Microscopic scales of linear tearing modes: a tutorial on boundary layer theory for magnetic reconnection

H. Betar, D. Del Sarto, M. Ottaviani, A. Ghizzo

J. Plasma Phys. (2022), *vol*. 88, 925880601
Published by Cambridge University Press

doi:10.1017/S0022377822001088

TUTORIAL

Microscopic scales of linear tearing modes: a tutorial on boundary layer theory for magnetic reconnection

H. Betar[1,2,†], **D. Del Sarto**[2,†], **M. Ottaviani**[3] **and A. Ghizzo**[2]

[1]Laboratoire M2P2, UMR CNRS 7340 – Université Aix-Marseille, F-13451 Marseille, France

[2]Institut Jean Lamour, UMR 7198 CNRS – Université de Lorraine, F-54000 Nancy, France

[3]CEA, IRFM, F-13108, Saint-Paul-lez-Durance, France

(Received 31 January 2022; revised 8 October 2022; accepted 12 October 2022)

We revise in detail and in a pedagogical way the analysis of the boundary layer theory of warm tearing modes in slab, reduced magnetohydrodynamics (MHD), when magnetic reconnection is driven by electron inertia and/or resistivity, and ion-sound Larmor radius effects are included. By comparison with the numerical solution of the corresponding eigenvalue problem, we interpret these results by means of a heuristic approach, which in the warm-electron regime, we show to be in general not feasible without knowledge of the scaling of the gradient of the magnetic flux function, differently from what happens in the cold-electron regimes. We put in evidence for a non-trivial relation between the first derivative of the magnetic flux function and of the velocity parallel to the neutral line, evaluated in its proximity, by thus providing insight to the multiple boundary layer analysis that Pegoraro & Schep (*Plasma Phys. Control. Fusion*, vol. 28, 1986, p. 647) first showed to be required in warm-tearing regimes. In this way, we also suggest and justify a general operational definition of the reconnecting layer width and we discuss the linear appearance of microscopic scales related to the gradients of the eigenfunctions of the tearing modes.

Key words: fusion plasma, astrophysical plasmas, plasma instabilities

Contents

1 Introduction **4**

2 Model equations and linear problem: general features **9**

2.1 Magnetic reconnection in tearing modes and formation of magnetic islands 10

2.2 Eigenvalue of the linear problem and reconnection rate in tearing-type modes 15

† Email addresses for correspondence: homam.betar@univ-amu.fr, daniele.del-sarto@univ-lorraine.fr

3 Boundary layer approach for tearing modes: large- and small-Δ' regimes 18
3.1 Orderings and instability parameter Δ' . . . 21
3.2 Small- and large-Δ' limits in slab geometry and in tokamaks . . . 23
3.3 Boundary layer integration of collisionless tearing in the previous literature 28

4 Boundary layer solution in the outer ideal region 30
4.1 A specific example of evaluation of $\Delta'(\psi_0; k)$ . . . 30

5 Equations in the non-ideal region 32
5.1 Differential equations in the non-ideal region . . . 33
5.2 Normalisation and distinction of the boundary layers . . . 34
5.3 Auxiliary function 'χ' and large- and small-Δ' limits . . . 36
5.3.1 Asymptotic estimate of χ_∞ in the small-Δ' limit . . . 36
5.3.2 Asymptotic estimate of χ_∞ in the large-Δ' limit . . . 36
5.4 Auxiliary equation for the function $\chi(\zeta)$ in the non-ideal region . . . 37
5.5 Wavelength limit and choice of integration via the equations for χ or for ψ and φ . . . 38

6 Solutions in the inner region: cold regime 39
6.1 Solution for $\bar{d}_e^2/\rho_s^2 \gg 1$: large-$\Delta'$ limit . . . 40
6.2 Solution for $d_e^2/\rho_s^2 \gg 1$: small-Δ' limit . . . 41

7 Solutions in the inner region: warm-electron regime 43
7.1 Equations in the non-ideal region for $\rho_s \gtrsim d_e$ . . . 44
7.2 Boundary layers in the non-ideal region for $\rho_s^2/d_e^2 \gg 1$ . . . 45
7.2.1 Outermost boundary layer . . . 45
7.2.2 Innermost boundary layer . . . 45
7.3 Integration strategy in the warm-electron regime for $\rho_s^2/\bar{d}_e^2 \gg 1$ . . . 46
7.3.1 Solution of the equation in the innermost interval ($x \ll \delta_1$) via integral representation of hypergeometric functions . . . 47
7.4 Solution of the auxiliary equation for $\rho_s^2/d_e^2 \gg 1$: large-Δ' limit . . . 49
7.4.1 Solution in the innermost layer $x \leq \delta_1$ . . . 50
7.4.2 Constraints at the origin . . . 51
7.4.3 Solution in the intermediate region, $\delta_1 \ll x \leq \delta_2$ . . . 51
7.4.4 Matching of solutions: scaling laws and eigenfunctions . . . 52
7.5 Solution of the linear equations for $\rho_s^2/d_e^2 \gg 1$: small-Δ' limit . . . 54
7.5.1 Matching and scalings in the non-ideal region $x \ll 1$ . . . 55
7.5.2 Approximated eigenmodes in the non-ideal region $x \ll 1$ . . . 57

8 Operational definition of the reconnecting layer width, δ, and other microscopic scales related to the eigenmodes 57
8.1 Notions of reconnecting layer and estimates of its width in previous literature . . . 58

https://doi.org/10.1017/S0022377822001088 Published online by Cambridge University Press

8.2 Operational definition of the reconnecting layer width, δ, and its scalings 60
8.3 Further micro-scales related to the gradients of the eigenmodes on the neutral line . . . 62
8.3.1 Asymptotic scalings of $\delta_\psi^{(2)}$ and of $\delta_\psi^{(4)}$ . . . 64
8.3.2 Asymptotic scalings of $\delta_\psi^{(2)}$ . . . 64
8.3.3 Asymptotic scalings of $\delta_\psi^{(4)}$ . . . 66

9 Heuristic derivation of the scaling laws of tearing modes 68
9.1 General hypotheses in the heuristic approach to the scaling estimate . . . 68
9.2 Heuristic derivation of the scaling laws in the cold-electron regime ($\rho_s^2 \ll \bar{d}_e^2$) . . . 70
9.3 Heuristic derivation of the scaling laws in the warm-electron regime ($\rho_s \gtrsim \bar{d}_e$) . . . 71

10 An ansatz about the 'generalisation' of the heuristic estimates: the role of the velocity gradient in the non-ideal region 72
10.1 Velocity gradient in the innermost non-ideal region . . . 72
10.2 A heuristic generalisation of the definition of the scale l_c . . . 73
10.3 Numerical evaluation of Δ' and Δ'_{v_y} . . . 74
10.4 Role of Δ'_{v_y} in heuristic-type estimates . . . 77
10.5 Significance of the inverse spatial scale Δ'_{v_y}: coherence with boundary layer calculations and comparison with previous work . . . 78

11 Summary and conclusions 81

A Appendix A. Derivation of the model equations for tearing modes in slab RMHD 83

B Appendix B. About alternative definitions of the reconnection rate 88

C Appendix C. Integration of the boundary layer equation via Fourier transformation 90
C.1 A brief historical review on the boundary layer approach to tearing-type equations in the Fourier space . . . 90
C.2 Comparison of the analysis of §§ 4–6 with the Fourier approach . . . 91

D Appendix D. An example of renormalisation of a differential equation 92

E Appendix E. Convergence and independence of the solutions of the hypergeometric form of the inner equation 93
E.1 Convergence of ψ_α and ψ_β . . . 93
E.2 Linear independence of ψ_α and ψ_β . . . 93

https://doi.org/10.1017/S0022377822001088 Published online by Cambridge University Press

F Appendix F. Heuristic estimation of the scaling laws by making use of the inverse gradient scale l_c and of Δ'_{v_y} 94

References 98

1. Introduction

Magnetic reconnection is one of the chief processes of conversion between electromagnetic energy and particle kinetic energy in magnetised plasmas (see, e.g. Biskamp 2000; Yamada, Kulsrud & Ji 2010). At the basis of extreme energy releasing phenomena that naturally occur in space plasmas, such as solar flares, coronal mass ejections or magnetic substorms, magnetic reconnection is of fundamental importance also in magnetically confined thermonuclear fusion plasma experiments: in fusion devices like tokamaks, it can cause disruptions (see, e.g. Wesson 1990), that is, the sudden loss of the magnetic confinement. This is usually due to magnetic island formation via tearing-like instabilities, and can affect the transport of matter and energy. Among the different scenarios, which have been devised since the first formulations of the 'magnetic reconnection' concept in the works by Giovanelli (1946), Hoyle (1949) and Dungey (1950), tearing-type modes (Furth, Killeen & Rosenbluth 1963) are the prototypical example of spontaneous reconnecting instabilities, that is, of magnetic perturbations that grow exponentially in time by inducing magnetic reconnection. Their 'explosive' behaviour in time make them the chief candidates for the explanation of several fast energy releasing events, which, both in Nature and in laboratory plasmas, are attributed to magnetic reconnection processes. Their theoretical modelling is however not trivial, since the mathematics required to solve the corresponding eigenvalue problem is complicated by some technical features that make its integration typically more complex than that of most linear instabilities. Notably, due to the multi-scale nature of the linear problem in which linear differential operators intervene, a boundary layer integration procedure is required.

Since Furth's remark (Furth 1963, 1964) of the relevance of electron inertia in allowing magnetic reconnection and since the early model by Furth (1964) and Coppi (1964*c*,*a*) for inertia-driven reconnecting instabilities, kinetic scale effects have attracted increasing attention in the attempt to model the rapid magnetic reconnection phenomena observed in low collisionality plasmas. After the seminal paper by Furth *et al.* (1963), in which the theory of resistive tearing modes was first formulated, several attempts have been made to include collisionless and/or kinetic physics in the linear tearing mode theory. Even if some works exist in which a full kinetic or girokinetic analytical treatment has been considered (Coppi, Laval & Pellat 1966; Laval, Pellat & Vuillemin 1966; Hazeltine & Ross 1975; Drake & Lee 1977; Cowley, Kulsrud & Hahm 1986; Daughton 1999; Daughton & Karimabadi 2005; Zocco & Schekochihin 2011; Connor, Hastie & Zocco 2012*b*), the complexity of the boundary layer analysis and of the heuristic assumptions on the ordering of the different microscopic scales makes the identification of the different reconnection regimes a quite difficult task, especially when two or more non-ideal magnetohydrodynamic (MHD) parameters enter in the reconnection rate. This is true even in a relatively simple fluid description extended to include non-ideal MHD effects.

For this reason, heuristic approaches have been developed to tackle the boundary layer problem with a simplified dimensional-like analysis, based on estimations about the characteristic gradients and about the balance of the terms of the linear equations. These techniques have been successfully used to recover the asymptotic scalings of the growth rate and of the reconnection layer width in the purely resistive and purely inertial regimes of reduced MHD (RMHD) instabilities. They are also often presented in textbooks on

https://doi.org/10.1017/S0022377822001088 Published online by Cambridge University Press

magnetic reconnection as a 'short-cut' procedure to obtain these results without carrying out the full boundary layer integration of the eigenmodes. Providing an estimate of the characteristic temporal and spatial scales of spontaneous reconnecting instabilities, and comparing them with the values inferred from experimental measures of reconnection events occurring in the laboratory or in Nature, are indeed among the elements of principal interest, in this context. Heuristic methods based on dimensional analysis have also proven to work for both small and large values of the Δ' instability parameter (Ottaviani & Porcelli 1995) and for the fastest growing mode in a large aspect ratio current sheet (Bhattacharjee *et al.* 2009; Comisso *et al.* 2013; Del Sarto *et al.* 2016). Moreover, they are generally used to obtain insight on the physics of the problem and on the interpretation of some non-trivial results of the boundary layer analysis (see, e.g. Drake & Lee 1977; Cowley *et al.* 1986). However, as we are going to discuss in this work, heuristic methods 'fail' to obtain the scalings first computed by Pegoraro & Schep (1986) and Porcelli (1991) with a boundary layer approach, when electron temperature effects are included, unless some further careful assumptions are made, which are related to the boundary layer decomposition of the spatial domain: whether it is possible to develop heuristc arguments which allow one to obtain these results without relying on further information from boundary layer analysis (or from numerical integration of the linear problem) is, at the moment, an open question.

One of the main purposes of this work is to revise in a tutorial way the linear analysis of tearing-type modes in these regimes, by discussing their analytical solutions in the coordinate space and by showing in this way the advantages and limitations of heuristic-type derivations. To the best of our knowledge, indeed, details of the analytical theory for this double-boundary layer approach have been seldom discussed in the existing literature. When this has occurred, the analysis was based on the solution of the eigenvalue problem in the Fourier space (Pegoraro & Schep 1986), or by using a different linear model based on a reduced fluid-kinetic approach (Zocco & Schekochihin 2011) and by taking a somewhat different analytical approach based on perturbation methods to solve the boundary layer equations that here we will tackle by direct integration instead.[1] It should be nevertheless recalled that other analytical works on this subject exist. In these, the boundary layer analysis of tearing modes is however complicated by further ingredients related, for example, to the geometry of the magnetic equilibrium profile (see, e.g. Militello *et al.* 2004; Connor *et al.* 2012*a*; Zocco, Helander & Weitzner 2020) or to the inclusion of full kinetic effects (see the references previously cited in this regard). Moreover, also in the few works that addressed these subjects with different approaches with respect to the one we develop here, most details of the complex analysis involved in the calculations were often not reported and are difficult to track.

To simplify the analysis and to show in a pedagogical way the essential features of the double boundary layer separation, we focus here on the limit of cold ions, which allows us to take a fluid closure for the latter, differently from the semi-kinetic models considered in practically all previous works that already treated this problem (see, e.g. Cowley *et al.* 1986; Pegoraro & Schep 1986; Pegoraro, Porcelli & Schep 1989; Porcelli 1991; Zocco & Schekochihin 2011). In particular, we rely on the equations of the two-fluid reduced-MHD model extended to include ion-sound Larmor radius effects, for which different derivations exist (Zank & Matthaeus 1992; Schep, Pegoraro & Kuvshinov 1994; Bergmans 2001; Del Sarto, Califano & Pegoraro 2006; Bian & Tsiklauri 2009), which are based on two different

[1] After acceptance of this manuscript the authors have become aware of another recent work (Granier *et al.* 2022), in which an integration of the boundary layer equations in the coordinate space has been performed in the warm-electron, small-Δ' regime of tearing modes.

https://doi.org/10.1017/S0022377822001088 Published online by Cambridge University Press

types of ordering between fluctuations of the ion density and of the guide field magnetic component (cf. Appendix A). Several more recent and refined gyrofluid models exist, which are based on the evolution of more than two scalar fields. However, the two-field model we focus on, which has been used in several nonlinear studies of different magnetic reconnection scenarios (see Kleva, Drake & Waelbroeck 1995; Cafaro *et al.* 1998; Grasso *et al.* 1999; Bergmans & Schep 2001; Del Sarto, Califano & Pegoraro 2003; Wang *et al.* 2011 to cite the earliest) or even of turbulence (Milosevich, Morrison & Tassi 2018), contains the whole essential physics of the problem. More specifically, it yields the same linear system to which all other, more refined, cold-ion models converge in the isothermal electron limit.

To accomplish our pedagogical purpose, we then give a step-by-step presentation of the boundary layer integration procedure in the coordinate space, with the aim of keeping it 'self-contained', that is, by trying to provide all the analytical tools useful for the purpose (e.g. element of complex analysis), when they result necessary for the algebra. By then comparing the analytical results with those obtained with a numerical eigen-solver (Betar *et al.* 2020) based on a multi-precision toolbox (Holoborodko 2012), we analyse the spatial behaviour of the corresponding eigenfunctions and we discuss the limitations and delicate points of heuristic estimations that are sometimes used as a 'quicker' alternative to full boundary layer calculations. Although the main focus of this article is on the warm-electron regime, we also consider, for comparison, the cold-electron limit, in which a single boundary layer analysis suffices. In particular, we consider in a unified way both the resistive and collisionless regimes, and we separately address the cold- and warm-electron regimes. Each regime is associated with some characteristic non-ideal parameter: the Lundquist number S^{-1}, related to resistivity; the electron skin depth d_e, related to electron inertia in the collisionless limit; and the ion-sound Larmor radius ρ_s, related to the electron temperature.

We thus discuss the results of the boundary layer analysis, which yields the asymptotic scaling (in terms of the non-ideal parameters ruling the reconnection process) of the growth rates and of some characteristic spatial scales associated with the eigenfunctions, as well as the approximated profile of the latter in some regions of the domain of integration. We then discuss the asymptotic estimates of the first derivatives of the current and velocity field on the neutral line. We also provide (to the best of our knowledge, for the first time) a formal quantitative definition of the reconnection layer width, which we argue to be valid in all reconnection regimes and which is given in terms of numerically measurable quantities that are related to the spatial profile of the eigenfunctions.

Then, in interpreting these quantities in terms of a heuristic approach, whose limitations in the warm-electron case we point out, we provide evidence that the introduction of the scale ρ_s makes a further characteristic 'mixed' scale appear in the collisionless large wavelength limit, which is *smaller* than d_e when $\rho_s > d_e$, since it scales like $\sim \rho_s^{-1/3} d_e^{4/3}$. Such a characteristic length, which in previous works (Porcelli 1991) had been already noted, is identifiable as the reconnecting layer width, in agreement both with the operational definition here proposed and with previous works that already recognised it as such (Zocco & Schekochihin 2011).

By discussing the boundary layer results in light of a heuristic dimensional-type approach, we also show a new, non-trivial relation between the first derivative of the magnetic flux function and the first derivative of the parallel velocity, which holds close to the neutral line. This velocity gradient displays characteristic scalings that depend on the wavelength regime. Information about these scalings is *a priori* not evident, and the analysis we provide on this subject at the end of this work suggests indeed that such information can not be obtained via simple dimensional analysis, if not in the cold-electron

https://doi.org/10.1017/S0022377822001088 Published online by Cambridge University Press

regimes. Nevertheless, introducing this scale length allows, in any reconnection regime, the writing of the scaling laws in a way that results to be perfectly symmetric between the small and large wavelength limit, provided the characteristic instability parameter of the small wavelength limit (i.e. the Δ' parameter of Furth *et al.* 1963) is replaced in the large wavelength limit by the gradient of the velocity (which we have here called Δ'_{v_y}, by analogy). This fact, and the correspondence between some characteristic scale length associated with this velocity gradient and scale lengths that in other works based on a kinetic approach have been interpreted in terms of inherently kinetic features (Drake & Lee 1977; Cowley *et al.* 1986; Ottaviani & Porcelli 1993; Zocco & Schekochihin 2011), suggests that the role of this quantity in the tearing mode linear dynamics deserves future investigation.

The structure of this article is as follows.

(i) In § 2, we discuss the model equations and some general aspects of magnetic reconnection which include: a brief historical review of the notion of magnetic reconnection associated with that of magnetic topology and some general features of tearing modes and of the magnetic structures they induce (§ 2.1); the notion of reconnection rate and its relation with the growth rate of the eigenvalue problem (§ 2.2).

(ii) In § 3, we introduce the notion of boundary layer, we discuss its relevance to tearing mode analysis and we outline the key points of the corresponding integration strategy. Then we introduce the notion of instability parameter (Δ') and the way it intervenes in the matching of the solutions between the ideal and non-ideal regions of the domain (§ 3.1). We discuss the wavelength regimes of the eigenmode solution, in terms of the amplitude of Δ', by pointing out similarities and differences between tearing modes in slab and in cylindrical geometry (§ 3.2). In § 3.3, we briefly review previous works in which a boundary layer analysis similar to the one we develop here has been discussed.

(iii) In § 4, we address the boundary layer integration by starting from the ideal region, where the hypotheses of ideal MHD hold, and we detail the integration procedure which allows the analytical evaluation of $\Delta'(k)$ in terms of the instability wavenumber k for a specific equilibrium profile, which exemplifies a larger class of equilibria (§ 4.1).

(iv) In § 5, we introduce the notions of 'generalised' resistivity and electron inertia, which allow a unified treatment of the resistive and collisionless case altogether, and we discuss the combination of the two non-ideal parameters. We then discuss the strategy for the identification of the integration layers in the non-ideal region via the general approximations valid in the non-ideal region (§ 5.1) and the criteria of normalisation (§ 5.2). We then introduce the auxiliary function, useful for the integration of the boundary layer problem in some regimes, by discussing its small and large wavelength limits (§ 5.3) and then its normalisation (§ 5.4). Finally, we outline the criteria that may make one prefer to perform the integration of the non-ideal equation by using the auxiliary equations rather than the equations for the two scalar fields (§ 5.5).

(v) In § 6, we solve the boundary layer problem in the cold-electron regimes. First we find the solution in the large-Δ' limit (§ 6.1) and then in the small-Δ' limit (§ 6.2).

(vi) In § 7, we address the warm-electron regimes: after discussing the general form of the equations in the non-ideal region (§ 7.1), we identify the two boundary layers of interest in this case (§ 7.2) and then we outline the integration strategy that will be pursued, by relying on the integral representation of hypergeometric functions

https://doi.org/10.1017/S0022377822001088 Published online by Cambridge University Press

(§ 7.3). First we consider the solution in the large-Δ' (§ 7.4) and then in the small-Δ' limit (§ 7.5).

(vii) In § 8, we address the problem of identifying the characteristic width of the reconnecting layer by relying on further hypotheses of physical character and by starting from the characteristic scales obtained from the boundary layer integration. After reviewing different notions of the reconnecting layer that have been adopted in the literature over the years (§ 8.1), we propose an operational definition of its width, related to the distance of the local maxima (or minima) of the current density from the neutral line, which can be useful for both experimental and numerical application, and which is shown via numerical integration to provide the same scalings of the inner layer width (§ 8.2). The asymptotic scalings of further characteristic spatial scales associated with the derivatives of the magnetic field and of the velocity profile on the neutral line are then estimated and compared to the scalings of the reconnecting layer width in different regimes (§ 8.3).

(viii) In § 9, we address the problem of the heuristic derivation of the scaling laws of tearing modes via dimensional analysis. After discussing the relevance and usefulness of the approach and after having outlined its general hypotheses (§ 9.1), we apply it to the 'textbook' example of the cold-electron regimes, where its efficiency is well established (§ 9.3). Then we show and discuss its 'failure' in the warm-electron regimes, where it yields wrong estimates with respect to those obtained from the boundary layer analysis (§ 9.3).

(ix) In § 10, starting from the physical insight brought by the analysis of the logical points which may lead to the wrong dimensional estimates in the warm-electron regime, we introduce a new characteristic scale length associated with the gradient of the velocity component parallel to the neutral line and evaluated close to it: by analogy with the instability parameter, we call it Δ'_{v_y} (§ 10.1). We then postulate a further estimate for the gradient of the magnetic flux function, which, depending on the reconnection regime, can be related to Δ'_{v_y} (§ 10.2). After having shown the convergence of a numerical procedure which allows the quantification of Δ'_{v_y} (§ 10.3), we show its relevance for the heuristic estimates: they can now lead to the correct results – although in the warm-electron regime, the procedure is not 'closed', since it is strongly suggested that the scale Δ'_{v_y} can not be obtained by simple dimensional analysis – and they can be cast in a 'symmetric form', in which the scalings in the large-Δ' limits mirror those of the small-Δ' limits provided the substitution $\Delta' \leftrightarrow \Delta'_{v_y}$ (§ 10.4). The significance of the inverse scale length Δ'_{v_y} is further discussed by comparison with results obtained in previous works on boundary layer calculations, in which a characteristic length displaying similar scalings in some regimes had been already noted (§ 10.5).

(x) Conclusions follow in § 11.

(xi) Further technical details are reported in the Appendices. These include: calculations related to the derivation of the model and a discussion of the relevant hypotheses (Appendix A); a brief discussion of alternative definitions found in literature for the notion of 'reconnection rate', which are not directly relevant to the problem we consider here (Appendix B); a discussion on the general strategy of integration of the boundary layer problem of tearing modes in the Fourier space, and a comparison of the equations we have integrated with those appearing in previous works available in the literature (Appendix C); a didactical example of normalisation of a differential

https://doi.org/10.1017/S0022377822001088 Published online by Cambridge University Press

equation (Appendix D); the proof of convergence and linear independence of the solution found in § 7.4 (Appendix E); and the detailed discussion of the logical steps, which allow one to generalise the heuristic estimate discussed in § 10.4 in terms of Δ'_{v_y} (Appendix F).

2. Model equations and linear problem: general features

We consider the reduced MHD limit, from now on noted as RMHD (Strauss 1976, 1977; Zank & Matthaeus 1992), and we consider the standard tearing equations in slab geometry ($\partial/\partial z = 0$) for a strongly magnetised plasma whose guide field component is along the z direction. Fluid incompressibility, valid for the bulk plasma at the leading $\boldsymbol{E}\times\boldsymbol{B}$-drift ordering and possibly with inclusion of drift-diamagnetic corrections (see Appendix A), allows us to reduce the number of independent vector components and therefore to consider a limited set of scalar quantities.

Choosing perturbations of the form $\sim f(x)\mathrm{e}^{\mathrm{i}ky+\gamma t}$+c.c. we linearise the equations around equilibria with an odd $B_y^0(x)$ component, which vanishes at $x = 0$, and with a null in-plane fluid velocity at equilibrium, $\boldsymbol{U}^0(x, y) = 0$. Here we have already used knowledge of the fact that the eigenmodes we are considering have low frequencies, so that $\omega/\gamma \sim 0$. This can be taken here as a verifiable heuristic assumption.

It can be shown that only two scalar fields are necessary. The relevant equations can be then represented by the equation for one of the in-plane components of $\boldsymbol{B}$ and by the equation for one of the in-plane components of the fluid velocity. These can be cast in the form of two coupled equations for the stream functions ψ and φ. Details about all these features, and bibliographical references as well, are provided in Appendix A.

In particular, $\psi(x, y, t)$ and $b(x, y, t)$ are the normalised scalar functions defining the magnetic field components, $\boldsymbol{B} = \boldsymbol{\nabla}\psi \times \boldsymbol{e}_z + b\boldsymbol{e}_z$, whereas $\varphi(x, y, t)$ is the stream function for the in-plane $\boldsymbol{E}\times\boldsymbol{B}$-drift velocity, $\boldsymbol{U}_\perp = -\boldsymbol{\nabla}\varphi \times \boldsymbol{e}_z$, expressing the normalised gradient of the electrostatic potential in RMHD. Here, the large guide field ordering allows us to completely neglect the dynamics related to the scalar function b.

Labelling with indices '0' and '1' the equilibrium quantities and first-order perturbations, respectively, the linearisation is then performed around equilibria of the form $\psi(x, y, 0) \equiv \psi_0(x)$, even with respect to $x = 0$, with $\phi(x, y, 0) = 0$. Normalised as indicated below and using, for simplicity of notation, the same symbols for the fields defined in the coordinate space and for their Fourier transform with respect to the y variable, the equations we will work with, read:

$$\gamma[\psi_1 - d_e^2(\psi_1'' - k^2\psi_1)] - \mathrm{i}k\varphi_1(\psi_0' - d_e^2\psi_0''') = -\mathrm{i}k\rho_s^2(\varphi_1'' - k^2\varphi_1)\psi_0' + S^{-1}(\psi_1'' - k^2\psi_1), \tag{2.1}$$

$$\gamma[\varphi_1'' - k^2\varphi_1] = \mathrm{i}k\psi_0'(\psi_1'' - k^2\psi_1) - ik\psi_1\psi_0'''. \tag{2.2}$$

We can also cast (2.1)–(2.2) in a matrix form (useful for the eigenvalue solution) as

$$\gamma\begin{pmatrix}\mathcal{F} & 0\\ 0 & \mathcal{L}\end{pmatrix}\begin{pmatrix}\psi_1\\ \varphi_1\end{pmatrix} = \begin{pmatrix}S^{-1}\mathcal{L} & \mathcal{B}\\ \mathcal{A} & 0\end{pmatrix}\begin{pmatrix}\psi_1\\ \varphi_1\end{pmatrix}, \tag{2.3}$$

where we have introduced the differential operators

$$\mathcal{L} \equiv \frac{\partial^2}{\partial x^2} - k^2, \quad \mathcal{F} \equiv 1 - d_e^2\mathcal{L}, \tag{2.4}$$

$$\mathcal{A} \equiv \mathrm{i}k(\psi_0'\mathcal{L} - \psi_0'''), \quad \mathcal{B} \equiv \mathrm{i}k\left[(\psi_0' - d_e^2\psi_0''') - \rho_s^2\psi_0'\mathcal{L}\right], \tag{2.5}$$

with $\mathcal{C}$ being the $\rho_s = 0$ limit of $\mathcal{B}$.

https://doi.org/10.1017/S0022377822001088 Published online by Cambridge University Press

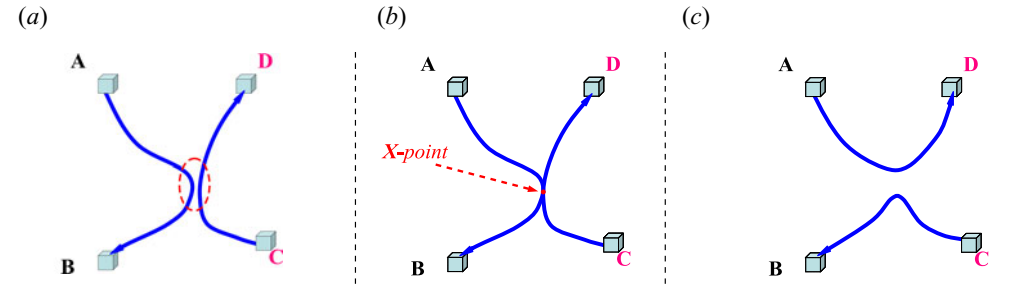

FIGURE 1. Cartoon schematising three steps of a simplified 2-D magnetic reconnection process that emphasises the notion of change of magnetic topology. (*a*) Two magnetic lines connecting different pairs of fluid elements, A $\leftrightarrow$ B and C $\leftrightarrow$ D, are twisted by the ideal fluid motion so as to locally generate strong spatial gradients, i.e. current densities. (*b*) Magnitude of the spatial gradients locally compensates the smallness of the non-ideal parameters in the generalised Ohm's law, by thus allowing the relaxation of the topological constraints that in the ideal limit, forbid the intersection of initially distinct magnetic lines; an *X*-point is formed. (*c*) Magnetic reconnection process undergone at the *X*-point, by which magnetic energy is dissipated and/or converted into other forms of plasma energy, which makes other magnetic configurations accessible to the plasma; the magnetic topology has globally changed as the magnetic lines now connect the pairs of fluid elements A $\leftrightarrow$ D and B $\leftrightarrow$ C.

The non-ideal parameters of the model are normalised to the reference scale length L_0. They correspond to the electron skin-depth, d_e, to the ion-sound Larmor radius, ρ_s, and to the Lundquist number, S. The reference length L_0 is chosen to be the equilibrium shear length a of $\psi_0(x)$ at $t = 0$, whereas times are normalised to the reference Alfvén time τ_A computed with respect to the in-plane equilibrium magnetic field component, evaluated sufficiently far from the neutral line.

Several derivations exist of (2.1)–(2.2). The parameter ρ_s, which violates the Lagrangian invariance of the parallel electron canonical momentum $F \equiv \psi - d_e^2 \nabla^2 \psi$, is related to electron parallel compressibility effects (Grasso *et al.* 1999). It is also considered to be a finite-Larmor-radius (FLR) effect, since in a strong guide field limit, it can be shown to be due to a component of the non-isotropic electron pressure tensor that enters in the equation of ψ via the diamagnetic drift component of the fluid electron velocity (see Schep *et al.* (1994) and Appendix A).

2.1. *Magnetic reconnection in tearing modes and formation of magnetic islands*

A magnetic reconnection process is characterised by the formation of an *X*-point, where initially distinct magnetic lines have connected thanks to non-ideal effects that become important as the gradients of the magnetic field components, i.e. the components of the current density, are large enough. As a result of the magnetic reconnection event, the plasma system typically relaxes to a final state of lower 'potential magnetic energy', the diminished energy being converted into plasma kinetic and internal energy as well as into electron acceleration. During this process, the 'magnetic topology' in the plasma changes since the connection of fluid elements is globally modified – see figure 1.

Non-ideal effects allow a local violation of the topological conservations implied by the ideal Ohm's law (Cowling 1933; Alfvén 1942; Batchelor 1950; Elsasser 1950*a*,*b*; Truesdell 1950; Lundquist 1951; Newcomb 1958), which would otherwise prevent initially distinct magnetic lines embedded in the plasma to intersect. Mathematically speaking, this kind of conservation is a consequence of the fact that Faraday–Ohm's law in an ideal MHD

https://doi.org/10.1017/S0022377822001088 Published online by Cambridge University Press

plasma,

$$\frac{\partial \boldsymbol{B}}{\partial t} = \boldsymbol{\nabla} \times (\boldsymbol{U} \times \boldsymbol{B}), \tag{2.6}$$

is equivalent, thanks to a well-known vector identity ($\boldsymbol{\nabla} \times (\boldsymbol{U} \times \boldsymbol{B}) = \boldsymbol{U}(\boldsymbol{\nabla} \cdot \boldsymbol{B}) - \boldsymbol{B}(\boldsymbol{\nabla} \cdot \boldsymbol{U}) + (\boldsymbol{B} \cdot \boldsymbol{\nabla})\boldsymbol{U} - (\boldsymbol{U} \cdot \boldsymbol{\nabla})\boldsymbol{B}$) combined with the continuity equation (Truesdell 1950), to a vector expression that corresponds to the null Lie-derivative of the vector field $\boldsymbol{B}/n$ dragged by the velocity field $\boldsymbol{U}$: this directly implies the Lagrangian invariance of magnetic lines from which a set of topological conservations follow, the most famous of which go under the names of '(Cowling–)Alfvén theorem' (Cowling 1933; Alfvén 1942), 'Woltjer invariants' Woltjer (1958) and 'connection theorem' (Newcomb 1958) – see (Tur & Yanovsky 1993; Kuvshinov & Schep 1997; Del Sarto *et al.* 2006) and references therein for a more detailed discussion; see, e.g. Dubrovin, Nivikov & Fomenko (1991, § III.23) for a definition of Lie derivative in tensor notation in the coordinate representation and Schouten (1989, § II.8) for the Lie-derivative of tensor densities of arbitrary 'weight' (cf. also Lovelock & Rund (1989, p. 105) for the notion of a 'relative tensor'). This is mathematically analogous to the set of topological conservations related to the fluid vorticity, which were well known to follow from the inviscid vorticity equation in a barotropic fluid (see Truesdell 1954). In this context, the Alfvén theorem of magnetic flux conservation in an ideal MHD plasma is the mirror correspondent of the Helmholtz–Kelvin theorem of vorticity conservation in ideal hydrodynamics (Batchelor 1950; Elsasser 1950*b*; Truesdell 1950; Axford 1984; Greene 1993). We incidentally note that some formal similarities can be also recognised in the eigenmode analysis of resistive tearing modes and of ideal instabilities in presence of viscosity in a Kolmogorov hydrodynamic flow (Fedele, Negulescu & Ottaviani 2021). In terms of the RMHD equations above, the Lagrangian invariance of magnetic lines is expressed by the ideal limit ($d_e = \rho_s = S^{-1} = 0$) of (2.1), although a finite ρ_s alone allows preservation of the ideal MHD topological conservation, provided a redefinition of the stream function of the velocity field $\boldsymbol{U}$ according to $\varphi \to \varphi - \rho_s^2 \nabla^2 \varphi$ (Pegoraro *et al.* 2004). In particular, in the collisionless regime, even the nonlinear evolution of tearing-type instabilities can be shown to be ruled by the conservation of Lagrangian invariants whose existence is related to the condition $\rho_s \neq 0$ (Cafaro *et al.* 1998; Grasso *et al.* 2001).

The early notion of *magnetic reconnection* has been formalised by Dungey (1950, 1953) after the intuitions by Giovanelli and Hoyle. The former one first noted the occurrence of solar flares in correspondence with regions of local inversion of the magnetic field perpendicular to the Sun surface, and thus made the hypothesis that this could have been a signature of a mechanism of conversion from the magnetic energy to the plasma kinetic energy allowed by resistivity (Giovanelli 1946); the second one conjectured that the same may have occurred also in the terrestrial magnetotail (Hoyle 1949). Resistivity is one of the non-ideal effects capable of violating alone the Lagrangian invariance of $\boldsymbol{B}$, so as the electron inertia, or the electron–electron viscosity, or a non-zero out-of-plane component of the rotational of the divergence of the pressure tensors, also are. All these non-ideal effects, together with other ones such as the Hall-term, can be synthetically expressed with the vector $\boldsymbol{\Phi}_\varepsilon$ in generalised Ohm's law, ε generally indicating the infinitesimally small parameter weighting the non-ideal contribution (we use the same normalisation of (2.1)–(2.2)):

$$\boldsymbol{E} + \boldsymbol{U} \times \boldsymbol{B} = \boldsymbol{\Phi}_\varepsilon. \tag{2.7}$$

Magnetic reconnection at least requires $\boldsymbol{\nabla} \times \boldsymbol{\Phi}_\varepsilon \neq 0$. Although ideal Ohm's law at the MHD scale takes the form of (2.7) with $\boldsymbol{\Phi}_\varepsilon = 0$, note that the dominant contribution to

https://doi.org/10.1017/S0022377822001088 Published online by Cambridge University Press

generalised Ohm's law, obtained by summing (A7)–(A8) multiplied by the respective charge over mass of the species, comes from electron momentum equation. That is, electrons fix the strongest 'frozen-in' condition between the plasma flow and the magnetic field, which, by neglecting all electron inertia, electron–electron viscosity and electron–ion viscosity (i.e. resistivity), and electron-pressure anisotropy, is expressed by the 'ideal Hall-MHD Ohm's law': $\boldsymbol{E}+\boldsymbol{u}^e\times\boldsymbol{B}=0\ \Leftrightarrow\ \boldsymbol{E}+\boldsymbol{u}^i\times\boldsymbol{B}=d_i(\boldsymbol{J}\times\boldsymbol{B})/n$. While at MHD scales, where $\boldsymbol{U}\simeq\boldsymbol{u}_i$, the frozen-in condition equally applies for both ions and electrons. At smaller spatial scales, the magnetic field can decouple from the ion fluid, but, as long as $\boldsymbol{E}+\boldsymbol{u}^e\times\boldsymbol{B}\simeq 0$ (or, better, as long as $\boldsymbol{E}+\boldsymbol{u}^e\times\boldsymbol{B}\simeq\nabla f$) holds, magnetic lines are dragged by the electron fluid flow. Note in this regard that (2.1) for the magnetic stream function ψ, corresponding to the z-component of Ohm's law, also expresses the variation of the z-component of the electron canonical momentum (cf. Appendix A).

The first analytical model of magnetic reconnection was the well-known Sweet–Parker model (Parker 1957; Sweet 1958), which assumes a steady inflow condition in an X-point: in this case, the resistive reconnection steadily occurs in one point (the X-point) of a static current sheet of finite elongation L and of large aspect ratio L/a, which asymptotically scales as S, when the Lundquist number is defined with respect to the current sheet thickness a, as in (2.1) – see figure 2(a) (when S is instead defined – let us call it S_L – with respect to the current sheet length, L, the scaling of the Sweet-Parker aspect ratio reads $L/a\sim S_L^{1/2}$). This steady reconnection scenario has been then extended to the inertia-driven regime by Wesson (1990), for applications to the sawtooth crash in tokamaks, and by Bulanov, Pegoraro & Sakharov (1992) for applications to reconnection in the electron-MHD regime. Variations to this model, in which a different choice of the boundary conditions around the reconnecting region has been made and different rates of magnetic reconnection have been obtained, have been done in subsequent works, starting from that of Petschek (1964) – see also (Vasyliunas 1975) and references therein.

Instead, the notion of a tearing mode, the first example of a spontaneous reconnecting instability, was formalised a few years later in the pioneering work by Furth *et al.* (1963). In this case, the current sheet is assumed to have *periodic* boundary conditions along the 'resonant line' where the wave vector of the linear perturbation is locally orthogonal to the equilibrium magnetic field. That is, if $\boldsymbol{B}_0(x_s)\cdot\boldsymbol{k}=0$, then the equation $x=x_s$ defines a resonant line in two dimensions and a resonant surface in three dimensions. After a translation of the reference amplitude of the sheared magnetic field component, it can always be assumed that the sheared equilibrium magnetic field is zero at $x=x_s$, and changes sign in its neighbourhood: therefore, in slab geometry, the resonant line is usually termed the '*neutral line*'. It can be seen from the energy principle that the $\boldsymbol{B}_0(x_s)\cdot\boldsymbol{k}=0$ condition minimises the stabilising role played by Alfvénic perturbations: this is why rational surfaces (m,n) in large aspect ratio tokamaks are candidate resonant surfaces for tearing-type instabilities. We recall that a rational surface in a tokamak is a magnetic surface characterised by the condition $q(r)=-m/n$. In the large aspect ratio limit, i.e. the 'cylindrical tokamak' approximation, the safety factor reads $q(r)=B_\varphi r/(B_\theta R)$, where B_φ and B_θ are respectively the toroidal and poloidal component of the magnetic field, and r and R are the minor and major radius of the tokamak, respectively. It is easy to verify that the condition $\boldsymbol{k}(r)\cdot\boldsymbol{B}(r)=0$ defines a rational surface for $\boldsymbol{k}=m/(2\pi r)\boldsymbol{e}_\theta+n/(2\pi R)\boldsymbol{e}_\varphi$. The harmonic perturbation along the neutral line direction (the wave vector k of (2.1)–(2.2)) induces a sinusoidal modulation of the perturbed magnetic field lines that gives rise to the characteristic '*magnetic island*' pattern: in this case, a pair of X-points (at the local minima of ψ_1) delimits each magnetic island, and an elliptic point for the magnetic field, called the O-point (at the local maximum of ψ_1),

https://doi.org/10.1017/S0022377822001088 Published online by Cambridge University Press

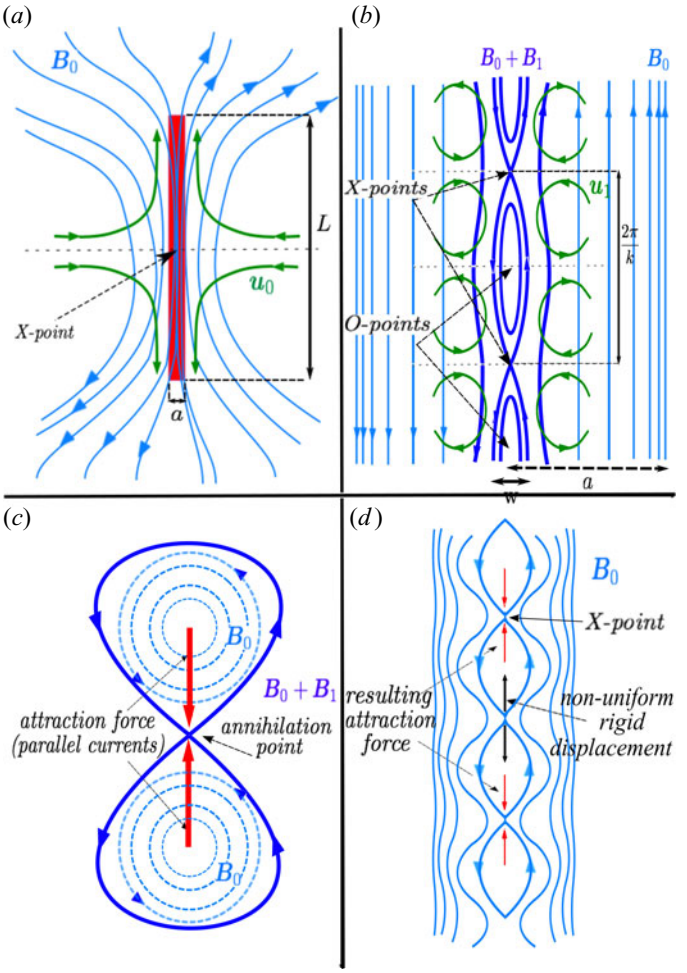

FIGURE 2. Comparison of four reconnection scenarios. (*a*) Sketch of the steady Sweet–Parker reconnection scenario. No particular hypotheses are done on the boundary conditions of the reconnecting current sheet, whereas steadiness and a specific scaling of the aspect ratio with non-ideal parameters like resistivity (i.e. $L/a \sim S^{-1}$, Parker 1957; Sweet 1958) or electron inertia (Wesson 1990) are required. The configuration does not represent an instability: no distinction is made between equilibrium and perturbed quantities. (*b*) Typical 'magnetic island' configuration in the tearing-type reconnection. Periodic boundary conditions along the neutral line are required and hyperbolic patterns of the velocity field near the *X*- and *O*-points develop together with the island formation. The wavenumber of oscillations of the mode fixes the number of magnetic islands which are generated. In the linear stage, the island width is $w \simeq \delta \ll a$. (*c*,*d*) Merger configuration (*c*) of two undisplaced line currents (Syrovatskii 1966*a*; Biskamp & Welter 1980; Kleva *et al.* 1995), which resembles (*d*) a non-periodic version of the 'coalescence instability' scenario. The latter concerns a periodic structure constituted by magnetic islands in a chain (Finn & Kaw 1977; Pritchett, Lee & Drake 1979; Bhattacharjee, Brunel & Tajima 1983). In the displaced current merger case, the attraction of two parallel current filaments squeezes the magnetic field that piles up and typically dissipates at the *X*-point: in this configuration, one may rather speak of 'magnetic annihilation' (cf. e.g. Priest & Sonnerup 1975; Watson & Craig 1998; Gu *et al.* 2019). In the coalescence instability scenario, a somewhat similar process occurs (an out-of-plane current density being associated with the *O*-point of each island) once a non-rigid displacement along the neutral line perturbs the periodic configuration by making the islands get closer, pairwise. Similarly, a periodic 2-D 'paving' of magnetic cell-like structures of different shape (not shown here) can be destabilised the same way by planar, non-rigid displacements (Longcope & Strauss 1993).

https://doi.org/10.1017/S0022377822001088 Published online by Cambridge University Press

is at the centre of the island – see figure 2(*b*) (see also White 1983, 1986) for a tutorial discussion about further features of tearing mode analysis that go beyond the purpose of the present work). In figure 2*c,d*), other reconnection scenarios related to the merger of current filaments (Syrovatskii 1966*a*; Biskamp & Welter 1980) and to the 'coalescence' of a chain of magnetic islands (Finn & Kaw 1977; Longcope & Strauss 1993) are shown for comparison.

As tearing-type modes are linear instabilities, they grow exponentially in time, which marks an important, fundamental difference with respect to the Sweet–Parker scenario: the structure of the reconnecting current sheet is not static but is altered by the current density associated with the tearing mode perturbation, which makes the magnetic island grow in thickness until nonlinear saturation of the instability (see Ottaviani *et al.* 2004 and references therein for a survey of different saturation scenarios). This dynamics is associated with hyperbolic patterns of the velocity field around both the X- and O-points, whereas only the hyperbolic flow at the X-point is required in the Sweet–Parker scenario. The hyperbolic flow at the X-point is responsible for the well-known quadrupole pattern of the stream function of the velocity field, and the elliptic and hyperbolic structure of ψ, φ and of their derived fields near the critical points (X and O) fix the symmetries of the eigenmode solutions. We incidentally note that this also provides a quite simple explanation (cf. Del Sarto *et al.* 2016, App. A) of the quadrupole pattern associated with the out-of-plane magnetic field component at the X-point, in the regime where the Hall term is dominant in the generalised Ohm's law (quadrupole structure which is often recognised as an experimental proxy of Hall-mediated reconnection – cf. e.g. Deng & Matsumoto 2001): in this regime, the Lagrangian invariance of the magnetic field is expressed with respect to the electron flow (see Fruchtman 1991; Pegoraro *et al.* 2004; Del Sarto *et al.* 2006), which is in turn associated with the in-plane current density, and therefore to the spatial modulation of the out-of-plane magnetic field. If the equilibrium magnetic profile is even with respect to the neutral line, as it is typically assumed in analytical models for tearing modes (as we will do here), the matrix operators of (2.3) commute with the parity operator inducing the transformation $x \leftrightarrow -x$, which makes tearing modes have a fixed parity in x. Taking into account the parity in y associated with the harmonic perturbation, the point symmetries of the ψ_1 and φ_1 fields near the critical points (X and O) for tearing modes developing in an even magnetic equilibrium can be summarised as

$$\text{X-point}: \begin{cases} \psi \text{ even in } x, & \text{even in } y, \\ \varphi \text{ odd in } x, & \text{odd in } y, \end{cases} \qquad \text{O-point}: \begin{cases} \psi \text{ even in } x, & \text{even in } y, \\ \varphi \text{ odd in } x, & \text{odd in } y. \end{cases} \tag{2.8}$$

These symmetries nonlinearly mix via the Poisson bracket operators, of which the terms of (2.1)–(2.2) are a rewriting, after linearisation (cf. (A1)–(A2), Appendix A). A local quadratic expansion of the eigenmodes near the critical points, which accounts for these nonlinear couplings, allows interesting insight in the early nonlinear, local dynamics of tearing-type instabilities (Pegoraro *et al.* 1995; Del Sarto *et al.* 2011).

We conclude by recalling that several effects, in addition to the inclusion of further non-ideal terms in Ohm's law, have been considered, over the years, in the linear theory of tearing modes in reduced MHD. These include the effect of flows parallel to the neutral line, which can have a stabilising effect on the tearing mode instability (Bulanov, Sakai & Syrovatskii 1979; Syrovatskii 1981; Faganello *et al.* 2010), and which can also make the latter compete with the Kelvin–Helmholtz instability (Hofmann 1974; Chen & Morrison 1990; Ofman *et al.* 1991; Chen, Otto & Lee 1997) – cf. also (Einaudi & Rubini 1986; Wang, Lee & Wei 1988; Bettarini *et al.* 2006; Li & Ma 2012) for a

https://doi.org/10.1017/S0022377822001088 Published online by Cambridge University Press

numerical linear study; the stabilising effect of an in-plane magnetic field component orthogonal to the neutral line (see Nishikawa 1982; Somov & Verneta 1988, 1989); the role of equilibrium density gradients, which via the diamagnetic drift frequency gives a time-resonant character to the so-called drift-tearing modes (Coppi 1965; Drake & Lee 1977; Coppi *et al.* 1979). These diamagnetic effects are particularly important in tokamaks, where they are related to the rotation of tearing structures and contribute to the nonlinear or resonant coupling of tearing modes with different mode numbers (see, e.g. Hicks, Carreras & Holmes 1984; Cowley & Hastie 1988; Fitzpatrick *et al.* 1993), but also influence their linear evolution and stability threshold (see, e.g. Mahajan *et al.* 1978, 1979; Migliuolo, Pegoraro & Porcelli 1991; Grasso, Ottaviani & Porcelli 2001; Yu 2010). In tokamaks, also temperature gradients may induce, in the framework of a gyrokinetic description, the onset of the so-called 'micro-tearing' modes (see, e.g. Hazeltine & Ross 1975; Drake & Lee 1977; Gladd *et al.* 1980; Connor, Cowley & Hastie 1990), which cause the formation of microscopic magnetic islands that can affect turbulent transport (see Doerk *et al.* 2011) and foster stochastic fluctuations of the magnetic field, which can in turn affect tearing modes (Carreras, Rosenbluth & Hicks 1981) and the magnetic confinement (see, e.g. Firpo 2015). Also, we recall that the linear tearing mode theory has been extended and adapted so as to study modes simultaneously and interdependently occurring on two (or more) sufficiently close resonant surfaces, i.e. the double- (or multiple-) tearing modes (Furth, Rutherford & Selberg 1973; Pritchett, Lee & Drake 1980; Wang *et al.* 2011); or to include the so-called 'neo-classical effects' related to pressure gradient and toroidal curvature in tokamak plasmas. Although the latter effects are intrinsically nonlinear, they can be self-consistently included in the study of the linear growth of the so-called 'neo-classical tearing' modes (NTMs, in specialised 'jargon'): these are modes developing out of a seed magnetic island (e.g. produced by previous tearing-type instabilities which have saturated and have become stable) and which are driven by the so-called 'boot-strap current' (see, e.g. Hahm 1988; Lütjens & Luciani 2002; Wilson 2012). In addition to the large number of works developed over the years on these subjects, attention has also been recently drawn to the role that a background plasma turbulence can have in driving the growth of NTMs (see, e.g. Muraglia *et al.* 2009, 2011; Agullo *et al.* 2017*a*,*b*; Choi 2021). These latter subjects are somewhat related (see, e.g. Brennan *et al.* 2002) to the further topic of forced magnetic reconnection, which has also been considered in the framework of tearing mode theory, by looking at the way an external forcing affects the stability and growth of the linear modes (see, e.g. Hahm & Kulsrud 1985; Wang & Bhattacharjee 1997; Fitzpatrick 2008). None of these subjects is however of further concern to us; here, in the following, we will focus on the linear problem related to (2.1)–(2.2) only, with respect to which of each of these ingredients would provide further elements of analytical complication that would lead us beyond the purpose of this work.

2.2. *Eigenvalue of the linear problem and reconnection rate in tearing-type modes*

In the literature, the notion of '*reconnection rate*', let us name it as $\mathcal{R}_{rc}$, formally refers to the rate at which the magnetic flux changes over time close to the X-point during a magnetic reconnection event associated with it. In general, we can write

$$\mathcal{R}_{rc} \equiv \frac{1}{\Phi_\Omega(\boldsymbol{B})}\frac{\mathrm{d}\Phi_\Omega(\boldsymbol{B})}{\mathrm{d}t}, \quad \Phi_\Omega(\boldsymbol{B}) \equiv \int_\Omega \boldsymbol{B}\cdot\mathrm{d}\boldsymbol{S}, \tag{2.9}$$

where Ω is the resonant surface, which, in a planar configuration, corresponds to the surface generated by translation of the neutral line along the invariant coordinate (z in the slab coordinate system we have chosen). If we assume the planar current sheet (or

https://doi.org/10.1017/S0022377822001088 Published online by Cambridge University Press

the neutral line) to be static and along the y direction, then $\Omega = \ell_y \ell_z$, where the extension of the length ℓ_y depends on the specific reconnection process considered.

The way this rate is evaluated clearly depends on the reconnection scenario which is considered. A few words on this topic are therefore useful, since the contrasting terminology acquired on this subject by specialised literature dealing with different reconnection scenarios (e.g. steady, Sweet–Parker-like versus tearing-type reconnection) can be sometimes confusing (cf. also Biskamp (2000, p. 54) for a brief discussion as well as Appendix B). This is especially important, since the reconnection rate is related to the rate at which magnetic energy is converted into other forms of plasma energy and therefore to the power released in the form of thermal energy and particle acceleration during a reconnection event. This subject is at the basis of many open questions turning around magnetic reconnection in both laboratory and astrophysical plasmas. These subjects, still debated, concern for example: the model capable of accounting for the short time scale of the sawtooth crash and of other reconnection-related disruptions in tokamaks (see, e.g. Wesson 1986, 2004; Porcelli, Boucher & Rosenbluth 1996; Boozer 2012; Jardin, Krebs & Ferraro 2020); a theoretical model of the fast release of energy during solar flares and coronal mass ejections (see, e.g. Shibata 1998; Cassak & Shay 2012; Aschwanden, Xu & Jing 2014; Aschwanden *et al.* 2016; Janvier 2017; Aschwanden *et al.* 2019; Aschwanden 2020); the mechanism of energy release at the basis of X-rays and γ-ray emissions (gamma-ray bursts) in pulsars, magnetars and nebulae (see, e.g. Lyutikov 2003; Tavani *et al.* 2011; Uzdensky 2011); the processes by which the kinetic and magnetic energy of the photospheric plasma are likely to heat up the expanding solar wind by a factor $\sim 10^6$ over the distance of just a solar radius, supposedly via reconnection in the turbulent coronal plasma (see, e.g. Leamon *et al.* 2000; Matthaeus & Velli 2011); the energy injected in the magnetosphere via solar wind–magnetosphere interactions and released during geomagnetic storms (see, e.g. Lakhina & Tsurutani 2016), and the impact that the ensuing space–weather perturbations may have on terrestrial biosphere and human activity (see National Research Council (2008) and further more specific studies like, e.g. Gopalswamy 2016; Nelson 2016; Eastwood *et al.* 2018; Knipp *et al.* 2018). Regardless of whether the tearing mode theory be actually relevant and capable to explain these phenomena or not, it should be noted that the comparison of theoretical estimates of the reconnection rate with the characteristic time scales directly measured or inferred from experiments or simulations is probably the main criterion presently used to assess the pertinence of tearing-type instabilities or of alternative magnetic reconnection models for these energy releasing processes.

The operational definition by which the reconnected flux can be computed according to (2.9) has been refined over time in different contexts, which also keep account of observational difficulties related to issues encountered in both direct experimental and numerical measurements (see Parker 1957; Petschek 1964; Syrovatskii 1966*a*,*b*; Bratenahl & Yeates 1970; Baum, Bratenahl & White 1971; Parker 1973; Schnack 1978; Park, Monticello & White 1984; Chen *et al.* 1997; Hesse, Forbes & Birn 2005; Comisso & Bhattacharjee 2016; Grasso *et al.* 2020). For the purpose of the present discussion, we here rely on the formal definition: combination of (2.9) with (2.7) via Faraday's law and Kelvin–Stokes theorem of circulation allows us to write

$$\mathcal{R}_{rc} = \frac{1}{\Phi_S(\boldsymbol{B})} \int_\Omega \left(\frac{\partial \boldsymbol{B}}{\partial t} - \boldsymbol{\nabla} \times (\boldsymbol{U} \times \boldsymbol{B}) \right) \cdot \mathrm{d}\boldsymbol{S} = -\frac{c}{\Phi_S(\boldsymbol{B})} \int_\Omega (\boldsymbol{\nabla} \times \boldsymbol{F}_\varepsilon) \cdot \mathrm{d}\boldsymbol{S}, \quad (2.10)$$

where the curl term in the first integral generally accounts for the evolution of the surface over which the magnetic flux is calculated, as it is dragged by the bulk plasma velocity

https://doi.org/10.1017/S0022377822001088 Published online by Cambridge University Press

$\boldsymbol{U}$. If the surface over which the flux is evaluated is static, like it can be chosen in the Sweet–Parker scenario or for non-propagating tearing-like modes, that contribution is null. This is the case in which we are interested, where we consider a non-evolving integration surface along the neutral line, whose extension in the y direction depends on the reconnection scenario considered, as it will be specified below. If, under this assumption, we specify the surviving terms of the first integral of (2.10) for the slab geometry, RMHD variables $\boldsymbol{B} = \boldsymbol{\nabla}\psi \times \boldsymbol{e}_z + b\boldsymbol{e}_z$ of (2.1)–(2.2), we can write $\mathrm{d}S = \mathrm{d}y\,\mathrm{d}z\,\boldsymbol{e}_x$ and therefore

$$\Phi_\Omega(\boldsymbol{B}) = \int_\Omega \boldsymbol{B}\cdot\mathrm{d}\boldsymbol{S} = \int_\Omega B_{x,1}\,\mathrm{d}y\,\mathrm{d}z = \int_{l_z}\mathrm{d}z\int_{l_y}\frac{\partial\psi_1}{\partial y}\,\mathrm{d}y. \tag{2.11}$$

Thus, posing the X-point to lay on the line $x = 0$, we obtain

$$\mathcal{R}_{rc} = \frac{\int_{l_y}\mathrm{d}y\;\partial^2\psi_1(0,y,t)/\partial t\partial y}{\int_{l_y}\mathrm{d}y\;\partial\psi_1(0,y,t)/\partial y}. \tag{2.12}$$

In the case of tearing modes, it is easy to see from the symmetries of the eigenmode solutions in (2.8) that it is appropriate to consider the integration interval in y to not have the X-point in the middle (otherwise the spatial integral would vanish). For a single tearing mode, the interval can be therefore taken to extend from the X-point to the O-point (although each O-point is delimited by two X-points, the periodicity of the configuration makes the numbering of X- and O-points be in a 1:1 correspondence). By construction, the eigenmode of the magnetic stream function has a separable dependence on time and on space of the form $\psi_1(x,y,t) = f(x,y)\mathrm{e}^{\gamma t}$. In reality, although we are here anticipating the formal results, as we will discuss in the next sections, it is easy to determine from the magnetic island shape that the solution is of the form $\psi_1(x,y,t) = g(x)\cos(ky)\mathrm{e}^{\gamma t}$, if $y = 0$ is taken at the O-point – cf. figure 2(*b*). Hence, one immediately obtains (the label *TM* standing for 'tearing mode')

$$\mathcal{R}_{TM}(k) = \gamma(k), \tag{2.13}$$

that is, for a tearing-type instability of wavenumber k, the notions of reconnection rate and of growth rate are equivalent. The quadratic dependence of the magnetic energy on ψ (cf. (A5)) trivially implies that for a single tearing mode, the rate at which magnetic energy $\mathcal{E}_B = \int|\boldsymbol{\nabla}\psi_1|^2\,\mathrm{d}x\,\mathrm{d}y$ is converted into other forms of energy during the linear stage of the instability is $2\mathcal{R}_{TM} = 2\gamma$.

Of course, if several tearing modes are simultaneously unstable, and/or if one or more reconnection instabilities are in their nonlinear stage, the identification $\mathcal{R}_{rc} \leftrightarrow \gamma(k)$ is not correct any longer, even if a dominant mode can be assumed to dominate the reconnection process. In these cases, an evaluation of the *global* reconnection rate in a given volume, more accurate at least from a numerical point of view, can be made by taking

$$\mathcal{R}_{rc} \simeq \frac{1}{2\mathcal{E}_c}\left|\frac{\partial\mathcal{E}_c}{\partial t}\right|, \tag{2.14}$$

where $\mathcal{E}_c$ is a component of the total energy (cf. (A5)) involved in the reconnecting process and the factor $1/2$ accounts for the quadratic relation between the fields and the energy components. Usually, $\mathcal{E}_c$ is the magnetic energy component $\mathcal{E}_B$, which in most reconnection regimes (see, e.g. White 1983, 1986) can be shown to provide the 'reservoir' of energy of the instability, which is 'dissipated' (or, more generally, converted into other forms) during the process. It should be however noted that in some regimes of tearing-like instabilities,

https://doi.org/10.1017/S0022377822001088 Published online by Cambridge University Press

numerically studied by using 'large' values of d_e/L_0 (i.e. $d_e/L_0 \lesssim 1$ but not asymptotically smaller than unity), the role of $\mathcal{E}_B$ has been observed to be played, instead, by the electron kinetic energy $\mathcal{E}_J = \int \mathrm{d}_e^2 |\nabla^2 \psi_1|^2 \,\mathrm{d}x\,\mathrm{d}y$ associated with the equilibrium current sheet (Del Sarto, Califano & Pegoraro 2005; Del Sarto *et al.* 2006). Also, the increase of some kinetic energy component could be used for the estimate of (2.14), if it assumed that the electromagnetic energy released during the reconnection event is dominantly transferred to particle heating and/or acceleration, or to radiation. This is the way by which, for example, the reconnection rate of processes at the basis of solar flares and coronal mass ejections, or of the sawtooth cycle in tokamaks, is indirectly inferred from observational measures.

Some alternative definitions of 'reconnection rate', provided in terms of *local* estimates of quantities, are also frequently used in the literature. These further definitions, briefly outlined and discussed in Appendix B for comparison, are not of concern for the purpose of this work, since they mostly deal with stationary reconnection or provide approximations to the more accurate (2.13), valid in the case of interest to us.

We conclude this section with a note on the notion of 'fast', often used in the literature for models devised in the attempt of modelling the rapid reconnection processes observed in Nature and in experiments, which display growth rates faster – in an asymptotic sense – than those predicted by the early reconnection models (i.e. resistive Sweet–Parker and resistive tearing modes). On the one hand, the notion of 'fast' has changed over the years, both depending on the specific reconnection context (space or laboratory) and on the physical process allowing a relative increase of the reconnection rate (e.g. electron inertia, the inclusion of the Hall-effect in Ohm's law, the accounting for other nonlinear effects, 3-D effects and secondary instabilities – see appendices of Del Sarto & Ottaviani 2017) for a short historical review on these subjects). On the other hand, it is unlikely that a primary spontaneous tearing mode developing on a *static* current sheet overtake values of order unity, when measured with respect to the normalisation time τ_A defined as below ((2.4)–(2.5)) – see Pucci & Velli (2014), Del Sarto *et al.* (2018), and § IX of Betar *et al.* (2020) for more detailed discussions. It is however worth noting that for linear tearing modes, the normalised growth rate evaluated from (2.1)–(2.2) typically becomes of the order of unity or, better, of some decimal fraction of it, when the shear length becomes comparable to the microscopic non-ideal scales of interest: that is, $\gamma\tau_A \sim O(10^{-1}) - O(1)$, when some among d_e, ρ_s or $(S^{-1}/\gamma)^{1/2}$ become of the order of $O(a/10) - O(a)$. However, this also generally means that we are out of the limits of applicability of the boundary layer theory (cf. § 3, next, and note that we leave aside, here, the open problem of discussing the validity of an extended fluid modelling at these kinetic scales): in this case, the analytical estimates of $\gamma(k)$, which we are going to develop below, are not applicable and a numerical computation is instead required. See figure 3 and table 2 of Del Sarto *et al.* (2011) for an example in the collisionless limit.

3. Boundary layer approach for tearing modes: large- and small-Δ' regimes

In this section, we start by describing the general strategy of integration with the boundary layer approach to solve the eigenvalue problem of (2.1)–(2.2). Then, we discuss the ordering and the instability parameter, which defines the unstable spectrum of wavenumbers, and its consequences on the classification of different reconnection regimes in both slab and toroidal geometries. Finally, we close the section by giving a brief review on previous works using the boundary layer integration in the collisionless regime.

There are no exact analytical solutions available for the general eigenvalue problem of (2.1)–(2.2). Approximated analytical solutions can be obtained by using a boundary layer approach as first shown for the purely resistive tearing by Furth *et al.* (1963) in the constant-ψ regime and by Coppi *et al.* (1976), Ara *et al.* (1978) and Basu & Coppi (1981)

https://doi.org/10.1017/S0022377822001088 Published online by Cambridge University Press

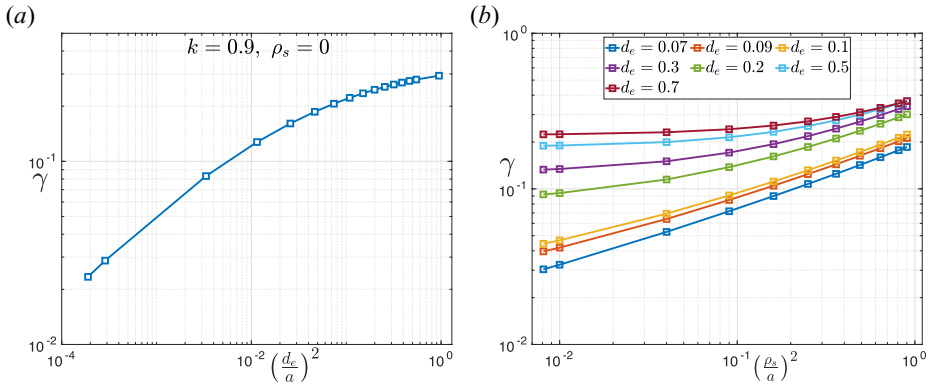

FIGURE 3. Growth rates of collisionless tearing modes numerically computed from (2.1)–(2.2) with the solver of Betar *et al.* (2020), for values of the non-ideal parameters at the limits of (or beyond the) applicability of boundary layer theory, and for a wavelength $ka \sim O(1)$ (likely value for modes on large aspect ratio current sheets having a microscopic thickness – a condition typically met, e.g. in MHD turbulence (see, e.g. Franci *et al.* 2016; Del Sarto & Pegoraro 2017; Franci *et al.* 2022). Note that once γ approaches unity, the effect of the non-ideal parameters on the magnetic equilibrium ψ_0 is not negligible anymore, and (2.1) and (2.2) in the resistive limit (not shown here) should be modified accordingly (cf. Appendix A). (*a*) Case of cold electrons. (*b*) Case of warm electrons, for different values of d_e/a and for values of ρ_s/a approaching one.

in the internal-kink regime. When kinetic-like effects are included, it is instead easier to solve the boundary layer problem if calculations are performed after doing a Fourier transform with respect to the variable x: this facilitates the analytical calculations since it lowers the order of the differential equations in the 'inner region', as it has been first shown by Pegoraro & Schep (1986) and Pegoraro *et al.* (1989).

The boundary layer approach consists in solving the linear problem in distinct overlapping regions. The number of regions depends on the non-ideal parameters that exist in the problem. Moreover, for the boundary layer approach to be applied, it is necessary that the normalised non-ideal parameters (e.g. $\varepsilon = S^{-1}$ or $\varepsilon = (d_e/a)^2$) be much smaller than unity, i.e. $\varepsilon \ll 1$. This makes it possible to perform an asymptotic analysis by expanding quantities in powers of ε, and also grants the scale separation between the boundary layers, since the characteristic width of the innermost layers, where ideal-MHD breaks down, is *a posteriori* found to scale with a multiplication of positive powers of the parameters 'ε' at play. Quantitatively speaking, comparison between theoretical estimates and numerical integration of the boundary layer problem indicates that the condition $\varepsilon \ll 1$ typically means that the microscopic scales (cf. end of § 2.2) related to the non-ideal terms capable of breaking the ideal MHD conservation of the magnetic topology be not larger than a fraction $\sim 10^{-1}$ of the equilibrium shear length a.

For example, for purely resistive or purely inertia-driven tearing modes in RMHD, the linear problem is solved in *two* distinct regions and the solutions are asymptotically matched in an intermediate layer, as shown in figure 4(*a*). In this case, the first region is the 'outer' region in which the plasma is assumed to be at ideal MHD force-balance equilibrium at spatial scales of the order of $L_0 = a$. The second region is the 'inner' one, in which a solution is sought for the differential equations while retaining the non-ideal parameters in the limit $x \ll 1$ (i.e. $x/L_0 \ll 1$ in dimensional coordinates). The characteristic size of the inner region is identified to correspond to the *reconnection layer width* (cf. § 8), whose characteristic thickness we hereafter call δ, with $\delta \to 0$ as the

https://doi.org/10.1017/S0022377822001088 Published online by Cambridge University Press

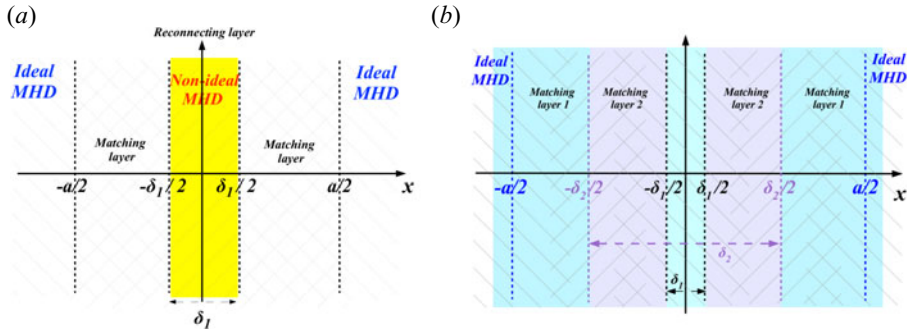

FIGURE 4. (*a*) Sketch of the boundary layer decomposition for the calculation of the tearing eigenmodes with asymptotic matching techniques, when a single boundary layer is sufficient (e.g. case of the resistive tearing first considered by Furth *et al.* 1963). The width δ of the inner boundary layer is here the natural candidate for the width of the 'reconnecting layer', although the latter is not formally defined, i.e. we can assume $\delta = \delta_1$ (an assumption we will support in § 8 with further arguments). (*b*) Sketch of the boundary layer decomposition when two boundary layers are required (e.g. case of the warm-collisionless RMHD). Note that the reconnecting layer width, which we call δ, is, again, *a priori* not defined but, as we will see (§ 8), further arguments can be found to identify it with the innermost layer width, i.e. $\delta = \delta_1$.

non-ideal parameters tend to zero. The inner region is therefore defined by the inequality $x/\delta \lesssim 1$.

Seen from the inner region, the convergence to some point in the outer domain is expressed with the limit $x/\delta \to \infty$ with respect to the 'stretched variable' x/δ. In the matching layer, this limit should match the limit $x/L_0 \to 0$ (or, simply, $x \to 0$ in normalised units) for quantities evaluated in the outer region.

When more than one non-ideal parameter is involved in the problem, applying the boundary layer approach becomes more difficult. This is due to the presence of at least two boundary layers and therefore of two matching regions (cf. figure 4*b*), whose characteristic widths, i.e. the normalisation scales for the asymptotic matching, say δ_2 and δ_1, depend on the spatial scales of the problem in a non-trivial way. Moreover, the notion of 'reconnection layer width', which we keep on naming δ, in this case is not *a priori* related to the width of one of the boundary layers, although, as we will see (§ 8), we can make it correspond to the extension of the innermost layer, δ_1.

Operationally speaking, the integration of tearing mode equations by means of the boundary layer approach, which we will detail in the nextsections, can be split in the following sequence of steps.

(i) *Solving the equations in the ideal MHD limit* provides the solution in the outer layer (the 'outer solution') and allows one to evaluate the instability parameter (the so-called Δ' parameter, see § 3.1), which identifies the range of wavenumbers that are tearing-unstable and allows one to distinguish among different wavelength regimes of reconnection – the constant-ψ or tearing regime, the large-Δ' or internal-kink regime, and the fastest growing mode in a continuum wavelength spectrum of slab tearing modes.

(ii) *Considering the equations in the non-ideal region* by assuming that the inverse spatial gradients are small enough to count the microscopic scales associated with the non-ideal parameters. This also allows some simplifications to the equations,

https://doi.org/10.1017/S0022377822001088 Published online by Cambridge University Press

related to the fact that the nth derivative with respect to x dominates over the nth power of k.

(iii) *Establishing, on heuristic basis, an ordering among terms of the non-ideal equations* depending on the value of the non-ideal microscopic parameters. This allows one to distinguish different boundary layers (cf. figure 4*b*) in which the non-ideal equations are differently approximated. This task becomes more complex as more non-ideal parameters are present, and is subordered to the consistency of the solutions *a posteriori* found after integration in each sub-region (hence, the 'heuristic' nature of the ordering of the terms in the equations).

(iv) *Integrating the non-ideal equations* in each sub-region, by taking the solution in the next-most, outer domain as a boundary condition. For example, with reference to figure 4(*b*), the outer solution in the ideal region provides the boundary condition in the matching layer II for the solution in the sub-domain $|x| \lesssim \delta_2/2$, which in turn provides the boundary condition in the matching layer I for the solution in the region $|x| \lesssim \delta_1/2$.

(v) Finally note that, in any case, constructing the global solution in the whole domain in an explicit form is a not evident task and often it is not possible, since the integral solutions in each non-ideal region may be not obtained in closed form. Nevertheless, *it is possible to obtain a quantitative estimate of the eigenvalues of the linear problem (i.e. the growth rate of the reconnecting mode) from the conditions on the solutions in the non-ideal region*. Similarly, other spatial scales of interest (which, by further arguments, can be *interpreted* as corresponding, e.g. to the reconnecting layer width, δ – cf. § 8) can be quantitatively evaluated.

3.1. *Orderings and instability parameter Δ'*

In the present section, we discuss the different orderings of the operators in the eigenvalue problem, which will allow us to obtain the governing equations in different regions of the domain, and we introduce the notion of an '*instability parameter*'.

In the outer, ideal MHD region, the ordering of different operators in (2.3) is

$$\gamma \sim 0, \quad \mathcal{L} \sim 1, \quad \mathcal{F} \simeq 1, \quad \mathcal{A} \sim 1, \quad \mathcal{B} = \mathcal{C} = \mathrm{i}k\psi_0' \sim 1. \tag{3.1}$$

Solving the equations resulting from this ordering allows us to obtain the solution in the outer region, ψ_{out}.

At the neutral line, the equilibrium magnetic field (shear field) vanishes and changes its sign when reconnection occurs. Therefore, this field should be an odd function in the vicinity of $x = 0$. Hence, ψ_0, whose x-derivative represents the shear field $B_y^0(x)$, is an even function. Moreover, close to the neutral line, $\psi_0(x)$ is continuous at least up to its first derivative. We then expand it as a Taylor series which, for symmetric tearing modes in slab geometry, has non-zero coefficients only for even powers of x,

$$\psi_0(x)|_{x\to 0} \simeq C_0 + C_2 x^2 + C_4 x^4 + \cdots . \tag{3.2}$$

Therefore, we can relate δ to the intensity of the equilibrium magnetic field and to the gradient of the associated current density inside of the inner layer, when looked at from the matching (or from the outer) region. So we write

$$\psi_0'\big|_{x\to 0} \sim \psi_0'''\big|_{x\to 0} \sim x|_{\mathrm{inner}} \simeq \delta. \tag{3.3}$$

Before going further, we note that condition (3.2) is too restrictive, in general, for slab tearing modes on magnetic equilibria that are not symmetric with respect to the shear

https://doi.org/10.1017/S0022377822001088 Published online by Cambridge University Press

coordinate. An example is provided by tearing modes in a cylinder, for which $C_1 = 0$ but $C_3 \neq 0$ (Bertin 1982; Militello *et al.* 2004, 2011). It must be also noted that the inner layer width, δ, has not yet been 'defined' here. As a quantity, it only explicitly appears in boundary layer calculations as a normalisation scale for the differential equations in the non-ideal region, whose boundaries are defined by the condition $|x|/\delta \sim O(1)$. To date, indeed, no general criterion exists to quantitatively define δ, whose estimation is made, when possible, thanks to further hypothesis and heuristic ansatz (e.g. comparison with the characteristic scales of the problem). In the present section, we therefore assume δ to be simply defined as the innermost layer width (in § 8, we will propose a quantitative general definition of δ, whose appropriateness in the different regimes we will prove numerically by comparing it with theoretical estimates).

Unless a large aspect ratio current sheet is considered, for which an almost continuous spectrum of wavenumbers can be destabilised that also allows k to be large, the further ordering $\partial_x \gg k$ is assumed for $x \ll 1$. This implies the following orderings inside the non-ideal region:

$$\mathcal{L} \simeq \partial_x^2, \quad \mathcal{F} = 1 - d_e^2\mathcal{L}, \quad \mathcal{A} = -k\delta(1-\mathcal{L}) \sim -k\delta\mathcal{L}, \quad \mathcal{B} = ik\delta\left[(1-d_e^2) - \rho_s^2\mathcal{L}\right]. \tag{3.4}$$

The corresponding equations are solved for the 'inner' functions $\psi_1 = \psi_{\rm in}$ and $\varphi_1 = \varphi_{\rm in}$.

The matching with the outer solution is assumed as a boundary condition to be imposed across an intermediate matching layer, where one must compare the asymptotic series $\sum a_n^{(\rm in)}(x/\delta)^n$ for $(x/\delta) \gg 1$ and $\sum_n a_n^{(\rm out)} x^n$ for $x \ll 1$ (we recall that all lengths appear here as normalised to $L_0 = a$), respectively representing the inner and outer solutions – see Bender & Orszag (1978, § 9). This translates in the condition

$$\lim_{x/\delta\to\pm\infty} a_m^{(\rm in)}\,(x/\delta)^m \simeq \lim_{x\to\pm 0} a_m^{(\rm out)}\,x^m \qquad \begin{array}{l}(\text{for } m \text{ that corresponds to}\\ \text{the leading term of the series}).\end{array} \tag{3.5}$$

Condition (3.5) is usually expressed in a looser notation as

$$\lim_{x/\delta\to\pm\infty} \psi_{\rm in}(x/\delta) = \lim_{x\to\pm 0} \psi_{\rm out}(x). \tag{3.6}$$

Although (3.6) formally compares the two numerical values of the limits of the eigenfunctions solving the differential equations, in the following, we will mean this expression as a shortcut writing of (3.5), as it is usually done in tearing mode analysis.

The dependence on the outer solution becomes then explicit through the relation

$$\int_{-\infty}^{+\infty} \psi_{\rm in}''\,{\rm d}\,(x/\delta) = \psi_{\rm out}(0)\Delta', \tag{3.7}$$

which introduces the instability parameter (Furth *et al.* 1963) related to the discontinuity which is met in the first derivative of $\psi_{\rm out}$ as $x \to \pm 0$,

$$\Delta'(k;\,\psi_0) \equiv \lim_{\epsilon\to 0} \frac{\psi'_{\rm out}(\epsilon) - \psi'_{\rm out}(-\epsilon)}{\psi_{\rm out}(0)}. \tag{3.8}$$

In the expression above, $\epsilon > 0$. Definition (3.8) enters in (3.6) as

$$\int_{-\infty}^{+\infty} \psi_{\rm in}''\,{\rm d}(x/\delta) = \psi'_{\rm in}(+\infty) - \psi'_{\rm in}(-\infty) = \psi'_{\rm out}(+0) - \psi'_{\rm out}(-0) = \psi_{\rm out}(0)\Delta', \tag{3.9}$$

where we have used the key fact that the outer solution $\psi_{\rm out}$ is continuous as $x/L_0 \to 0$ while this is generally not the case for its derivative $\psi'_{\rm out}$ (as it is found *a posteriori* when solving the inner equation for tearing-type modes).

https://doi.org/10.1017/S0022377822001088 Published online by Cambridge University Press

The linear problem in the inner region is closed by combining (3.7) with the relation that can be established between $\psi_{\rm in}$ and $\varphi_{\rm in}$. According to the inner region ordering, (2.2) becomes $\gamma\varphi_{\rm in}'' = {\rm i}kx\psi_{\rm in}''$. Therefore,

$$\int_{-\infty}^{+\infty} \psi_{\rm in}''\, {\rm d}\,(x/\delta) = -({\rm i}\gamma/k) \int_{-\infty}^{+\infty} \frac{\varphi_{\rm in}''}{x/\delta}\, {\rm d}\,(x/\delta)\,. \tag{3.10}$$

It must be however noted that when more than one non-ideal parameter is involved and/or when the microscopic scale of variation of ψ and φ differ (this happens, for example, in 2-D electron-MHD (Bulanov *et al.* 1992), where the fluid stream function is related to the fluctuation b of the B_z magnetic component and an equation for b replaces that for φ), the matching procedure above requires more care, as we are going to see in § 7. In these cases, more than two boundary layers must be considered and the corresponding solutions must be matched – see Pegoraro & Schep (1986), Porcelli (1991) and Bulanov *et al.* (1992). These are the cases for which heuristic estimations are difficult, since a different width must be associated with each boundary layer (e.g. δ_2 and δ_1, with $\delta_1 < \delta_2$). In this kind of analysis, the width of each layer appears as the characteristic normalisation scale, say $l_{\rm norm}$, with respect to which to consider the limits $x/l_{\rm norm} \ll 1$ and $x/l_{\rm norm} \gg 1$ while performing the asymptotic matching in the intermediate region between the layers. In this sense, the limit $\varepsilon \to 0$ of (3.8) also must be reinterpreted, which we should read as $\varepsilon = |x|/l_{\rm norm}$ for $l_{\rm norm} = L_0 = a$. At the same time, also the relations between Δ' and the spatial gradients of $\varphi_{\rm in}$ expressed by combinations of (3.7) and (3.10) become non-trivial, as we will discuss in § 10.

3.2. *Small- and large-Δ' limits in slab geometry and in tokamaks*

For each eigenvalue problem in slab geometry, the numerical value of Δ' depends both on the choice of the magnetic equilibrium profile and on the value of k. A classification of regimes of slab tearing modes can be generally done depending on the numerical comparison of $(\Delta')^{-1}$ and of the innermost layer width, δ_1, regardless of the number of boundary layers involved. For simplicity of notation, we generically use for them the symbol δ, although it is only later (§ 8) that we will provide some argument to identify the 'reconnecting layer width'. In particular, one speaks of a *small-Δ'* limit for $\Delta'\delta \ll 1$ and of a *large-Δ'* limit for $\Delta'\delta \gg 1$.

Once the scaling of δ on the non-ideal parameters involved is known, the large- and small-Δ' limits in slab geometry can be made to respectively correspond to the small and large wavelength limits of the tearing dispersion relation, which for each reconnection regime can be defined with respect to the comparison of $kL_0 = ka$ with powers of the non-ideal parameters involved (as it has been discussed for example by Bulanov (2017) for the purely resistive case).

In particular, since Δ' defined through (3.7)–(3.8) is, when analytically obtained (cf. example below – § 4.1), a continuous function of the variable k, the large wavelength limit can be postulated to correspond to a power-law dependence of the kind

$$\lim_{ka\to 0} \Delta'(ka) = (ka)^{-p}, \quad p > 0, \tag{3.11}$$

where p depends on the initial equilibrium profile (Del Sarto *et al.* 2016; Pucci *et al.* 2018; Betar *et al.* 2020). While the limit above corresponds to $\Delta' \to \infty$, the marginal stability condition $a\Delta'(ka) \to 1$ is approached as $ka \to 1$.

A fundamental difference between large- and small-Δ' tearing-type modes in tokamak devices and their corresponding small- and large-k limits in slab geometry must be

https://doi.org/10.1017/S0022377822001088 Published online by Cambridge University Press

however remembered, when the results of the two models are compared: in tokamak devices, the wave vector is *fixed* by the resonant surface on which reconnection occurs, and the large- or small-Δ' condition is therefore determined by the specific shape of the unstable magnetic profile (sometimes in turn determined by some ideal instability, which has previously occurred and which has modified the otherwise stable magnetic configuration). In slab Cartesian geometry, instead, the transition between the small- and large-Δ' limit occurs by moving along the k interval for a *fixed*, tearing-unstable magnetic profile, and depends on the aspect ratio of the associated current sheet (see figure 5).

We remark indeed that the distinction between small- and large-Δ' limits has been historically introduced to characterise, in terms of the instability parameter Δ' defined by Furth *et al.* (1963), two different types of unstable modes observed in tokamaks. In tokamak physics, for positive values of Δ', a distinction is made between the *tearing mode* or *constant-ψ mode*, first studied in the cylindrical geometry approximation by Furth *et al.* (1963) (and which formally corresponds to $\Delta'\delta \ll 1$) and the *internal kink mode* or $m = n = 1$ *non-ideal kink mode*, first identified in cylindrical geometry by Coppi *et al.* (1976) (and which formally has $\Delta' = \infty$) (we recall indeed that, even if $\Delta' < 0$, ideal instabilities (i.e. the 'ideal kink mode') can also occur in a tokamak, depending on the value of the safety factor q – cf. Wesson (1990), § 6). In a cylindrical tokamak approximation, these two modes generally occur on different magnetic surfaces and for specific values of the wavenumbers, and also display different relations between the eigenfunctions φ_1 and ψ_1: differently from the tearing mode, for which the fluid displacement $\xi \equiv k^2\varphi_1/\gamma$ is proportional to $\sim \psi_1/x$, the internal kink mode corresponds to a rigid displacement $\xi \sim const.$ of the plasma inside the inner region; more specifically, for the internal kink mode, $\xi \sim const.$ in the whole subdomain $r \leq r_s$, where r_s is the radius of the resonant surface, whereas $\xi = 0$ for $r > r_s$ (see, e.g. Porcelli 1987; Del Sarto & Ottaviani 2017 for a more detailed discussion). It has been however shown by Ara *et al.* (1978) that, thanks to the formal analogy between the two corresponding eigenvalue problems in cylindrical and Cartesian geometry, the transition between the two types of modes can be modelled in a slab geometry configuration by varying the value of the wavenumber for a fixed magnetic equilibrium and for fixed values of the non-ideal parameters. This corresponds to a transition between the small- and the large-Δ' limits. In this context, both the tearing (constant-ψ) mode and the internal-kink mode of tokamak physics can be considered as examples of tearing-type modes when modelled in slab, Cartesian geometry. In this case, a larger 'free energy' can be associated with tearing-type modes in the large-Δ' limit. This is the approach we take here.

Another fundamental difference between tearing and internal kink modes in tokamaks on the one side, and tearing-type modes in slab geometry on the other side, is the fact that in slab geometry, it makes sense to identify a further wavenumber 'regime' that is characterised by the condition $\Delta'\delta \sim 1$ (see Loureiro, Schekochihin & Cowley 2007; Bhattacharjee *et al.* 2009; Del Sarto *et al.* 2016; Betar *et al.* 2020) at the varying of the non-ideal parameters involved. This wavelength limit, which is met thanks to the possibility to perform a 'continuous' transition from $\Delta'\delta \ll 1$ to $\Delta'\delta \gg 1$, corresponds to the *fastest growing mode* that can be destabilised in a periodic current sheet when a continuum spectrum of wavenumbers is admitted (see Furth *et al.* 1963, appendix D, and also Biskamp 1982). Its scaling is exemplified in figure 6 for the case of purely resistive tearing modes (i.e. $d_e = 0$, $\rho_s = \nu = 0$ in (2.1)–(2.2)) destabilised on an equilibrium profile $\psi_0 = \cos(x/a)$, whose $\Delta'(k)$ formula has been discussed by Ottaviani & Porcelli (1993, 1995) and for which the scaling $\gamma_M \sim S^{-1/2}$ can be deduced (dashed line in the figure).

https://doi.org/10.1017/S0022377822001088 Published online by Cambridge University Press

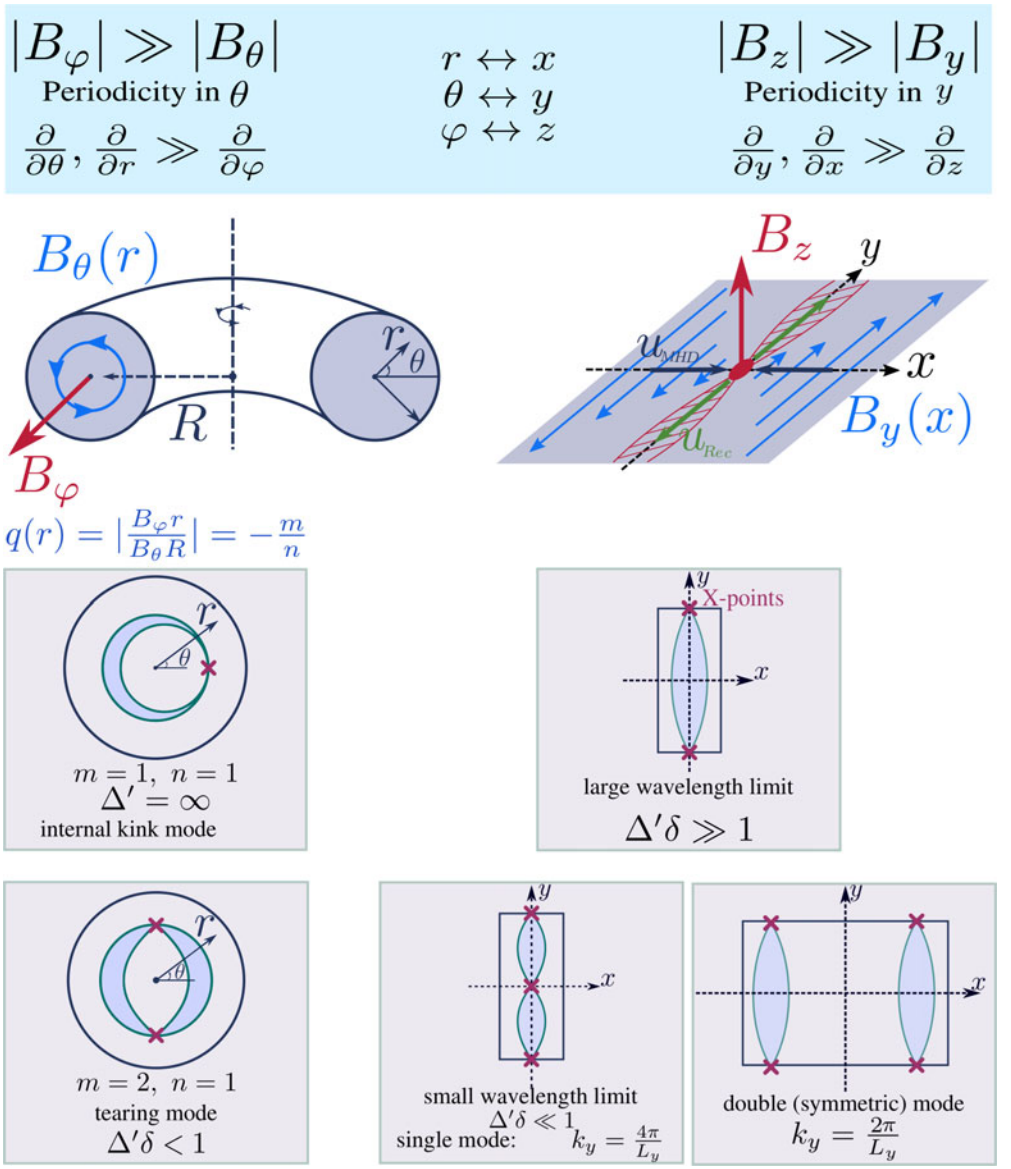

FIGURE 5. Scheme of the correspondence between linear reconnecting instabilities in the RMHD slab geometry limit and in the RMHD 'cylindrical tokamak' approximation, which is compatible with the strong guide field assumption (Strauss 1976). At the bottom of the figure, we highlight the fact that the slab geometry easily allows modelling both of tearing modes of different wavenumber (centre frame) and of the double tearing mode, i.e. the tearing-like instability simultaneously occurring on two sufficiently close resonant surfaces (Furth *et al.* 1973), of which we have shown here only the symmetric case (rightmost frame). Note however that we have considered here the 'cylindrical tokamak', or 'large aspect ratio tokamak' approximation, in the strict limit of $\partial/\partial\varphi \to 0$, which maps into the $\partial/\partial z \to 0$ assumption that we consider in this article. In reality, the RMHD modelling also allows for inclusion of the neglected derivatives with respect to the axis-symmetric coordinate ordered as $\partial/\partial\varphi \sim \partial/\partial z \sim \varepsilon_B$, in terms of the ratio ε_B between the in-plane and the guide magnetic field components at equilibrium (cf. (A11) and discussion in the last paragraph of Appendix A).

https://doi.org/10.1017/S0022377822001088 Published online by Cambridge University Press

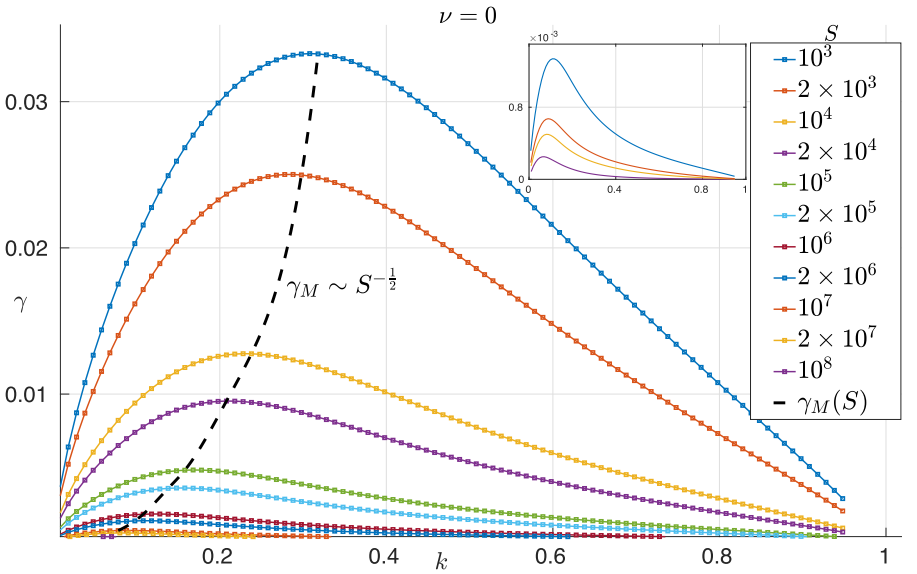

FIGURE 6. Dispersion relation of the purely resistive tearing as a function of ka (dots correspond to numerically computed values), evaluated for the equilibrium $\psi_0 = \cos(x/a)$. The smaller box is a 'zoom' of the plot for low values of γ, which correspond to the range of smaller values of S^{-1} indicated in the caption. The dashed line corresponds to the fastest mode scaling, which for $\psi_0 = \cos(x/a)$ is $\gamma_M \sim S^{-1/2}$. This can be obtained by using in (24) of Del Sarto *et al.* (2016) the value $p = 2$, which can be deduced from the $ka \ll 1$ limit of the corresponding $\Delta'(ka)$ formula (see Ottaviani & Porcelli 1993 or (8) of Ottaviani & Porcelli 1995). An 8th-order accurate scheme has been used here for integration on a uniform grid by using the solver discussed by Betar *et al.* (2020).

When tearing modes are destabilised in a large aspect ratio, *periodic* current sheet, so that also the $\Delta'\delta \sim 1$ modes are excited, several magnetic islands emerge and mutually interact during the nonlinear evolution, e.g. via the coalescence instability (cf. § 2.1), by moving along the neutral line. This dynamics is due to the superposition of several unstable modes with different wavenumbers and growth rates, among which the fastest mode is obviously the dominant one. In general, an aspect ratio L/a of the order of $\sim$20 is sufficient to grant the instability of a wavenumber sufficiently close to the fastest growing mode Velli & Hood (1989) – see also figure 1 of Betar *et al.* (2020). In this scenario, the 'soliton-like' behaviour of magnetic islands, noted already by Biskamp (1982) in his early simulations, has earned them the name of 'plasmoids' (see, e.g. Biskamp & Welter 1989; Biskamp 1996; Shibata & Tanuma 2001; Loureiro *et al.* 2007; Bhattacharjee *et al.* 2009), by analogy with the similarly behaving 'plasma blobs', also termed 'plasmoids', that have been identified and referenced in astrophysical plasma literature since the end of the sixties (Cowling 1967). Plasmoid structures displaying 'soliton-like' features have been observed in space plasmas, in particular, in magnetotail reconnection processes (see, e.g. early works such as those by Hones (1979) and Birn & Hones (1981) or later works such as Hautz & Scholer (1987), Scholer (1987) and also Lin, Cranmer & Farrugia (2008), for a review of the usage of the term plasmoid in this context) and – although in a different geometrical setting – they have been also observed in connection to coronal mass ejections, arguably induced by reconnection processes in the solar corona (see, e.g. early works such as Pneuman 1983; Gosling & McComas 1987). In this sense, in the recent literature, the term

https://doi.org/10.1017/S0022377822001088 Published online by Cambridge University Press

'plasmoid regime' of reconnection (Uzdensky, Loureiro & Schekochihin 2010; Huang & Bhattacharjee 2010; Comisso *et al.* 2018; Zhou *et al.* 2021) is typically used to identify both tearing reconnection in the $\Delta'\delta \sim 1$ wavelength limit (cf. the early numerical study by Biskamp (1986) on the instability of a Sweet–Parker current sheet to tearing modes) and the generation of magnetic islands in current sheets developed as a consequence of a turbulent motion. Here, the formation of 'plasmoids' is observed, either numerically (see Biskamp & Welter 1989; Biskamp & Bremer 1994; Wei *et al.* 2000; Servidio *et al.* 2009, 2011; Wan *et al.* 2013; Franci *et al.* 2017 and several more recent works) or by experimental measurements (see, e.g. Nishizuka *et al.* 2015; Kumar *et al.* 2019; Yan *et al.* 2022). We recall in this regard that also the term '*plasmoid instability*' has been used in recent literature, with reference to the tearing instability associated with the fastest growing mode, which is destabilised on a Sweet–Parker current sheet of length L, and for which a scaling $\gamma_M \sim S_L^{1/4}$ is obtained (Tajima & Shibata 1997; Loureiro *et al.* 2007; Bhattacharjee *et al.* 2009). The diverging scaling with respect to a vanishing non-ideal parameter – otherwise impossible for a spontaneous reconnecting instability – is here due to the fact that the fastest growing mode develops in this case as a 'secondary' reconnection process to a primary steady reconnection scenario (cf. figure 2): for $S_L^{-1} = 0$, the Sweet–Parker reconnection does not occur, by thus forbidding the onset of the tearing modes. Due to the violently unstable nature of the tearing mode developing in the Sweet–Parker scenario, the possibility to measure, in Nature, a steady, Sweet–Parker-like reconnecting current sheet has been first questioned and discussed by Pucci & Velli (2014).

Interpreting the magnetic islands observed in current sheets developed by turbulence as due to tearing mode instabilities is an hypothesis which is grounded on the assumption that a standard Fourier representation can be used in a Wentzel–Kramers–Brillouin (WKB)-sense also for reconnecting modes in a non-periodic, large aspect ratio current sheet. In this case, the fastest growing mode can be assumed to be, in an asymptotic sense, the dominant reconnecting instability. Although a proof of the correctness of this assumption for finite length current sheets has not been provided yet, this kind of approach has attracted since the beginning much attention in the context of both space plasmas (see, e.g. Cross & van Hoven 1971; Van Hoven & Cross 1971) and solar physics (see, e.g. Priest 1976; Velli & Hood 1989), and has been more recently been considered for applications to secondary instabilities to primary reconnection processes (see, e.g. Tajima & Shibata 1997; Shibata & Tanuma 2001; Tanuma *et al.* 2001; Loureiro *et al.* 2005; Daughton & Scudder 2006; Drake *et al.* 2006; Loureiro *et al.* 2007; Bhattacharjee *et al.* 2009; Landi *et al.* 2015; Tenerani *et al.* 2015; Del Sarto *et al.* 2016; Del Sarto & Ottaviani 2017; Papini, Landi & Del Zanna 2019*b*; Singh *et al.* 2019) and to reconnection in turbulence (see, e.g. Pucci & Velli 2014; Loureiro & Uzdensky 2016; Tenerani *et al.* 2016; Comisso *et al.* 2018; Papini *et al.* 2019*a*; Betar *et al.* 2020; Kowal *et al.* 2020; Pucci *et al.* 2020; Schekochihin 2020; Tenerani & Velli 2020; Franci *et al.* 2022) in the context of the so-called 'turbulent (or turbulence-mediated or turbulence-driven) reconnection' scenario (Matthaeus & Lamkin 1986; Strauss 1988; Loureiro *et al.* 2009; Matthaeus & Velli 2011; Schekochihin 2020) – not to be confused with the study of 'turbulent-driven magnetic island' in tokamaks (cf. end of § 2.1). This topic is not of concern here, where we consider strictly periodic current sheets only. We therefore direct the interested reader to the aforementioned references. A survey of the scalings of the fastest growing mode in different reconnection regimes (among which the collisionless regimes we consider in the following) for periodic current sheets can be found in (Betar *et al.* 2020).

In the remainder of the article, we just focus on the formal solution of the eigenvalue problems in a slab current sheet in the $\Delta'\delta \ll 1$ and $\Delta'\delta \gg 1$ limits. In this regard, we note that, in a few cases, a closed form of the integral (3.7) has been provided: in resistive

https://doi.org/10.1017/S0022377822001088 Published online by Cambridge University Press

and collisionless regimes, formulae involving integration in the Fourier space have been provided by Pegoraro & Schep (1986), Pegoraro *et al.* (1989), Schep *et al.* (1994), Basu & Coppi (1981) and Porcelli (1991). These calculations provide the available analytical formulae for the growth rates in the 'internal-kink' and 'constant-ψ' RMHD, collisionless regimes.

Table 1 summarises the known results of the boundary layer analysis for the regimes of reconnection of interest in this article. The general dispersion relation for RMHD tearing modes, from which the large- and small-Δ' limits can be obtained, has been written as in Del Sarto & Ottaviani (2017, appendix C) in terms of a characteristic scale length δ_L that coincides with the relevant layer width δ in the large- and small-Δ' regimes. In §§ 5–7, we will detail the analytical calculations that allow the relevant limits of these dispersion relations to be recovered.

Finally, we draw attention to the fact that the definition (3.8) in a slab geometry changes meaning as soon as the condition $\Delta'\delta \gtrsim 1$ is achieved, since application of (3.11) for $ka \ll 1$ and $\Delta'\delta \sim 1$ formally implies a dependence of k on δ. In general, indeed, $(\Delta')^{-1}$ *becomes a microscopic scale* as soon as $\Delta' L_0 \gg 1$, and for $\Delta'\delta \gtrsim 1$, the condition $(\Delta'(k))^{-1} \ll \delta$ is satisfied by a range of wavenumbers that depend on the non-ideal parameters which define δ.

3.3. *Boundary layer integration of collisionless tearing in the previous literature*

In the following, we will discuss the method that can be used to find the analytical solution of the boundary layer problem associated with the scalings of table 1.

Differently from Pegoraro & Schep (1986) and Porcelli (1991), who tackled the boundary layer calculations in the Fourier space, we are going to address the integration in the coordinate space: although a little more cumbersome, if one's interest is limited to obtaining the eigenvalue scaling alone, the analysis performed in the coordinate space allows a more intuitive understanding of the physics of the problem. Moreover, it spares one from the sometimes non-trivial task of reversing the Fourier transform so as to obtain the eigensolutions in the coordinate space. To the best of our knowledge, these kinds of calculations in the coordinate space for the warm-electron regime ($\rho_s \gtrsim d_e$) have never been reported in the literature, before.

Only in the work by Zocco & Schekochihin (2011) have some details of the analysis for the double boundary layer integration in the presence of two matching layers been discussed in the coordinate space (see appendix B therein). However, in that work, a different analytical approach has been taken for the integration of a different analytical reduced-MHD model including ion-FLR effects in the warm-collisionless regime. In particular, starting from gyrokinetic equations, these authors derived a reduced model consisting of three equations corresponding: to the scalar potential related to the $\boldsymbol{E}\times\boldsymbol{B}$ drift velocity (φ); to the parallel component of the vector potential ($A_\parallel = -\psi$); and to the 'reduced' electron distribution function (g_e, therein), which accounts for the moments of the electron distribution function, except for the density and the mean parallel velocity. The equation describing the evolution of g_e is there coupled to the other two equations via the perturbation of the parallel electron temperature ($\delta T_{e,\parallel}$). In the linear limit, the latter can be written in terms of φ: this allowed the authors to obtain the customary system of two slab-geometry tearing equations for φ and ψ, although modified with respect to (2.1)–(2.2) we consider here, because of the contribution of the gyrokinetic ion operator that appears in the vorticity equation after integration of the ion gyrokinetic equation (Pegoraro & Schep 1981); this contribution clearly vanishes in the limit of null ion temperature in which we are interested. In this way, Zocco and Schekochihin looked for asymptotic analytical solutions of the boundary layer problem in the coordinate space by identifying two distinct

https://doi.org/10.1017/S0022377822001088 Published online by Cambridge University Press

RMHD orderings	'General' dispersion relation $\left(\text{for } Q=\frac{\gamma}{kd_e},\quad \delta_L=\frac{\gamma}{kd_e}Q^{1/2}d_e\right)$	$\Delta'\delta\gg 1$		$\Delta'\delta\ll 1$	
		δ_{LD}	γ_{LD}	δ_{SD}	γ_{SD}
$d_e\gg\rho_s$	$\Delta'\delta_L=-\frac{\pi}{8}Q\frac{\Gamma[(Q-1)/4]}{\Gamma[(Q+5)/4]}$	d_e	kd_e	$\Delta' d_e^2$	$(\Delta')^2kd_e^3$
$S^{-1}>\rho_s^{1/2}\gamma^{1/4}$	Same as above for $d_e\to(S\gamma)^{-1/2}$	$k^{-4/7}\times$ $\rho_s^{-5/7}S^{-4/7}$	$k^{6/7}\times$ $\rho_s^{4/7}S^{-1/7}$	$k^{-2/3}\Delta'^{1/3}$ $\times(\rho_sS)^{-2/3}$	$k^{2/3}\Delta'^{2/3}$ $\times\rho_s^{2/3}S^{-1/3}$
$\rho_s>d_e\neq 0$	$\Delta'\delta_L=\pi\frac{\delta_L^2}{d_e\rho_s}\left(\frac{1}{1-\frac{\pi}{2}\frac{\delta_L^3}{d_e\rho_s^2}Q^3}\right)$	$\rho_s^{-1/3}d_e^{4/3}$	$kd_e^{1/3}\rho_s^{2/3}$	$\Delta' d_e^2$	$\Delta' kd_e\rho_s$
$\rho_s^{1/2}\gamma^{1/4}\gg S^{-1}$	Same as above for for $d_e\to(S\gamma)^{-1/2}$	$k^{-1/3}S^{-1/3}$	$k^{2/3}S^{-1/3}$	$\Delta'^{1/5}\times$ $(kS^{-2/5})$	$\Delta'^{4/5}\times$ $k^{2/5}S^{-3/5}$

TABLE 1. Known scalings available in the previous literature as obtained from a boundary layer analysis in the collisionless and resistive regimes. The general dispersion relation of Porcelli (1991) and Ottaviani & Porcelli (1995) for $d_e^2\gg\rho_s^2$ and that of Porcelli (1991) and Comisso *et al.* (2013) for $\rho_s>d_e\neq 0$ are reported. In both cases, we have adopted the notation used in Del Sarto & Ottaviani (2017, appendix C), from which the small and large wavelength limits can be obtained once $\delta_L\to\delta$ is assumed and some estimation is made for $\delta=\delta_{LD}$ or $\delta=\delta_{SD}$. The general dispersion relation valid in all wavelength limits of the cold-electron resistive regimes (Ara *et al.* 1978) and of the warm-electron resistive regimes (Pegoraro & Schep 1986) is not reported explicitly but it can be obtained from the collisionless cases previous substitution $d_e\to(S\gamma)^{-1/2}$. Note that, although available since the early solutions of the boundary layer calculations, the scalings of δ_{LD} and of δ_{SD} we have reported here in the different regimes have not been always pointed out in the related, reference works. These scalings correspond indeed to the characteristic width of the innermost boundary layer (i.e. δ_1) in each reconnection regime, but the identification of the latter as the reconnecting layer width requires indeed further hypotheses which are discussed in § 8.

layers: the electron and the ion regions whose widths are defined by the reconnection layer width δ and by the ion-sound Larmor radius (ρ_s), respectively. However, differently from the approach we are going to develop below, in which we will look for a direct integration of the asymptotic solutions in the warm-collisionless regime, these authors solved the linear equations in the two asymptotic regions for the warm-collisionless regime by using perturbation methods (Zakharov & Rogers 1992). By matching the asymptotic solutions, they then recovered the scaling laws first evaluated in the Fourier space (Porcelli 1991).

In the remainder of the article, we will treat both the collisionless and resistive limits in a unified way, by separately considering the warm ($\rho_s \gtrsim d_e$) and cold ($d_e \gg \rho_s$) regimes. Then, we will specify the results of the dispersion relation in each reconnection regime. We will thus reobtain the resistive scaling laws first computed by Furth *et al.* (1963) in the cold-electron regime and by Pegoraro & Schep (1986) in the warm-electron regime, and the collisionless scaling laws first evaluated by Coppi (1964*c*,*a*) in the cold-electron limit and by Porcelli (1991) in the warm one.

In Appendix C, we make a brief review of previous works which have approached boundary layer calculations in the Fourier space (included are some more recent works which explicitly made a comparison between eigenmode solutions in the real and in the Fourier space – Connor *et al.* 2012*b*), and we compare some key points of that procedure with the integration procedure that we follow in this work.

4. Boundary layer solution in the outer ideal region

We now turn our attention to solve the linearised equations in the ideal MHD region.

In the outer region and sufficiently far from the reconnection layer, a steady force balance condition in ideal MHD can be assumed. Therefore, the terms weighted by the non-ideal parameters can be neglected. In this case, using $\psi_1 = \psi_{\rm out}$, $\varphi_1 = \varphi_{\rm out}$, (2.1)–(2.2) become

$$\varphi_{\rm out} = -\frac{{\rm i}\gamma}{k\psi_0'}\psi_{\rm out}, \tag{4.1}$$

$$\psi_{\rm out}'' = \left(k^2 + \frac{\psi_0'''}{\psi_0'}\right)\psi_{\rm out}. \tag{4.2}$$

Equation (4.1) says that ψ_1 and φ_1 have opposite spatial parity and are de-phased by $\pi/2$, i.e. $\psi_1 \sim \cos(ky)$ versus $\varphi_1 \sim \sin(ky)$ if $y = 0$ is assumed at an O-point.

It is also evident that solving (4.2) gives the outer solution ($\psi_1 = \psi_{\rm out}$) which is unequivocally determined by the equilibrium profile ψ_0 and by k. Using (4.1), one can so obtain also the eigenmodes $\varphi_{\rm out}$. The number of inner regions depends instead on the number of non-ideal parameters involved in the problem.

A class of magnetic equilibria of particular interest is provided by those fulfilling the condition $\lim_{|x|\to\infty}(\psi_0'''/\psi_0') = $ constant, for which a quite general integration procedure can be devised, as we are going to discuss in the specific example below.

4.1. *A specific example of evaluation of* $\Delta'(\psi_0; k)$

Having in mind the numerical results to be presented in the next sections, let us solve the outer equations for the equilibrium profile

$$\psi_0'(x) = \frac{\tanh(x)}{\cosh^2(x)}, \tag{4.3}$$

which is the one used by Betar *et al.* (2020) to obtain the scalings to which we will make comparison. This profile was first proposed by Porcelli *et al.* (2002). Substituting

https://doi.org/10.1017/S0022377822001088 Published online by Cambridge University Press

the previous relation into (4.2), one finds

$$\psi''_{\rm out} - \left(\alpha^2 - \frac{12}{\cosh^2(x)}\right)\psi_{\rm out} = 0, \tag{4.4}$$

where $\alpha^2 = k^2 + 4$ and $\psi_0'''/\psi_0' = 4 - 12/\cosh^2(x)$. Grasso first evaluated the corresponding Δ', reported by Porcelli *et al.* (2002), by looking for a polynomial solution expressed in powers of $\tanh(x)$ (D. Grasso, private communication 2017). Here, we formally revise the problem, and we reduce (4.4) to a Legendre-type equation that can be shown to be valid for different kinds of equilibria, which we will discuss elsewhere.

First, we notice that $\lim_{x\to\infty}\cosh^{-2}(x) = 0$. This represents a main requirement if one seeks to apply periodic boundary conditions on the problem by considering ψ_0 as a periodic function in x with spatial period of infinite extension. Therefore, far enough from the neutral line where the reconnection event takes place, the hyperbolic term in (4.4) can be neglected and (4.4) becomes

$$\psi''_f - \alpha^2\psi_f = 0, \tag{4.5}$$

whose solution is

$$\psi_f(x) = Ae^{-\alpha x}, \tag{4.6}$$

with A an integration constant. One then expects the solution of (4.4) to take the form

$$\psi_{\rm out}(x) = \psi_f(x)f(x) = Ae^{-\alpha x}f(x). \tag{4.7}$$

Substituting the previous equation in (4.4), one obtains

$$f'' - 2\alpha f' + \frac{12}{\cosh^2(x)}f = 0. \tag{4.8}$$

Motivated by the fact that $\tanh'(x) = \cosh^{-2}(x)$, we perform the change of variables $z = \tanh(x)$. Then, (4.8) for $f(z)$ reads

$$(1 - z^2)f'' - 2(z + \alpha)f' + 12f = 0, \tag{4.9}$$

where the ‘’ refers to the derivation with respect to z. The neutral line is now at $z = \tanh(x) = 0$. When $\alpha = 0$, (4.9) becomes a Legendre equation of order three (we recall that a Legendre equation of order p reads $(1 - z^2)f'' - 2zf' + p(p + 1)f = 0$ – see Abramowitz & Stegun 1964, § 8.1.1). This equation has two regular singular points occurring at $z = \pm 1$ ($x \to \pm\infty$), and one of its two linearly independent solutions is a polynomial of third degree. This reads

$$f = a + bz + cz^2 + dz^3, \tag{4.10}$$

where the coefficients can be found by substituting the polynomial solution into (4.9) and equating to zero the coefficients with equal powers of z. After obtaining these coefficients, using $z = \tanh(x)$ and (4.7), the outer solution of (4.2) becomes

$$\psi_{\rm out} = Ae^{-\alpha|x|}\left\{1 + \frac{6\alpha^2 - 9}{\alpha(\alpha^2 - 4)}\tanh(|x|) + \frac{15}{(\alpha^2 - 4)}\tanh^2(|x|) + \frac{15}{\alpha(\alpha^2 - 4)}\tanh^3(|x|)\right\}. \tag{4.11}$$

The equation in the outer region accepts both an even and an odd solution. The even solution is the one required for tearing modes (the magnetic island shape is symmetric

https://doi.org/10.1017/S0022377822001088 Published online by Cambridge University Press

with respect to the neutral line – cf. also (2.8)). This solution displays a discontinuity in $\psi'_{\rm out}$ at $x = 0$. Taking the limit of the first derivative of (4.11),

$$\lim_{x\to\pm 0} \psi'_{\rm out} = A\left\{\mp\sqrt{k^2+4} \pm \frac{6k^2+15}{k^2\sqrt{k^2+4}}\right\}, \tag{4.12}$$

we obtain, using (3.8),

$$\Delta' = 2\frac{-k^4+2k^2+15}{k^2\sqrt{k^2+4}}. \tag{4.13}$$

It follows that $\Delta' > 0$ when $k \in [0, \sqrt{5}]$, which represents the spectrum of unstable wavenumbers to tearing-type instabilities for the equilibrium profile given by (4.3).

The outer solution for the case in which the magnetic equilibrium is given by Harris' profile $\psi'_0(x) = \tanh(x)$ (Harris 1962) can be obtained in the same manner, as already noted by Furth (1963) (§ 4, therein). In this case, the equivalent of (4.9) is a Legendre equation of degree $p = 2$. Therefore, $f(z) = a + bz$, which leads to an even solution $\psi_{\rm out}(x) = \psi_0 e^{-k|x|}\{k + \tanh(|x|)\}$. Following the same arguments as before, one recovers the result $\Delta' = 2(1/k - k)$, where the instability condition $\Delta' > 0$ is met when $k \in [0, 1]$ (Furth *et al.* 1963). The point we underline here is that the solution of the outer equation and the evaluation of Δ' by splitting the problem in (4.5)–(4.6) can be, in principle, used for a quite large class of magnetic equilibria.

As anticipated, the condition $\Delta' > 0$ determines the spectrum of unstable wavenumbers for a given equilibrium profile. This can be formally seen as related to the change of concavity that the solution ψ_1 must undergo while moving from the outer to the inner region, for the singular eigenfunction obtained in the ideal-MHD limit to become 'regular', thanks to the presence of non-ideal effects that allow reconnection (Furth *et al.* 1963). In general, exponentially growing solutions of the linear problem are obtained when $\Delta' > 0$ (cf. figure 7).

5. Equations in the non-ideal region

After having solved the linearised equations in the ideal MHD region, we are now interested in finding their solutions in the non-ideal region. We thus begin this section by introducing a 'generalised resistivity', which allows us to cast the linear equations in a unique form that can be applied to both the collisionless and resistive regimes. For analytical purposes that will become evident in the following, in this section, we also normalise the linear system with respect to an arbitrary characteristic length – say ℓ – which will be later specified in each subdomain and in each regime. Then, we will introduce an auxiliary function χ related to both scalar fields ψ_1 and φ_1, which allows us to combine the inner layer equations into a single equation. It is this equation that, in some reconnection regimes, will be later approximated in each subdomain of the boundary layer approach and which will be solved analytically according to the strategy detailed in § 3.

For the analytical integration of the linear problem, it is first useful to introduce a parameter that includes both the resistive and inertia-related non-ideal terms in Ohm's law by thus highlighting their 'almost symmetric' contributions in (2.1). This can be equivalently done in terms of the 'generalised resistivity', as first suggested by Furth (1963) (§ 5 therein), which, in the normalised units we use, reads

$$\bar{S}^{-1} \equiv S^{-1} + \gamma d_e^2, \tag{5.1}$$

or in the form of a 'generalised electron skin depth', as done by Porcelli (1991) (note that Porcelli (1991) uses the symbol Δ in place of the $\bar{d}_e$ we adopt here), by expressing the

https://doi.org/10.1017/S0022377822001088 Published online by Cambridge University Press

Lundquist number in terms of the normalised electron–ion collision rate, ν_{ei}, as $S^{-1} = d_e^2 \nu_{ei}/2$, so as to write

$$\bar{d}_e^2 \equiv d_e^2 + \frac{S^{-1}}{\gamma} = d_e^2 \left(1 + \frac{1}{2}\frac{\nu_{ei}}{\gamma}\right). \tag{5.2}$$

In either case, the second left-hand side term and the last right-hand side term of (2.1) can be re-absorbed into a single contribution that formally accounts for both resistive and inertial effects, the latter being therefore interpretable, in the form γd_e^2, as a 'collisionless resistivity'. Using for example (5.2), we rewrite (2.1) as

$$\gamma[\psi_1 - \bar{d}_e^2(\psi_1'' - k^2\psi_1)] - \mathrm{i}k\varphi_1(\psi_0' - d_e^2\psi_0''') = -\mathrm{i}k\rho_s^2(\varphi_1'' - k^2\varphi_1)\psi_0'. \tag{5.3}$$

In the following, when we will analytically integrate the linear problem in the non-ideal region, it will be more convenient to start from (2.2) and (5.3), of which we will then take the appropriate collisional or collisionless limits. Specialising the parameters $\bar{S}^{-1}$ or $\bar{d}_e$ to the purely resistive or purely collisionless limits is meaningful for linear tearing modes, because of the extremely narrow region of the parameter space in which both S^{-1} and d_e appreciably contribute to the asymptotic scalings (Betar *et al.* 2020). A transition from resistive to inertia-dominated regimes can instead be relevant to the onset of secondary collisionless modes over primary resistive tearing modes (Del Sarto & Ottaviani 2017), provided the applicability of the WKB approximation we spoke of in § 3.2 for secondary tearing instabilities developing on finite length, large-aspect ratio current sheets generated by the primary reconnection event. In this case, the possibility of having a transition of regime depends on both the rescaling of the shear length and of the magnetic field amplitude of reference (see Del Sarto *et al.* 2018).

A further distinction will be made between the 'cold' regime $\bar{d}_e^2 \gg \rho_s^2$ (discussed in § 6) and the opposite 'warm' regime $\rho_s^2 \gg \bar{d}_e^2$ (discussed in § 7). The reason why we are going to treat the two cases separately is due to the fact that the normalisation scales that define the extent, in an asymptotic sense, of the innermost boundary layer domain (i.e. δ_1 of figure 4*b*) turn out to be different, depending on whether ρ_s is negligible or not with respect to d_e (or to $(S^{-1}/\gamma)^{1/2}$). The asymptotic scaling of the layer width, δ_1, also determines, via the matching conditions, the scalings of the reconnection rate γ. It follows that the 'cold' collisionless solution cannot be obtained as a trivial limit $\rho_s \to 0$ of the solution obtained for the 'warm' case.

Operationally speaking, we will solve the inner equations using the generalised electron skin depth of (5.3), so we will first formally recover the collisionless results of Coppi (1964*c*), Coppi (1964*a*) and Porcelli (1991). Then, we will comment about the correspondence of these results with those obtained by Furth *et al.* (1963), Coppi *et al.* (1976), Ara *et al.* (1978), Pegoraro & Schep (1986) and Pegoraro *et al.* (1989) when resistivity dominates over electron inertia.

5.1. *Differential equations in the non-ideal region*

The fact non-ideal effects are important in a region which is microscopic with respect to the equilibrium shear scale a, allows us to use (3.2) so as to write $\psi_0'(x) \approx 2xC_2 = x\,\psi_0''|_{x=0} \equiv xJ_0$, where we have named $J_0 \equiv \psi_0''(x)|_{x=0}$ the value (normalised to B_0 and $L_0 = a$) of the second derivative of the equilibrium flux function at the neutral line. Using the ordering given by (3.4), (5.2)–(2.1) become

$$\gamma\psi_1 - \gamma\bar{d}_e^{\,2}\psi_1'' = \mathrm{i}kJ_0x\varphi_1 - \mathrm{i}kJ_0\rho_s^2x\varphi_1'', \tag{5.4}$$

$$\gamma\varphi_1'' = \mathrm{i}kJ_0x\psi_1''. \tag{5.5}$$

https://doi.org/10.1017/S0022377822001088 Published online by Cambridge University Press

It can be noted that a direct comparison between the relative weight of the parameters $\bar{d}_e^{\,2}$ and ρ_s^2 in (5.4) can be done after eliminating φ_1'' in (5.4) via (5.5). Doing so, (5.4) takes the form

$$\gamma\psi_1 = \mathrm{i}kJ_0x\varphi_1 + \gamma\left(\bar{d}_e^{\,2} + \rho_s^2\frac{k^2J_0^2}{\gamma^2}x^2\right)\psi_1''. \tag{5.6}$$

The coefficient multiplying ψ_1'' at the right-hand side of (5.6) can be read as a generalised, space-dependent, 'Lundquist number', i.e. it can be assimilated to a space-dependent resistivity/conductivity. (In more complex reconnection models based on a gyrokinetic modelling and including also ion-FLR effects, it can be shown (Cowley *et al.* 1986; Zocco & Schekochihin 2011) that the generalised conductivity, which rules the collisionless reconnection process inside the innermost layer dominated by electron dynamics, takes a rational-polynomial form of the kind $\sigma_e = (a + b(x/\delta_1))/(c + d(x/\delta_1)^2 + e(x/\delta_1)^4)$, where δ_1 is the innermost reconnecting layer width and a, b, c, d and e are coefficients that depend on the plasma parameters. This form has been used by Connor *et al.* (2012*b*) to obtain, via Fourier-space integration, a general dispersion relation encompassing drift-tearing modes, kinetic Alfvén modes and the internal kink mode at low values of the plasma β parameter.) To have magnetic reconnection, i.e. to allow for the existence of tearing-type unstable modes, the coefficient $\bar{d}_e^{\,2}$ must be non-null since ρ_s^2 alone does not allow the relaxation of the topological constraints forbidding the intersection and breaking of initially distinct magnetic lines (cf. § 2.1). Once the importance of the $\bar{d}_e^{\,2}$ term in the non-ideal region is established, one sees that the condition for which the last term in parenthesis of (5.6) is negligible in a subdomain of the integration domain, even for a non-vanishing value of ρ_s, is

$$\frac{\rho_s^2}{\bar{d}_e^{\,2}} \ll \left(\frac{\gamma}{kxJ_0}\right)^2. \tag{5.7}$$

This assumption will be later done in some regimes and will be heuristically verified.

5.2. *Normalisation and distinction of the boundary layers*

More in general, to solve the system (5.4)–(5.5) with the boundary layer approach, further hypotheses are done about the relative magnitude of the different contributions inside of the inner layer, and some auxiliary function (traditionally noted as χ) relating φ_1 to ψ_1 via (5.5) is introduced, depending on the Δ'-regime, so as to bring the system to a single ordinary differential equation (ODE). In each regime, appropriate normalisation of the spatial scales can be therefore chosen so as to better identify the extension of the sub-intervals of the inner region, where some term dominates over or is negligible with respect to the others. This is why, in the following, in the reconnection regimes and Δ' limits which will be of interest, at each time, we will perform several changes of variable based on different normalisation choices.

This is an important step in the boundary layer procedure, since it is at this level that one introduces the layer widths δ_1 or δ_2 (cf. figure 4), although only implicitly: in practice, a 'stretched' coordinate is introduced by referring the coordinate x to a characteristic length, say ℓ, which replaces x in different subdomains of the non-ideal region. It is when the limits $|x|/\ell \gg 1$ or $|x|/\ell \ll 1$ will be taken for the purpose of finding solutions of the differential equations within the boundary layer approach that the length ℓ will be identified as the layer width, e.g. δ_2 or δ_1. Also note that the length ℓ may initially depend on some unknown parameter like the eigenvalue γ: its scaling, and therefore that of ℓ and

https://doi.org/10.1017/S0022377822001088 Published online by Cambridge University Press

subsequently that of the layer width to which it corresponds, will be therefore determined *a posteriori*, from the conditions on the solutions obtained by integrating and matching the equations for small and large values of these stretched variables. Note that since the initial choice of each length scale ℓ is essentially arbitrary, it must be *a posteriori* verified for consistency that, asymptotically, $\delta_1 \ll \delta_2 \ll 1$ (when both δ_2 and δ_1 are expressed in units of $L_0 = a$).

It is also worth stressing that the identification of each boundary layer is subordered to the identification of the negligibility of some term of the non-ideal equations. This means that we must have knowledge of the relative ordering of the non-ideal parameters at play (for example, had we wanted to include viscosity, a third scale length – let us say λ_ν – would have appeared. If the hypothesis $\lambda_\nu \gg \rho_s \gtrsim \bar{d}_e$ had been fulfilled, one could have *a priori* expected three subdomains in the non-ideal region: one where ν alone dominates, one where *both* ν *and* ρ_s in principle dominate, and one where all three non-ideal parameters are in principle important. Then, one should evaluate if, in the two innermost regions, specific conditions can be satisfied so that the dominant contribution of one or two non-ideal terms alone can be isolated: this possibly refines further the subdomains of interest for the purpose of the integration. It is at this level that we finally *define* the boundary layers, with respect to which the matching conditions will be fixed), or, if this is not the case, specific assumptions must be done on them by separately considering the different possible combinations, until in each case, the 'thinnest' sub-domain is this way singled out: this is the innermost region where the eigenmode solution must be first integrated by imposing the boundary conditions from outside.

As an example of general interest for the calculations that we are going to develop next, we can consider a normalisation of (5.4)–(5.5) to an arbitrary length ℓ, which we will specify later, in each case examined. This will also let us get rid of some 'superfluous' parameters in the equations. We thus define

$$\zeta = \frac{x}{\ell}, \quad \mathcal{G} = \frac{\gamma}{k\ell J_0}, \quad \tilde{\varphi}_1 = -\mathrm{i}\frac{\gamma}{k\ell J_0}\varphi_1(\zeta), \quad \tilde{\psi}_1 = \psi_1(\zeta), \tag{5.8}$$

which allow us to re-write (5.4)–(5.5) as

$$\tilde{\psi}_1 - \left(\frac{\bar{d}_e^2}{\ell^2} + \frac{\rho_s^2}{\ell^2}\frac{\zeta^2}{\mathcal{G}^2}\right)\tilde{\psi}_1'' = -\frac{\zeta}{\mathcal{G}^2}\,\tilde{\varphi}_1, \tag{5.9}$$

$$\tilde{\varphi}_1'' = \zeta\,\tilde{\psi}_1'', \tag{5.10}$$

where both functions $\tilde{\varphi}_1$ and $\tilde{\psi}_1$ depend now on ζ.

We note that $\mathcal{G}$ depends on γ, which generally makes both quantities complex numbers: they are real for usual tearing-type instabilities, which, in the absence of diamagnetic effects related to equilibrium density gradients, do not propagate; instead, they are purely imaginary if the magnetic profile is stable. Because of this feature, in the following, it will be useful to perform some integration in the complex plane.

Also note that if $\ell = 1$ (in units of $L_0 = a$), then, in dimensional units, we can write $\mathcal{G} = \gamma\tau_0/(ka)$, where $\gamma\tau_0$ expresses the growth rate of the unstable mode measured with respect to the 'natural timescale' $\tau_0 \sim \sqrt{mn_0/(4\pi)}(c/J_0)$, which equals here the transition time of a shear Alfvén wave across the shear length a (cf. Betar *et al.* 2020). Therefore, $\mathcal{G}|_{\ell=1} \ll 1$ in an asymptotic sense, as long as the wavenumber is fixed and then ka is unordered with respect to $\gamma\tau_0$. If, instead, the scale ℓ is microscopic, the ordering of $\mathcal{G}$ with respect to unity must be *a posteriori* evaluated.

https://doi.org/10.1017/S0022377822001088 Published online by Cambridge University Press

5.3. *Auxiliary function 'χ' and large- and small-Δ' limits*

The strategy by which the inner equations are integrated depends on mathematical features that we are going to discuss in detail in each specific regime and wavelength limit on which they depend (see also § 5.5). In general, some approximations and hypotheses are required, since they allow us to combine (5.9)–(5.10) into a single equation. An integration strategy which is particularly efficient, especially in the large-Δ' limit, consists in casting the equations for $\tilde{\psi}_1$ and $\tilde{\varphi}_1$ into an equation for an auxiliary variable, even with respect to ζ, which is typically noted $\chi(\zeta)$, after the notation first chosen for it by (Coppi *et al.* 1976; Ara *et al.* 1978)

$$\chi(\zeta) \equiv \zeta \tilde{\psi}_1'(\zeta) - \tilde{\psi}_1(\zeta). \tag{5.11}$$

This is directly connected to (5.10), of which it is an integral. Indeed, we have

$$\tilde{\varphi}_1''(\zeta) = \chi'(\zeta) \quad \Longrightarrow \quad \tilde{\varphi}_1'(\zeta) = \chi(\zeta) - \lim_{\zeta\to\infty} \chi(\zeta) = \chi(\zeta) - \chi_\infty. \tag{5.12}$$

In the last passage, we have named χ_∞ the value of $\chi(\zeta)$ as $\zeta \to \infty$. Note that in boundary layer calculations, when ℓ will be identified as δ_2 or δ_1, the limit $\zeta \to \infty$ for which χ_∞ is defined must be taken in the matching layer outside of the innermost layer, but still inside the non-ideal region, i.e. for $\delta_1 \ll x \ll 1$ (in units of $L_0 = a$): since $\tilde{\varphi}_1'$ represents the $y-$component of the velocity, it approaches zero as $\zeta \to \infty$ inside the ideal region. Determining the asymptotic behaviour of χ_∞ at both limits of the unstable wavelength spectrum is important since the scaling laws of the eigenvalue problem depend on it (Ara *et al.* 1978). In practice, depending on whether χ_∞ is zero or not, the differential equation for χ is homogeneous or not (see (5.19) below). These topics are discussed in the remainder of this section by considering, for simplicity, the case of a single boundary layer (i.e. assuming $\ell = \delta_1$).

5.3.1. *Asymptotic estimate of χ_∞ in the small-Δ' limit*

In the case of the small-Δ' limit and when $x \to 0$, according to the definition of $\chi(\zeta)$ and to the matching condition $\lim_{\zeta\to\infty} \tilde{\psi}_1(\zeta) \sim \lim_{x\to 0} \psi_{\mathrm{out}}(x)$, one finds

$$\chi_\infty = \lim_{\zeta\to\infty} \chi(\zeta) \sim \lim_{x\to 0} x\psi_{\mathrm{out}}'(0) - \psi_{\mathrm{out}}(0) \simeq -c_0, \quad \text{(constant-}\psi\text{ ordering)}. \tag{5.13}$$

In this case, we have used the 'constant-ψ' approximation (Furth *et al.* 1963), i.e. the fact that in the small-Δ' regime, the inner solution tends to a constant value $\psi_1(0)$ when it approaches the innermost region. Such constant value is approximatively obtained already from the $x \to 0$ limit of the outer solution $\psi_{\mathrm{out}}(x)$, so that in this wavelength limit, we can write $\lim_{x\to 0} \psi_{\mathrm{out}}(x) = c_0$.

The constant-ψ ordering can be assumed and heuristically verified after integration of the eigenmode problem for the single boundary layer limit (cf. Furth *et al.* 1963; White 1983), and in the small-Δ' regime, it can be shown to be equivalent to the condition $\delta_1\Delta' \ll 1$. In this case, we can also estimate $\lim_{x\to 0} x\psi_1'(x) \sim \lim_{x\to 0} x\Delta'\psi_{\mathrm{out}}(x) \sim \delta_1\Delta' c_0$, where in the last passage, we have (over)estimated $\lim_{x\to 0} x$ by the extent of the innermost layer width: owing to the $\Delta'\delta_1 \ll 1$ condition, the last passage of (5.13) is thus justified, whence one deduces

$$\chi_\infty = -c_0, \quad \text{for } \delta_1\Delta' \ll 1. \tag{5.14}$$

5.3.2. *Asymptotic estimate of χ_∞ in the large-Δ' limit*

In the large-Δ' limit for $x \to 0$, instead, one finds that $\chi_\infty = 0$. This has been first discussed by Coppi *et al.* (1976) and Ara *et al.* (1978), where it has been shown that the

https://doi.org/10.1017/S0022377822001088 Published online by Cambridge University Press

vanishing of $\chi(\zeta)$ far out from the resonant region (equivalent to the innermost layer in our notation) is consistent with the rigid plasma displacement that characterises the internal kink mode in a cylindrical tokamak: in the notation and slab geometry assumption we use in this work, this corresponds to write $\tilde{\varphi}_1(\zeta) = -\gamma\zeta$ for $|\zeta| \leq 1$ and $\tilde{\varphi}_1(\zeta) = 0$ for $|\zeta| > 1$ (cf. also Porcelli 1987; Del Sarto & Ottaviani 2017), whence the condition $\chi_\infty = 0$ immediately follows by direct comparison with the definition in (5.12). An alternative way to look at the consistency of this result is to consider the Taylor expansion of the outer solution given by (4.7):

$$\psi_{\rm out}(x) \sim c_0 + c_1|x| \implies \psi_{\rm out} \sim c_0 + c_1|x| \implies \Delta' \sim \frac{2c_1}{c_0}. \tag{5.15}$$

This solution formally holds in the outermost matching layer, where the instability parameter Δ' is defined by neglecting non-ideal effects, i.e. by taking the limit $x \to 0$ of the eigenmode in the ideal region. Therefore, the use of $\lim_{x\to 0}\psi_{\rm out}(x)$ to match the solution $\lim_{\zeta\to\infty}\psi_1(\zeta)$ is *a priori* not always justified. This however is not the case of the large-Δ' limit, in which it can be *a posteriori* shown, from heuristic arguments (see Ottaviani & Porcelli (1995) for the 'cold' reconnection regime) or by numerical integration, that the discontinuity in the derivative of $\psi_{\rm out}$ occurs in a position which gets progressively closer to the neutral line, as long as the numerical value of $\Delta'(k)$ increases (cf. also §§ 8–10). In this limit, using therefore $\lim_{\zeta\to\infty}\tilde{\psi}_1 \simeq \lim_{x\to 0}\psi_{\rm out}(x)$ combined with (5.15) in the definition of (5.11), one finds

$$\lim_{\zeta\to\infty}\chi(\zeta) \sim c_1|x| - c_0 - c_1|x| = -c_0 \sim \frac{c_1}{\Delta'}. \tag{5.16}$$

The fact that $c_0 \to 0$ as Δ' increases is shown in figure 7, where the spatial profile of ψ_1, obtained after numerical integration of the purely resistive regime (for $S^{-1} = 10^{-5}$), is shown for the values of $\Delta'(k) = -19.19$ (green curve), $\Delta'(k) = 48.9$ (blue curve) and $\Delta'(k) = 3.2766$ (orange curve), evaluated using (4.13) for $k = 10, 0.1$ and 1.7, respectively. Thus, in the large-Δ' limit where $\Delta' \to \infty$, (5.16) implies that

$$\chi_\infty = 0 \quad \text{for } \Delta' \to \infty. \tag{5.17}$$

The fact that condition $\Delta' \to \infty$ can be replaced by Δ' larger than the inverse of some characteristic scale length will be discussed in § 10. As already anticipated (§ 3.2), this condition can be generally read as $\Delta'\delta_1 \gg 1$.

5.4. *Auxiliary equation for the function $\chi(\zeta)$ in the non-ideal region*

Definitions in (5.11)–(5.12) can be used to cast (5.9) in an equation for $\chi(\zeta)$. For analytical convenience, i.e. to facilitate the substitution of variables, it is preferable to evaluate the derivative of (5.9) after it has been divided by ζ. After opportunely regrouping the terms of the equation so obtained, the result reads

$$(\zeta\tilde{\psi}_1' - \tilde{\psi}_1) - \frac{\bar{d}_e^2}{\ell^2}(\zeta\tilde{\psi}_1''' + \tilde{\psi}_1'' - 2\tilde{\psi}_1'') - \frac{1}{\mathcal{G}^2}\frac{\rho_s^2}{\ell^2}\zeta^2(\zeta\tilde{\psi}_1''' + \tilde{\psi}_1'') = -\frac{1}{\mathcal{G}^2}\zeta^2\tilde{\varphi}_1', \tag{5.18}$$

which can be rewritten as

$$\left(\frac{\bar{d}_e^2}{\ell^2} + \frac{\rho_s^2}{\ell^2}\frac{\zeta^2}{\mathcal{G}^2}\right)\chi'' - 2\frac{\bar{d}_e^2}{\ell^2}\frac{\chi'}{\zeta} - \left(1 + \frac{\zeta^2}{\mathcal{G}^2}\right)\chi = -\frac{\zeta^2}{\mathcal{G}^2}\chi_\infty. \tag{5.19}$$

In the following, we will take different limits of this equation, depending on the tearing regime and wavelength limit considered. We emphasise that to give to the right-hand side

https://doi.org/10.1017/S0022377822001088 Published online by Cambridge University Press

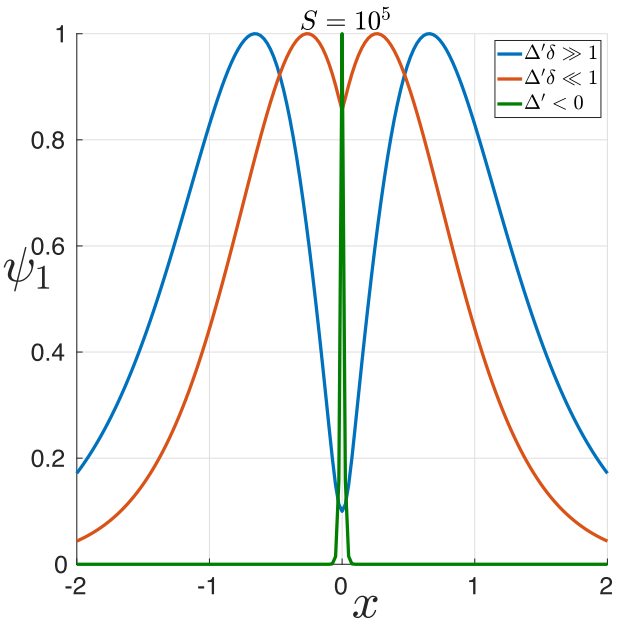

FIGURE 7. Profile of the eigenfunction ψ_1 in the purely resistive regime, computed via the numerical solver of Betar *et al.* (2020) for $S^{-1} = 10^{-5}$ and $k = 10$ (green curve), $k = 1.7$ (orange curve) and $k = 0.1$ (blue curve). These three values are respectively exemplificative of: the stable regime ($\Delta' = -19.19 < 0$, green curve); of the small-Δ' wavelength limit ($\Delta' = 3.2766$, red curve); and of the large-Δ' wavelength limit ($\Delta' = 48.9$, blue curve). In the stable case ($\Delta' < 0$), the eigenfunction does not change concavity as x approaches the neutral line, whereas for the unstable tearing-type solutions obtained for $\Delta' > 0$, the value $c_0 \equiv \lim_{x\to 0} \psi_1(x)$ decreases approaching zero as the value of $\Delta'(k)$ increases approaching $+\infty$.

term χ_∞ of (5.19) the geometrical (and physical) meaning we have previously discussed in terms of the boundary layer theory, the length ℓ must correspond to the layer width, δ_2 or δ_1 (depending on whether we are in the case of figure 4), to which the solution ψ_{out} obtained in the ideal region is matched.

5.5. *Wavelength limit and choice of integration via the equations for χ or for ψ and φ*

The choice of performing the integration by using (5.4)–(5.5) for ψ_1 and φ_1, rather than (5.19) for χ, clearly depends on analytical convenience. In general, we note that this choice can be biased by the ease by which the boundary conditions imposed by the solution obtained in the outer, ideal region, are 'transferred' to the solution in the innermost region. The asymptotic matching generally poses some constraints on the integration constants in each subdomain, but it is easy to see that, operationally speaking, these conditions take different and quite 'appealing' forms in the small- and large-Δ' limits, depending on whether one looks at the equation for ψ_1 or at the auxiliary equation for χ, respectively. In particular, the following are observed.

(i) In the *small-Δ' limit*, it is usually more convenient to perform the integration on the equation for ψ_1, for which the boundary conditions imposed from the ideal region are directly implemented by making explicit the dependence on Δ' via (3.7) and (3.10). In this case, the constraint imposed by the solution ψ_{out} in the ideal region can be directly used on the integration of the innermost equation in the form of the

https://doi.org/10.1017/S0022377822001088 Published online by Cambridge University Press

constant-ψ condition. Indeed, if we define $c_0 \equiv \lim_{x\to 0} \psi_{\rm out}(x)$ and we heuristically assume the constant-ψ condition to be valid, the latter implies that $\psi_1 \simeq c_0$ *both* in the innermost region $|x| \leq \delta_1$ and in the possible intermediate region $\delta_1 < |x| \leq \delta_2$. Therefore, also when two boundary layers are present, the constant-ψ condition can be directly implemented in the integration of the innermost equation, by thus practically allowing one to 'bypass' the procedure of matching between the solutions in the ideal and in the intermediate region, and then between the solutions in the intermediate and in the innermost region[2] (at least for the purpose of establishing the dispersion relation, i.e. to find the asymptotic scalings of the eigenvalue). However, as the matching occurs in the boundary layer with the ideal region, it is generally more convenient to maintain the normalisation to the intermediate layer width, also when two layers are present. This approach will be used in §§ 6.2 and 7.5.

(ii) In the *large-Δ' limit*, it is instead usually more convenient to perform the integration on the auxiliary equation, since in this case, the constraint imposed by the outer solution $\psi_{\rm out}$ on the solutions in the non-ideal region is simply expressed as $\chi_\infty = 0$ (cf. § 5.3.2). From an operational point of view, this realises the matching between the ideal and the intermediate region. The dispersion relation is therefore directly obtained by solving the non-ideal equation for $\chi_\infty = 0$ in case a single boundary layer is present, or by matching the innermost solution and the intermediate solution (both sought under the constraint $\chi_\infty = 0$) if two boundary layers are present. This approach will be used in §§ 6.1 and 7.4.

6. Solutions in the inner region: cold regime

Let us first discuss the reconnection regime with both cold electrons and ions. The linear problem has been first solved in the small-Δ' wavelength limit by Furth *et al.* (1963) in the resistive regime and by Coppi (1964*c*,*a*) in the inertial regime, using boundary layer calculations in the coordinate space. A solution of the linear problem in the large-Δ' wavelength limit has been first provided in the resistive regime by Coppi *et al.* (1976) and has been extended in the collisionless regime by Porcelli (1991). In this latter work, the calculations in the Fourier space, with which Pegoraro & Schep (1986) also recovered the resistive results of Furth *et al.* (1963) and Coppi *et al.* (1976), have been extended to the purely collisionless regime. We will come back to these more recent works relying on the integration in the Fourier space in § 7, where we will discuss the 'warm' reconnection regime including FLR effects related to parallel electron compressibility (i.e. a kind of diamagnetic effect).

The reason for which we start from the case of cold species is that, from the point of view of the boundary layer theory, the 'cold' regime in which we neglect ρ_s-related terms in (2.1)–(2.2) is both conceptually and analytically simpler than the 'warm' tearing regime (cf. figure 4). Since we consider the cold limit $\bar{d}_e^2 \gg \rho_s^2$ which encompasses the case $\rho_s = 0$, to ensure convergence of the solution with the $\rho_s = 0$ limit, we assume the validity of the condition (5.7) in the whole integration domain. We can verify *a posteriori* its validity, once the eigenvalue problem is solved.

We also mention here that the analytical results we are going to obtain below have been numerically verified by Betar *et al.* (2020) to be valid for $\bar{d}_e^{\,2} > \rho_s^2/100$, i.e. for $\bar{d}_e \gtrsim \rho_s/10$.

[2] In (Granier *et al.* 2022) it has been pointed out that in the warm small-Δ' regime the equation for φ_1 changes of form while moving from the layer of width δ_2 to the innermost layer of width δ_1: while this would formally require to carry out the full boundary layer calculation for its integration, doing so only yields negligible additive corrections of order $O(\delta_1/\rho_s) \ll 1$ to the growth rate scalings.

https://doi.org/10.1017/S0022377822001088 Published online by Cambridge University Press

6.1. *Solution for $\bar{d}_e^2/\rho_s^2 \gg 1$: large-$\Delta'$ limit*

Assuming heuristically the validity of (5.7), we neglect the second term in parentheses in (5.9). The restriction to the large Δ'-limit, in which the condition in (5.17) holds, suggests that we make use of the auxiliary function $\chi(\zeta)$ defined by (5.11), which leads us to consider the appropriate limit of (5.19):

$$\chi'' - \frac{2}{\zeta}\chi' - \frac{\ell^2}{\bar{d}_e^2}\left(1 + \frac{\zeta^2}{\mathcal{G}^2}\right)\chi = 0. \tag{6.1}$$

The structure of the equation *suggests* that we take $\ell \equiv \bar{d}_e$ as the normalisation length to be used in the definitions of (5.8). This means that we postulate

$$\delta_1 = \bar{d}_e, \tag{6.2}$$

which, at least for $\bar{d}_e = d_e$, is evidently consistent with the asymptotic condition $\delta_1 \ll 1$. A solution to (6.1) can be sought in the form

$$\chi_1 = e^{-\alpha\zeta^2}. \tag{6.3}$$

Substituting it in (6.1) yields

$$2\alpha = 1, \quad 4\alpha^2 = \frac{1}{\mathcal{G}^2}. \tag{6.4}$$

Using the first part of (5.8) and combining the two conditions above, gives

$$\gamma = k\bar{d}_e J_0. \tag{6.5}$$

This result can be specialised both to the fully collisionless ($\bar{d}_e^2 = d_e^2$) and to the fully collisional ($\bar{d}_e^2 = S^{-1}/\gamma$) internal-kink regime. We recall in this regard that numerical analysis (Betar *et al.* 2020) confirms that the parameter space interval where both inertial and resistive effects non-negligibly combine is very narrow, so that tearing modes can be usually considered either as fully collisionless or as fully resistive.

In the collisionless limit, we thus recover the result of (Porcelli 1991)

$$\gamma = kd_e J_0 \quad \delta_1 \sim d_e. \tag{6.6}$$

In the resistive case, (6.6) specialises to the result of (Coppi *et al.* 1976)

$$\gamma = k^{2/3} J_0^{2/3} S^{-1/3}, \quad \delta_1 \sim k^{-1/3} J_0^{-1/3} S^{-1/3}. \tag{6.7}$$

Substitution of the results of (6.6) and (6.7) for $x \sim \delta_1$ in (5.7) makes it equivalent to the condition $\rho_s^2/\bar{d}_e^2 \ll 1$ from which we started, thus verifying *a posteriori* its correctness.

The scalings in (6.6) and (6.7)), in contrast to those of the large-Δ' limit of the warm-collisionless regime, can be obtained using a heuristic-type derivation based on dimensional estimates, as we are going to prove in § 9.3.

Finally, some words about the second solution of (6.1), which we have neglected, since it can be shown that it is not of interest to the tearing instability problem. To this purpose,

https://doi.org/10.1017/S0022377822001088 Published online by Cambridge University Press

we can look for a solution of the form $\chi_2(\zeta) = u(\zeta)\,\chi_1(\zeta)$. Substituting $\chi = \chi_2$ in (6.1) and using the fact that χ_1 already solves it, one obtains, after a little algebra,

$$u''\chi_1 + 2u'\left(\chi_1' - \frac{\chi_1}{\zeta}\right) + u\chi_1'' = 0. \tag{6.8}$$

Further substitution of (6.3) into the equation above yields

$$u'' - \left(4\alpha\zeta + \frac{2}{\zeta}\right)u' = 0, \tag{6.9}$$

which, defining $w = u'$, can be brought to a directly integrable form:

$$\frac{\mathrm{d}w}{w} = 4\alpha\zeta\,\mathrm{d}\zeta + \frac{2\,\mathrm{d}\zeta}{\zeta} \implies w(\zeta) = w_0\,\zeta^2 e^{2\alpha\zeta^2}, \tag{6.10}$$

w_0 being a constant of integration. Specialising the result for $\alpha = 1/2$, integrating w once to find u and then substituting the result in $\chi_2 = u\chi_1$, one obtains

$$\chi_2 = \mathrm{i}\sqrt{\frac{\pi}{2}}\mathrm{erf}\left(\frac{\mathrm{i}\zeta}{\sqrt{2}}\right)e^{-(\zeta^2/2)} + \zeta, \tag{6.11}$$

which is odd and unbounded when $\zeta \to \infty$. Therefore, for our purposes, the solution χ_2 can be disregarded since its spatial parity is not compatible with that of tearing modes (i.e. it is not compatible with the formation of X-points).

6.2. *Solution for $d_e^2/\rho_s^2 \gg 1$: small-Δ' limit*

In the small-Δ' limit, the boundary layer analysis mirrors that of the paper by Furth *et al.* (1963) if the resistive limit $\bar{d}_e^2 \to S^{-1}/\gamma$ is considered. In general, regardless of the form of $\bar{d}_e$, we can here use the 'constant-ψ' approximation stating that $\tilde{\psi}_1(\zeta) \to c_0$ as $\zeta \to 0$ (cf. (5.15)). However, instead of using the auxiliary equation (5.19), in this case, it is more convenient to consider (5.9) in which $\tilde{\psi}_1''$ has been eliminated by using (5.10) since, after combination with the constant-ψ limit, this yields an equation for the function $\tilde{\varphi}_1(\zeta)$ that can be brought to an integrable form more easily than the equation for $\chi(\zeta)$:

$$\tilde{\varphi}_1'' - \frac{\zeta^2}{\mathcal{G}^2}\frac{\ell^2}{\bar{d}_e^2}\tilde{\varphi}_1 = c_0\frac{\ell^2}{\bar{d}_e^2}\,\zeta. \tag{6.12}$$

Note that in this equation, the length ℓ is so far left unspecified. In practice, at this stage of the calculations, it can be taken $\ell = 1$, which would be still consistent with the constant-ψ limit with respect to which the substitution $\tilde{\psi}_1(0) \simeq c_0$ has been done. The identification of a proper normalisation length defining the boundary layer width can be done after a further change of variable that leads (6.12) to an integrable form in which the boundary layer integration can be more easily performed. Equation (6.12) for $\ell = 1$ can be indeed brought to the form

$$\Phi'' - z^2\Phi = z \tag{6.13}$$

after the change of variables and coordinates

$$z = \left(\mathcal{G}\bar{d}_e\right)^{-1/2}\zeta, \quad \Phi = \left(\frac{\bar{d}_e}{\mathcal{G}^3}\right)^{1/2}\left(\frac{\tilde{\varphi}_1}{c_0}\right). \tag{6.14}$$

The normalisation of Eq. (6.12) is detailed in Appendix D as a didactical example of how to generally proceed to find the normalisation coefficients of a differential equation. In the

https://doi.org/10.1017/S0022377822001088 Published online by Cambridge University Press

limit $\bar{d}_e^2 \to S^{-1}/\gamma$, (6.13) is the equation of the resistive tearing mode studied by Furth *et al.* (1963), whose solution has been provided by Basu & Coppi (1976), Coppi *et al.* (1976) and Ara *et al.* (1978) (cf. (III.26) and (III.27) and appendix A in the latter) in the closed integral form:

$$\Phi = -\frac{1}{2} z \int_0^1 (1-t^2)^{-1/4} e^{-(1/2)tz^2}\, \mathrm{d}t. \tag{6.15}$$

The scaling of the eigenvalue γ and its dependence on the amplitude of the instability parameter Δ' can be made explicit by comparing the eigenfunction $\Phi(z)$ to $\varphi_1(x/\delta_2)$ in the matching condition expressed by (3.7), which also allows us to identify the layer width δ_2: combining (3.7) and (3.10) (where we re-introduce the quantity J_0) yields

$$\psi_{\mathrm{out}}(0)\Delta' = -\mathrm{i}\frac{\gamma}{kJ_0} \int_{-\bar{X}'}^{+\bar{X}'} \frac{\varphi_1''(x')}{x'}\, \mathrm{d}x', \tag{6.16}$$

where Δ' is defined by (3.8), $x' = x/\delta_1$ and $\bar{X}' = \bar{X}/\delta_1$ is indicative of some point of the matching region such that $\delta_1 \ll \bar{X} \ll 1$ in units of $L_0 = a$. Connection with (6.13) follows from noticing that (6.14) implies:

$$\left.\frac{\mathrm{d}^2\tilde{\varphi}_1}{\mathrm{d}\zeta^2}\right|_{\ell=1} = c_0 \left(\frac{1}{\bar{d}_e \mathcal{G}^3}\right)\Bigg|_{\ell=1}^{1/2} \left(\frac{\mathrm{d}z}{\mathrm{d}\zeta}\right)^2 \frac{\mathrm{d}^2\Phi}{\mathrm{d}z^2} = c_0 \left(\frac{\mathcal{G}}{\bar{d}_e^3}\right)\Bigg|_{\ell=1}^{1/2} \frac{\mathrm{d}^2\Phi}{\mathrm{d}z^2}. \tag{6.17}$$

This authorises us to identify

$$x' = \frac{x}{\delta_1} \longrightarrow z = \frac{x}{(\mathcal{G}\bar{d}_e)|_{\ell=1}^{1/2}}, \quad -\mathrm{i}\frac{\gamma}{kJ_0}\frac{\mathrm{d}^2\varphi(x')_1}{\mathrm{d}x'^2} \longrightarrow c_0 \left(\frac{\mathcal{G}}{\bar{d}_e^3}\right)\Bigg|_{\ell=1}^{1/2} \frac{\mathrm{d}^2\Phi}{\mathrm{d}z^2}, \tag{6.18}$$

which now fixes the boundary layer width to be

$$\delta_1 = (\mathcal{G}\bar{d}_e)\big|_{\ell=1}^{1/2} = \sqrt{\frac{\gamma \bar{d}_e}{k}}, \tag{6.19}$$

whose consistency with the condition $\delta_1 \ll 1$ must be verified once $\mathcal{G}|_{\ell=1}$ is explicitly obtained. Substituting then $\psi_{\mathrm{out}}(0) \simeq \lim_{\zeta\to 0} \tilde{\psi}_1(\zeta) = c_0$ and using (6.18) makes (6.16) become

$$\Delta' = \left(\frac{\mathcal{G}}{\bar{d}_e^3}\right)\Bigg|_{\ell=1}^{1/2} \int_{-\bar{Z}}^{+\bar{Z}} \frac{\Phi''}{z}\, \mathrm{d}z, \tag{6.20}$$

where $\bar{Z} = \bar{X}/(\mathcal{G}\bar{d}_e)|_{\ell=1}^{1/2}$. The integral in the previous equation is convergent, let us call its value $I \equiv \int_{-\infty}^{+\infty} (\Phi''/z)\, \mathrm{d}z \simeq \int_{-\bar{Z}}^{\bar{Z}} (\Phi''/z)\, \mathrm{d}z$. Then, using the definition in (5.8) for $\ell = 1$,

https://doi.org/10.1017/S0022377822001088 Published online by Cambridge University Press

one obtains

$$\gamma = k\bar{d}_e^3(\Delta')^2\left(\frac{J_0}{I^2}\right). \tag{6.21}$$

In the inertia-dominated regime, $\bar{d}_e = d_e$, one recovers the well-known result by Coppi (1964*c*,*a*), later re-obtained by Porcelli (1991):

$$\gamma = k(\Delta')^2 {d_e}^3\left(\frac{J_0}{I^2}\right), \quad \delta_1 = \frac{\Delta' d_e^2}{I}. \tag{6.22}$$

In taking the resistive limit, $\bar{d}_e = (S^{-1}/\gamma)^{1/2}$, one obtains instead the classical result of Furth *et al.* (1963), later recovered by Pegoraro & Schep (1986):

$$\gamma = k^{2/5}(\Delta')^{4/5}S^{-3/5}\left(\frac{J_0}{I^2}\right)^{2/5}, \quad \delta_1 = \frac{k^{-2/5}(\Delta')^{1/5}S^{-2/5}}{(J_0 I^2)^{2/5}}. \tag{6.23}$$

In both cases (6.22) and (6.23), the asymptotic condition $\delta_1 \to 0$ as $d_e \to 0$ or $S^{-1} \to 0$ is verified.

7. Solutions in the inner region: warm-electron regime

Let us now consider the boundary layer problem in the 'warm' reconnecting regime by limiting our attention to the case of cold ions, consistent with (2.1) and (2.2).

Extending the analysis to include ion temperature effects related to FLR corrections in the fluid description of these low frequency modes is possible, but generally it requires relying on reduced models (i.e. 'gyrofluid' models), in which the ion response related to the separation between the motion of particles and of gyrocentres is obtained by starting from the gyrokinetic Vlasov equation. Fluid models of reconnection, in which this has been done, typically differ because of the way the gyrokinetic operator is approximated and because of the number of scalar fields that are retained in the description (see, e.g. Pegoraro & Schep 1981, 1986; Pegoraro *et al.* 1989; Porcelli 1991; Schep *et al.* 1994; Loureiro & Hammett 2008 for essentially two-field models, and, e.g. Aydemir (1992), Zakharov & Rogers (1992), Dorland & Hammett (1993), Smolyakov, Pogutse & Hirose (1995), Pogutse, Smolyakov & Hirose (1998), Waelbroeck, Hazeltine & Morrison (2009), Zocco & Schekochihin (2011), Waelbroeck & Tassi (2012), Connor *et al.* (2012*b*) and Tassi, Sulem & Passot (2016) for other gyrofluid models retaining more than two scalar fields). A common feature of linear tearing analysis build on these gyrofluid models, as well as on other descriptions retaining kinetic features at a more fundamental level (see Drake & Lee 1977; Cowley *et al.* 1986; Rogers *et al.* 2007), is the 'symmetric' way by which ion and electron temperature effects enter in the dispersion relation in regimes where an estimate of the growth rate of tearing-type modes is analytically available. This symmetry is expressible via the formal substitution $\rho_s^2 \to \rho_s^2 + \rho_i^2$ in the dispersion relations which we are going to discuss in the remainder of this work. In regimes of the parameter space that go beyond the applicability of the analytical predictions by Pegoraro & Schep (1986), Pegoraro *et al.* (1989) and Porcelli (1991), a departure from the symmetry between ρ_s and ion-Larmor-radius effects associated with the parameter $\rho_i = \rho_s\sqrt{T_i/T_e}$ has been numerically observed in the growth rate of the internal-kink mode (Del Sarto *et al.* 2011). Dealing with these subjects would include some complicacy about the build of the linear model, which are unnecessary with respect to the purpose of the present work. This is why we neglect them here.

We therefore start from (5.4) and (5.5). Since the problem has now two characteristic spatial scales, namely $\bar{d}_e$ and ρ_s, the identification of the two boundary layers will require

https://doi.org/10.1017/S0022377822001088 Published online by Cambridge University Press

us to perform two subsequent normalisations and approximations of the terms of the aforementioned equations. Since we are now restricting to the parameter range where ρ_s^2 is not negligible with respect to $\bar{d}_e^2$, we can assume $\rho_s^2 \gtrsim \bar{d}_e^2$. A natural choice for choosing a first normalisation scale defining the 'largest' non-ideal region of interest is therefore to pose $\ell = \rho_s$. We note that identifying this as a boundary layer width or not is a further logical step, whose appropriateness depends on the kind of approximations of the equations and integration strategies that can be possibly performed with respect to the stretched variable x/ρ_s. This is what we are going to discuss below.

Also note that for economy of symbols – let us say – in this section, we will use some symbols used in the changes of variables of § 6 with a different definition that will be given in each specific case (this will concern, in particular, the definition of ζ, $\mathcal{G}$ and the use of the '$\tilde{\cdot}$' to label some normalised quantities).

7.1. *Equations in the non-ideal region for $\rho_s \gtrsim d_e$*

As we enter the non-ideal region from the ideal one, when $x < 1$, the first non-ideal characteristic scale that is encountered under the hypotheses previously done is $\rho_s > d_e$. This is the first scale length with respect to which we can *try* to identify a boundary layer: aiming to single out a subdomain in the $x \ll 1$ range where only ρ_s possibly matters, we start by fixing $\ell = \rho_s$ in (5.8), so that (5.9) and (5.10) become

$$\tilde{\psi}_1 - \left(\frac{\bar{d}_e^2}{\rho_s^2} + \frac{\tilde{\zeta}^2}{\tilde{\mathcal{G}}^2}\right)\tilde{\psi}_1'' = -\frac{\tilde{\zeta}}{\tilde{\mathcal{G}}^2}\tilde{\varphi}_1, \quad \tilde{\varphi}_1'' = \tilde{\zeta}\,\tilde{\psi}_1'', \tag{7.1}$$

with

$$\tilde{\zeta} = \frac{x}{\rho_s}, \quad \tilde{\mathcal{G}} = \frac{\gamma}{k\rho_s J_0}, \quad \tilde{\varphi}_1 = -i\tilde{\mathcal{G}}\varphi_1(\tilde{\zeta}), \quad \tilde{\psi}_1 = \psi_1(\tilde{\zeta}). \tag{7.2}$$

The auxiliary equation (5.19) specialises to

$$\left(\frac{\bar{d}_e^2}{\rho_s^2} + \frac{\tilde{\zeta}^2}{\tilde{\mathcal{G}}^2}\right)\tilde{\chi}'' - 2\frac{\bar{d}_e^2}{\rho_s^2}\frac{\chi'}{\tilde{\zeta}} - \left(1 + \frac{\tilde{\zeta}^2}{\tilde{\mathcal{G}}^2}\right)\tilde{\chi} = -\frac{\tilde{\zeta}^2}{\tilde{\mathcal{G}}^2}\,\tilde{\chi}_\infty. \tag{7.3}$$

Equation (7.3) can be shown to be equivalent to (B42) of Zocco & Schekochihin (2011), although the latter has been obtained from a four-field system which also accounts for the dynamics of the reduced electron guiding centre contribution and for the parallel electron temperature perturbation (g_e and $\delta T_{\parallel,e}$, respectively, therein). These authors also solved the boundary layer problem in the coordinate space, but – also because of the different system of equations they started from – they took a different path with respect to the one we take here, in which we tackle the integration of the inner equation directly in the different wave length limits of interest. In this sense, the comparison between the boundary layer integration procedure of the aforementioned article and the one we are going to outline here is not immediate, although possible, since some different operational assumptions in the definition of the boundary layers and in the analytical technique of integration have been used in that work and in the present one. In their work, Zocco & Schekochihin (2011) identified two non-ideal integration regions where ion physics and electron physics were respectively dominating. In these two regions, they sought the solutions of their auxiliary equation, from which they computed the magnetic flux function ψ in the electron and ion region ($A_{\parallel,e}$ and $A_{\parallel,i}$ in their notation, respectively, which, in this work, map into the solution ψ that we will compute in the innermost and outermost non-ideal regions) by assuming in the large- and small-wavelength limit some heuristic

https://doi.org/10.1017/S0022377822001088 Published online by Cambridge University Press

orderings (*a posteriori* verified) in terms of Δ' and what they named the 'reconnection region' ($\delta_{\rm in}$, in their notation). As we will later discuss (§ 8), the characteristic width of their 'reconnection region', $\delta_{\rm in}$, differs from that of the innermost boundary layer that we are going to identify (δ_1). However, in some regimes, δ_{in} can be interpreted in the light of a further characteristic scale length, which we will introduce in § 10 (namely, what we will call $(\Delta'_{v_y})^{-1}$). In the following, we are going to adopt an integration procedure based on the integral representation of hypergeometric functions, whereas, in their work, (Zocco & Schekochihin 2011) used a perturbative method to obtain a closed form solution for $A_{\parallel,e}$. Note that, so far, the boundary layers have not yet been identified here.

7.2. *Boundary layers in the non-ideal region for $\rho_s^2/d_e^2 \gg 1$*

We now specialise the condition $\rho_s \gtrsim d_e$ by making the assumption $\rho_s^2/\bar{d}_e^2 \gg 1$, which requires a sufficiently large scale separation between $\bar{d}_e$ and $\rho_s \geq \bar{d}_e$. Note that this is henceforth the strongest assumption about the relative ordering of the non-ideal parameters at play, which is done in this analysis for tearing modes in the warm-electron regime. Nevertheless, the quantitative results obtained in this way are usually applied also for $\rho_s \gtrsim \bar{d}_e$: numerical calculations in a wide interval of the parameter space (Betar *et al.* 2020) suggest that the condition $\rho_s > \bar{d}_e/10$ can be assumed for the validity of the results we are going to obtain below. In the interval $\rho_s/10 \lesssim \bar{d}_e \lesssim 10\rho_s$, a transition from power-law scalings of the cold limit of § 6 to those of the warm limit that we are going to discuss here is observed.

7.2.1. *Outermost boundary layer*

Assuming $\rho_s^2/\bar{d}_e^2 \gg 1$, (7.1) becomes

$$\tilde{\psi}_1 - \frac{\tilde{\zeta}^2}{\bar{\mathcal{G}}^2}\tilde{\psi}_1'' = -\frac{\tilde{\zeta}}{\bar{\mathcal{G}}^2}\tilde{\varphi}_1, \quad \tilde{\varphi}_1'' = \tilde{\zeta}\tilde{\psi}_1'' \tag{7.4}$$

and (7.3) reads

$$\tilde{\chi}'' - \left(1 + \frac{\tilde{\mathcal{G}}^2}{\tilde{\zeta}^2}\right)\tilde{\chi} = -\tilde{\chi}_\infty. \tag{7.5}$$

These equations must be assumed to be valid in an interval where spatial scales are comparable to ρ_s but larger than $\bar{d}_e$, that is, $\bar{d}_e/\rho_s \lesssim \tilde{\zeta} \ll 1$, where the first inequality is meant in the sense discussed above. Therefore, restriction to this interval formally corresponds to take $\bar{d}_e = 0$ in (5.4). The integration of (7.8) and the matching of their solutions with $\psi_{\rm out}$ of the ideal region via (3.5) and (3.6) formally identifies the outermost boundary layer of width

$$\delta_2 = \rho_s. \tag{7.6}$$

7.2.2. *Innermost boundary layer*

Of course, since the formation of the X-point via reconnection requires $\bar{d}_e \neq 0$, a second, innermost boundary layer can be defined in a region where both scales $\bar{d}_e$ and ρ_s matter. The width δ_1 of this second boundary layer does not necessarily correspond to the scale $\bar{d}_e$ (if it were so, the condition $\delta_1 \ll \delta_2$ would require $\bar{d}_e \ll \rho_s$, which is an even stronger restriction than that defining the validity of (7.6)). To identify this inner boundary layer, we can look back to (7.1) and (7.3) or to ((5.9) and (5.10) and (5.19)) and notice that the two terms in parentheses, in which there is an explicit dependence on both ρ_s and $\bar{d}_e$, are comparable (regardless of the definition of ℓ and $\mathcal{G}$) if $(\zeta\rho_s)^2/(\mathcal{G}\bar{d}_e)^2 \sim 1$. In dimensional

https://doi.org/10.1017/S0022377822001088 Published online by Cambridge University Press

units, this means $xk\rho_s J_0/(\gamma\bar{d}_e) \sim 1$, which suggests that we introduce the normalisation scale $\ell = \gamma\bar{d}_e/(k\rho_s J_0)$. Using then in (5.9) and (5.10) the change of coordinates and variables expressed by

$$\zeta = \frac{x}{\ell} = \frac{xk\rho_s J_0}{\gamma\bar{d}_e}, \quad \mathcal{G} = \frac{\rho_s}{\bar{d}_e}, \quad \varphi_1 = -\mathrm{i}\mathcal{G}\varphi_1(\zeta), \quad \psi_1 = \psi_1(\zeta), \tag{7.7}$$

we write

$$\psi_1 - \frac{\bar{d}_e^2}{\ell^2}\left(1+\zeta^2\right)\psi_1'' = -\frac{\zeta}{\mathcal{G}^2}\varphi_1, \quad \varphi_1'' = \zeta\psi_1''. \tag{7.8}$$

Using the definition of $\mathcal{G}$ in (7.7) and the fact that $\rho_s^2/\bar{d}_e^2 \gg 1$, one sees that in this interval, $\zeta\varphi_1/\mathcal{G}^2 \sim \zeta^2\psi_1\bar{d}_e^2/(J_0^2)\rho_s^2 \ll \psi_1$ so that (7.8) can be approximated as

$$\psi_1 - \frac{\bar{d}_e^2}{\ell^2}\left(1+\zeta^2\right)\psi_1'' = 0, \quad \varphi_1'' = \zeta\psi_1'', \tag{7.9}$$

and with the same normalisation, (7.3) (or (5.19)) becomes

$$(1+\zeta^2)\chi'' - \frac{2}{\zeta}\chi' - \frac{\ell^2}{\bar{d}_e^2}\chi = -\zeta^2\chi_\infty. \tag{7.10}$$

Note that *in the definitions above, we have used the same symbols for ℓ, $\mathcal{G}$ and ζ, previously introduced in (5.8)*, since the different regime of interest here should not induce any confusion with those symbols used in § 6. Also note that to avoid unnecessary burdens to notation in the following calculations, *we have used for $\psi_1(\zeta)$ and $\varphi_1(\zeta)$ the same symbol that we use everywhere else for $\psi_1(x)$ and $\varphi_1(x)$*. This, also, should not cause any confusion as the argument of the function will be later specified in the few cases where the two meanings could be confounded.

Later in this section, we will proceed with the integration of these solutions and with their matching. It is therefore reasonable to postulate the innermost layer width to be

$$\delta_1 = \frac{\gamma\bar{d}_e}{k\rho_s J_0}, \tag{7.11}$$

which we will later show to be the case, indeed, although we remind that the identification $\delta_1 \to \ell$ formally requires us to *a posteriori* verify that $\delta_1 \ll \rho_s \ll 1$. From now on, we will therefore write δ_1 defined by (7.11) in place of ℓ defined by (7.7).

7.3. *Integration strategy in the warm-electron regime for $\rho_s^2/\bar{d}_e^2 \gg 1$*

We can now better establish the integration strategy for this problem, which has been generally outlined at the end of § 3. We have identified three overlapping spatial intervals of the integration domain in which different limits of the eigenvalue equations hold. For practical reasons, these can be identified in terms of the variable $\tilde{\zeta}$ introduced in (7.1) and (7.2).

(i) The innermost region $x \le \delta_1$, where $\delta_1 = \gamma\bar{d}_e/(k\rho_s J_0)$, to be yet quantified, and (7.9)- and (7.10) are valid. This integration domain applies for $\tilde{\zeta} \ll 1$, i.e. for $x \ll \rho_s$.
(ii) The intermediate region $\delta_1 \ll x \le \delta_2$ where $\delta_2 = \rho_s$ and (7.4) and (7.5) hold. This integration domain applies for $\tilde{\zeta} \sim 1$, i.e. for $\delta_1 \ll x \ll a$.

https://doi.org/10.1017/S0022377822001088 Published online by Cambridge University Press

(iii) The outer region valid for x such that $\delta_2 \ll x$, whose governing equations are those of ideal MHD. Here, (4.2) is used. This integration domain applies for $\tilde{\zeta} \gg 1$, i.e. for $x \sim a$.

Two matching regions can be therefore identified.

(a) In the interval $\delta_1 < x < \delta_2$, the solution $\chi(\zeta)$ of (7.10) is matched with solution $\tilde{\chi}(\tilde{\zeta})$ of (7.5) according to $\lim_{\zeta\to\infty} \chi(\zeta) = \lim_{\tilde{\zeta}\to 0} \tilde{\chi}(\tilde{\zeta})$.

(b) In the interval $\delta_2 < x < a$, the solution $\tilde{\chi}(\tilde{\zeta})$ of (7.5) (corresponding to $\tilde{\psi}_1(\tilde{\zeta})$ and $\tilde{\varphi}_1(\tilde{\zeta})$ of (7.4)) is matched with the solutions $\psi_{\text{out}}(x)$ and $\varphi_{\text{out}}(x)$ of (4.1) and (4.2) according to $\lim_{\tilde{\zeta}\to\infty} \tilde{\psi}_1(\tilde{\zeta}) = \lim_{x\to 0} \psi_{\text{out}}(x)$ and $\lim_{\tilde{\zeta}\to\infty} \tilde{\varphi}_1(\tilde{\zeta}) = \lim_{x\to 0} \varphi_{\text{out}}(x)$.

Notice that the matching conditions also generally depend on the wavelength range, that is, on the value of Δ', which rules the solution in the ideal region. This can influence the integration strategy, as outlined in § 5.5.

Before solving (7.1) or (7.3) in both the inner and the outer regions, and then matching the corresponding solutions to obtain the general solution of the problem, it is useful to discuss (see § 7.3.1) a general method that can be used to solve equations having the form of (7.9). This method is based on the integration in the complex plane via representation by means of hypergeometric functions.

7.3.1. *Solution of the equation in the innermost interval ($x \ll \delta_1$) via integral representation of hypergeometric functions*

Equation (7.9) is a second-order ordinary differential equation that in the complex plane has three singular points at $\zeta = \pm i$ and $\zeta = \infty$. Therefore, employing some transformations, it can be written in the standard form of a hypergeometric equation. This suggests that we look for the solution of (7.9) and (7.10) in terms of hypergeometric functions. Inspired by the integral representation of hypergeometric functions, we can thus look for a solution of (7.9) of the form

$$\psi_1 = \frac{1}{2\pi \mathrm{i}} \oint_C F(s)(1+\zeta^2)^s \,\mathrm{d}s, \tag{7.12}$$

where C is a closed contour in the complex plane which starts at $-\infty$ of the real axis, goes around the singularities of the function $F(s)$ (it will turn out that these singularities are given by an infinite number of simple poles of $F(s)$) and then returns back to $-\infty$. This representation will allow us to employ the residue theorem which states that ψ_1 equals the sum of residues enclosed by the contour C. The second derivative of ψ_1 becomes

$$\psi_1'' = \oint_C 2s(2s-1)F(s)(1+\zeta^2)^{s-1}\,\mathrm{d}s - \oint_C 4s(s-1)F(s)(1+\zeta^2)^{s-2}\,\mathrm{d}s. \tag{7.13}$$

Shifting the operator in the second term by taking $s' = s+1$, (7.13) reads

$$\psi_1'' = \oint_C 2s(2s-1)F(s)(1+\zeta^2)^{s-1}\,\mathrm{d}s - \oint_C 4s(s+1)F(s+1)(1+\zeta^2)^{s-1}\,\mathrm{d}s. \tag{7.14}$$

Substituting the previous relation in (7.9), one obtains an expression stating that the integral of $(1+\zeta^2)^s$ times a function of s equals zero. A sufficient condition for its validity

https://doi.org/10.1017/S0022377822001088 Published online by Cambridge University Press

is to set to zero the function of s, which reads

$$[2s(2s-1)-(\delta_1/\bar{d}_e)^2]F(s)-4s(s+1)F(s+1)=0. \tag{7.15}$$

To get an insight on the form of $F(s)$, let us write $F(s+k)$ in terms of $F(s)$ by using (7.15). After a little algebra, we obtain

$$F(s+1)=\frac{\left(s-\frac{\alpha}{2}\right)\left(s-\frac{\beta}{2}\right)}{s(s+1)}F(s), \tag{7.16}$$

where $\alpha=\frac{1}{2}-\nu$, $\beta=\frac{1}{2}+\nu$ and $\nu=(1/4+(\delta_1/\bar{d}_e)^2)^{1/2}$. Then,

$$F(s+j)=\frac{\left(s-\frac{\alpha}{2}\right)_j\left(\frac{s-\beta}{2}\right)_j}{(s)_j(s+1)_j}F(s), \tag{7.17}$$

where

$$(q)_j\equiv q(q+1)\cdots(q+j-1)=\frac{\Gamma(q+j)}{\Gamma(q)} \tag{7.18}$$

is the so-called 'Pochhammer symbol' defined in terms of the Γ-function (see Abramowitz & Stegun 1964, § 6.1.22). Motivated by the form of (7.17) one can look for a function $F(s)$ expressed as a combination of Gamma functions, that is,

$$F(s)=\frac{\Gamma(s+a)\Gamma(s+b)}{\Gamma(s+c)\Gamma(s+d)}. \tag{7.19}$$

If, by comparison with (7.17), we choose $c=0$ and $d=1$, (7.15) becomes

$$\left(a+b+\frac{1}{2}\right)s+ab+\left(\frac{\delta_1}{2\bar{d}_e}\right)^2=0. \tag{7.20}$$

The previous equation should be satisfied for any value of s. Therefore, one obtains

$$a+b+\frac{1}{2}=0,\quad ab+\left(\frac{\delta_1}{2\bar{d}_e}\right)^2=0, \tag{7.21}$$

which has the following solutions:

$$a=-\frac{\alpha}{2},\quad b=-\frac{\beta}{2},\quad \alpha=\frac{1}{2}-\nu,\quad \beta=\frac{1}{2}+\nu,\quad \nu=\left(\frac{1}{4}+\frac{\delta_1^2}{\bar{d}_e^2}\right)^{1/2}. \tag{7.22}$$

Here, a and b are real numbers because $(\delta_1/\bar{d}_e)^2$ is also a real number, whence it is evident that the singularities of $F(s)$ are points on the real axis. Using (7.22), $F(s)$ reads

$$F(s)=\frac{\Gamma\left(s-\frac{\alpha}{2}\right)\Gamma\left(s-\frac{\beta}{2}\right)}{\Gamma(s)\Gamma(s+1).} \tag{7.23}$$

One sees that $F(s)$ has two series of simple poles at

$$s=\frac{\alpha}{2}-m,\quad s=\frac{\beta}{2}-m,\quad m=0,1,2,3,\ldots. \tag{7.24}$$

It is also clear that the previous poles are associated with two series of residues. The first one is obtained by taking the limit $s=\alpha/2-m$ in the evaluation of the residue of

https://doi.org/10.1017/S0022377822001088 Published online by Cambridge University Press

$F(s)(1+\zeta^2)^s$,

$$\psi_\alpha = \mathrm{Res}_\alpha \equiv \sum_{m=0}^{\infty} \lim_{s\to\alpha/2-m} \left[(s+m)\Gamma\left(s-\frac{\alpha}{2}\right)\right] \frac{\Gamma(-\nu-m)(1+\zeta^2)^{\alpha/2-m}}{\Gamma\left(\frac{5}{4}-\frac{\nu}{2}-m\right)\Gamma\left(\frac{1}{4}-\frac{\nu}{2}-m\right)}$$

$$= \sum_{m=0}^{\infty} \frac{(-1)^m}{m!} \frac{\Gamma(-\nu-m)}{\Gamma\left(\frac{5}{4}-\frac{\nu}{2}-m\right)\Gamma\left(\frac{1}{4}-\frac{\nu}{2}-m\right)} (1+\zeta^2)^{\alpha/2-m}, \tag{7.25}$$

where the limit in the previous equation is obtained using the property $\Gamma(s+1) = s\Gamma(s)$, which leads to

$$\lim_{s\to-m}(s+m)\Gamma(s) = \lim_{s\to-m}(s+m)\frac{\Gamma(s+1)}{s}$$

$$= \lim_{s\to-m}(s+m)\frac{\Gamma(s+m+1)}{s(s+1)\cdots.(s+m-1)(s+m)} = \frac{(-1)^m}{m!}. \tag{7.26}$$

The second series of the residues can be calculated taking the limit $s = \beta/2 - m$. Then,

$$\psi_\beta = \mathrm{Res}_\beta = \sum_{m=0}^{\infty} \frac{(-1)^m}{m!} \frac{\Gamma(\nu-m)}{\Gamma\left(\frac{5}{4}+\frac{\nu}{2}-m\right)\Gamma\left(\frac{1}{4}+\frac{\nu}{2}-m\right)} (1+\zeta^2)^{\beta/2-m}. \tag{7.27}$$

Therefore, using the residue theorem ($\oint_C f(z)\,\mathrm{d}z = 2\pi i \sum_{z\in C} \mathrm{Res}[f(z)]$), and substituting in (7.12), ψ_1 becomes

$$\psi_1 = \psi_\alpha + \psi_\beta. \tag{7.28}$$

We recall that this solution is valid as long as $x \ll \delta_2$, i.e. $x \ll \rho_s$.

The same result could be found by using the Frobenius method (see, e.g. Bender & Orszag 1978, § 3.3) by assuming a power series solution of the form $\psi_1 = \sum_{m=0}^{\infty} g_m(1+\zeta^2)^{\lambda-m}$: after substituting ψ_1 in (7.9) and using $g_0 \neq 0$, the indicial equation leads to $\lambda_1 = \alpha/2$ and $\lambda_2 = \beta/2$, where α and β are given by (7.22). The coefficients g_m for both λ_1 and λ_2 can be found by equating the coefficients of the powers of ζ to zero. In this way, one obtains again (7.25)–(7.28).

A discussion about both the convergence and the independence of solutions (7.25) and (7.27) is in Appendix E.

7.4. *Solution of the auxiliary equation for $\rho_s^2/d_e^2 \gg 1$: large-Δ' limit*

We now solve the auxiliary equation (7.10) in the large-Δ' limit. Its detailed analytical investigation becomes essential in this wavelength limit since, as we will see in § 9.3, the 'standard' heuristic derivation here (surprisingly) fails to recover the correct scaling laws.

In this wavelength limit, the solution of the auxiliary equation in the innermost region can be matched directly to the solution obtained in the outermost non-ideal region by setting $\chi_\infty = 0$, as discussed in § 5.5. From this matching, we will obtain the scaling laws for both the growth rate and the reconnecting layer width.

https://doi.org/10.1017/S0022377822001088 Published online by Cambridge University Press

7.4.1. *Solution in the innermost layer $x \leq \delta_1$*

We can solve (7.10) by following the same line of thought used to solve (7.9), as described in § 7.3.1: we thus assume a solution of the form

$$\chi(\zeta) = \frac{1}{2\pi i} \oint_C G(s)(1+\zeta^2)^s \, \mathrm{d}s. \tag{7.29}$$

After calculating the first and second derivative of (7.29) with respect to ζ, and substituting them into (7.10), one obtains the condition

$$[2s(2s-1) - (\delta_1/\bar{d}_e)^2]G(s) - 4(s+1)^2 G(s+1) = 0. \tag{7.30}$$

By noticing the similarity of the previous relation with (7.15), we look for a $G(s)$ of the form

$$G(s) = \frac{\Gamma(s+a)\Gamma(s+b)}{\Gamma^2(s+1)} = \frac{F(s)}{s}. \tag{7.31}$$

We recall that the previous equation has been written by assuming $c = d = 1$ in (7.19), and this allows us to eliminate the $(s+1)^2$ coefficient in (7.30). In (7.31), we have also used $\Gamma^2(s+1) = s\Gamma(s)\Gamma(s+1)$. This choice leads us again to (7.21) and, therefore, to the same values for a and b which are given by (7.22), meaning that both (7.19) and (7.31) have the same infinite series of poles, as can be expected from the definition of χ expressed by (7.29). Therefore, the general solution of (7.10) reads

$$\chi_{\mathrm{in}}(\zeta) = \chi_\alpha(\zeta) + \chi_\beta(\zeta), \tag{7.32}$$

where

$$\chi_\alpha(\zeta) = \sum_{m=0}^{\infty} \frac{(-1)^m}{m!} \frac{\Gamma(-\nu-m)}{\Gamma^2\left(\frac{5}{4} - \frac{\nu}{2} - m\right)} (1+\zeta^2)^{\alpha/2-m}, \tag{7.33}$$

$$\chi_\beta(\zeta) = \sum_{m=0}^{\infty} \frac{(-1)^m}{m!} \frac{\Gamma(\nu-m)}{\Gamma^2\left(\frac{5}{4} + \frac{\nu}{2} - m\right)} (1+\zeta^2)^{\beta/2-m}. \tag{7.34}$$

We close the discussion in this section by noticing that the leading terms in (7.32) are $(1+\zeta^2)^{\alpha/2}$ and $(1+\zeta^2)^{\beta/2}$. Therefore, we can look for an approximate asymptotic solution of the form

$$\chi_{\mathrm{in}}(\zeta) \approx \chi_{\mathrm{in}}^{\mathrm{appr}}(\zeta) = A(1+\zeta^2)^{\alpha/2} + B(1+\zeta^2)^{\beta/2} + C, \tag{7.35}$$

where A, B and C are constants. Their values will be estimated by matching the solutions in the different regions and by applying the constraints at $\zeta = 0$, which we are going to obtain in § 7.4.2. Note that for limit $\zeta \to \infty$, (7.35) can be further approximated to

$$\chi_{\mathrm{in}}(\zeta) \approx \chi_{\mathrm{in}}^{\mathrm{appr}}(\zeta) = A\zeta^\alpha + B\zeta^\beta + C. \tag{7.36}$$

https://doi.org/10.1017/S0022377822001088 Published online by Cambridge University Press

7.4.2. *Constraints at the origin*

Any solution of the auxiliary equation must satisfy the constraints below that follow from the definition of $\chi(\zeta)$ in (5.11) and from (7.9) at $\zeta = 0$:

$$\psi_1''(0) = \frac{\delta_1^2}{\bar{d}_e^2}\psi_1(0) = \chi''(0) = -\frac{\delta_1^2}{\bar{d}_e^2}\chi(0), \tag{7.37}$$

$$\psi_1^{iv}(0) = \frac{\delta_1^2}{\bar{d}_e^2}\psi_1''(0) - 2\frac{\delta_1^2}{\bar{d}_e^2}\psi_1(0) = -2\left(1 - \frac{1}{2}\frac{\delta_1^2}{\bar{d}_e^2}\right)\psi_1''(0) = -2\frac{\delta_1^2}{\bar{d}_e^2}\left(1 - \frac{1}{2}\frac{\delta_1^2}{\bar{d}_e^2}\right)\psi_1(0), \tag{7.38}$$

$$\chi^{iv}(0) = 3\psi_1^{iv}(0) = -6\left(1 - \frac{1}{2}\frac{\delta_1^2}{\bar{d}_e^2}\right)\psi_1''(0) = -6\left(1 - \frac{1}{2}\frac{\delta_1^2}{\bar{d}_e^2}\right)\chi''(0) = 6\frac{\delta_1^2}{\bar{d}_e^2}\left(1 - \frac{1}{2}\frac{\delta_1^2}{\bar{d}_e^2}\right)\chi(0). \tag{7.39}$$

These expressions will be later used in the asymptotic matching, so as to determine the free coefficients in the expression of $\chi_{\rm in}^{\rm aprr}$ in (7.35).

7.4.3. *Solution in the intermediate region, $\delta_1 \ll x \leq \delta_2$*

In this region, we look for a solution $\tilde{\chi}(\tilde{\zeta})$ of (7.3). Being interested in the large-Δ' limit, we can pose $\tilde{\chi}_\infty = 0$. Equation (7.3) then becomes the homogeneous equation

$$\tilde{\chi}'' - \left(1 + \frac{\tilde{\mathcal{G}}^2}{\tilde{\zeta}^2}\right)\tilde{\chi} = 0, \tag{7.40}$$

where '' refers to the derivative with respect to $\tilde{\zeta} = x/\rho_s$. This equation belongs to the family of modified Bessel equations (see Abramowitz & Stegun 1964, § 9.6.1). In fact, it can be transformed into the standard modified Bessel equation via the change of variable $\chi\tilde{\zeta} = \tilde{\zeta}^{1/2}u(\tilde{\zeta})$ that leads to

$$\tilde{\zeta}^2 u'' + \tilde{\zeta}u' - \left(\tilde{\zeta}^2 + \nu^2\right)u = 0, \tag{7.41}$$

where ν is given by the last of (7.22). The only solution of the previous equation that is bounded when $\tilde{\zeta} \to \infty$ (or equivalently, when $x \to \infty$) is the modified Bessel function of the second kind, that is, $u(\tilde{\zeta}) = \mathcal{K}_\nu(\tilde{\zeta})$. Therefore, (7.40) has the solution

$$\tilde{\chi}_{\rm mid}(\tilde{\zeta}) = \tilde{\zeta}^{1/2}\mathcal{K}_\nu(\tilde{\zeta}), \tag{7.42}$$

the label '$_{\rm mid}$' standing for the intermediate region domain $\delta_1 \ll x \leq \delta_2$ where it is defined. Its asymptotic behaviour as $\tilde{\zeta} \to 0$ is given by

$$\begin{aligned}\tilde{\chi}_{\rm mid}^{\rm appr} &\equiv \lim_{\tilde{\zeta}\ll 1}\tilde{\chi}_{\rm out}(\tilde{\zeta}) = \lim_{\tilde{\zeta}\ll 1}\tilde{\zeta}^{1/2}\mathcal{K}_\nu(\tilde{\zeta}) = \lim_{\tilde{\zeta}\ll 1}\tilde{\zeta}^{1/2}\left(\frac{\pi}{2}\right)\frac{\mathcal{I}_{-\nu}(\tilde{\zeta}) - \mathcal{I}_\nu(\tilde{\zeta})}{\sin(\pi\nu)} \\ &\sim \frac{2^\nu}{\Gamma(1-\nu)}\tilde{\zeta}^\alpha - \frac{2^{-\nu}}{\Gamma(1+\nu)}\tilde{\zeta}^\beta,\end{aligned} \tag{7.43}$$

where we used the relation in § 9.6.2 of Abramowitz & Stegun (1964). Here, α and β are once more given by (7.22), and $\mathcal{I}_\nu(\tilde{\zeta})$ is the modified Bessel function of the first kind,

$$\mathcal{I}_\nu(\tilde{\zeta}) \equiv \left(\frac{\tilde{\zeta}}{2}\right)^\nu \sum_{m=0}^{\infty}\frac{\left(\frac{\tilde{\zeta}^2}{4}\right)^m}{m!\Gamma(\nu+m+1)}. \tag{7.44}$$

https://doi.org/10.1017/S0022377822001088 Published online by Cambridge University Press

7.4.4. *Matching of solutions: scaling laws and eigenfunctions*

The scaling laws for both the growth rate γ and the width of the innermost layer, δ_1, are obtained from matching the solutions in the innermost and intermediate regions of the domain. This formally closes the eigenvalue problem.

To accomplish this, we start by estimating the second and the fourth derivative of $\chi_{\rm in}^{\rm appr}(\zeta)$ at $\zeta = 0$. Then we will apply the constraints at the origin written in § 7.4.2 and the condition $\lim_{\zeta\to\infty}\chi(\zeta) = \lim_{\tilde\zeta\to 0}\tilde\chi(\tilde\zeta)$, that is, $\lim_{\zeta\to\infty}\chi_{\rm in}^{\rm appr}(\zeta) = \lim_{\tilde\zeta\to 0}\tilde\chi_{\rm mid}^{\rm appr}(\tilde\zeta)$, so as to obtain the equations that will allow us to find A, B and C, and, finally, the scaling laws.

First of all, from the matching of (7.43) with (7.36), we obtain

$$A = \frac{2^{\nu}}{\Gamma(1-\nu)}\left(\frac{\delta_1}{\rho_s}\right)^{\alpha}, \quad B = -\frac{2^{-\nu}}{\Gamma(1+\nu)}\left(\frac{\delta_1}{\rho_s}\right)^{\beta}. \tag{7.45}$$

Taking the second and the fourth derivatives of $\chi_{\rm in}^{\rm appr}$ (we here omit superscript 'appr' to simplify the notation), one finds

$$\chi_{\rm in}(0) = A + B + C, \tag{7.46}$$

$$\chi_{\rm in}''(0) = A\alpha + B\beta, \tag{7.47}$$

$$\chi_{\rm in}^{iv}(0) = 6A\alpha\left(\frac{\alpha}{2} - 1\right) + 6B\beta\left(\frac{\beta}{2} - 1\right). \tag{7.48}$$

Then, using the constraint on the second derivative given by (7.37) and (7.47),

$$C = -A\left(1 + \alpha\left(\frac{\bar d_e}{\delta_1}\right)^2\right) - B\left(1 + \beta\left(\frac{\bar d_e}{\delta_1}\right)^2\right). \tag{7.49}$$

The constraints on the fourth derivative in (7.39) and on (7.48) instead lead to

$$A\alpha\left(\alpha - \left(\frac{\delta_1}{\bar d_e}\right)^2\right) + B\beta\left(\beta - \left(\frac{\delta_1}{\bar d_e}\right)^2\right) = 0. \tag{7.50}$$

Combining the previous equation with (7.45), one obtains

$$-\frac{A}{B} = \frac{\beta\left(\beta - \left(\delta_1/\bar d_e\right)^2\right)}{\alpha\left(\alpha - \left(\delta_1/\bar d_e\right)^2\right)} = 2^{2\nu}\left(\frac{\delta_1}{\rho_s}\right)^{-2\nu}\frac{\Gamma(1+\nu)}{\Gamma(1-\nu)}, \tag{7.51}$$

where we used $\alpha - \beta = -2\nu$. For small values of $(\delta_1/\bar d_e)$, (7.22) gives $\nu \approx 1/2$, $\alpha \approx -(\delta_1/\bar d_e)^2$ and $\beta \approx 1$; therefore, (7.51) becomes

$$\frac{1}{2}\left(\frac{\bar d_e}{\delta_1}\right)^4\left(1 - \left(\frac{\delta_1}{\bar d_e}\right)^2\right) = 2\frac{\Gamma\left(\frac{3}{2}\right)}{\Gamma\left(\frac{1}{2}\right)}\left(\frac{\rho_s}{\delta_1}\right). \tag{7.52}$$

Using $\Gamma(3/2) = \Gamma(1/2)/2 = \sqrt{\pi}/2$ and $(\delta_1/\bar d_e)^2 \ll 1$ (to be verified *a posteriori*), the equation above implies

$$\delta_1 \sim \rho_s^{-1/3}\bar d_e^{4/3} \tag{7.53}$$

https://doi.org/10.1017/S0022377822001088 Published online by Cambridge University Press

whence, using the definition in (7.11), one obtains

$$\gamma \sim k\rho_s^{2/3}\bar{d}_e^{4/3}. \tag{7.54}$$

Specialising (7.53) and (7.54) to the purely resistive regime, $\bar{d}_e = (S^{-1}/\gamma)^{1/2}$, one recovers the result of Pegoraro & Schep (1986) for the growth rate (cf. (33) therein and also (20) in Pegoraro *et al.* 1989) and of Zocco & Schekochihin (2011) for δ_1 (cf. δ_η in (B100), therein),

$$\gamma \sim k^{6/7}\rho_s^{4/7}S^{-1/7}, \quad \delta_1 \sim k^{-4/7}\rho_s^{-5/7}S^{-4/7}. \tag{7.55}$$

Specialising the same equations to the purely collisionless regime, $\bar{d}_e = d_e$, one recovers instead the result of Porcelli (1991) for both for the growth rate ((8), therein) and for the innermost layer width (quantity σ, defined therein above (7); see also Bhattacharjee, Germaschewski & Ng 2005),

$$\gamma \sim k\rho_s^{2/3}d_e^{1/3}, \quad \delta_1 \sim \rho_s^{-1/3}d_e^{4/3}. \tag{7.56}$$

In both the purely resistive and the collisionless case, the conditions $\delta_1^2 \ll \bar{d}_e^2$ and $\delta_1 \ll \delta_2 \sim \rho_s$ we had previously heuristically assumed, are *a posteriori* verified.

Finally, by looking at the definition of χ, it is obvious that $\psi_1 \approx \chi_{\text{in}}^{\text{appr}}$ when $x \ll \delta_1$, since $x\psi_1' \sim x\psi_1/\delta_1 \ll 1$. Therefore, substituting the values of ν, α, β, $\mathcal{G}$ and δ_1 in (7.35), one obtains for the inner layer

$$\lim_{x\ll\delta_1}\psi_1 \simeq \frac{2^{1/2}}{\Gamma(1/2)}\left(\frac{\delta_1}{\rho_s}\right)^{-\delta_1^2/\bar{d}_s^2}\left(1+\frac{x^2}{\delta_1^2}\right)^{-\delta_1^2/\bar{d}_s^2} - \frac{2^{-1/2}}{\Gamma(3/2)}\left(\frac{\delta_1}{\rho_s}\right)\left(1+\frac{x^2}{\delta_1^2}\right)^{1/2} + \left(\frac{\delta_1}{\rho_s}\right)\left(1+\frac{\bar{d}_s^2}{\delta_1^2}\right). \tag{7.57}$$

Integrating (5.12) and using (7.35), one finds for $x \ll \delta_1$,

$$\lim_{x\ll\delta_1}\varphi_1 \simeq \sum_{m=0}^{\infty}\left[\frac{2^{1/2}}{\Gamma(1/2)}\left(\frac{\delta_1}{\rho_s}\right)^{-\delta_1^2/\bar{d}_s^2}\binom{-\delta_1^2/\bar{d}_s^2}{m}_b - \frac{2^{-1/2}}{\Gamma(3/2)}\left(\frac{\delta_1}{\rho_s}\right)\binom{-1/2}{m}_b\right]\left(\frac{x}{\delta_1}\right)^{2m+1} + \left(\frac{\delta_1}{\rho_s}\right)\left(1+\frac{\bar{d}_s^2}{\delta_1^2}\right)\left(\frac{x}{\delta_1}\right), \tag{7.58}$$

where

$$\binom{r}{m}_b = \frac{r(r-1)\cdots(r-m+1)}{m!} = \frac{(r)_m}{m!} \tag{7.59}$$

is the usual binomial coefficient, generalised for real values of the argument r.

Notice that for $x \leq \delta_1$, the dominant term in (7.58) is the one with $m = 0$. Therefore, to the lowest order, φ can be approximated as $\varphi \sim x$. Figure 8 shows the spatial profile of ψ_1, $\chi_{\text{in}}^{\text{appr}}$ and $x\psi_1'$ in blue, black and orange colours, respectively, in a sub-interval of the integration domain. These profiles have been computed numerically by solving the eigenvalue problem for ψ_1 and φ_1 with the solver of Betar *et al.* (2020) and using the definitions in (7.36). We can this way numerically verify that $\chi_{\text{in}}^{\text{aprr}} \approx \psi_1$ within the innermost layer with $|x| \ll \delta_1$, in agreement with the previous discussion.

The eigenfunctions (7.57) and (7.58) agree with the behaviour of the perturbed current density profile provided by Pegoraro & Schep (1986) in the inner layer for the warm-resistive regime ($\bar{d}_e = (S^{-1}/\gamma)^{1/2}$), which had been already numerically verified by Betar *et al.* (2020).

https://doi.org/10.1017/S0022377822001088 Published online by Cambridge University Press

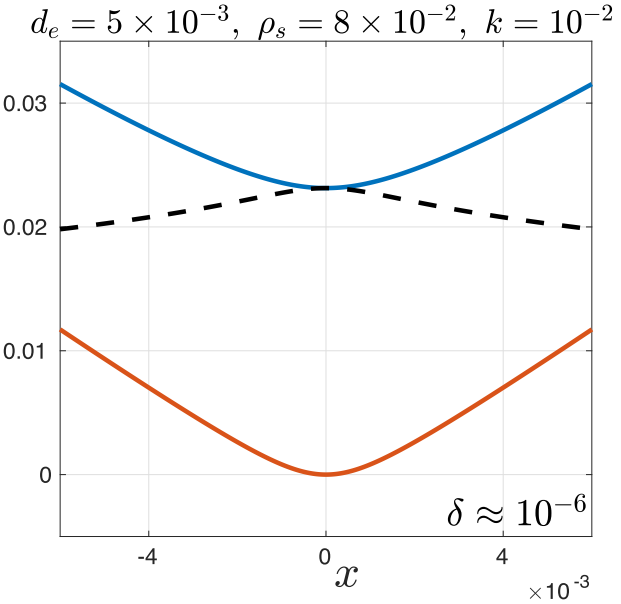

FIGURE 8. Profiles of ψ_1 (blue), $\chi_{\rm in}^{\rm appr}$ of (7.46) (black-dashed) and $x\psi_1'$ (orange) in the reconnection layer around the neutral line: these profiles are obtained by numerical integration of the complete eigenvalue problem and should be compared to the approximated analytical solutions ((7.57) and (7.58)). The width of reconnection layer, evaluated as it will be specified in § 7, is $\delta = \delta_1 \simeq 10^{-6}$. The physical parameters of the numerical integration performed with the solver of Betar *et al.* (2020) in the large-Δ' limit are shown in the figure.

7.5. *Solution of the linear equations for $\rho_s^2/d_e^2 \gg 1$: small-Δ' limit*

In the small-Δ' limit, we use again the constant-ψ approximation, as we already did in the integration of the cold-electron limit in § 6.2. Figure 9 shows the appropriateness of this assumption also in the warm-electron regime: it displays the profile of ψ_1 numerically computed with the eigenvalue solver of Betar *et al.* (2020) in the collisionless regime for $d_e = 2 \times 10^{-2}$, $\rho_s = 5 \times 10^{-3}$ and for a value of $k = 1.7$, which corresponds to $\Delta'(k) = 3.3$ and $\delta_1 \simeq 2.4 \times 10^{-6}$ (evaluated according to the definition in (8.3) – see later).

Therefore, we write $\psi_1 = c_0$ in the whole non-ideal region and, as discussed in § 5.5, this allows us to more conveniently perform the integration by looking at the equations for ψ_1 and φ_1 rather than the auxiliary equation. In this way, (7.1) can be combined in the form

$$\left(1 + \frac{\rho_s^2}{\bar{d}_e^2}\frac{\tilde{\zeta}^2}{\tilde{\mathcal{G}}^2}\right)\tilde{\varphi}_1'' = \frac{\rho_s^2}{\bar{d}_e^2}\frac{\tilde{\zeta}^2}{\tilde{\mathcal{G}}^2}\tilde{\varphi}_1 + c_0\frac{\rho_s^2}{\bar{d}_e^2}\tilde{\zeta}. \tag{7.60}$$

The results of § 8.3 in the small-Δ' cold-electron limit are recovered by neglecting the $\rho_s^2\tilde{\zeta}^2\tilde{\varphi}_1''/(\bar{d}_e^2\tilde{\mathcal{G}}^2)$ contribution in the left-hand side term of (7.60). Its presence here makes an intermediate matching region also appear in this wavelength limit.

This can be seen in figure 10, where the results of a numerical integration performed in the small-Δ' limit of the warm collisionless regime ($\bar{d}_e = d_e$) with the solver of Betar *et al.* (2020) are shown. The blue curve corresponds to the $\rho_s^2\tilde{\zeta}^2\tilde{\varphi}_1''/(\bar{d}_e^2\tilde{\mathcal{G}}^2)$ term in (7.60). Its strong variation close to the neutral line is concentrated in a narrow region much

https://doi.org/10.1017/S0022377822001088 Published online by Cambridge University Press

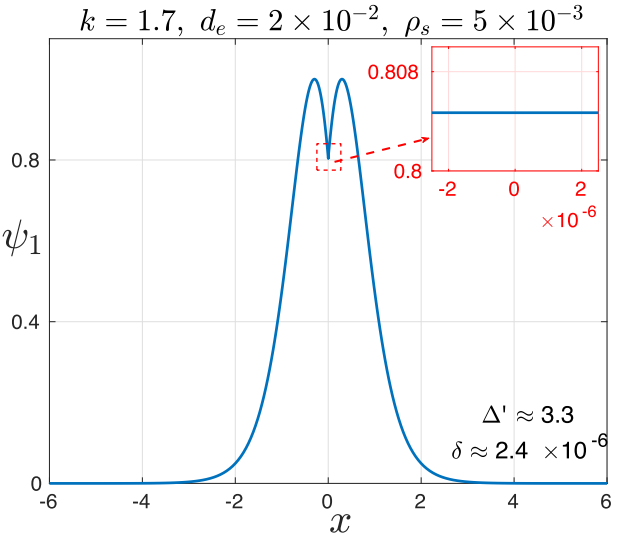

FIGURE 9. Spatial profile of ψ_1, numerically computed with the eigenvalue solver of Betar *et al.* (2020) in the collisionless regime for a choice of the parameters $d_e = 2 \times 10^{-2}$, $\rho_s = 5 \times 10^{-3}$, and for a value of $k = 1.7$. These values correspond to $\Delta'(k) = 3.3$ and to $\delta = \delta_1 \simeq 2.4 \times 10^{-6}$, evaluated according to the definition in (8.3) introduced next. The smaller box inserted at the top right-hand corner of the figure shows a zoom of the solution inside the innermost layer of width $\sim \delta = \delta_1$, in which the appropriateness of the constant-ψ_1 condition is evidenced.

smaller than $\delta_2 = \rho_s$, which is of the order of δ_1 (evaluated from the numerically computed eigenfunction, as it will be discussed in § 8). The green curve corresponds instead to the $\tilde{\varphi}_1''$ term in (7.60), i.e. to the first left-hand side contribution between parentheses, whereas the orange curve corresponds to the first term on the right-hand side of (7.60), $\rho_s^2\tilde{\zeta}^2\tilde{\varphi}_1/(\bar{d}_e^2\tilde{\mathcal{G}}^2)$. This term can be neglected with respect to the one corresponding to the blue curve. For completeness, the contribution of the last right-hand side term of (7.60), $c_0\rho_s^2\tilde{\zeta}^2/\bar{d}_e^2$, is shown as the black, dashed line. From the comparison of these contributions, one verifies the appropriateness of the hypotheses justifying (7.4).

Thus, an intermediate region, corresponding to the interval $\delta_1 < |x| \lesssim \delta_2$ of § 7.2.1, can be recognised: here, (7.4) hold, which we can combine in the form

$$\tilde{\zeta}\tilde{\varphi}_1'' = \tilde{\zeta}\tilde{\varphi}_1 + c_0\bar{\mathcal{G}}^2. \tag{7.61}$$

However, as discussed in § 5.5, it is not necessary here to first perform the integration of (7.61), since the constant-ψ condition holds in this case also in the innermost region.

7.5.1. *Matching and scalings in the non-ideal region $x \ll 1$*

Combining (7.8) is in practice equivalent – except for the chosen normalisation – to neglecting the $\sim \tilde{\zeta}^2\tilde{\varphi}_1/$ term in (7.60). Using the latter, where we recall lengths are normalised to ρ_s, we write

$$\tilde{\varphi}_1'' = c_0\frac{\rho_s^2}{\bar{d}_e^2}\frac{\tilde{\zeta}}{1 + \rho_s^2\tilde{\zeta}^2/(\bar{d}_e^2\tilde{\mathcal{G}}^2)}. \tag{7.62}$$

https://doi.org/10.1017/S0022377822001088 Published online by Cambridge University Press

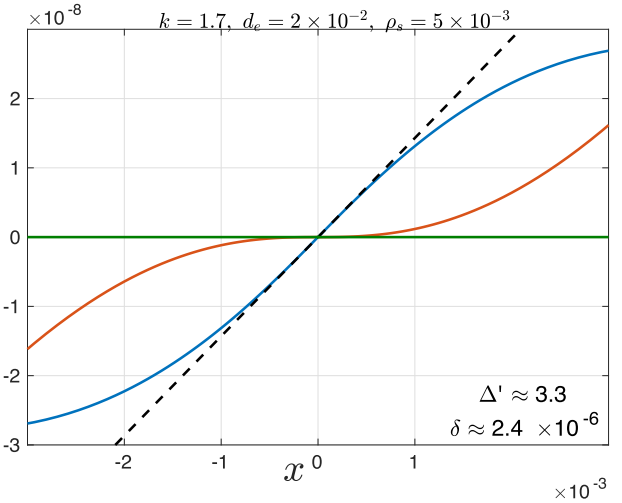

FIGURE 10. Comparison of the spatial profiles of the terms $\rho_s^2/(\bar{d}_e^2\tilde{\mathcal{G}}^2) \times \tilde{\zeta}^2\tilde{\varphi}_1''$ (blue curve), of $\rho_s^2/(\bar{d}_e^2\tilde{\mathcal{G}}^2) \times \tilde{\zeta}^2\tilde{\varphi}_1$ (orange curve) and of $\tilde{\varphi}_1$ (green curve) of (7.60), in a region of the domain with width $|x| < \delta_2 = \rho_s$. The parameters of the numerical integration performed with the eigen-solver of Betar *et al.* (2020) in the small-Δ' limit are shown at the top of the figure. The value of $\delta = \delta_1$ in the bottom right corner has been evaluated according to the definition in (8.3).

The equivalent of (3.10), obtained after integration of the second of (7.1) (cf. it also with (6.16)) reads

$$\int_{-\tilde{Z}}^{+\tilde{Z}} \tilde{\psi}_1''\,\mathrm{d}\tilde{\zeta} = \int_{-\tilde{Z}}^{+\tilde{Z}} \frac{\tilde{\varphi}_1''}{\tilde{\zeta}}\,\mathrm{d}\tilde{\zeta}, \tag{7.63}$$

where $\tilde{Z} = X/\rho_s \gg 1$ is a matching point in the interval $\delta_1 \ll X \ll \delta_2$ in units of $L_0 = a$. Use of (3.9) allows one to establish the matching conditions with the outer solution by making explicit the dependence on Δ': writing therefore $\int_{-\tilde{Z}}^{+\tilde{Z}} \tilde{\psi}_1'' = c_0\Delta'$ and substituting (7.62) in (7.63), one obtains

$$c_0\Delta' = \int_{-\tilde{Z}}^{+\tilde{Z}} \frac{\tilde{\varphi}_1''}{\tilde{\zeta}}\,\mathrm{d}\tilde{\zeta} = c_0\frac{\rho_s^2}{\bar{d}_e^2}\int_{-\tilde{Z}'}^{+\tilde{Z}'} \frac{\mathrm{d}\tilde{\zeta}}{1+\varrho^2\tilde{\zeta}^2} = c_0\frac{\rho_s^2}{\varrho\bar{d}_e^2}\arctan(\varrho\tilde{\zeta})\Big|_{-\tilde{Z}}^{+\tilde{Z}}, \tag{7.64}$$

where $\varrho \equiv \rho_s/(\bar{d}_e\tilde{\mathcal{G}})$. Taking the asymptotic limit $\tilde{Z} \to \infty$ and using $\arctan(\varrho\tilde{\zeta})|_{-\infty}^{+\infty} = \pi$, (6.16) reads

$$c_0\Delta' = c_0\pi\frac{\rho_s^2\tilde{\mathcal{G}}}{\bar{d}_e} \implies \gamma = \sqrt{\pi}J_0 k\rho_s\bar{d}_e\Delta' \implies \delta_1 \sim \Delta'\bar{d}_e^2, \tag{7.65}$$

where in the last passage, we have used the definition in (7.11) of $\delta_1 = \gamma\bar{d}_e/(k\rho_s J_0)$. We can thus explicate the scalings above in the purely collisionless and purely resistive limits.

https://doi.org/10.1017/S0022377822001088 Published online by Cambridge University Press

In the former, taking $\bar{d}_e = d_e$, one obtains

$$\gamma \sim J_0 k \Delta' \rho_s d_e, \quad \delta_1 \sim \Delta' d_e^2, \tag{7.66}$$

that is, the result of Porcelli (1991) (cf. the discussion between (8) and (9), therein). Taking instead $\bar{d}_e = S^{-1/2}\gamma^{-1/2}$, one obtains

$$\gamma \sim J_0^{2/3}(k\Delta')^{2/3}\rho_s^{2/3}S^{-1/3}, \quad \delta_1 \sim J_0^{-1/3}k^{-2/3}(\Delta')^{1/3}\rho_s^{-2/3}S^{-2/3}, \tag{7.67}$$

that is, the result first obtained by Pegoraro & Schep (1986) for the growth rate (cf. (39), therein) and by Zocco & Schekochihin (2011) for δ_1 (which maps into δ_η of (B.96), therein).

7.5.2. *Approximated eigenmodes in the non-ideal region $x \ll 1$*

Approximated expressions for the eigenmodes can be obtained by integrating (7.62) twice, and by calculating the second of these integrals by parts: one finds the following approximate formula for the eigenfunction $\tilde{\varphi}_1(x/\delta_2)$ in a spatial interval $x \lesssim \delta_2 \simeq \rho_s$ that covers the whole non-ideal region:

$$\varphi_1(x) \simeq \frac{c_0\delta_1^3}{2\bar{d}_e^2}\left\{\left(\frac{x}{\delta_1}\right)\ln\left(1+\left(\frac{x}{\delta_1}\right)^2\right) + 2\arctan\left(\frac{x}{\delta_1}\right) - 2\left(\frac{x}{\delta_1}\right)\right\}. \tag{7.68}$$

Substituting (7.68) into (7.62), using the second part of (7.8) and integrating twice by parts, gives an approximated expression for ψ_1:

$$\psi_1(x) \simeq c_0 + \frac{c_0\delta_1^2}{\bar{d}_e^2}\left\{\left(\frac{x}{\delta_1}\right)\arctan\left(\frac{x}{\delta_1}\right) - \frac{1}{2}\ln\left(1+\left(\frac{x}{\delta_1}\right)^2\right)\right\}. \tag{7.69}$$

From the expressions above, it is straightforward to find closed forms for both the magnetic field components and the current density perturbations, using their definitions $B_x(x) \equiv k\psi_1$, $B_y(x) \equiv -\partial\psi_1/\partial x$, and $J_z(x) \equiv -\delta^2\psi_1/\partial x^2$ and (7.69). These lead to

$$B_x(x) = -k\sin(ky)\psi_1(x), \quad B_y(x) = -\frac{k\delta_1 c_0}{\bar{d}_e^2}\arctan\left(\frac{x}{\delta_1}\right), \tag{7.70}$$

$$J_z(x) = -\frac{c_0}{\bar{d}_e^2}\frac{1}{1+\left(\frac{x}{\delta_1}\right)^2}. \tag{7.71}$$

In the appropriate limits, this equation corresponds to (74) of Pegoraro & Schep (1986) and to (31) of Betar *et al.* (2020).

8. Operational definition of the reconnecting layer width, δ, and other microscopic scales related to the eigenmodes

We have seen (§§ 6 and 7) that the boundary layer calculations allow one to determine the asymptotic scaling of the width of the layers, where approximate solutions of the eigenfunctions can be analytically evaluated. These characteristic widths appear as normalisation scales δ_1 and δ_2, which, although sometimes can be seen as 'natural', being suggested by the comparison of some terms in the equations (as in the cases we previously considered), are *a priori* arbitrary and are essentially determined by the algebra.

https://doi.org/10.1017/S0022377822001088 Published online by Cambridge University Press

Recognising some of these scales as indicative of the reconnecting layer width requires instead further insight (and hypothesis) of physical nature.

This is the subject we discuss in this section, where we are going to provide an operational definition allowing the measurement of the reconnecting layer width, δ, which is in agreement with previous theoretical assumptions (i.e. theoretical definitions based on some physical insight that have been used in the previous literature), and which can be useful for both numerical and experimental quantitative estimates. The appropriateness of this definition is then shown by direct comparison with boundary layer calculations of §§ 6 and 7 and by numerical verification of its asymptotic scaling.

By analysing some local properties of the derivatives of the eigenfunctions close to or on the neutral line, we also identify the asymptotic scalings of some microscopic scales, which are associated with the inverse of these spatial gradients. The relevance of these scale lengths will be shown again by comparison between the results of the boundary layer calculations and the numerical results.

To this purpose, we use the adaptive multi-precision solver discussed by Betar *et al.* (2020), which had been specifically developed to address the generalised eigenvalue problem in a slab periodic box of dimension $[-L_x/2, L_x/2]$, for k assigned. This solver uses a compact finite difference scheme of tunable precision for the derivatives on a non-uniform grid along the x-direction. The use of a non-uniform grid and of tunable precision in the calculation allow us to resolve the inner layer even for microscopic, realistic values of the non-ideal parameters: the grid spacing in the inner layer can be so chosen to be much smaller than in the outer layer to save computing time without loosing accuracy. In that work, we verified the numerical scalings predicted by boundary layer calculations in different reconnection regimes. Although the scalings in the small-Δ' regime are insensitive of the magnetic equilibrium profile, this is not the case for the large-Δ' limit, as it had been already noted in a series of works by Cross & van Hoven (1971), Van Hoven & Cross (1971), Van Hoven & Cross (1973*b*) and Van Hoven & Cross (1973*a*): in both (Betar *et al.* 2020) and in the present article, the numerical results refer to the equilibrium profile (4.3) in a numerical box with $L_x = 4\pi$.

8.1. *Notions of reconnecting layer and estimates of its width in previous literature*

The *reconnecting layer width* δ, meant as the extension of the interval around the neutral line, where the reconnection process takes place and is mostly localised, is *not per se unequivocally defined* via boundary layer calculations. Its identification requires further ansatz based on physical assumptions. Because of this, in most of the early reference papers about boundary layer calculations performed in the warm fluid–electron regime, the notion of 'reconnecting layer width' has not been explicitly used (cf. Pegoraro & Schep 1986; Pegoraro *et al.* 1989; Porcelli 1991). In this context, an early notion of 'layer width', identifiable as δ, has just been used in some kinetic models for tearing modes (cf. Drake & Lee 1977; Mahajan *et al.* 1978, 1979; Cowley *et al.* 1986). In particular, in some of these works (Drake & Lee 1977; Cowley *et al.* 1986), it has been referenced as the '*electron layer width*', because of its identification with the microscopic region dominated by electron dynamics, in contraposition to the broader 'ion layer width', where non-ideal effects are important, but at scales larger than those of electrons. In this sense, δ has been made to actually correspond to the innermost layer width, which we have named δ_1 (the 'ion layer' being practically correspondent to δ_2). This identification, which also agrees with the assumption made in cold-electron regimes (practically since the first work of Furth *et al.* (1963) – cf. also Ottaviani & Porcelli 1995) where a single non-ideal layer can

https://doi.org/10.1017/S0022377822001088 Published online by Cambridge University Press

be identified, has been made more explicit in later works (Bhattacharjee *et al.* 2005; Zocco & Schekochihin 2011; Connor *et al.* 2012*b*).

The physical argument which is at the basis of the identification $\delta \to \delta_1$, and which has been more or less explicitly stated in different works on tearing mode analysis, grounds on the idea that it is the innermost subdomain which contains the essential non-ideal physics allowing the reconnection process. For example, for $\rho_s > \bar{d}_e$, the non-ideal region extending up to $x/\rho_s \sim 1$ is not of interest in this sense, coherently with the fact that ρ_s does not allow, *per se*, the onset of tearing instabilities: it is only in the innermost layer of width δ_1 that both electron inertia (d_e) or resistivity (S^{-1}) and ion-sound FLR effects (ρ_s) are important. Because of this, δ_1 is the natural candidate to be identified as the characteristic microscopic region where magnetic lines dragged there by the flow can intersect, by thus violating the frozen-in condition. And since this cannot occur as long as magnetic lines are frozen in the electron flow (cf. comment on (2.7)), this layer is arguably dominated by electron physics, whence the appropriateness of naming it the '*electron layer*.'

Alternative, yet similar, expressions have been frequently used in the literature to characterise the layer where the electron frozen-in condition is violated. In this regard, it is worth mentioning the '*dissipation region (or layer)*', named this way with reference to the dissipation of magnetic flux in resistive reconnection (see, e.g. among many others, Parker 1973; Mandt, Denton & Drake 1994; Shay *et al.* 1998), and the probably even more common expression, '*(electron) diffusion region*'. Introduced with initial reference to the resistive magnetic diffusion in Sweet–Parker-like steady reconnection processes – see, e.g. Sonnerup (1973) and Vasyliunas (1975) – the latter expression is currently used to identify the reconnecting layer in any reconnection processes, and thus also in all regimes of tearing-type modes (see, e.g. Drake & Kleva 1991; Hesse, Forbes & Birn 1999; Le *et al.* 2013) and several other works, especially connected to astrophysical plasma research). All these notions fit with the idea of identifying the extension of the reconnecting layer with that of the reconnecting current sheet. In practically all works on magnetic reconnection explicitly touching on the subject, the scale length δ is more or less explicitly assimilated also to the characteristic width of the '*(reconnecting) current layer (or sheet)*'.

However, in spite of the vast scientific literature, spanning almost seven decades, which addresses the subject of characterising the reconnecting layer in different reconnection scenarios and regimes, no precise and generally acquired operational definition seems to exist for it. Identifying the reconnecting region and measuring the spatial profile of physical quantities inside of it is a crucial element for the modelling of reconnection processes observed in Nature or in experiments (cf. e.g. Bratenahl & Yeates 1970; Yamada *et al.* 1997; Vaivads *et al.* 2004; Yamada *et al.* 2010). Even identifying its position and extension from measurements may be a non-trivial task, and indeed specific proxies are sought for this purpose in different reconnection regimes (e.g. the quadrupolar pattern of the magnetic field for Hall-reconnection, etc.). Also, when reconnection is known or is expected to occur because of tearing-type modes, for which quite accurate analytical estimates are available, quantitative information on δ obtained from measurements can give insight on important features of the reconnection process (we will dedicate §§ 9 and 10 of this work to this point and to the heuristic interpretation of the boundary layer calculation). Moreover, once compared with theoretical estimates, this quantitative information can give indication on the dominant non-ideal effects at play. We recall indeed that the scale δ_1 obtained from boundary layer calculations is not 'trivial' (cf. §§ 9 and 10): for example, in the large-Δ' limit of the $\rho_s > \bar{d}_e$ regime, we have seen the scale δ_1 to be *asymptotically smaller than both* $\bar{d}_e$ *and* ρ_s. At the same time, despite this information being available since the first boundary layer calculations performed in the Fourier space in the warm electron regime, its interpretation in physical terms has not

https://doi.org/10.1017/S0022377822001088 Published online by Cambridge University Press

been univocal: while practically all early works agreed on recognising the non-ideal ion region to have extension of the order of ρ_s, the width of the current layer has been instead differently identified, on the basis of slightly different physical arguments, often depending on further hypotheses or heuristic estimates. For example, the current width in the linear, large-Δ', warm-collisionless regime has been also estimated to be larger than d_e (see, e.g. Drake & Kleva 1991; Ottaviani & Porcelli 1995), on the basis of the heuristic arguments developed by Drake & Lee (1977), Cowley *et al.* (1986) and then re-discussed by Zocco & Schekochihin (2011), or of the order of $\sim d_e$ (see, e.g. Grasso *et al.* 1999), based on the simple argument that d_e is the characteristic scale related to the reconnection process in collisionless regimes (see, e.g. Vasyliunas 1975). The distinction between current layer width and reconnecting layer width, which was done by Zocco & Schekochihin (2011), is a subtle point to which we will return later, at the end of § 10.5.

From all these argument follows the interest in seeking *a priori* estimates of δ, which can be of general acceptance and do not ground on boundary layer calculations but can be directly implemented by starting from experimental or numerical data.

In the context of nonlinear numerical simulations of tearing mode reconnection, different examples of the estimate of δ have been proposed in the literature. Sometimes, δ has been identified in terms of the global profile of the eigenmode superposed on the equilibrium function. For example, Ali, Li & Kishimoto (2014) have measured the width of the current sheet as the distance between the local minima of $J_{z,1}(x, y_0) + J_{z,0}(x)$ with respect to the coordinate x, and for y_0 that corresponds to the ordinate of the X-point. The current layer width has also been identified (Tenerani *et al.* 2015) by evaluating the distance between the local minima of what here we would name $B_{x,1}(x, y_0) \sim \psi_1(x)\cos(k(y - y_0))$. It can be noted that the estimate of Tenerani *et al.* (2015) relates to the numerical evaluation we later give of the inverse scale length D' (cf. (10.10) and figure 14) rather than of δ. In the context of the aforementioned work, this is however coherent since in the simulations of Tenerani *et al.* (2015), the instability of a large aspect ratio current sheet is studied, where a fastest growing mode exists (as evidenced already by Furth *et al.* 1963) for which $\Delta' \sim 1/\delta$ (cf. Loureiro *et al.* 2007; Bhattacharjee *et al.* 2009; Del Sarto *et al.* 2016; Betar *et al.* 2020). In the nonlinear simulations of Papini *et al.* (2019*b*), instead, the reference value for δ has been taken by evaluating the full width (with respect to, let us say, the x coordinate) at half-maximum of the total current J_z minus its average background value, that is, δ has been evaluated as the width at half-height of a local estimation of $J_{z,1}(x)$.

8.2. *Operational definition of the reconnecting layer width, δ, and its scalings*

Here, we propose a quantitative, operational definition for the *measurement* of δ, which differs with respect to those previously suggested in the way we estimate the current layer width, at least for tearing-type reconnection. We start indeed by noting that, in agreement with the well-known identification 'reconnecting layer $\leftrightarrow$ current sheet', this layer can be identified as the region around the neutral line in which the current density related to the perturbation is concentrated. In our notation, this current density is $J_{z,1} = -\nabla^2\psi_1$. Inside of this region, a velocity field is also concentrated, corresponding to an outflow parallel to the neutral line outwardly directed from the X-point, which is a hyperbolic point of the flow (see sketch in figure 11). In the notation used here, such a velocity field is $v_{y,1} = -\varphi_1'$.

The profiles of $J_{z,1}(x)$ and of $v_{y,1}(x)$ close to the neutral line (cf. figure 12) are qualitatively analogous, so that both their respective characteristic 'thicknesses' could be taken as candidates for δ. Therefore, by referring to the eigenfunctions only, we here consider the distance from the neutral line of the local maxima (or minima) of the gradient of the current density (J_z') and to the distance from the neutral line of the local maxima (or minima) of the vorticity (φ''). Since these two distances can in principle differ, we

https://doi.org/10.1017/S0022377822001088 Published online by Cambridge University Press

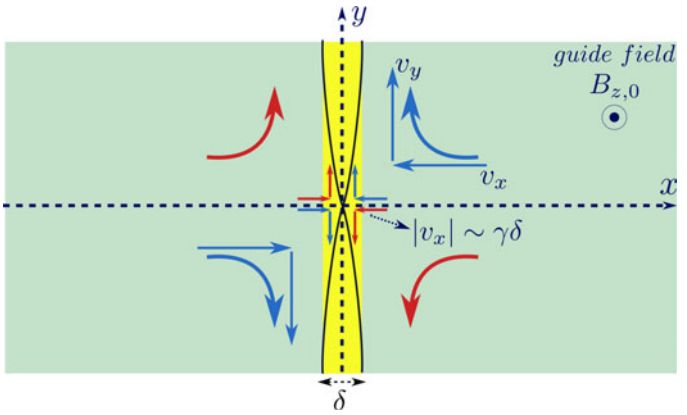

FIGURE 11. Sketch of the hyperbolic pattern of the velocity field associated with linear perturbations around the X-point. The yellow stripe represents the reconnecting layer in the vicinity of the neutral line, where a current sheet $J_{z,1}$ of width $\sim \delta$ is concentrated (the width of the magnetic island, instead, may well trespass the width of this region, during its nonlinear evolution – cf. caption of figure 2). Note that the estimate $v_{x,1} \sim \gamma\delta$, with $v_{x,1} = -ik\varphi_1$, holds inside of this region, whereas the $v_{y,1} = \varphi_1'$ component exhibits a change of sign on the neutral line and therefore displays a strong gradient across the $\Delta x \simeq \delta$ interval.

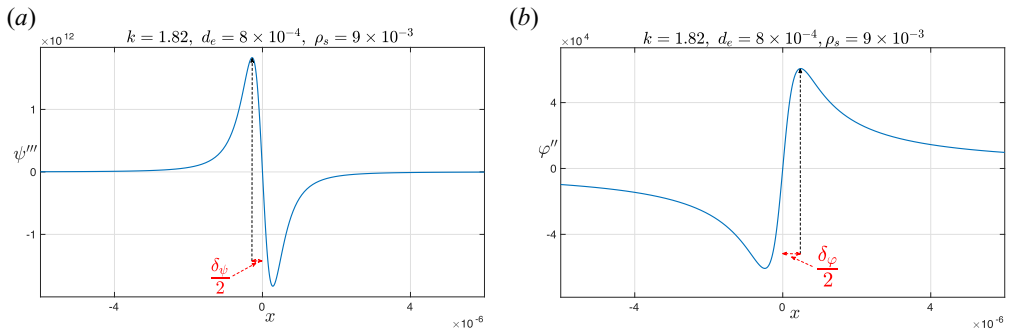

FIGURE 12. Examples of evaluation of the half-width of the current layer as the distance of the local maxima (minima) of $\psi_1''' = -J_{z,1}'$ (*a*) and of φ_1'' (*b*) from the neutral line (the parameters of the numerical calculation are indicated at the top of the panels).

respectively name them δ_ψ and δ_φ:

$$\delta_\psi \ : \quad J_{z,1}''\big|_{x=\delta_\psi} = \psi_1^{iv}\big|_{x=\delta_\psi} = 0, \qquad \delta_\varphi \ : \quad v_{y,1}''\big|_{x=\delta_\phi} = \varphi_1'''\big|_{x=\delta_\varphi} = 0. \tag{8.1}$$

As shown in figure 12, δ_ψ and δ_φ can be easily calculated once the profile of the corresponding eigenfunction has been computed.

A numerical scan performed in the whole parameter range of the regimes considered by Betar *et al.* (2020) indicates that δ_ψ and δ_φ approximatively display the same asymptotic scaling, as shown in figure 13, as an example, for the warm-collisionless reconnection regime. We can so write $\delta_\psi \sim \delta_\varphi$, even if a proportionality factor not much different from unity is present (for example, we measured $\delta_\varphi \simeq 2\delta_\psi$ in warm-collisionless RMHD with $\rho_s/d_e \simeq 10$), which seems to display a weak dependence on the non-ideal parameters involved, at least in the parameter range we have numerically investigated.

https://doi.org/10.1017/S0022377822001088 Published online by Cambridge University Press

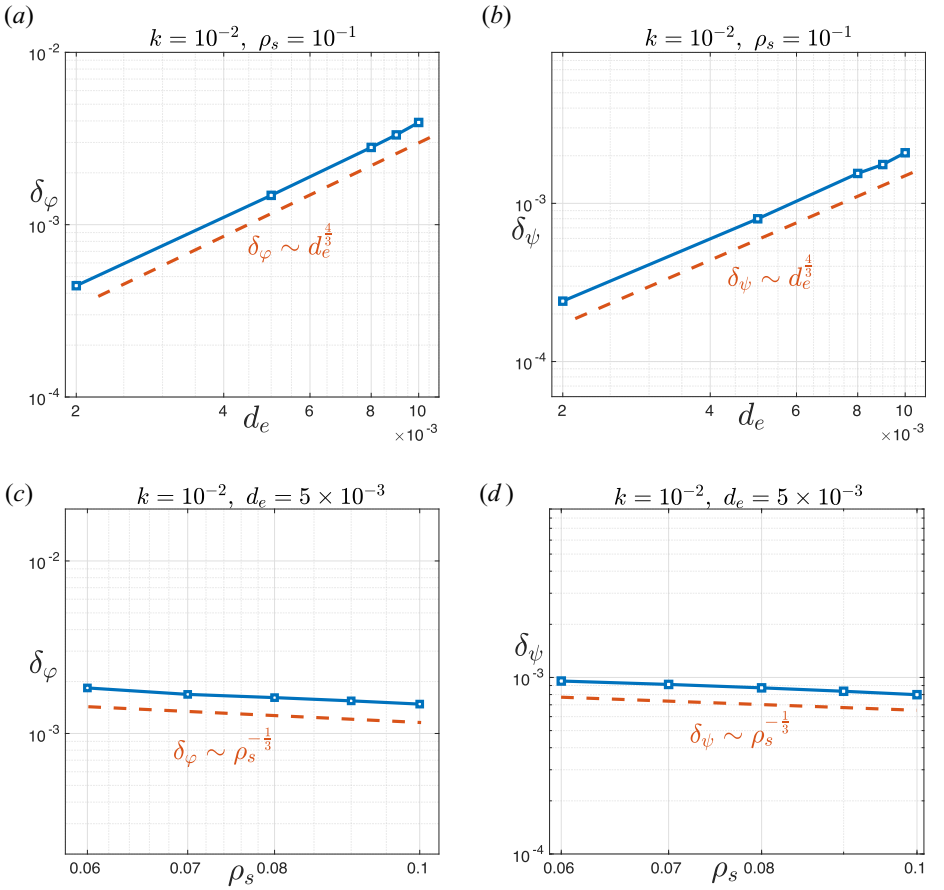

FIGURE 13. Scalings of δ_φ (*a*,*c*) and δ_ψ (*b*,*d*) calculated using the definitions given by (8.1). The scalings, shown on the different panels, prove that these two quantities follow the same scaling laws.

Based on the coherence with the numerical results that show the correspondence of the scalings of δ_1 with those of δ_ψ in all the reconnection regimes considered (also when electron–electron viscosity is included – see Betar *et al.* 2020),

we identify δ *as twice the distance from the neutral line of theinflection point of* J_z. (8.2)

Accordingly, we propose to operationally *define* the layer width as

$$\delta \equiv \delta_\psi \sim \delta_1. \tag{8.3}$$

The symbols δ_{SD} and δ_{LD} can be therefore used to indicate $\delta \equiv \delta_\psi \sim \delta_1$ in the small- and large-Δ' regimes.

8.3. *Further micro-scales related to the gradients of the eigenmodes on the neutral line*

A further ensemble of characteristic spatial scales of the system is provided by the normalised derivatives of the eigenfunctions evaluated on the neutral line. These can be shown to be related to combinations of powers of the non-ideal parameters and of δ_1.

https://doi.org/10.1017/S0022377822001088 Published online by Cambridge University Press

We define

$$\delta_{\psi}^{(N)} \equiv \left| \frac{\psi_1^{(N)}}{\psi_1} \right|_{x=0}^{-(1/N)}, \quad N = 2, 4, 6, \ldots, \tag{8.4}$$

where N is the order of the derivative with respect to the shear variable x.

These length scales can be related to the local expansion of the eigenfunctions in a neighbourhood of $x = 0$. Using the fact that both ψ_1 and $v_{y,1}(x) = \varphi_1'(x)$ are even and are continuous, at least up to the third derivative with respect to x, we can write

$$\psi_1(x) \simeq c_0 \left\{ 1 \pm \frac{1}{2} \left(\frac{x}{\delta_{\psi}^{(2)}} \right)^2 \pm \frac{1}{4!} \left(\frac{x}{\delta_{\psi}^{(4)}} \right)^4 \pm \ldots \right\}, \tag{8.5}$$

$$v_y(x) = \varphi_1'(x) \simeq q_0 \left\{ 1 \pm \frac{1}{2} \left(\frac{x}{\delta_{v_y}^{(2)}} \right)^2 \pm \frac{1}{4!} \left(\frac{x}{\delta_{v_y}^{(4)}} \right)^4 \pm \ldots \right\}. \tag{8.6}$$

Note that the coefficients of (8.6) are related to those of (8.5). Using indeed $\mathrm{d}\varphi_1(\zeta)/\mathrm{d}\zeta = \zeta \mathrm{d}\psi_1(\zeta)/\mathrm{d}\zeta - \psi_1(\zeta) - \chi_\infty$ (cf. (5.11) and (5.12)) for $\zeta = x/\delta_1$, whence $\mathrm{d}x/\mathrm{d}\zeta = \delta_1$, and taking into account the normalisation of $\varphi_1(\zeta)$, i.e. $\varphi_1(\zeta) = A\varphi_1(x)$ with $A = -i\gamma/(k\delta_1 J_0)$ in the cold-electron regime and $A = -i\rho_s/d_e$ in the warm-electron regime, one obtains

$$\frac{\mathrm{d}\varphi_1}{\mathrm{d}x} = \frac{x}{A\delta_1} \frac{\mathrm{d}\psi_1}{\mathrm{d}x} - \frac{\psi_1}{A\delta_1} - \frac{\chi_\infty}{A\delta_1}. \tag{8.7}$$

Direct substitution of ((8.5) and (8.6)) into (8.7) and comparison of equal powers of x yields

$$q_0 \sim -\frac{c_0}{A\delta_1} - \frac{\chi_\infty}{A\delta_1}, \quad \delta_{v_y}^{(N)} \sim \left(1 + \frac{\chi_\infty}{c_0} \right)^{1/N} (N-1)^{1/N} \delta_{\psi}^{(N)}. \tag{8.8}$$

Using then (5.14) and (5.17), we can write

$$q_0 \sim \frac{O(\Delta'\delta_1)}{A\delta_1} \quad \text{for } \Delta'\delta_1 \ll 1, \quad q_0 \sim -\frac{c_0}{A\delta_1} \quad \text{for } \Delta'\delta_1 \gg 1. \tag{8.9}$$

Notice that the first of (8.9) is of scarce utility here, since not accurate enough: the estimate (5.14), which identifies $\chi_\infty \sim -c_0$ by neglecting possible corrections roughly estimable as being of the order of $\sim O(\Delta'\delta_1)$, cannot be indeed used for the present calculations, as it would always yield $v_y(0) = 0$. This does not generally agree with the analytical results of the boundary layer calculations in the small-Δ' limit (cf. e.g. figure 14*c* obtained via numerical integration of the eigenvalue problem). Therefore, when needed, depending on the reconnecting regime and wavelength limit considered next, we will rely on a more accurate estimate obtained from the boundary layer solution found in the case of interest.

The scalings of some of the length scales $\delta_{\psi}^{(N)}$ are easily found to be related to those of δ_1 (and hence of $\delta \sim \delta_\psi$). This can be proven analytically. A possibility, quite generally applicable, consists in combining ((2.1) and (2.2)) by using $\varphi_0(0) = 0$ with the local expansion

$$\psi_0(x) \simeq C_0 + \frac{C_2}{2} x^2 + \frac{C_4}{4!} x^4 + \mathcal{O}(x^4), \tag{8.10}$$

and in differentiating the eigenfunctions the number of times which is needed. Note the correspondence $C_2 = J_0$ in the notation used in previous sections. The sought scalings

https://doi.org/10.1017/S0022377822001088 Published online by Cambridge University Press

can be obtained by balancing the dominant terms of the equations while taking the limit $x \to 0$, and by using the scalings of γ and δ_1 obtained from boundary layer calculations. An alternative procedure consists in the direct evaluation of these derivatives from the approximated eigenmode solutions close to the neutral line, once they are obtained by integration of the boundary layer problem.

Here, below (§ 8.3.1), we use the second procedure to compute $\delta_\psi^{(2)}$ and the former to obtain $\delta_\psi^{(4)}$.

8.3.1. *Asymptotic scalings of $\delta_\psi^{(2)}$ and of $\delta_\psi^{(4)}$*

The scalings that can be obtained for $\delta_\psi^{(2)}$ and $\delta_\psi^{(4)}$ in the different regimes are summarised in table 2.

The estimate of $\delta_\psi^{(2)}$ is of interest, since it provides a direct estimate of the peak amplitude of the current density on the neutral line during the linear stage of the tearing mode evolution. According to the values in table 2, $J_z|_{x=0} \simeq c_0/\bar{d}_e$. Also, the scale of $\delta_{v_y}^{(2)}$ is of potential interest, since it gives the characteristic curvature with respect to x of the velocity profile $v_y(x)$ on the neutral line. While, according to (8.8) and (8.9), $\delta_{v_y}^{(2)} \sim \bar{d}_e$ in the large-Δ' limit, in the small-Δ' limit, its value is typically asymptotically smaller, since it depends on the estimate of $(1 + \chi_\infty/c_0) \ll 1$ (cf. e.g. (8.21) for the cold-electron limit). These estimates are likely to be relevant for the study of the stability of the Bickley jet (Bickley 1937) related to the $v_y(x)$ velocity component, which, especially in the cold collisionless, large-Δ' regimes, nonlinearly develops along the neutral line and for $d_e^2 \gg \rho_s^2$, leads to a turbulent regime via the onset of secondary Kelvin–Helmholtz instabilities (Del Sarto *et al.* 2003, 2006). A similar feature had been observed also in early nonlinear simulations of the collisionless internal-kink mode in cylindrical geometry (Biskamp & Sato 1997) and had motivated dedicated studies of the stability of the Bickley jet in the presence of a background magnetic field aligned to it (Biskamp, Schwarz & Zeiler, 1998). The destabilisation via Kelvin–Helmholtz of a Bickley jet developing during the nonlinear stage of the collisionless reconnection process has been confirmed also in nonlinear simulations of tearing modes in three-dimensional geometry (Grasso, Borgogno & Pegoraro 2007; Grasso *et al.* 2009, 2020).

The estimate of $\delta_\psi^{(4)}$ is also of interest, since it intervenes in the modelling of the nonlinear current sheet evolution, which in the purely collisionless regime has been shown to shrink exponentially in time (Ottaviani & Porcelli 1993, 1995).

Below, we separately evaluate $\delta_\psi^{(2)}$ and $\delta_\psi^{(4)}$ so to prove the scalings reported in the table.

8.3.2. *Asymptotic scalings of $\delta_\psi^{(2)}$*

The scaling of $\delta_\psi^{(2)}$ follows from (2.1), which, in the purely collisionless limit, both 'cold' and 'warm', implies the conservation of the electron canonical momentum on the neutral line because of (8.10): $\partial_t(\psi - d_e^2\nabla^2\psi)|_{x=0} = 0$. The result can be formally extended to the resistive regime by relying again on the generalised electron skin depth $\bar{d}_e$. More precisely, regardless of the value of ρ_s, we obtain from (2.1)

$$\delta_\psi^{(2)} = \frac{\bar{d}_e}{\sqrt{1 + k^2\bar{d}_e^2}} \simeq \bar{d}_e, \tag{8.11}$$

https://doi.org/10.1017/S0022377822001088 Published online by Cambridge University Press

Length scale	Cold regimes				Warm regimes			
	collisionless		resistive		collisionless		resistive	
	$\Delta'\delta_1 \ll 1$	$\Delta'\delta_1 \gg 1$	$\Delta'\delta_1 \ll 1$	$\Delta'\delta_1 \gg 1$	$\Delta'\delta_1 \ll 1$	$\Delta'\delta_1 \gg 1$	$\Delta'\delta_1 \ll 1$	$\Delta'\delta_1 \gg 1$
$\delta_\psi^{(2)}$	d_e		$(S\gamma)^{-1/2}$		d_e		$(S\gamma)^{-1/2}$	
$\delta_\psi^{(4)}$	$\sqrt{d_e\delta_{SD}}$	$\sqrt{d_e\delta_{LD}}$	$\dfrac{\delta_{SD}^{-1/2}}{(S\gamma)^{1/4}}$	$\dfrac{\delta_{LD}^{-1/2}}{(S\gamma)^{1/4}}$	$\sqrt{d_e\delta_{SD}}$	$\sqrt{d_e\delta_{LD}}$	$\dfrac{\delta_{SD}^{-1/2}}{(S\gamma)^{1/4}}$	$\dfrac{\delta_{LD}^{-1/2}}{(S\gamma)^{1/4}}$

TABLE 2. Scaling of the spatial scales associated with the second- and fourth-order derivative of $\psi_1(x)$, evaluated on the neutral line $x = 0$ in different reconnection regimes and wavelength limits. In each regime, δ_{SD} and δ_{LD} are those of table 1 and correspond to the different values of δ_1 evaluated in §§ 6 and 7.

since in both the large- and small-Δ' regimes, purely resistive or purely inertial, $k^2\bar{d}_e^2 \ll 1$. The above expression can also be approximatively written as

$$\left.\frac{\psi_1''}{\psi_1}\right|_{x=0} \simeq \frac{1}{\bar{d}_e^2} \quad \Longrightarrow \quad \delta_\psi^{(2)} \simeq \bar{d}_e. \tag{8.12}$$

The corresponding scalings in table 2 descend from (8.12), after the relevant parameter and wavelength limits are considered.

8.3.3. *Asymptotic scalings of* $\delta_\psi^{(4)}$

To evaluate $\delta_\psi^{(4)}$, we should differentiate the solutions ψ_1 obtained in each reconnection regime and wavelength limit. Save for the warm-electron, large-Δ' limit, where the last equality of (7.38) immediately gives $|(d^4\psi_1/d\zeta^4)/\psi_1|_{\zeta=0} \simeq 2\delta_1^2/\bar{d}_e^2 + O(\delta_1^4/\bar{d}_e^4)$, whence $\delta_\psi^{(4)}$ can be rapidly evaluated by using $\zeta = x/\delta_1$ and then $\delta_1 = \mathrm{d}x/\mathrm{d}\zeta$, in all other cases, some more algebra is required. It is therefore interesting to look if it is possible to address all the regimes and cases in a unified way. To this purpose, we can combine (8.10) and (8.5) and (8.6) with the limit $x \to 0$ of the second-order derivative of (2.1) and of the first-order derivative of (2.2) with respect to x. Having introduced once more $\bar{d}_e$ so as to treat the inertial and resistive cases all together, we obtain

$$\gamma\left((1+k^2\bar{d}_e^2)\psi_1'' - \bar{d}_e^2\psi_1^{iv}\right)|_{x=0} \simeq \mathrm{i}2C_2k\left(\rho_s^2\varphi_1''' - \varphi_1'\right)|_{x=0}, \tag{8.13}$$

$$\gamma\varphi_1'''|_{x=0} \simeq \mathrm{i}k\left(C_2\psi_1'' - C_4\psi_1\right)|_{x=0}. \tag{8.14}$$

Combining them and using (8.6),

$$\gamma^2\left((1+k^2\bar{d}_e^2)\psi_1'' - d_e^2\psi_1^{iv}\right)|_{x=0} \simeq -2C_2k^2\rho_s^2(C_2\psi_1'' - C_4\psi_1)|_{x=0} - \mathrm{i}2C_2k\gamma q_0. \tag{8.15}$$

Finally, using (8.12),

$$-\frac{\bar{d}_e^4}{1+k^2\bar{d}_e^2}\left.\frac{\psi_1^{iv}}{\psi_1}\right|_{x=0} \simeq -1 - 2(C_2)^2\frac{k^2}{1+k^2\bar{d}_e^2}\frac{\rho_s^2}{\gamma^2} + 2C_2\frac{k^2}{1+k^2\bar{d}_e^2}\frac{\bar{d}_e^2}{\gamma^2}\left(\rho_s^2C_4 - \mathrm{i}\frac{\gamma q_0}{kc_0}\right). \tag{8.16}$$

At this point, we specialise the result to the cold and to the electron limits.

Cold-electron limit

In the cold limit $\rho_s = 0$, using $A = -\mathrm{i}\gamma/(k\delta_1 J_0)$, $q_0 \sim -c_0/(A\delta_1)$ or $\sim -2c_0/(A\delta_1)$ (cf. (8.9)), we can so distinguish two cases.

(*a*) One case is for $k^2\bar{d}_e^2\delta_1/\gamma^2 \sim d_e \ll 1$, which corresponds to the large-Δ' limit, in which we obtain the scaling

$$\left|\frac{\psi_1^{iv}}{\psi_1}\right|_{x=0} \simeq \frac{1}{\bar{d}_e^4} \quad \Longrightarrow \quad \delta_\psi^{(4)} \simeq \bar{d}_e \sim \delta_1 \sim \sqrt{\bar{d}_e\delta_{LD}}. \tag{8.17}$$

(*b*) The second case is for $k\bar{d}_e^2q_0/(c_0\gamma) \gg 1$, which is true in the small-Δ' limit, for which $\gamma\bar{d}_e/k \sim \delta_1^2$ (cf. (6.19), but for which a better estimate of q_0, as given by the first part of (8.9), must be found. To this purpose, we can directly use the solution found for $\Phi(z) = (\bar{d}_e k^3 J_0^3/\gamma^3)^{1/2}\varphi_1(x(kJ_0)^{1/2}/(\gamma\bar{d}_e)^{1/2})$ from boundary

https://doi.org/10.1017/S0022377822001088 Published online by Cambridge University Press

layer calculations performed in this regime (§ 6.2). We first take the derivative of (6.15):

$$\frac{\mathrm{d}\Phi}{\mathrm{d}z} = -\frac{1}{2}\int_0^1 (1-t^2)^{-1/4} e^{-(1/2)tz^2}\,\mathrm{d}t + z^2\int_0^1 t(1-t^2)^{-1/4} e^{-(1/2)tz^2}\,\mathrm{d}t. \quad (8.18)$$

Since $z \propto x$, we can evaluate $Q_0 \equiv \Phi'(z)|_{z=0}$ and then relate it to $q_0 = \varphi_1'(x)|_{x=0}$. From (8.18), we obtain

$$Q_0 = -\frac{1}{2}\int_0^1 \frac{\mathrm{d}t}{(1-t^2)^{1/4}} = -\int_0^{\pi/4} \sqrt{1-2\sin^2(u)}\,\mathrm{d}u = -\mathcal{E}\left(\frac{\pi}{4}\middle|\,2\right), \quad (8.19)$$

where in the last passage, we have made the changes of variables of integration $t = \sin\theta$ and $u = \theta/2$, and where $\mathcal{E}$ is the incomplete elliptic integral of second kind (see Gradshteyn & Ryzhik 2015, (8.2) in § 8.111). Using (6.14), we thus find

$$q_0 = \mathrm{i}\frac{c_0\gamma}{k\bar{d}_e J_0} Q_0 = -\mathrm{i}\frac{c_0\gamma}{k\bar{d}_e J_0}\mathcal{E}\left(\frac{\pi}{4}\middle|\,2\right). \quad (8.20)$$

Finally, using (6.21), one finds

$$q_0 = -\mathrm{i}\frac{c_0\left(\Delta'\bar{d}_e\right)^2}{I^2}\mathcal{E}\left(\frac{\pi}{4}\middle|\,2\right). \quad (8.21)$$

This leads to

$$\left.\frac{\psi_1^{iv}}{\psi_1}\right|_{x=0} \simeq -\mathrm{i}2\frac{C_2}{I^2}\mathcal{E}\left(\frac{\pi}{4}\middle|\,2\right)\frac{k\Delta'}{\gamma}, \quad (8.22)$$

that is,

$$\left|\left.\frac{\psi_1^{iv}}{\psi_1}\right|_{x=0}\right| \simeq \frac{1}{\Delta'\bar{d}_e^3} \quad \Longrightarrow \quad \delta_\psi^{(4)} \simeq \sqrt{\bar{d}_e\delta_{SD}}. \quad (8.23)$$

Warm-electron limit

In the warm limit $\rho_s > \bar{d}_e$, we can assume instead the first term of (8.22) to be always dominant at the right-hand side and greater than unity, so as to write

$$\left.\frac{\psi_1^{iv}}{\psi_1}\right|_{x=0} \simeq 2C_2^2\frac{k^2}{\gamma^2}\frac{\rho_s^2}{\bar{d}_e^4}. \quad (8.24)$$

Using finally the definition (7.11), we obtain, in both the small- and large-Δ' limits,

$$\left|\left.\frac{\psi_1^{iv}}{\psi_1}\right|_{x=0}\right| \simeq \frac{1}{\bar{d}_e^2\delta_1^2} \quad \Longrightarrow \quad \delta_\psi^{(4)} \simeq \sqrt{\bar{d}_e\delta_1}. \quad (8.25)$$

Specialising $\bar{d}_e$ in the purely inertial or purely resistive regime and taking the relevant scalings in the large-Δ' allows us to complete table 2.

https://doi.org/10.1017/S0022377822001088 Published online by Cambridge University Press

9. Heuristic derivation of the scaling laws of tearing modes

In previous sections, we obtained the growth rate scaling law by analytically solving the eigenvalue problem in the warm- and cold-collisionless regimes. To solve the equations, we expanded the equilibrium profile around the neutral line using a Taylor series. Therefore, despite the cumbersome analysis developed to find them, the eigenfunctions so obtained are merely approximations and not 'exact' solutions of the problem. The complexity of the boundary layer approach is also evident, which leads to differential equations of hypergeometric nature.

A complementary approach is possible, which, in some cases as we are going to see, allows the estimate of the scalings of both the growth rate and of the reconnecting layer width by providing some more physical insight about the analytical assumption made in the boundary layer formalism. This method is based on some heuristic orderings of the terms in the inner layer equations, and on balancing these terms together to obtain the scaling laws via dimensional analysis – see Drake & Lee (1977) and Cowley *et al.* (1986) for an application to kinetic tearing, Betar *et al.* (2020) for an application to the cold resistive and viscous-resistive regimes, and Drake & Kleva (1991) for an application to secondary instabilities to a primary tearing-type mode. Although it has not been detailed, this approach has been also used to get the collisionless scalings of tearing modes in Ottaviani & Porcelli (1995). An analogous approach is at the basis of the available theoretical estimates of the scalings of the reconnecting rate in the whistler-mediated reconnection scenario (Mandt *et al.* 1994) and of the reconnecting rate in Hall-MHD reconnection (Biskamp, Schwarz & Drake 1995, 1997). Heuristic ansatz on the scaling of the gradients of the tearing eigenfunction have been revealed to be useful also for quantitative estimates – which have been numerically verified *a posteriori* – about the time and spatial behaviour of the reconnecting current sheet during its nonlinear, collisionless evolution (Ottaviani & Porcelli 1993, 1995). More in general, heuristic estimates are of fundamental importance to allow insight on the physical interpretation of less evident analytical results (see, e.g. Drake & Lee 1977; Cowley *et al.* 1986 for tearing modes and Grasso *et al.* (1999) for the interpretation of the physical meaning of ρ_s in reduced MHD reconnection).

While this heuristic method, with some variations, is frequently presented in textbooks as a shortcut procedure to find the scalings of the cold-electron, resistive tearing mode (see, e.g. Biskamp 2000, § 4.1.1; Schnack 2009, Lecture 34; Boyd & Sanderson 2003, § 5.3.1, to give some examples), its application cannot be clear when more than one boundary layer exists, as it is in the case of warm-electron tearing modes. Discussing this point is therefore of general interest: this is what we are going to do in this section, where we compare the heuristic approach to the boundary layer analysis presented in previous sections. In particular, we are going to show that further information is required to get consistent results from the heuristic analysis to get the correct scalings when $\rho_s \gtrsim d_e$. From preliminary analysis, this information appears not to be immediately available from *a priori* arguments. This suggests that the heuristic approach should be carefully handled, when electron temperature effects (and, more in general, FLR effects) are included, since it could lead to incorrect estimates, as we are going to show below.

9.1. *General hypotheses in the heuristic approach to the scaling estimate*

Let us first outline the general hypotheses, which allow one to recover the correct scaling laws by dimensional analysis in the textbook-like examples of the purely resistive and of the purely inertial tearing mode analysis.

https://doi.org/10.1017/S0022377822001088 Published online by Cambridge University Press

We first re-write the eigenvalue equations for $x \ll 1$ (i.e. $x/a \ll 1$ in dimensional units), in the non-ideal region:

$$\psi_1 - \mathrm{i}\frac{kx}{\gamma} J_0 \varphi_1 = \bar{d}_e^2 \psi_1'' + \frac{\rho_s^2}{\gamma^2} k^2 x^2 J_0^2 \psi_1'', \tag{9.1}$$

$$\varphi_1'' = -\mathrm{i}\frac{kx}{\gamma} J_0 \psi_1'', \tag{9.2}$$

where (9.2) was used to express the second term on the right-hand side of (9.1), and resistivity has been included in the parameter $\bar{d}_e^2$.

The usual heuristic estimations, as they have been successfully used for both the purely collisionless and purely resistive regimes, are based on the following ideas.

(i) There is a characteristic scale, say l_c, for the gradient of ψ_1, which we are going to quantitatively define in the following. It allows one to estimate $\psi_1' \sim \psi_1/l_c$ at some point x in the neighbourhood of the neutral line.
(ii) A single characteristic microscopic scale exists for both the first derivative of ψ_1' and φ_1: this corresponds to the inner layer width, δ, which we operationally define according to (8.3), (this can be proven via numerical integration of the equations – see later).
(iii) We can generally assume $\delta \leq l_c$.

We then add a further assumption that can be *a posteriori* verified (also numerically), and somewhat generalises the examples for which the heuristic approach has been successfully applied in the past.

(iv) l_c is the largest characteristic scale length in the matching layer with the ideal-MHD solution. That is, in a neighbourhood of the neutral line, we write the estimates

$$\psi_1' \sim \frac{\psi_1}{l_c}, \quad \psi_1'' \sim \frac{\psi_1}{\delta l_c}. \tag{9.3}$$

The two characteristic scales that naturally appear when a distinction has been made between the large-Δ' and small-Δ' limits are $(\Delta')^{-1}$ and δ. Accordingly, in the small-Δ' limit, $l_c = (\Delta')^{-1}$ with $\Delta'\delta \ll 1$, while in the large-Δ' limit, $l_c = \delta$ and $\Delta'\delta \gg 1$. This argument suggests the following scalings (Ottaviani & Porcelli 1995):

$$\frac{\psi_1''}{\psi_1} \sim \frac{1}{\delta^2} \quad \text{for } (\Delta'\delta \gg 1), \qquad \frac{\psi_1''}{\psi_1} \sim \frac{\Delta'}{\delta} \quad \text{for } (\Delta'\delta \ll 1). \tag{9.4}$$

Note that, differently from (8.12), where the ratio ψ_1''/ψ_1 is evaluated exactly on the neutral line ($x \equiv 0$), in the estimates of (9.4), it is evaluated in the neighbourhood of the line (i.e. $x \simeq 0$).

After approximating $x \sim \delta$ in the inner layer, (9.2) gives

$$\varphi_1'' \sim \frac{k\delta}{\gamma} J_0 \psi_1'', \tag{9.5}$$

which is true in all tearing regimes. All further estimates rely on assumptions about the relative ordering between the terms of the equations. In what follows, we will discuss the derivation of the scaling laws in the different regimes by using this method: it will prove to be successful in the cold-collisionless limit, but we will see that it fails in the warm-collisionless regime.

https://doi.org/10.1017/S0022377822001088 Published online by Cambridge University Press

9.2. *Heuristic derivation of the scaling laws in the cold-electron regime ($\rho_s^2 \ll \bar{d}_e^2$)*

In these regimes, we can take $\rho_s = 0$. Therefore, the second term on the right-hand side of (9.1) vanishes.

For reasons of 'economy of thought' and of convenience about the generalisability of the heuristic approach, which will be discussed next (cf. comments on (10.4) in § 10.1), we now follow a procedure, which, although practically equivalent to those that can be found in classical textbook examples, slightly differs from most of them, as far as some ansatz are concerned: in particular, we are not going to make use of the estimate $\varphi_1'' \sim \varphi_1/\delta_1^2$, otherwise typically used, and which can be verified to be valid in the cold-electron regimes.

We then start by balancing the remaining terms of (9.1) and (9.2). This leads us to

$$\psi_1 \sim \bar{d}_e^2 \psi_1'', \quad \varphi_1 \sim \frac{\gamma}{k\delta J_0}\psi_1, \quad \varphi_1 \sim \frac{\gamma \bar{d}_e^2}{k\delta J_0}\psi_1''. \tag{9.6}$$

Differentiating twice the second part of (9.6) and using (9.5), one gets

$$\gamma \sim k\delta J_0, \tag{9.7}$$

which is valid for both wavelength limits and in both the collisionless and resistive regimes. Substituting (9.4) in the first part of (9.6), one obtains

$$\delta \sim \bar{d}_e \quad \text{for } (\Delta'\delta \gg 1), \quad \delta \sim \bar{d}_e^2 \Delta' \quad \text{for } (\Delta'\delta \ll 1). \tag{9.8}$$

It can be noticed that, looking at the physical aspects, the first of the conditions in (9.6) is the result of the balance between the two terms directly involved in the process of energy conversion that is related to magnetic reconnection: the magnetic potential ψ_1 on the one side, and, on the other side, the electron kinetic energy $d_e^2\psi_1''$ in the collisionless limit or the energy dissipated by Ohm's law in the resistive limit, $S^{-1}\psi_1''$.

At this point, it is convenient to treat the purely inertial and the purely collisionless case separately.

(*a*) *Collisionless case*.
Substituting $\bar{d}_e \to d_e$ and (9.8) into (9.7) yields

$$\gamma \sim J_0 k d_e \quad \text{for } \Delta'\delta \gg 1, \quad \gamma \sim J_0 k (\Delta')^2 d_e^3 \quad \text{for } \Delta'\delta \ll 1. \tag{9.9}$$

The corresponding scalings of the width of the reconnecting layer read

$$\delta \sim d_e \quad \text{for } \Delta'\delta \gg 1, \quad \delta \sim \Delta' d_e^2 \quad \text{for } \Delta'\delta \ll 1. \tag{9.10}$$

These are the scaling laws of Porcelli (1991) that we have analytically obtained in § 6.

(*b*) *Resistive case*.
Substituting instead $\bar{d}_e \to S^{-1/2}/\gamma^{1/2}$ and proceeding as above yields the scalings of Furth *et al.* (1963) and Coppi *et al.* (1976) (see also Ottaviani & Porcelli 1995), which we have also already obtained in § 6:

$$\gamma \sim J_0^{2/3} k^{2/3} S^{-1/3} \quad \text{for } \Delta'\delta \gg 1, \quad \gamma \sim J_0^{2/5} k^{2/5} (\Delta')^{4/5} S^{-3/5} \quad \text{for } \Delta'\delta \ll 1), \tag{9.11}$$

$$\delta \sim J_0^{-1/3} k^{-1/3} S^{-1/3} \quad \text{for } \Delta'\delta \gg 1, \quad \delta \sim J_0^{-2/5} k^{-2/5} (\Delta')^{1/5} S^{-2/5} \quad \text{for } \Delta'\delta \ll 1. \tag{9.12}$$

https://doi.org/10.1017/S0022377822001088 Published online by Cambridge University Press

9.3. *Heuristic derivation of the scaling laws in the warm-electron regime ($\rho_s \gtrsim \bar{d}_e$)*

If we now follow an analogous approach in the warm-collisionless regime, problems arise suggesting some (or all) of the hypotheses made at points (i)–(iii) and in (9.3)–(9.5) to not be correct. Let us see why.

In this regime, the second term on the right-hand side of (9.1) does not vanish. Therefore, it is expected that this term will be of the same order of the first right-hand side term at the boundary of the inner layer (i.e. at $|x| \simeq \delta$). Balancing these two terms yields

$$\frac{\gamma}{kJ_0} \sim \frac{\rho_s}{\bar{d}_e}\delta. \tag{9.13}$$

By balancing the first left-hand side terms of (9.1), one estimates $\psi_1 \sim \bar{d}_e^2\psi_1''$. For the small-$\Delta'$ limit, one has $\psi_1''/\psi_1 \sim \Delta'/\delta \sim 1/\bar{d}_e^2$, meaning $\delta \sim \Delta'\bar{d}_e^2$. Therefore, for the $\Delta'\delta \ll 1$ limit, one obtains

$$\gamma \sim J_0 k\Delta'\rho_s\bar{d}_e, \quad \delta \sim \Delta'\bar{d}_e^2. \tag{9.14}$$

These scaling laws for γ and δ are identical to those given by (7.65) which we analytically derived in § 7.5. That is, they allow us to recover the small-Δ' limit of the scalings of (Pegoraro & Schep 1986).

Following the same line of thought to find the scaling laws of the large-Δ' limit, one would expect, as discussed in § 9, that the largest scale l_c equals δ since this time, $\delta \gg (\Delta')^{-1}$. Therefore, $\psi_1 \sim \bar{d}_e^2\psi_1''$ gives $\delta \sim \bar{d}_e$, which differs from the scaling in (7.53). Proceeding with this argument, after substituting $\delta \sim \bar{d}_e$ in (9.13), the scaling $\gamma \sim k\rho_s$ is obtained. This also differs from the scaling law obtained analytically in (7.54) and which, instead, has been numerically verified (Betar *et al.* 2020). No numerical evidence in the range $\rho_s \gtrsim \bar{d}_e$ has been found of the scalings $\delta \sim \bar{d}_e$ and $\gamma \sim k\rho_s$. Also note that $\gamma \sim k\rho_s$ does not display any explicit dependence on $\bar{d}_e$, which contains the non-ideal parameters that allow magnetic reconnection (and which should make $\gamma \to 0$ as $\bar{d}_e \to 0$). We therefore conclude the scalings $\delta \sim \bar{d}_e$ and $\gamma \sim k\rho_s$ to be wrong.

This implies that the generalisability of the heuristic approach to the warm regimes is not evident and further information about the estimates of the relevant quantities is needed.

Even if this problem is not solved yet, and a closed set of equations for the heuristic estimates is not available when $\rho_s \gtrsim \bar{d}_e$, in the next subsection, we investigate this possibility by introducing a new characteristic scale-length of the system associated with the gradient of the velocity component parallel to the neutral line, and which we postulate to be related to the gradient of the magnetic flux function at the boundaries of the 'outer region': although so far we must rely on its numerical estimate, we are going to show that this allows us to use a heuristic-type approach to get the correct scaling laws of the growth rate and of the inner layer width in all reconnection regimes here considered. In this sense, introducing this scale length at least allows us to generalise the heuristic procedure to warm-electron regimes, although this generalisation remains so far incomplete, due to the lack of a procedure apt to *a priori* estimate this scale length. Moreover, the asymptotic scaling of this quantity can be shown to correspond to that of a characteristic scale length, which in both Porcelli (1991) and Zocco & Schekochihin (2011) has been obtained as a normalisation length in boundary layer integration procedure. In these works, it had been related to the width $> \delta_1$ of the domain sub-interval in which the solution of the innermost equation is valid in the large-Δ' limit.

https://doi.org/10.1017/S0022377822001088 Published online by Cambridge University Press

10. An ansatz about the 'generalisation' of the heuristic estimates: the role of the velocity gradient in the non-ideal region

A critical ingredient of the previous analysis is the estimate of the characteristic length, l_c, related to the first derivative of the magnetic stream function in the non-ideal region. Let us focus on the $\rho_s \gtrsim \bar{d}_e$ regime, where heuristic estimates display problems. Using $\psi_1 \sim \bar{d}_e^2 \psi_1''$ and (9.13), we see that the scale length l_c enters in the estimates of the growth rate and of the reconnecting layer width as

$$\gamma \sim J_0 \frac{k\rho_s \bar{d}_e}{l_c}, \quad \delta \sim \frac{\bar{d}_e^2}{l_c}. \tag{10.1}$$

In both the collisionless and resistive regimes, the correct estimates are recovered in the small-Δ' limit when $l_c \sim (\Delta')^{-1}$, whereas they are incorrect in the large-Δ' limit if we assume $l_c \sim \delta$. This suggests looking for another reasonable estimate for l_c, in this case.

The strategy we pursue here is therefore to look for a third 'effective' scale length for l_c, different from Δ' and δ, that would allow us to recover the correct scaling from (10.1) in the large-Δ' limit, and to verify its relevance and appropriateness by means of numerical calculations.

10.1. *Velocity gradient in the innermost non-ideal region*

The likely candidate we propose for an alternative definition of l_c is the inverse of the logarithmic jump in the component of the derivative of the fluid velocity parallel to the neutral line and evaluated at $x = \pm\delta$, which we name Δ'_{v_y}, in (loose) analogy with the usual Δ' defined for the magnetic stream function ψ_1:

$$\Delta'_{v_y} \equiv \frac{v_y'(\delta) - v_y'(-\delta)}{v_y(\delta)} = \frac{\varphi_1''(\delta) - \varphi_1''(-\delta)}{\varphi_1'(\delta)}. \tag{10.2}$$

It must be noted that in (10.2), we have used the 'whole' eigenfunction φ_1, differently from what happens in the definition of Δ', in which only the 'outer' eigenfunction ψ_{out} is involved. This fact is important for the numerical computation of both Δ'_{v_y} and Δ', as it will be discussed in § 10.3. Definition (10.2) and the identification $\delta = \delta_1$ means that $1/\Delta'_{v_y}$ represents the characteristic scale length of the velocity gradient at the boundary of the innermost layer, i.e. the 'electron diffusion region'.

Evaluating (9.2) at $x = \delta$ and $x = -\delta$, and using the definition (10.2), we obtain

$$\gamma \Delta'_{v_y} \varphi_1'|_{x=\delta} = \mathrm{i}k\delta J_0 \, (\psi_1''|_{x=\delta} + \psi_1''|_{x=-\delta}). \tag{10.3}$$

Using the fact that $\psi_1''(\delta) = \psi_1''(-\delta)$ and assuming the validity of condition (9.3) at $x = \delta$, we find

$$\left.\frac{\gamma \varphi_1'}{k\psi_1}\right|_{x=\delta} = \frac{2\mathrm{i}J_0}{l_c \Delta'_{v_y}}. \tag{10.4}$$

Equation (10.4) expresses a constraint on the product $l_c \Delta'_{v_y}$ which depends on the scaling of γ, and on the profiles of $v_y = \varphi_1'$ and of ψ_1. It should be noted that in the cold-electron regimes, the correct scalings can be obtained via heuristic approach using the hypothesis $\varphi_1''|_{x\simeq\delta} \sim \varphi_1/\delta_1^2$ (see, e.g. Biskamp 2000, § 4.1.1). Should this assumption be always correct, the scaling $l_c \sim (\Delta_{v_y})^{-1} \sim \delta_1$ would be always obtained in the large-Δ' limit regardless of the reconnection regime, but this estimate does not allow us to recover

https://doi.org/10.1017/S0022377822001088 Published online by Cambridge University Press

the correct scalings when $\rho_s \gtrsim \bar{d}_e$. However, although so far the asymptotic scaling of Δ'_{v_y} is not known, considering the results that we have found to be valid in the cold-electron regimes, we can expect that, at least for $\rho_s = 0$ and in the large-Δ' limit, the quantity Δ'_{v_y} be related to (actually, 'be proportional to the inverse of') δ_1.

10.2. *A heuristic generalisation of the definition of the scale l_c*

Based on the remarks above, we *heuristically postulate* the definition:

$$l_c \sim \max\{(\Delta')^{-1}, (\Delta'_{v_y})^{-1}\}, \tag{10.5}$$

which we will later show (§ 10.4) to be indeed consistent with all other definitions and hypotheses, and thus, arguably correct. It can be *a posteriori* verified that the results would have been equally consistent even if we had developed the arguments which follow using the alternative definition $l_c \sim \max\{(D')^{-1}, (\Delta'_{v_y})^{-1}\}$, based on the further inverse scale length D', which we introduce below, in (10.10), and whose scaling we numerically compute later, in different regimes. Definition (10.5) has been chosen, here, since Δ' is always *a priori* known, whereas the evaluation of D', too, requires a numerical integration of the boundary layer problem. According to heuristic definition (10.5), in the small-Δ' limit, we expect $l_c \sim (\Delta')^{-1} \gg (\Delta'_{v_y})^{-1}$, whereas in the large-$\Delta'$ limit, we expect $l_c \sim (\Delta'_{v_y})^{-1} \gg \Delta'$. From (10.5), the transition between the two limits is therefore ruled by the asymptotic scaling of the ratio $\gamma\varphi'_1/(k\psi_1)$. In particular, regardless of the reconnection regime (resistive or collisionless, warm or cold), we must have

$$\left.\frac{\gamma\varphi'_1}{k\psi_1}\right|_{x=\delta} \sim \frac{\Delta'}{\Delta_{v_y}} \ll 1 \quad (\text{for } \Delta'\delta \ll 1), \qquad \left.\frac{\gamma\varphi'_1}{k\psi_1}\right|_{x=\delta} \sim O(1) \quad (\text{for } \Delta'\delta \gg 1). \tag{10.6}$$

The first of the conditions in (10.6) can be however *a posteriori* refined and re-formulated as a condition on the ratio $(\gamma\varphi''_1)/(k\psi_1)$, which reads

$$\left.\frac{\gamma\varphi''_1}{k\psi_1}\right|_{x=\delta} \sim O(1) \quad (\text{for } \Delta'\delta \ll 1). \tag{10.7}$$

This condition follows from (9.2) combined with the second part of (9.3) and from the knowledge we have about the scalings of δ and γ in terms of l_c: using the estimates $l_c\delta \sim d_e^2$ and $l_c\delta \sim S^{-1}/\gamma$ that we obtain by specialising $\bar{d}_e$ to the collisionless and resistive regimes, respectively, we obtain

$$\left.\frac{\gamma\varphi''_1}{k\psi_1}\right|_{x=\delta} \sim \frac{\delta}{d_e^2} \quad (\text{collisionless}), \qquad \left.\frac{\gamma\varphi''_1}{k\psi_1}\right|_{x=\delta} \sim \frac{\gamma\delta}{S^{-1}} \quad (\text{resistive}). \tag{10.8}$$

Equation (10.9) is then *verified* in all reconnection regimes once we substitute the relevant known scalings we have already evaluated from boundary layer theory into (10.8). Also, using the definition of Δ'_{v_y} of (10.2), the two equations in (10.8) result to be compatible with the second part of (10.6). In conclusion, we can therefore write the constraints:

$$\begin{cases} \left.\dfrac{\gamma\varphi''_1}{k\psi_1}\right|_{x=\delta} \sim O(1) \\ \left.\dfrac{\gamma\varphi'_1}{k\psi_1}\right|_{x=\delta} \sim \dfrac{\Delta'}{\Delta_{v_y}} \ll 1 \end{cases} \quad (\text{for } \Delta'\delta \ll 1), \qquad \left.\frac{\gamma\varphi'_1}{k\psi_1}\right|_{x=\delta} \sim O(1) \quad (\text{for } \Delta'\delta \gg 1). \tag{10.9}$$

https://doi.org/10.1017/S0022377822001088 Published online by Cambridge University Press

These conditions can be taken to be generally discriminating for the transition from the small- to the large-Δ' scaling relations in any reconnection regimes.

It must be however emphasised that, while both (10.6) and (10.8) are self-consistently *deduced* from the specific hypotheses we have made so far, (10.7) must be *heuristically assumed*, since, although *a priori* reasonable and compatible with the first of conditions (10.6), it does not follow from the other hypotheses, but it is just verified once the scalings of γ and δ are found.

The discussion and the analysis we are going to develop next (§ 10.4) seems to suggest that accomplishing this latter task in the context of the heuristic derivation may not be feasible. Nevertheless, we will numerically prove the correctness of the hypotheses (i)–(iii) of § 9 and we will show that definitions (10.4) and (10.5) are consistent with the estimates of the correct scalings, provided the scaling of Δ'_{v_y} is known. In doing so, we will elucidate (cf. Appendix E) the logical points of the heuristic approach in the different tearing regimes by pointing out when an *a priori* self-consistent estimate can be done or not, and, in the second case, which information is missing. Before doing so, we need however to first discuss how to numerically evaluate Δ'_{v_y}, which must be compared with the numerical value of Δ' and of δ, the latter of which has been already discussed in § 8. This is what we are going to do in § 10.3.

10.3. *Numerical evaluation of Δ' and Δ'_{v_y}*

Let us first look at a numerical procedure that allows us to quantify the inverse scale lengths Δ' and Δ'_{v_y} defined by (3.8) and (10.2), respectively.

Of course, because of the definition in (3.8), the values of Δ' are always independent of the non-ideal parameters. The numerical evaluation of $\Delta'(k)$ becomes therefore trivial whenever an analytical formula that depends only on k and on the equilibrium profile can be obtained (cf. (4.13)).

Then, for the evaluation of Δ'_{v_y}, the definition in (10.2) may be operationally used, although it is procedurally quite demanding: it requires to compute first the eigenfunction φ_1, then its first and second derivative, and then to evaluate them at $x = \delta$, a value which can be numerically obtained by using the definition in (8.3) and by following the procedure sketched in figure 12.

It is however possible to 'speed up' the calculation of the scalings of both Δ' and Δ_{v_y}, by relying on an alternative numerical procedure.

This procedure mimics the numerical evaluation of Δ' that is made possible *only in the small-Δ' limit*, thanks to the geometrical interpretation that can be given of the instability parameter in terms of a local expansion of the outer solution (Furth *et al.* 1963): we recall that by using $\psi_{\text{out}} \approx c_0 + c_1|x|$ as $|x| \to 0$, then $\Delta' = 2c_1/c_0$ (cf. §§ 5.3.1 and 5.3.2). These two coefficients can be evaluated by measuring the value of ψ_{out} and of the slope of the tangent to ψ_{out} close to $x = 0$.

This idea can be borrowed so as to evaluate analogous quantities defined with respect to the *total* solutions ψ_1 and φ_1: noting that, graphically speaking, both ψ_1 and φ'_1 still display a linear behaviour with respect to x as $x \to \delta$, both in the small- and large-Δ' limits, we write $\psi_1|_{x\to\delta} \approx c_0 + c_1|x|$ and $v_y|_{x\to\delta} = \varphi'_1|_{x\to\delta} \approx q_0 + q_1|x|$. Note that these approximations are consistent with the local expansions (8.5) and (8.6), which are valid, instead, for $x \ll \delta$. Therefore, once the corresponding eigenfunctions have been numerically computed, at $|x| \sim \delta$, we can evaluate

https://doi.org/10.1017/S0022377822001088 Published online by Cambridge University Press

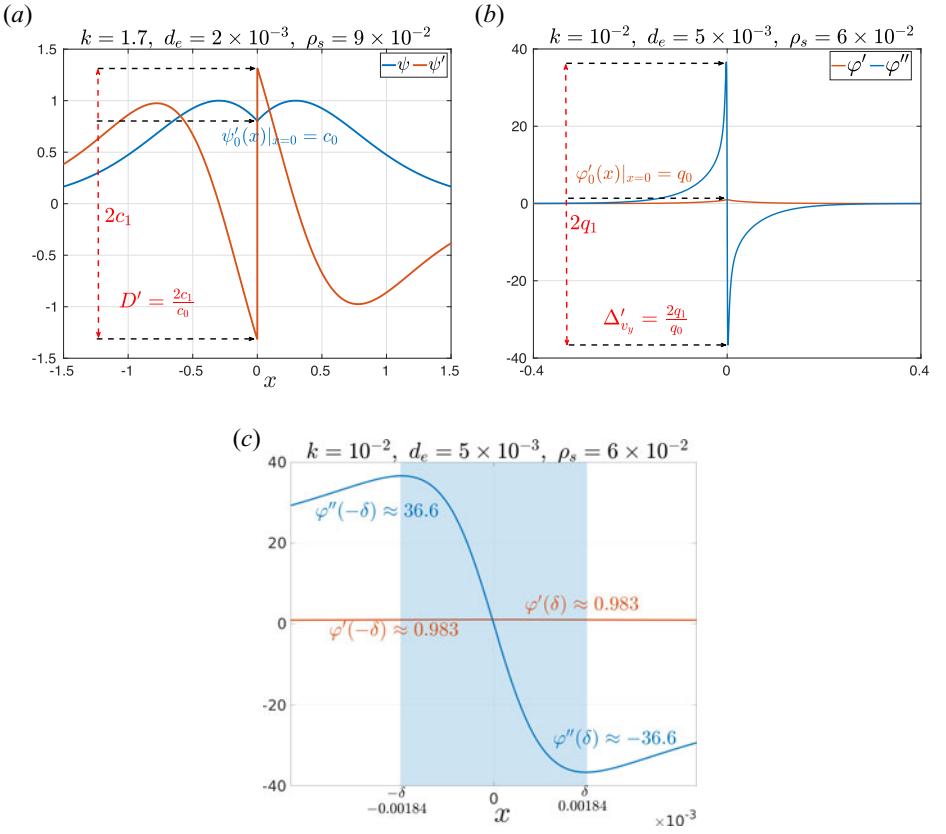

FIGURE 14. (*a*) Example of numerical evaluation of the coefficients c_0 and c_1 of (10.10), once the profile of $\psi_1(x)$ and of its derivatives $\psi_1'(x)$ have been computed for $|x| \geq \delta$ in a neighbourhood of $x = \delta$. (*b*) Analogous example of evaluation of q_0 and q_1 of (10.10) from φ_1' and φ_1'', calculated once the eigenfunction φ_1 has been computed; in this example, $\Delta'_{v_y} \approx 73.82$. (*c*) A zoomed version of panel (*b*) in which the inner region, here of width $\delta \approx 0.00184$ (computed according to the method outlined in § 8), is shaded in light-blue colour. All the values required to estimate Δ'_{v_y} using (10.2) are here shown; it is this way that $\Delta'_{v_y} \approx 74.48$ is obtained, in very good agreement with the result computed with the alternative method sketched in panel (*b*).

(see figure 14)

$$D' \equiv 2\frac{c_1}{c_0}, \quad \Delta'_{v_y} = 2\frac{q_1}{q_0}. \tag{10.10}$$

In particular, due to the smallness of δ, the coefficients c_1, c_0 and q_0, q_1 can be numerically computed as shown in figure 14, by measuring the values of ψ_1 and φ_1 and of the peak values of their derivatives close to $x = 0$.

We have verified that the scalings obtained for Δ'_{v_y} in this way agree with those directly computed by first evaluating δ and by then using the definition in (10.2), as shown in figure 14(*b*,*c*), and that $D' = \Delta'$ in the small-Δ' limit.

Figure 15 displays the scaling laws of $(D')^{-1}$, $(\Delta'_{v_y})^{-1}$ and δ, numerically computed according to the operational definitions given by (10.10) and (8.3), respectively, in the cold-collisionless regime at $\rho_s = 0$: the different characteristic lengths are shown in

https://doi.org/10.1017/S0022377822001088 Published online by Cambridge University Press

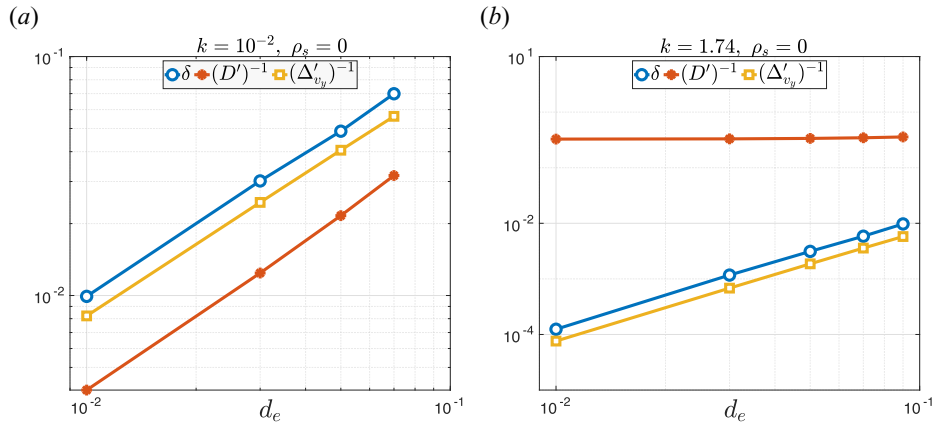

FIGURE 15. Examples of scaling laws of D', Δ'_{v_y} (cf. (10.10)) and δ with respect to d_e, for $\rho_s = 0$. The large-Δ' limit is in panel (a), the small-Δ' in panel (b). The values of D' and Δ'_{v_y} are computed numerically according to the procedure sketched in figure 14. In the small-Δ' limit, the values of Δ', obtained from (4.13), coincide with the orange line in panel (b).

figure 15(a) for the large-Δ' limit, and in figure 15(b) for the small-Δ' limit. Figure 16 shows the corresponding scaling laws for the tearing modes in the warm-collisionless regimes at $\rho_s \neq 0$. The dependence of $(D')^{-1}$, $(\Delta'_{v_y})^{-1}$, and δ on the electron skin depth (d_e) is in figure 16(a,c), the dependence on the ion-sound Larmor radius (ρ_s) is in figure 16(b,d); both the large-Δ' limit (figure 16(a,b)) and the small-Δ' limit (figure 16(c,d)) are considered.

Numerical results prove that, as it could be expected, D' of (10.10) coincides with the definition of Δ' only in the small-Δ' limit, where we can indeed state that $\psi_1(x)|_{x\to\delta^+} \simeq \psi_{\text{out}}(x)|_{x\to\delta^+}$ (cf. figure 15b, and figure 16c,d). In this limit, D' can be therefore taken as an accurate estimate of Δ', in spite of the fact that the latter is formally defined by evaluating the derivatives of ψ_{out} at a distance from the neutral line much larger than δ. This is made possible by the fact that in this large wavelength limit, the outer solution must match the inner one in an overlapping region that gets sufficiently close to $|x| = \delta$. That is, the constant-ψ hypothesis holds in the whole non-ideal region, down to the innermost layer.

Different is the result in the large-Δ' limit: in the cold-collisionless regime, $(D')^{-1}$ displays the same asymptotic scaling of δ, except for a numerical factor (cf. figure 15a), and these scaling laws are the same as for $(\Delta'_{v_y})^{-1}$; in the warm-collisionless regime, instead, both $(D')^{-1}$ and $(\Delta'_{v_y})^{-1}$ display the same asymptotic scalings $(D')^{-1} \sim (\Delta'_{v_y})^{-1} \sim \rho_s^{1/3} d_e^{2/3}$ (figure 16a,b) which are non-trivial, since they differ from $\delta_{LD}^{-1} \sim \rho_s^{1/3} d_e^{4/3}$. Analogous results, not shown here, are found in the warm-resistive, large-Δ' limit, in which, for these quantities, we obtain also an explicit dependence on k: $(D')^{-1} \sim (\Delta'_{v_y})^{-1} \sim k^{-2/7} \rho_s^{-1/7} S^{-2/7}$ and $\delta \sim k^{-4/7} \rho_s^{-5/7} S^{-4/7}$.

For summary, we recall here the scalings of Δ'_{v_y} that have been numerically obtained in the different regimes:

$\Delta'_{v_y} \sim \delta_{SD}^{-1}$ (warm/cold and collisionless/resistive regimes at small-Δ');
$\Delta'_{v_y} \sim \delta_{LD}^{-1}$ (cold and collisionless regimes at large-Δ');

https://doi.org/10.1017/S0022377822001088 Published online by Cambridge University Press

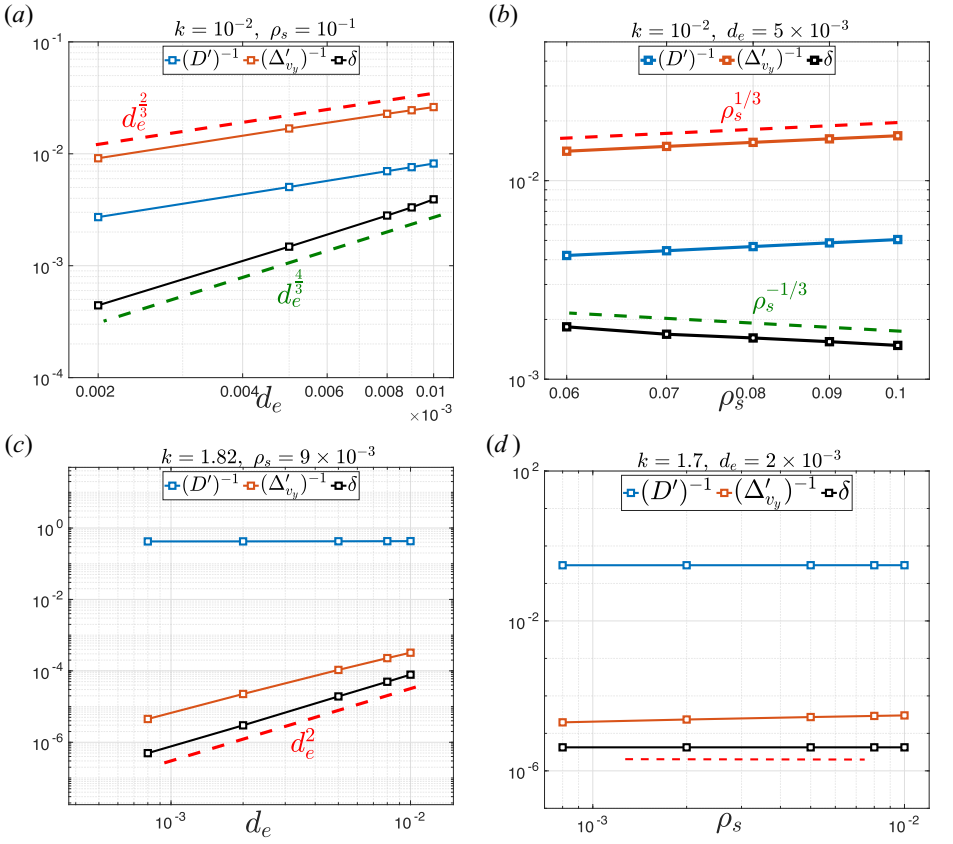

FIGURE 16. Examples of scaling laws of D', Δ'_{v_y} (cf. (10.10)) and δ for $\rho_s \neq 0$. Panels (*a*,*b*) correspond to the large-Δ' limit, whereas panels (*c*,*d*) correspond to the small-Δ' limit. The values of D' and Δ'_{v_y} are computed numerically according to the procedure sketched in figure 14. Notice that D' and δ are independent of ρ_s in the small-Δ' limit (cf. panel *d*). In the small-Δ' limit, the values of Δ' obtained from (4.13) coincide with the blue lines in panels(*c*,*d*).

$$\Delta'_{v_y} \sim \rho_s^{-1/3} d_e^{-2/3} \qquad \text{(warm-collisionless regime at large-}\Delta'\text{)};$$
$$\Delta'_{v_y} \sim k^{-2/7} \rho_s^{1/7} S^{-2/7} \qquad \text{(warm-resistive regime at large-}\Delta'\text{)}.$$

10.4. *Role of Δ'_{v_y} in heuristic-type estimates*

It is easy to verify that combining the estimates in (10.1) with the definition in (10.5) and with the *scalings numerically obtained* for Δ'_{v_y}, the correct scaling laws obtained in §§ 6 and 7 can be recovered in both the warm-collisionless and warm-resistive regimes.

This is discussed in detail in Appendix F, in which the logical steps of the procedure are singled out and identified, thus providing insight on the physical interpretation of the analytical results of the boundary layer calculations. In particular, the main hypotheses on which this (partial) heuristic approach relies and the corresponding results in all collisionless regimes, both 'warm' and 'cold', are summarised in tables 3–5 of Appendix F, where the logical steps of the procedure are presented as statements and formulae.

https://doi.org/10.1017/S0022377822001088 Published online by Cambridge University Press

There are two main results of this analysis.

(i) Introducing the scale length Δ'_{v_y} and postulating the definition in (10.5) make it possible to obtain the scaling laws, which are, in principle, correct in all regimes and wavelength limits; however, in the large-Δ' warm-electron regime, the procedure results to be not 'closed', in the sense that the estimation of the scaling law of Δ'_{v_y} seems to be not possible by simple dimensional analysis.
(ii) Quite interestingly, using the definition in (10.5), the scaling laws of all reconnection regimes can be cast in a form which is perfectly symmetric in the small- and large-Δ' limit, with respect to the substitution $\Delta' \leftrightarrow \Delta'_{v_y}$.

These results, on the one hand, suggest to us that introducing the inverse scale length Δ'_{v_y} is a promising ingredient in the attempt to extend the heuristic-type analysis. On the other hand, however, finding the further constraint that makes it possible to obtain *a priori* all the sought algebraic scalings without resorting to numerical analysis and by mere dimensional analysis seems an elusive task. The logical steps identified in the tables of Appendix F, as well as some further insight on the interpretation of the boundary layer results, which follows from the heuristic approach and which we are going to discuss below (§ 10.5), could imply the heuristic analysis to be intrinsically not applicable in some regimes. This problem becomes manifest, in particular, in the large-Δ' limit when $\rho_s \neq 0$, in which the scaling of Δ'_{v_y} is a non-trivial power law combination of the scales ρ_s and $\bar{d}_e$. Nevertheless, the coherence of the results summarised in tables 3–5 supports the consistency of the heuristic 'ansätze' we have made so far.

In particular, the logical steps identified in tables 3–5 show that the difference between the warm and cold regimes lies in the balance condition $\psi_1 \sim ikx\varphi_1/\gamma\varphi_1$, which is valid in the cold regimes only (hypothesis [T6.H2] of table 5), and which is replaced by the balance expressed by hypothesis [T5.H2] of table 4 when $\rho_s \neq 0$. Condition [T6.H2] expresses indeed the validity of (4.1), in turn related to the inverse scale Δ', down to the boundary layer at the frontier with the innermost region: this means that the newly introduced scale $(\Delta'_{v_y})^{-1}$ is redundant in this regime with respect to δ and Δ'^{-1} (as, however, it was evident already from the heuristic-type approach discussed in § 9.3). We have indeed seen from the numerical results summarised at the end of § 10.3 that the scaling of $(\Delta'_{v_y})^{-1}$ turns out to always coincide with that of δ. Such a 'closure' condition for Δ_{v_y} is lost at $\rho_s \neq 0$, when hypothesis [T6.H2] is replaced by hypothesis [T5.H2], which leads to the general constraint $\gamma \sim k\rho_s(\delta/l_c)^{1/2}$: here, a value different from that of δ or $(\Delta')^{-1}$, with respect to which the transition from the small- to the large-Δ' limits is measured, is in principle admitted for l_c.

10.5. *Significance of the inverse spatial scale Δ'_{v_y}: coherence with boundary layer calculations and comparison with previous work*

Some insight about the physical significance of the characteristic spatial scales associated with Δ'_{v_y} is obtained from comparison of their scalings with identical asymptotic scalings which can be obtained from some boundary layer results available in the previous literature (Pegoraro & Schep 1986; Cowley & Hastie 1988; Porcelli 1991; Zocco & Schekochihin 2011) and from related works discussing the implications of these results (Ottaviani & Porcelli 1995; Grasso *et al.* 1999).

Combination of (10.5) (i.e. hypothesis T4.H1) with hypotheses T5.H3 or T6.H3 allows the identification of the small- and large-Δ' limits, say $\Delta'\delta \gtrless 1$, expressed in each

https://doi.org/10.1017/S0022377822001088 Published online by Cambridge University Press

reconnection regime in terms of l_c and thus in terms of Δ'_{v_y}:

$$\Delta'\delta \gtrless 1 \quad \Leftrightarrow \quad \begin{cases} \Delta' d_e \gtrless \max\left\{\dfrac{1}{\Delta' d_e}, \dfrac{1}{\Delta'_{v_y} d_e}\right\} & \text{(collisionless)}, \\ \Delta' S^{-1} \gtrless \max\left\{\dfrac{\gamma}{\Delta'}, \dfrac{\gamma}{\Delta'_{v_y}}\right\} & \text{(resistive)}. \end{cases} \tag{10.11}$$

In this regard, it is interesting to compare, e.g. the conditions for the warm-collisionless case with the similar conditions in Grasso *et al.* (1999) that have been written (cf. (17) and paragraphs below (18) therein) as

$$\Delta' d_e > \min\left\{1, \left(\frac{d_e}{\rho_s}\right)^{1/3}\right\}, \quad \Delta' d_e < 1, \tag{10.12}$$

based on the results of the boundary layer calculations in the Fourier representation by Porcelli (1991) (cf. conditions on '$\lambda_H \equiv -\pi/\Delta'$' in between (7) and (9) therein). Substitution of the scalings numerically found for Δ'_{v_y} in § 10.3 for $\rho_s^2 \gg d_e^2$ into the collisionless condition of (10.11) gives

$$\underbrace{\Delta' d_e > \max\left\{\frac{1}{\Delta' d_e}, \left(\frac{\rho_s}{d_e}\right)^{1/3}\right\}}_{\text{(large-}\Delta'\text{)}}, \qquad \underbrace{\Delta' d_e < \max\left\{\frac{1}{\Delta' d_e}, \Delta' d_e\right\}}_{\text{(small-}\Delta'\text{)}}, \tag{10.13}$$

which are indeed compatible with the conditions in (10.12), once $(\Delta' d_e)^2 < 1$ is deduced from the second part of (10.13) in the small-Δ' limit and therefore $\Delta' d_e < 1$ is assumed, with $\Delta' d_e \sim 1$ fixing the threshold value also for the first inequality of (10.13).

In this regard, we notice that the non-trivial characteristic scale length associated with the asymptotic scaling, which we have numerically found for Δ'_{v_y} in the large-Δ', warm-electron limit, naturally emerges from the boundary layer analysis developed by Pegoraro & Schep (1986); Porcelli (1991): here, the general dispersion relation encompassing both the small- and large-Δ' limits can be written in terms of $\bar{d}_e$ as (to this purpose, we can just substitute $d_e \to \bar{d}_e$, e.g. in (25) of Ottaviani & Porcelli 1995)

$$\frac{\pi}{2}\gamma^2 = -\frac{\pi\rho_s}{\Delta'} + \frac{\rho_s^2 \bar{d}_e}{\gamma}. \tag{10.14}$$

Naming $\gamma_{LD} \sim (2/\pi)^{1/3}\bar{d}_e^{1/3}\rho_s^{2/3}$ the solution obtained in the $\Delta' \to \infty$ limit, which we already recovered in previous sections, one sees that the opposite, small-Δ' limit is obtained when the condition

$$\frac{\pi\rho_s}{\Delta'} \gg \frac{\rho_s^2 \bar{d}_e}{\gamma_{LD}} \quad \Leftrightarrow \quad \Delta' \ll \frac{1}{2\rho_s^{1/3}\bar{d}_e^{2/3}} \quad \Longrightarrow \quad \Delta' \ll \Delta'_{v_y} \tag{10.15}$$

is satisfied, where in the last passage, we have used the numerical result we previously found in this wavelength limit, $\Delta'_{v_y} \sim \rho_s^{-1/3}\bar{d}_e^{-2/3}$. The rightmost condition of (10.15) is consistent indeed with the constraints in (9.4), previously found via the heuristic estimates discussed in § 10.2. This suggests that Δ'_{v_y} may provide a physical interpretation of the

https://doi.org/10.1017/S0022377822001088 Published online by Cambridge University Press

appearance of this characteristic scale length in boundary layer calculations, performed in the framework of the two-fluid model we consider here.

This interpretation is however somewhat different from that provided by Ottaviani & Porcelli (1995), and which was based on the previous boundary layer calculations (Cowley *et al.* 1986; Pegoraro & Schep 1986; Porcelli 1991) performed by starting from a charge density equation in which polarisation effects were taken into account through the gyrokinetic particle response. In that modelling framework, the scale-length $\rho_s^{1/3}\bar{d}_e^{2/3} \gg \delta_1$ was noted by Ottaviani & Porcelli (1995) to correspond to the distance from the neutral line at which γ_{LD} becomes comparable to the phase-velocity $k_\parallel(x)v_{\rm th}^e = (\boldsymbol{k}\cdot\boldsymbol{B}_0(x)/B_0)v_{\rm th}^e$, and below which the isothermal electron closure would formally break down. As already noted in the same work, however, the appropriateness of the isothermal condition, assumed to be valid for the purpose of the boundary layer calculations, had been numerically verified to a good extent in some previous works (Berk, Mahajan & Zhang 1991; Coppi & Detragiache 1992) and, more recently, its validity has been supported by the numerical studies of Perona, Eriksson & Grasso (2010). Relating the scale $\rho_s^{1/3}\bar{d}_e^{2/3}$ to the failure of the isothermal closure is thus consistent with the interpretation provided in further – and in part preceding– works based on a kinetic approach (Drake & Lee 1977; Cowley *et al.* 1986; Zocco & Schekochihin 2011). In these works, such a critical distance was shown by heuristic arguments (see Drake & Lee 1977; Cowley *et al.* 1986, § V) to correspond to the characteristic width of the current layer, determined by the balancing of the total current generated by the parallel electron pressure gradients with the current generated by the (reconnecting) parallel electric field. Instead, in § 8 and in Betar *et al.* (2020), we have numerically proven the current sheet to be concentrated around the neutral line in a region of width δ_1. The subtle point here may be in the meaning which can be given to the notion of 'characteristic width of the current layer', since it is true that, while the inflection points around the peak of $J_{z,1}$ are numerically found to be located at a distance δ_1 from the neutral line (cf. definition in (8.3)), the profile of the inner solution (i.e. the solution found in the 'electron region') extends beyond this distance. In particular, the matching with the outermost non-ideal solution (i.e. the solution in the 'ion region') is not to be meant as a matching in a single point, but rather as an asymptotic matching valid over an intermediate layer, whose distance from the neutral line in the warm-electron regime can be of the order of $\rho_s^{1/3}\bar{d}_e^{2/3}$. This latter point of view is in agreement with the notion of 'inner solution width', to which Zocco & Schekochihin (2011) make reference: the characteristic width of the inner solution, which is named $\delta_{\rm in}$ in the notation of their work, differs from the width of the inner layer, which we have here named $\delta_1 = \delta$, and satisfies $\delta_1 < \delta_{\rm in} < \delta_2$.

If we look in detail at the boundary layer analysis carried out by these latter authors in the warm-electron regime, we see that the scalings they *a posteriori* obtained (cf. (B56) and (B101) in the 'Collisionless two fluid limit' and 'Resistive two fluid limit' of that work) for the normalisation scale $\delta_{\rm in}$, coincide in the large-Δ' limit with the scalings of $(\Delta'_{v_y})^{-1}$ that we have detailed at the end of § 10.3. In particular, for the regime that we can write as $\rho_s \gtrsim \bar{d}_e$, these authors identified the small- and large-Δ' conditions, which we have here generally expressed as $\Delta'\delta_1 \ll 1$ and $\Delta'\delta_1 \gg 1$, respectively, via the conditions $\Delta'\delta_{\rm in} \ll 1$ and $\Delta'\delta_{\rm in} \gg 1$, instead. Using the correspondence $\delta_{\rm in} \to (\Delta'_{v_y})^{-1}$, these conditions would map into $\Delta' \ll \Delta'_{v_y}$ and $\Delta' \gg \Delta'_{v_y}$, the former of which is consistent with (9.4). It should be however noted that the scale $\delta_{\rm in}$ appears in the boundary layer analysis of Zocco & Schekochihin (2011) as a consequence of a normalisation choice of the non-ideal equations of their model ((B35)–(B36) therein), which differs with respect to the one we have detailed in § 7: while the scalings of their outermost and innermost non-ideal layers are *a posteriori* found to coincide with those of the scales δ_2 and δ_1 that we introduced in §§ 7.2.1

https://doi.org/10.1017/S0022377822001088 Published online by Cambridge University Press

and 7.2.2, these authors chose instead $\delta_{\rm in} \equiv (\sqrt{2}\rho_s\delta_1)^{1/2}$ as a normalisation scale of the innermost equations (our δ_1 mapping into δ of (B28) of their work), and they subsequently ordered the terms of the tearing equations with respect to this spatial scale. The scalings of the relevant quantities have been thus obtained there, via some heuristic ansatz on the width of the integral at the left-hand side of the equivalent of (3.7), in the form in which they obtained it (cf. (B46), therein). To evaluate the integral, which depends on φ_1'' (cf. (3.10)), the terms in the corresponding auxiliary equation ((B42) therein), which are related to integrand via $\varphi_1'' = \chi'$, have been so ordered in relation to the characteristic width $\delta_{\rm in}$. This approach is at the basis of the ordering of the wavelength regime in terms of the product $\Delta'\delta_{\rm in}$, which differs from the ordering in terms of the product $\Delta'\delta_1$, which we have here adopted, instead. The coherence of the results obtained in the two approaches, also emphasises the margin of arbitrariness in the choice of the normalisation scale, with respect to which it is possible to define the width of the boundary layers and to perform the integration and matching, after some appropriate approximations of the terms in the equations are assumed on heuristic basis. This makes possible the interpretation of $\delta_{\rm in}$ as the width of the solution in the innermost equation, information which is not evident if one follows instead the normalisation procedure we have adopted in this work. At the same time, it should be noticed that the scale $(\Delta'_{v_y})^{-1}$ seems to be not generally identifiable as the $\delta_{\rm in}$ obtained by Zocco & Schekochihin (2011): although the correspondence between the scalings of $\delta_{\rm in}$ obtained by these authors and the scaling of $(\Delta'_{v_y})^{-1}$ that we have obtained holds in the large-Δ' limit, it fails in the small-Δ' limits (cf. their (B54) and (B97) with the scalings at the end of § 10.3).

In summary, while on the one hand, we note the agreement of the results obtained by solving the boundary layer equations in the different models and with integration techniques that rely on slightly different heuristic hypotheses, on the other hand, we note that the appearance of the characteristic scale, which, in previous works, has been interpreted in terms of inherently kinetic features, in the MHD model of § 2, can be instead entirely related to 'fluid-like' features associated with the gradients of the velocity field in the non-ideal region. It should be also noticed, in this regard, the care with which conclusions drawn by heuristic estimates based on dimensional analysis must be dealt with: although it is comforting that different models of tearing mode analysis yield the same quantitative results, their physical interpretation is a more delicate issue, which requires further insight based on the consistency of the specific hypothesis of each model and therefore may not be univocal. In particular, the symmetry between the scaling laws in the small- and large-Δ' limits with respect to the substitution $\Delta' \leftrightarrow \Delta'_{v_y}$, which we have detailed in tables 3–5, suggests that the quantity Δ'_{v_y}, in this modelling related to inherently 'fluid' features, play a general, important role in the tearing mode regimes, which may deserve further investigations.

11. Summary and conclusions

We have reviewed the solution of the boundary layer problem for collisionless and resistive tearing instabilities in slab geometry, in both the small- and large-Δ' limits. The calculations in the warm regime, in which two matching regions are required, have been solved in the coordinate space by using the integral representation of hypergeometric functions to integrate the differential equations of the boundary layer approach (§§ 6 and 7). To the best of our knowledge, this kind of analysis has not been presented before, elsewhere, and in the present work, emphasis is put on a pedagogical derivation of the results. In this way, we have recovered the results first obtained by Pegoraro & Schep (1986), Pegoraro *et al.* (1989) and Porcelli (1991) in a Fourier representation.

https://doi.org/10.1017/S0022377822001088 Published online by Cambridge University Press

While developing this analysis, we have also been able to make a direct comparison (§ 6) with calculations in the coordinate space that had been earlier performed in the cold-collisionless regime and in the purely resistive regime of tearing modes, where a single matching region is required (Furth *et al.* 1963; Coppi 1964*c*; Ara *et al.* 1978), and with other calculations in the coordinate space that had been carried out in the warm-collisionless regime in the presence of warm ions (Zocco & Schekochihin 2011).

Then, by making reference to the results of the boundary layer calculations, we have been able to relate the inverse of the derivatives of the eigenfunctions evaluated on the neutral line to specific scalings with respect to the non-ideal parameters, which had not been noted before (§ 8.3). We have also shown the relation of the inverse of these derivatives with the reconnecting layer width, δ, whose operational definition, which we had previously verified in different reconnection regimes (Betar *et al.* 2020), we have here discussed for the first time (§ 8). These characteristic length scales, which can be useful for numerical diagnostics, are summarised in table 5.

We have interpreted in § 9 the results of the boundary layer analysis in light of heuristic derivations for the scalings of the growth rate and for the characteristic width of the reconnection layer, by following a dimensional analysis procedure that had been already successfully used in previous works but only when $\rho_s = 0$. In this way, we have highlighted in § 9.3 how the heuristic approach alone fails to provide the correct scaling when the ion-sound Larmor radius is not negligible ($\rho_s \gtrsim \bar{d}_e$).

Then, thanks to the operational definition we have given of δ, and by relying on both the heuristic estimates and the numerical solutions of the eigenvalue problem, we have shown a further non-trivial relation between the first derivative of ψ_1, evaluated close to the neutral line, and the gradients of the velocity component parallel to it (§ 10). We have, in this way, introduced an inverse characteristic scale length which we have named Δ'_{v_y}, because of its analogy with the classical Δ' parameter. Using this (inverse) scale length, we have therefore shown, both analytically and numerically, that, for the purpose of heuristic estimates, we can generally assume $\psi_1'|_{x=\delta} \sim \psi_1|_{x=\delta}/l_c$ with $l_c = \max\{(\Delta')^{-1}, (\Delta'_{v_y})^{-1}\} \gtrsim , \delta$. Knowing the asymptotic scaling of Δ'_{v_y}, an estimate of both δ and γ can be made in any RMHD reconnection regime (§ 10.4) by just using dimensional analysis.

It is interesting to note that, from an experimental point of view, density fluctuations n_1 are easier to be measured than magnetic perturbations ψ_1, and that the former can be related to the fluid stream function perturbation via $n_1 \sim \nabla^2\varphi$. In general, then, the estimate of the spatial gradients of φ_1 from experimentally measured profiles of the density may be more reliable than the evaluation of the spatial gradients of ψ_1. In this context, the characterisation of the large- and small-Δ' limits we have provided in § 10 with (10.6), or, more generally, the relation between the value of $\Delta'_{v_y} = (\varphi_1''/\varphi_1')|_{x=\delta} \sim \Delta'_{v_y}/2$ (cf. definition in (10.2)) and the scaling of δ or of the other scales detailed at the end of § 10.3, may be of interest.

Finally, we note that the introduction of the inverse scale Δ'_{v_y} makes the scaling laws in the large-Δ' limit mirror those in the small-Δ' limit provided the substitution $\Delta' \leftrightarrow \Delta'_{v_y}$.

Acknowledgements

This article was written in honour of F. Pegoraro's 70th birthday. It is our pleasure to recall his fundamental contributions to the linear and nonlinear theory of reconnecting instabilities in plasmas. The authors thank Miho Janvier (IAS CNRS – Université Paris-Saclay, France) and Chiara Marchetto (ISC-CNR Milano, Italy) for useful discussions about some bibliographical references. The authors are grateful to the 'Maison

de la simulation Lorraine' for partial time allocation on the cluster Explor (Project No. 2019M4XXX0978).

Editor Alex Schekochihin thanks the referees for their advice in evaluating this article.

Funding

This work was carried out within the framework of the French Federation for Magnetic Fusion Studies (FR-FCM) and of the Eurofusion consortium and received funding from the Euratom research and training programme 2014–2018 and 2019–2020 under grant agreement No. 633053 (WPEDU fundings obtained through FR-FCM AAP 2017–2021 'Evolution of current sheets in low-collision plasmas', in particular, are gratefully acknowledged). The views and opinions expressed herein do not necessarily reflect those of the European Commission. Neither the European Union nor the European Commission can be held responsible for them.

Declaration of interests

The authors report no conflict of interest.

Appendix A. Derivation of the model equations for tearing modes in slab RMHD

Different derivations exist in the literature of the set of tearing equations we have considered in this paper. For the inclusion of finite ion-sound Larmor radius effects in a two-field model under the strong (infinite) guide field hypothesis, we direct the reader for example to Schep *et al.* (1994), Kuvshinov, Pegoraro & Schep (1994), Bergmans (2001) and Del Sarto *et al.* (2006). Here below, we repropose however their complete derivation, with more details than in previous articles.

Despite the different procedures proposed over the years to obtain (2.1) and (2.2), it is agreed that their nonlinear form reads

$$\frac{\partial}{\partial t}(\psi - d_e^2\nabla^2\psi) + [\varphi, \psi - d_e^2\nabla^2\psi] = \rho_s^2[\nabla^2\varphi, \psi] + S^{-1}\nabla^2\psi, \tag{A1}$$

$$\frac{\partial}{\partial t}(\nabla^2\varphi) + [\varphi, \nabla^2\varphi] = [\psi, \nabla^2\psi]. \tag{A2}$$

The above equations have been written using the standard 'Poisson's bracket' notation, $[f(x, y, t), g(x, y, t)] \equiv \partial_x f \partial_y g - \partial_y f \partial_x g$. Each bracket term can be thus related to a convection term associated with one of the two scalar function involved, e.g.

$$[f, g] = (\nabla f \times \nabla g) \cdot \boldsymbol{e}_z = \underbrace{(\boldsymbol{e}_z \times \nabla f)}_{\boldsymbol{u}_f} \cdot \nabla g. \tag{A3}$$

Also note that in (2.1), the equilibrium contribution has been removed from the $S^{-1}\nabla^2\psi$ term for the sake of linear analysis, since, in the asymptotic limit $S^{-1} \ll 1$, the time scale of resistive dissipation of the magnetic equilibrium is *a posteriori* found to be much longer than that of the tearing-type instability.

The appropriateness of (A1) and (A2), and notably of the ρ_s^2-related contribution, is supported by comparison of the linear dispersion relation obtained in the collisionless regime ($\eta = \nu = 0$) with that obtained from the full Vlasov–Maxwell system in the same geometry configuration, that is, $\boldsymbol{B}^0 = \boldsymbol{B}_\perp^0 + B_z^0\boldsymbol{e}_z$ and $\boldsymbol{k} = \boldsymbol{k}_\perp + k_z\boldsymbol{e}_z$: the dispersion relation of shear kinetic-Alfvén waves (see e.g. Hasegawa & Uberoi 1982, pp. 19–21) is

https://doi.org/10.1017/S0022377822001088 Published online by Cambridge University Press

indeed recovered,

$$\omega^2 = c_{A,\perp} k_\perp \sqrt{\frac{1+k^2\rho_s^2}{1+k^2 d_e^2}}, \tag{A4}$$

where $c_{A,\perp}$ is the Alfvén velocity evaluated with the perpendicular magnetic component, only. Also note that (A1) and (A2) can be combined to give an equation for the energy conservation in the form

$$\frac{\partial}{\partial t}\int\int \left(\underbrace{|\nabla\psi|^2}_{\mathcal{E}_B} + \underbrace{d_e^2|\nabla^2\psi|^2}_{\mathcal{E}_J} + \underbrace{|\nabla\varphi|^2}_{\mathcal{E}_{\rm kin}} + \underbrace{\rho_s^2|\nabla^2\varphi|^2}_{\mathcal{E}_{\rm int}} \right) {\rm d}x\,{\rm d}y = 2S^{-1}\int\int |\nabla^2\psi|^2\,{\rm d}x\,{\rm d}y, \tag{A5}$$

where $\mathcal{E}_B, \mathcal{E}_J, \mathcal{E}_{\rm kin}, \mathcal{E}_{\rm int}$ stand for the energy contributions respectively related to the in-plane magnetic field, to the current density (or electron kinetic energy), to the ion kinetic energy and to the internal energy (in turn related to the electron thermal energy and to their parallel compressibility along magnetic lines – see Grasso *et al.* 1999).

The difference among the 'different' RMHD models which lead to the same set of (A1) and (A2) is in the weight that must be attributed to the different terms of the nonlinear equations with respect to the expansion parameters that have been adopted.

Here below, we focus on the first derivation proposed by Pegoraro & Schep (1986) and Schep *et al.* (1994); Kuvshinov *et al.* (1994) and that has been later re-discussed by Bergmans (2001) and Del Sarto *et al.* (2006). In this framework, (A1) and (A2) can be shown to follow from the z-component of the electron momentum equation, which gives (A1), and from the charge continuity equation, which gives (A2), under the assumption that $\boldsymbol{\nabla} = (\partial_x, \partial_y, 0)$ and that the gradient of the equilibrium density, and of its fluctuations as well, are smaller than the equilibrium quantity.

We start from the fluid equations for the species α, and we assume the ion pressure to be negligible with respect to the electron temperature (i.e. we take the cold-ion limit). The continuity and momentum equations can be written in dimensionless form, normalised to the MHD scales, as

$$\frac{\partial n^\alpha}{\partial t} + \boldsymbol{\nabla}\cdot(n^\alpha \boldsymbol{u}^\alpha) = 0, \tag{A6}$$

$$d_e^2\left(\frac{\partial \boldsymbol{u}^e}{\partial t} + \boldsymbol{u}^e\cdot\boldsymbol{\nabla}\boldsymbol{u}^e\right) = -d_i\left(\boldsymbol{E} + \boldsymbol{u}^e\times\boldsymbol{B} - \frac{\boldsymbol{J}}{S}\right) - \rho_s^2\frac{\boldsymbol{\nabla}\cdot\boldsymbol{\Pi}^e}{n^e}, \tag{A7}$$

$$d_i^2\left(\frac{\partial \boldsymbol{u}^i}{\partial t} + \boldsymbol{u}^i\cdot\boldsymbol{\nabla}\boldsymbol{u}^i\right) = d_i\left(\boldsymbol{E} + \boldsymbol{u}^i\times\boldsymbol{B} - \frac{\boldsymbol{J}}{S}\right). \tag{A8}$$

Above, the ion skin depth $d_i = d_e\sqrt{m_i/m_e}$ has been further introduced and the pressure tensor $\boldsymbol{\Pi}^e$ has been normalised to the electron density times an electron reference temperature. This, after normalisation to the MHD scales, makes the squared ion-sound Larmor radius appear (normalised to the equilibrium shear length).

From now on, we will refer the symbol $\perp$ to the components that are orthogonal to the guide field direction (i.e. $\boldsymbol{e}_z$), that is, that lie on the (x, y)-plane. Note that this differs from another notation, frequently used for example in tokamak geometry, in which the direction 'parallel' and 'perpendicular' are referred to the *total* magnetic field. The latter choice is generally more appropriate for the most general RMHD modelling, which we recall has

https://doi.org/10.1017/S0022377822001088 Published online by Cambridge University Press

been first introduced by Strauss (1976, 1977) in toroidal geometry and then in the so-called 'cylindrical tokamak' approximation, by ordering the ratio between the toroidal and the poloidal gradients to be comparable to the ratio between the poloidal and toroidal magnetic components. Our choice of notation is here justified by the assumption of translation invariance for the equivalent to the 'toroidal' component (i.e. $\partial_z = 0$), corresponding to the large guide field component too (cf. figure 5).

One of the two equations we will focus on is the z-component of Ohm's law, which, for reasons we will show next, is more convenient to rewrite in the form:

$$-E_z - \frac{d_e^2}{d_i}\frac{\partial u_z^e}{\partial t} - \boldsymbol{u}_\perp^e \cdot \left[\boldsymbol{B}\times\boldsymbol{e}_z + \frac{d_e^2}{d_i}\nabla u_z^e\right] = -S^{-1}J_z + \frac{\rho_s^2}{d_i}\frac{\nabla\cdot\boldsymbol{\Pi}^e}{n^e}\cdot\boldsymbol{e}_z. \tag{A9}$$

The other one is the charge continuity equation (i.e. the sum over species of (A6) multiplied by q^α/n^α), which, using the quasi-neutrality condition $q^e n^e + q^i n^i = 0$, we can rewrite as

$$q^e\boldsymbol{u}_\perp^e\cdot\nabla(\ln n^e) + q^i\boldsymbol{u}_\perp^i\cdot\nabla(\ln n^i) + \nabla\cdot(q^e\boldsymbol{u}_\perp^e + q^i\boldsymbol{u}_\perp^i) = 0. \tag{A10}$$

The two equations above will be then specialised by approximating the fluid equations in terms the expansion parameters:

$$\varepsilon_B \equiv \frac{|\boldsymbol{B}_\perp^0|}{B_z^0}, \quad \varepsilon_m \equiv \frac{m_e}{m_i}. \tag{A11}$$

The electromagnetic field components are written in terms of the scalar quantities of interest as

$$\boldsymbol{B} = \underbrace{B_z^0\nabla\psi\times\boldsymbol{e}_z}_{\boldsymbol{B}_\perp} + \underbrace{B_z^0(1+b_1)}_{B_z^0+B_z^1}\boldsymbol{e}_z, \quad \boldsymbol{E} = -\underbrace{\nabla\phi}_{\boldsymbol{E}_\perp} - \underbrace{\frac{1}{c}\frac{\partial\psi}{\partial t}\boldsymbol{e}_z}_{E_z}. \tag{A12}$$

Since we assume $\boldsymbol{J} = (c/4\pi)\nabla\times\boldsymbol{B}$, it follows $\nabla\cdot\boldsymbol{B} = 0$ and

$$\boldsymbol{J}_\perp = \frac{c}{4\pi}\nabla\times b\boldsymbol{e}_z, \quad J_z = -\frac{cB_z^0}{4\pi}\nabla^2\psi. \tag{A13}$$

After normalisation to the MHD scales, the fluid stream function $\varphi = \phi/(cB_z^0)$ appears as related to the electrostatic potential. Because of the uniform guide field hypothesis, the scalar function b also coincides with the first-order perturbation of the B_z component.

We furthermore assume $|\boldsymbol{B}_\perp^1| \sim |\boldsymbol{B}_\perp^0| \sim \varepsilon_B B_z^0$, whence it follows

$$\frac{\partial}{\partial t} \sim \frac{c_{A,\perp}}{L_0} \sim \varepsilon_B\frac{B_z^0}{L_0}, \tag{A14}$$

and we assume the charged particle dynamics along z to be mostly due to the electrostatic acceleration. This means that the ion velocity component along z, u_z^i, is ε_m times smaller than the electron velocity component, u_z^e, which is instead comparable in amplitude to both $\boldsymbol{u}_\perp^e$ and $\boldsymbol{u}_\perp^i$. This also means that $J_z \equiv q_i n_i u_z^i + q_e n_e u_z^e = q_e n_e u_z^e + \mathcal{O}(\varepsilon_m)$. In normalised units, $\boldsymbol{J} = n^e(\boldsymbol{u}^i - \boldsymbol{u}^e)$, and therefore

$$u_z^e = d_i\frac{\nabla^2\psi}{n_e} + \mathcal{O}(\varepsilon_m). \tag{A15}$$

The idea is then to use these hypotheses combined with a strong guide field limit so to consider the drift-ordering expansion for the $\boldsymbol{u}_\perp^\alpha$ fluid velocities. Using the standard

https://doi.org/10.1017/S0022377822001088 Published online by Cambridge University Press

procedure, we obtain from (A7) and (A8)) and (A12) the normalised velocity components:

$$\boldsymbol{u}^e_\perp = \underbrace{\boldsymbol{e}_z \times \nabla\varphi + (\boldsymbol{e}_z \times \nabla\psi)u^e_z - \frac{\rho_s^2}{d_i}\boldsymbol{e}_z \times \frac{\nabla \cdot \boldsymbol{\Pi}^e}{n_e} - S^{-1}\boldsymbol{e}_z \times \boldsymbol{J}_\perp}_{\text{1st order}} + \underbrace{\mathcal{O}(\varepsilon_m^{1/2}\varepsilon_B^2)}_{\text{2nd order}}, \tag{A16}$$

$$\boldsymbol{u}^i_\perp = \underbrace{\boldsymbol{e}_z \times \nabla\varphi - S^{-1}\boldsymbol{e}_z \times \boldsymbol{J}_\perp + \mathcal{O}(\varepsilon_m\varepsilon_B)}_{\text{1st order}} - \underbrace{d_i\left(\frac{\partial}{\partial t}\nabla\varphi + [(\boldsymbol{e}_z \times \nabla\varphi)\cdot\nabla]\nabla\varphi\right)}_{\text{2nd order}} + \mathcal{O}(\varepsilon_B^3). \tag{A17}$$

The $\mathcal{O}(\varepsilon_m\varepsilon_B)$ neglected terms in (A17) are due to the $(\boldsymbol{e}_z \times \nabla\psi)u^i_z$ contribution of the first-order drift-expansion. We note that the terms neglected in both equations are comparable if we order $\varepsilon_m \sim \varepsilon_B^2$.

Equations (A1) and (A2)) follow then from substitution of (A16) and (A17)) into (A9) and (A10) after a few further specific hypotheses. They are:

(i) the ordering $B^1_z/B^0_z = b \sim \varepsilon_B^2$, which also implies $|\boldsymbol{J}_\perp| \sim \varepsilon_B^2$; and
(ii) the assumption that the anisotropic electron pressure components are given by the first-order FLR corrections to a double adiabatic-type pressure tensor.

The original derivation had been obtained by Schep *et al.* (1994) in the strictly collisionless limit, in which, in the geometry of interest to us, the pressure tensor components including FLR 'gyrofluid' corrections can be written in dimensional units as

$$\boldsymbol{\Pi}^e = \begin{pmatrix} P^e_\perp + \dfrac{P^e_\perp}{\Omega_e}\left(\dfrac{\partial u^e_x}{\partial y} + \dfrac{\partial u^e_y}{\partial x}\right) & \dfrac{P^e_\perp}{\Omega_e}\left(\dfrac{\partial u^e_y}{\partial y} - \dfrac{\partial u^e_x}{\partial x}\right) & \dfrac{P^e_\perp}{\Omega_e}\left(\dfrac{\partial u^e_z}{\partial y}\right) \\ \dfrac{P^e_\perp}{\Omega_e}\left(\dfrac{\partial u^e_y}{\partial y} - \dfrac{\partial u^e_x}{\partial x}\right) & P^e_\perp - \dfrac{P^e_\perp}{\Omega_e}\left(\dfrac{\partial u^e_x}{\partial y} + \dfrac{\partial u^e_y}{\partial x}\right) & -\dfrac{P^e_\perp}{\Omega_e}\left(\dfrac{\partial u^e_z}{\partial x}\right) \\ \dfrac{P^e_\perp}{\Omega_e}\left(\dfrac{\partial u^e_z}{\partial y}\right) & -\dfrac{P^e_\perp}{\Omega_e}\left(\dfrac{\partial u^e_z}{\partial x}\right) & P^e_\parallel \end{pmatrix}. \tag{A18}$$

The components of matrix (A18) can be obtained by following a standard procedure (see e.g. Thompson 1961; Roberts & Taylor 1962; MacMahon 1965 for the ion case and Cerri *et al.* (2013) for a recent re-derivation for both species in the strictly collisionless limit). We make the further hypothesis that

$$P^e_\parallel \simeq P^e_\perp = n^e T^0 \tag{A19}$$

with T^0 reference electron temperature (uniform in space and constant in time). Since normalisation to the MHD reference quantities means that $\boldsymbol{u}^e$ is normalised to $c_{A,\perp} = d_i\Omega_i$ and spatial derivatives are normalised to $1/a$, using $\Omega_i/\Omega_e \simeq \varepsilon_m$, the combination of (A3),

https://doi.org/10.1017/S0022377822001088 Published online by Cambridge University Press

(A15), (A18) and (A19) gives:

$$\frac{\rho_s^2}{d_i}\frac{(\boldsymbol{\nabla}\cdot\boldsymbol{\Pi}^e)}{n^e}\cdot\boldsymbol{e}_z = \varepsilon_m d_i \frac{\rho_s^2}{n^e}\left(\frac{\partial n^e}{\partial x}\frac{\partial}{\partial y}\left(\frac{\nabla^2\psi}{n^e}\right) - \frac{\partial n^e}{\partial y}\frac{\partial}{\partial x}\left(\frac{\nabla^2\psi}{n^e}\right)\right)$$
$$= \varepsilon_m d_i \rho_s^2 \left[\ln n^e, \frac{\nabla^2\psi}{n^e}\right], \tag{A20}$$

$$\frac{\rho_s^2}{d_i}\boldsymbol{e}_z \times \frac{\boldsymbol{\nabla}\cdot\boldsymbol{\Pi}^e}{n^e} = \frac{\rho_s^2}{d_i}\boldsymbol{e}_z \times \boldsymbol{\nabla}(\ln n^e) + \mathcal{O}\left(\varepsilon_m\varepsilon_B\left|\frac{\boldsymbol{\nabla} n^e}{n^e}\right|\right). \tag{A21}$$

Note that, in (A21), FLR corrections contribute with terms $\sim \varepsilon_m\varepsilon_B$ smaller than the isotropic diamagnetic drift term: comparison with the neglected terms of (A16) and (A17) shows that they can be disregarded.

We can now rewrite (A9) without collisions as

$$\frac{\partial}{\partial t}\left(\psi - d_e^2\frac{\nabla^2\psi}{n^e}\right) + \boldsymbol{u}_\perp^e\cdot\boldsymbol{\nabla}\left(\psi - d_e^2\frac{\nabla^2\psi}{n^e}\right) = \varepsilon_m d_i\rho_s^2\left[\ln n^e, \frac{\nabla^2\psi}{n^e}\right]. \tag{A22}$$

From substitution of (A21) into (A16), we get, using $d_e^2 = \varepsilon_m d_i^2$,

$$\boldsymbol{u}_\perp^e\cdot\boldsymbol{\nabla}\left(\psi - d_e^2\frac{\nabla^2\psi}{n^e}\right) = \left[\varphi, \psi - d_e^2\frac{\nabla^2\psi}{n^e}\right] - \frac{\rho_s^2}{d_i}[\ln n^e, \psi]$$
$$+ \varepsilon_m d_i\rho_s^2\left[\ln n^e, \frac{\nabla^2\psi}{n^e}\right] + \mathcal{O}(\varepsilon_B^3) + \mathcal{O}(\varepsilon_m^{1/2}\varepsilon_B^2). \tag{A23}$$

Note the presence of a $[\ln n^e, \nabla^2\psi/n^e]$ term, identical to that of (A21), which is here due the diamagnetic drift contribution in the convection term $\boldsymbol{u}_\perp^e\cdot\boldsymbol{\nabla}u_z^e$ of the electron momentum equation. We can then write

$$\frac{\partial}{\partial t}\left(\psi - d_e^2\frac{\nabla^2\psi}{n^e}\right) + \left[\varphi, \psi - d_e^2\frac{\nabla^2\psi}{n^e}\right] = \frac{\rho_s^2}{d_i}[\ln n^e, \psi] + \mathcal{O}(\varepsilon_B^3) + \mathcal{O}(\varepsilon_m^{1/2}\varepsilon_B^2). \tag{A24}$$

The exact cancellation of the bracket terms proportional to $\varepsilon_m d_i\rho_s^2$ is known as 'gyroviscous (or, better 'gyrofluid') cancellation' (see Roberts & Taylor 1962). The terms involved are however at least $\varepsilon_m^{1/2}$ smaller than the other ones, even when d_e and ρ_s are left unordered with respect to ε_B or ε_m. Equation (A1) in the collisionless limit is finally recovered once we use continuity equations for ions and quasi-neutrality. From (A6), the continuity equation for ions can be rewritten as

$$\frac{\partial}{\partial t}\ln n^i + [\varphi, \ln n^i] = d_i\frac{\partial}{\partial t}\nabla^2\varphi + d_i[\varphi, \nabla^2\varphi] + \mathcal{O}(\varepsilon_B^3). \tag{A25}$$

Only the first-order $\boldsymbol{E}\times\boldsymbol{B}$ term of (A17) survives as a contribution to the convection term $\boldsymbol{u}_\perp^i\cdot\boldsymbol{\nabla}\ln n^i$, since we can heuristically order $|\boldsymbol{\nabla}\ln n^i| \sim \varepsilon_B$. Equation (A25) leads us to solve $\mathrm{d}(\ln n^i)/\mathrm{d}t = d_i\,\mathrm{d}(\nabla^2\varphi)/\mathrm{d}t$, of which we can take the solution $\ln n^i = d_i\nabla^2\varphi$ that verifies the heuristic hypothesis about the ordering of the spatial gradient of $\ln n^i$. From quasi neutrality, we finally write

$$\ln n^e = d_i\nabla^2\varphi, \tag{A26}$$

which brings (A24) to the form (A1) once we approximate $n^e \simeq n^0$ (i.e. $n^e \simeq 1$ in normalised units) in the left-hand side gradients of $\nabla^2\psi/n^e$.

https://doi.org/10.1017/S0022377822001088 Published online by Cambridge University Press

The equation for $\nabla^2\varphi$ is finally obtained from (A10) using the same approximation of the density n^e. Such equation follows from combining (A25) with the electron continuity equation, which, using (A16), reads

$$\frac{\partial}{\partial t}\ln n^e + [\varphi, \ln n^e] + d_i\left[\psi, \frac{\nabla^2\psi}{n^e}\right] + \mathcal{O}(\varepsilon_B^3) = \mathcal{O}(\varepsilon_m^{1/2}\varepsilon_B^2). \tag{A27}$$

Note that the $[\psi, \nabla^2\psi/n^e]$ contribution comes from the only non-null divergence term of (A16), that is, from $\boldsymbol{\nabla}\cdot((\boldsymbol{e}_z\times\boldsymbol{\nabla}\psi)u_z^e)$.

When collisions are included, the $+S^{-1}\nabla^2\psi$ contribution is recovered at the right-hand side of (A22) and (A23). In principle, the pressure tensor (A18) should be modified so as to include 'gyroviscous' corrections. These are provided, for example, by the model of Braginskii (1958). However, as long as the cold ion limit is formally assumed, so as to get rid of the ion temperature contribution, the corrections to the components of $\boldsymbol{\Pi}^e$ due to electron-ion viscosity are ε_m smaller than S^{-1}, and thus are also negligible in (A18). The last, further contribution we should care about is an additional $+S^{-1}\nabla^2 b \sim \mathcal{O}(S^{-1}\varepsilon_B^2)$ term at the right-hand side of (A25), which comes from the divergence of the $-S^{-1}\boldsymbol{e}_z\times\boldsymbol{J}_\perp$ term of ion drift velocity, (A17). This term is negligible under the further assumption $S^{-1}\ll d_i$. It must be noted that the latter choice is consistent with the fact that this two-field set of equations correspond to the extended MHD model in which the Hall term is neglected.

The quantitative comparison between the derivation here presented and that suggested by Kleva *et al.* (1995), Wang & Bhattcharjee (1995) and Bian & Tsiklauri (2009), in which the ρ_s^2-related Poisson bracket is interpreted as associated with the Hall-term contribution in Ohms' law – see also Del Sarto *et al.* (2006) and appendices of Del Sarto *et al.* (2016) – will be discussed elsewhere.

We finally recall that although in this modelling we assumed, since the beginning, strict translational invariance along z, i.e. $\partial/\partial z = 0$, the RMHD modelling in a strong guide field, large aspect ratio tokamak with toroidal coordinates (r, θ, φ) allows for the inclusion of the derivatives along φ that are ordered $\partial/\partial\varphi \sim \varepsilon_B\partial/\partial\theta$, i.e. $k_\varphi \sim \varepsilon_B k_\theta$ (Strauss 1976, 1977). This maps into a Cartesian 'extended-slab' RMHD modelling that includes the derivatives along z as corrections of order ϵ_B with respect to the perpendicular derivatives, i.e. $\partial/\partial z \sim \varepsilon_B\partial/\partial y$ or $k_z \sim \varepsilon_B k_y$ (see, e.g. Matthaeus & Lamkin 1986 or Biskamp 2000, p. 17). In the simplest, cold-electron limit, these corrections lead to further terms $+\partial\varphi_1/\partial z$ and $+\partial\nabla^2\psi_1/\partial z$ on the right-hand side of (A1) and (A2), respectively. The role of these terms, as well as of further ρ_s^2-related contributions linked to the parallel electron compressibility in the nonlinear evolution of tearing modes with different helicities, has been first investigated in an extended version of model equations (A1) and (A2) by Grasso *et al.* (2004) and Borgogno *et al.* (2005).

Appendix B. About alternative definitions of the reconnection rate

In the literature, alternative quantitative definitions exist, which, for historical reasons, are typically associated with the term 'reconnection rate', although they have been formulated under the hypothesis of steady reconnection. In the notation and geometry choice we make here, this alternative estimate of the reconnection rate can be written as

$$\mathcal{R}_{\text{steady}} = \frac{1}{L_0}U_x\big|^{\text{at some } x\neq 0}_{\text{near } X\text{-point}}. \tag{B1}$$

This definition originates from the Sweet–Parker model (Parker 1957), in which the rate at which the magnetic flux is reconnected, normalised with respect to the reference length

https://doi.org/10.1017/S0022377822001088 Published online by Cambridge University Press

L_0, is estimated as the component of the velocity $\boldsymbol{U}$ *perpendicular* to the neutral line such that

$$(U_x B_y)|^{\text{at some } x\neq 0}_{\text{near } X\text{-point}} = \mathcal{F}_z|^{\text{at some } x\neq 0}_{\text{near } X\text{-point}}. \tag{B2}$$

This relation holds in the neighbourhood of the neutral line under steadiness assumptions, for which the out-of-plane component of the electric field (E_z), which in planar reconnection is completely inductive (i.e. $E_z = -\partial\psi/\partial t$), is zero – cf. (2.7). In this case, the velocity U_x gives the rate per unit length L_0 at which the magnetic field lines are pushed and merged at the X-point.

Quantitative estimates of $\mathcal{R}_{\text{steady}}$ can be obtained by arguments relying on the continuity of the flow, which relate the velocity U_x, at which the magnetic field is dragged to the X point, to the velocity U_x at which, after reconnection has occurred, the field is transported out of it, along the neutral line ($U_x L \simeq U_y a$ – cf. figure 2*a*). These arguments also require a force balance condition implying that the upstream velocity U_y, evaluated close to the neutral line and sufficiently far from the X-point, is of the order of the Alfvén velocity evaluated with respect to B_y: these arguments allow one to relate $U_x|_{\text{near } X\text{-point}}$ to the dissipation mechanism given by $\mathcal{F}_z$ (Parker 1957; Petschek 1964; Parker 1973; Park *et al.* 1984; Wesson 1990).

Note that in the tearing mode scenario the reference length L_0 is a macroscopic quantity associated with the shear length a of the magnetic equilibrium, i.e. $L_0 = a$. In the first astrophysical applications of the steady reconnection scenario, instead, in which a distinction between equilibrium and perturbed quantities is not required, the macroscopic reference length was usually assumed to be of the order of the current sheet length L, i.e. $L_0 = L \gg a$, since the shear length a of the magnetic field $B_y(x)$ associated with the reconnecting current sheet was, in those contexts, a microscopic quantity. Thus, an alternative definition of 'reconnection rate per unit length L' is often met in the literature. This was defined by Petschek (1964) analogously to the Alfvénic Mach-number, from which it takes the symbol, as

$$M_{\text{rec}} = \frac{U_y|_{\text{near } X\text{-point}}}{U_x|_{\text{far from } X\text{-point}}} \simeq \frac{U_y|_{\text{near } X\text{-point}}}{c_A(L)}, \tag{B3}$$

where $c_A(L)$ is the Alfvén velocity evaluated in terms of B_y, measured sufficiently far from the neutral line along the neutral line $x = 0$, in a region where ideal MHD is valid. In the steady reconnection scenario, this definition is practically equivalent to (B1).

Finally, a further alternative definition of the reconnection rate is also often adopted,

$$\tilde{\mathcal{R}}_{\text{rec}} = \frac{1}{E_\parallel}\frac{\mathrm{d}E_\parallel}{\mathrm{d}t}\bigg|_{X\text{-point}}, \quad E_\parallel \equiv \frac{\boldsymbol{E}\cdot\boldsymbol{B}}{B}. \tag{B4}$$

We conclude by noting that while no ambiguity exists for the evaluation of the reconnection rate in the tearing-type instabilities with fixed wavenumber on which we are interested in this work, the situation becomes of course more complex in experimental contexts or in nonlinear numerical simulations of reconnection processes, especially if several reconnection sites (X-points) are simultaneously present and dynamically evolve in time. In those cases, estimates based on local measures like those provided by (2.13), (B3) and (B4) are of course more appealing for practical reasons. Their use for getting numerical values to be compared with scalings predicted by specific reconnection models should be however handled with care, since the way precision issues are determined in the measurement of numerical or experimental values is often unlikely to be sufficient to discriminate between a reconnection scenario or the other, e.g. in assessing the regime

https://doi.org/10.1017/S0022377822001088 Published online by Cambridge University Press

of reconnection events secondary to primary ones. Conversely, theoretical arguments supporting the existence or not of some specific regime are likely to provide a more accurate guide for the operational definition of reconnection rate that should be adopted in each case (cf. reference quoted just before (2.10)).

Appendix C. Integration of the boundary layer equation via Fourier transformation

Tackling the integration of tearing modes in the Fourier space with respect to the variable x is particularly useful since the overall order of the differential equations results is lowered (note that $\psi_0 \sim x \to \mathrm{d}/\mathrm{d}k_x$, whereas $\psi_1^{(N)} \to\sim k_x^N \hat{\psi}_1$). This approach is possible since the eigenfunctions we seek are bounded at each time with respect to the x variable. Also note that Fourier representation is quite natural in the mathematical treatment of the gyrokinetic operator in the Vlasov–Poisson equation which, at some level of the analysis, must be treated when FLR effects of electrons and/or of ions are included. However, while the integration in the Fourier space may be more efficient, from an analytical point of view, for obtaining the dispersion relation and the asymptotic scalings of γ and $\delta \sim \delta_1$, it has the drawback of requiring further analysis – not always trivial – for the computation of the eigenfunction profile in closed form in the coordinate space (i.e. the inverse Fourier transforms of the eigenfunctions integrated in the k_x-space must be evaluated).

C.1. *A brief historical review on the boundary layer approach to tearing-type equations in the Fourier space*

Fourier analysis was probably first applied to integrate interchange-type eigenmodes of MHD-type equations by Coppi (1964*b*), and was used in the tearing mode problem by Ara *et al.* (1978) to find approximate solutions of the inner equations from which to estimate the weight of ion–ion viscosity in the dispersion relation via a variational approach. A more detailed Fourier approach to tearing-type equations has been developed by Pegoraro & Schep (1981) to model low-frequency modes in toroidal tokamak geometry. This approach, which has been later used in several other specific reconnection models, consists in performing the Fourier transformation with respect to the stretched variable ζ of (5.9) and (5.10), and then combining the inner-layer equations for ψ_1 and φ_1 into a single equation for ψ_1. The integration of the tearing-type equations including FLR effect of both ions (for which a continuity equation was derived from a gyrokinetic one) and electrons (of which the isothermal limit was taken) has been first detailed by Pegoraro & Schep (1986), using the ballooning representation, and then, starting from a different kinetic model and using a somewhat different approach, by Cowley *et al.* (1986). The technique detailed by Pegoraro & Schep (1986) has been further used for the internal $m = 1$ kink mode in high-β regimes (Pegoraro *et al.* 1989). Relying on the same type of analysis, Porcelli (1991) derived the scaling laws for the collisionless regime in which magnetic reconnection occurs due to finite electron inertia and in combination with FLR effects. The Fourier analysis was also applied to investigate the scaling laws of the collisionless reconnection instabilities occurring in high frequency fluid regimes where ions form a neutralising background (Bulanov *et al.* 1992; Attico, Califano & Pegoraro 2000, 2001). The integration of tearing-type modes in Fourier space was then extended to other regimes in which electron temperature gradients at equilibrium are admitted and finite electron β effects are included, while a full gyro-kinetic model is taken for describing the ion response: motivated by the operational regime of large-size tokamaks, which is expected to fall in the semi-collisional regimes where the width of the semi-collisional region is much smaller that the ion Larmor radius and finite β-effects are expected to play an important role, Connor *et al.* (2012*b*) investigated tearing-type instabilities in low$-\beta$ and high-β

https://doi.org/10.1017/S0022377822001088 Published online by Cambridge University Press

regimes and the transition between them by relying on integration in the Fourier-space. In doing so, these authors also made a comparison of the solutions they obtained with those previously found in the coordinate space by Cowley *et al.* (1986). Here, solutions of tearing equations in the semi-collisional limit were obtained by starting from a full kinetic model and by performing an expansion of the eigenfunctions in powers of the ratio between the integration layer width over the ion Larmor radius. The technique used by Connor *et al.* (2012*b*) is analogous to the boundary layer approach discussed by Pegoraro & Schep (1981, 1986): using the fact that the dynamics of ions decouples from that of electrons at a distance of the order of the ion gyro-radius, the system of equations in each region was first transformed into a single equation for the current density in the Fourier space. Then, for the low$-\beta$ regime, the current density equation for ions was solved by Connor *et al.* (2012*b*) in Fourier space, while that for electrons was solved in real space. These solutions were made to match each other at some intermediate layer, while the solution in the ion region was also required to match that in the ideal MHD region, located far from the resonance surface. The technique to find the solution in the ion and electron regions consisted in expanding and matching the current density in powers of β. This method leads to a general dispersion relation that extends that of previous models by including four branches: the ion drift mode, the drift tearing mode, and other two branches corresponding to the kinetic Alfvén waves which couple to drift tearing modes for finite values of β.

C.2. *Comparison of the analysis of §§ 4–6 with the Fourier approach*

In the analysis of §§ 4–6, we have considered the low$-\beta$ regime with isothermal electrons, no equilibrium density fluctuations and cold ions, which rules out the coupling with drift modes while the coupling with kinetic Alfvén waves is restricted to the branch described by (A4). It is easy to show the essential points of the Fourier approach of Pegoraro & Schep (1986) discussed above, by making a direct comparison with the equations discussed in §§ 4–6 by Fourier transforming (5.9) and (5.10), and to combine them together so as to write a single equation for the Fourier components of the current density. To this purpose, let us first define Fourier transform for a function $f(\zeta)$ as

$$\hat{f} = \int_{-\infty}^{+\infty} f(\zeta) \mathrm{e}^{\mathrm{i}q\zeta}\, \mathrm{d}\zeta, \quad \zeta = \frac{x}{\sigma}, \quad q = k_x \sigma, \tag{C1}$$

where we have re-called the definition of the stretched variable, and therefore the relation of the 'stretched' Fourier coordinate q with k_x, the standard Fourier-conjugate wavenumber of x. For the scale σ, we have used the same notation of Porcelli (1991). In the notation adopted throughout the present manuscript, it would read indeed δ_1 or δ_2. Multiplying (5.9) and (5.10) by $\mathrm{e}^{\mathrm{i}q\zeta}$ and integrating from $-\infty$ to $+\infty$ while using the definition (C1), one obtains respectively

$$\frac{q^2}{\hat{\mathcal{G}}^2}\frac{\mathrm{d}^2\hat{\psi}_1}{\mathrm{d}q^2} - \left(1 + \frac{q^2}{\hat{\mathcal{G}}^2}\right)\hat{\psi}_1 = -\mathrm{i}d_e^2\frac{\mathrm{d}\hat{\tilde{\varphi}}}{\mathrm{d}q}, \quad \hat{\tilde{\varphi}} = -\mathrm{i}\frac{\mathrm{d}\hat{\psi}_1}{\mathrm{d}q}. \tag{C2}$$

Taking the derivative of the second equation in (C2) with respect to q and substituting the results in the former, one finds

$$\left(d_e^2 + \frac{q^2}{\hat{\mathcal{G}}^2}\right)\frac{\mathrm{d}^2\hat{\psi}_1}{\mathrm{d}q^2} - \left(1 + \frac{q^2}{\hat{\mathcal{G}}^2}\right)\hat{\psi}_1 = 0. \tag{C3}$$

This equation represents an eigenvalue problem for the eigenfunction $\hat{\psi}_1$. For analytical convenience, it is however useful to transform it in an eigenvalue problem for the current

https://doi.org/10.1017/S0022377822001088 Published online by Cambridge University Press

density $\hat{J}_1 = q^2\hat{\psi}_1$. After this substitution, one obtains

$$\left(d_e^2\hat{\mathcal{G}}^2 + q^2\right)\frac{\mathrm{d}^2}{\mathrm{d}q^2}\left(\frac{\hat{J}_1}{q^2}\right) - (q^2\hat{\mathcal{G}}^2 + 1)\hat{J}_1 = 0. \tag{C4}$$

This is the cold-ion limit of (3) of Porcelli (1991). The equivalence is evident once the following correspondence between variables and parameters of the aforementioned reference and those of §§ 4–6 are established: $\Gamma = \gamma$, $\Delta^2 = d_e^2(1 + S^{-1}/\gamma) \to d_e^2$, and $\rho_\tau = (\rho_s^2 + \rho_i^2)^{1/2} \to \rho_s$.

Here, we do not discuss further the solution of (C4), since it represents a specific case of the equation already solved by Pegoraro & Schep (1981, 1986) and further used by Pegoraro *et al.* (1989), Porcelli (1991), Attico *et al.* (2000, 2001) and Connor *et al.* (2012*b*).

Appendix D. An example of renormalisation of a differential equation

Consider (6.12) that we rewrite here for convenience as

$$\frac{\tilde{\varphi}_1''}{c_0} - \frac{A}{BC}\zeta^2\frac{\tilde{\varphi}_1}{c_0} = \frac{A}{B}\zeta, \tag{D1}$$

where

$$A \equiv \ell^2, \quad B \equiv \bar{d}_e^2, \quad C \equiv \mathcal{G}^2. \tag{D2}$$

As an example, let us consider the case in which also the scale ℓ is non-trivial (i.e. $\ell \neq 1$). From the point of view of physical dimensions, (6.12) and (D1) are already written in dimensionless form but we want to check if it is possible to bring them to the 'cleaner' form of (6.13), after further renormalisation of quantities. Suppose then to multiply (D1) by $A^aB^bC^c$, where a, b, c are here numerical coefficients to be determined *a posteriori*. Estimating, just for the purpose of dimensional analysis, $\tilde{\varphi}_1'' \sim \tilde{\varphi}_1/\zeta^2$, we obtain the following system:

$$A^aB^bC^c\left(\frac{\tilde{\varphi}_1}{c_0}\right)\zeta^{-2} \sim 1, \quad A^{a+1}B^{b-1}C^{c-1}\left(\frac{\tilde{\varphi}_1}{c_0}\right)\zeta^2 \sim 1, \quad A^{a+1}B^{b-1}C^c\zeta \sim 1. \tag{D3}$$

The choice of fixing all right-hand side coefficients equal to a number is made possible by the fact that the number of independent conditions is equal to or larger than the number of unknown coefficients a, b, c: the parameters A, B and C can be thus completely absorbed in the redefinition of ζ and $\tilde{\varphi}_1/c_0$. This is the case also when the scale ℓ is absent, i.e. when $\ell = A = 1$. When the number of parameters is larger than the number of constraints, some further parameter(s) corresponding to a dimensional combination(s) of powers of $A, B, \ldots$ will appear in the renormalised equations. The system above can be therefore solved to find that the values of the sought coefficients are $a = -3/4$, $b = 3/4$, $c = -1/4$. This means that we can define

$$\left.\begin{aligned} z &\equiv A^{a+1}B^{b-1}C^c\zeta = A^{1/4}B^{-1/4}C^{-1/4}\zeta, \\ \Phi &\equiv A^{-a-1}B^{-b+1}C^{-c-1}\left(\frac{\tilde{\varphi}_1}{c_0}\right) = A^{-1/4}B^{1/4}C^{-3/4}\left(\frac{\tilde{\varphi}_1}{c_0}\right). \end{aligned}\right\} \tag{D4}$$

For $\ell = 1$, this corresponds to (6.13).

https://doi.org/10.1017/S0022377822001088 Published online by Cambridge University Press

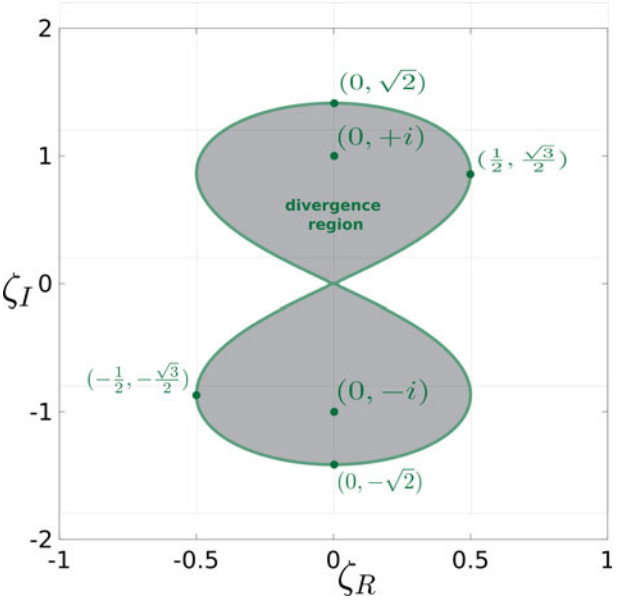

FIGURE 17. The region where the solutions ψ_α and ψ_β diverge is here displayed in a grey colour inside two lobes that join each other at $\zeta = 0$. Outside these two lobes, both series converge.

Appendix E. Convergence and independence of the solutions of the hypergeometric form of the inner equation

We here discuss some technical details about the solutions ((7.25) and (7.27)) of the innermost equation, which we have obtained by evaluation of the residues of its hypergeometric form.

E.1. *Convergence of ψ_α and ψ_β*

Following the ratio test of sequences for the coefficients of $(1+\zeta^2)^s$, one finds $\lim_{m\to\infty} g_{m+1}/g_m = 1$, meaning that the power series (7.25) and (7.27) converge when $\|1+\zeta^2\| > 1$. This region covers all the complex plane, except when $\zeta = 0$. In the complex plane, the boundary corresponding to the convergence radius $\|1+\zeta^2\| = 1$ is given by

$$(1 + \zeta_R^2 - \zeta_I^2)^2 + 4\zeta_R^2\zeta_I^2 = 1, \tag{E1}$$

which is a curve forming two lobes joining at $\zeta = 0$ and intersecting the $\zeta_R = 0$ axis at $\zeta_I = \sqrt{2}$, while the maximum width of the lobes occur at $\zeta_R = \pm 1/2$ and $\zeta_I = \pm\sqrt{3}/2$.

The region inside the lobes of figure 17 represents the divergence region, which includes the singular points at $\zeta_I = \pm i$.

E.2. *Linear independence of ψ_α and ψ_β*

It is not difficult to prove that the two solutions given by (7.25) and (7.27) are linearly independent in the domain of convergence, say $\mathcal{D}_{\alpha,\beta}$, where both ψ_α and ψ_β are defined. One way to prove this is to show that their Wronskian is non-zero everywhere in $\mathcal{D}_{\alpha,\beta}$. An easier way to proceed is to investigate the independence of the leading terms in both

https://doi.org/10.1017/S0022377822001088 Published online by Cambridge University Press

series. Taking $m = 0$, (7.25) and (7.27) become

$$\psi_{\alpha,0} = \frac{\Gamma(-\nu)}{\Gamma\left(\frac{5}{4} - \frac{\nu}{2}\right)\Gamma\left(\frac{1}{4} - \frac{\nu}{2}\right)}(1+\zeta^2)^{\alpha/2}, \quad \psi_{\beta,0} = \frac{\Gamma(\nu)}{\Gamma\left(\frac{5}{4} + \frac{\nu}{2}\right)\Gamma\left(\frac{1}{4} + \frac{\nu}{2}\right)}(1+\zeta^2)^{\beta/2}. \tag{E2}$$

The coefficients in the two previous relations are non-zero. Therefore, if $\alpha \neq \beta$, then $\psi_{\alpha,0}$ and $\psi_{\beta,0}$ are linearly independent, and so are ψ_α and ψ_β. However, if $\alpha = \beta$, then $\nu = 0$. Using the definition of the Γ function for positive and negative arguments, this means that the growth rate γ is purely imaginary. Therefore, in this case, the configuration is stable to tearing-type modes, which is not a case of interest here.

Another interesting remark related to (7.25) and (7.27) is that they are even functions with respect to ζ. Due to this symmetry, we expect that there is also an odd solution with respect to ζ which will be obviously linearly independent of the even solutions. The existence of this additional solution would apparently raise a paradox, because we would now have three independent solutions: the two independent even solutions ψ_α and ψ_β, and one odd solution, whereas a second-order ODE cannot have more than two linearly independent solutions. This apparent paradox can be solved by observing that going from $\zeta = 0^+$ to $\zeta = 0^-$ in the complex plane by passing through $\zeta = 0$ is not possible for any of the two series, because both ψ_α and ψ_β diverge there. Therefore, one should follow one of the lobes drawing the boundary of the divergence region in the complex plane (see figure 17), that is, one of the lobes encircling the singularities at $\zeta = \pm i$. Thus, to construct this solution, one can use a linear combination of the two series. This combination can be obtained using the integral representation and by choosing a path C_α (or C_β, alternatively) that goes around the poles associated with the exponent α (or β) by thus avoiding those of β (or α).

Appendix F. Heuristic estimation of the scaling laws by making use of the inverse gradient scale l_c and of Δ'_{v_y}

Here we discuss the logical steps of a unified heuristic procedure which would make it possible to deduce the correct scalings in any regime and wavelength limit among those considered in this work, were the scaling of Δ'_{v_y} be always deductible: in any regime, we obtain a scaling law, which is symmetric with respect to that of the small-Δ' limit prior to the substitution of $\Delta' \leftrightarrow \Delta'_{v_y}$. The proposed procedure, however, is 'self-consistent' in all regimes with the exception of the large-Δ', warm-electron limit, where the scaling of Δ'_{v_y} appears to be *a priori* non-deducible via dimensional analysis. To facilitate the identification and presentation of the logical steps of the proposed heuristic procedure, they are summarised as statements and formulae in tables 3–5.

In particular, in table 3, we recall the approximated linear equations, definitions and general constraints we rely upon, as well as the conclusions that can be drawn for them regardless of the reconnection regime considered.

Finally, in table 5, we consider the cold-tearing regimes ($\rho_s = 0$), both collisionless and resistive, by showing how the heuristic approach that takes Δ'_{v_y} into account works and still provides the good scalings. Although having introduced the new scale Δ'_{v_y} makes the heuristic procedure slightly longer than the one discussed in § 9.3, it allows one to appreciate the 'symmetry' between Δ' in the small-Δ' limit and Δ'_{v_y} in the large-Δ' limit also in these cold-electron regimes. More importantly, and differently from the warm-reconnection regimes, it becomes manifest that for $\rho_s = 0$, it is possible to close

https://doi.org/10.1017/S0022377822001088 Published online by Cambridge University Press

General hypotheses and conditions for a heuristic-type approach

Approximation	[T4.E1]	$\psi_1 - \frac{ik}{\gamma} x J_0 \varphi_1 \simeq d_e^2 \psi_1'' - \frac{\mathrm{i}kJ_0}{\gamma}\rho_s^2 x\varphi_1'' + \frac{S^{-1}}{\gamma}\psi_1''$
Equations	[T4.E2]	$\varphi_1'' \simeq -\frac{ikJ_0}{\gamma} x\psi_1''$
Definitions	[T4.D1]	$\delta: \quad \psi_1^{(iv)}(\delta) = 0$
	[T4.D2]	$l_c: \quad \psi_1'(\delta) \sim \frac{\psi_1(\delta)}{l_c}$
	[T4.D3]	$\Delta'_{v_y} \equiv \frac{\varphi_1''(\delta) - \varphi_1''(-\delta)}{\varphi_1'(\delta)} = \frac{2\varphi_1''(\delta)}{\varphi_1'(\delta)}$
	[T4.C1]	$\left.\frac{\gamma\varphi_1'}{k\psi_1}\right\|_{x=\delta} \sim \frac{2}{l_c\Delta'_{v_y}}$ (from T4.E2, T4.D2–T4.D3)
Constraints	[T4.C2a]	$\left.\frac{\gamma\varphi_1''}{k\psi_1}\right\|_{x=\delta} \sim O(1)$ $(\Delta'\delta \ll 1)$
	[T4.C2b]	$\left.\frac{\gamma\varphi_1'}{k\psi_1}\right\|_{x=\delta} \sim O(1)$ $(\Delta'\delta \gg 1)$
Hypotheses	[T4.H1]	$l_c \sim \max\{(\Delta')^{-1}, (\Delta'_{v_y})^{-1}\} \gtrsim \delta$
	[T4.H2]	$\psi_1''(\delta) \sim \frac{\psi_1(\delta)}{l_c\delta}$
Results 1	[T4.R1a]	$l_c \sim O(1) \Rightarrow l_c \sim (\Delta')^{-1} \gtrsim (\Delta'_{v_y})^{-1}$ (from T4.C2a, T4.D3 T4.C1 and T4.H1)
	[T4.R1b]	$l_c \sim (\Delta'_{v_y})^{-1} \gtrsim (\Delta')^{-1}$ (from T4.C21 and T4.Cb)

TABLE 3. Starting equations, definitions and assumptions based on general constraints that we take for the heuristic-type approach in all reconnection regimes. Equations [T4.E1–T4.E2] are the eigenmode equations ((2.1) and (2.2)) in which we have assumed k to be negligible with respect to the inverse scale of the spatial gradients of the eigenfunctions. Equations [T4.D1–T4.D3] are the operational definitions we have given in §§ 8, 9 and 10 of δ, l_c and Δ'_{v_y}, respectively. Equations [T4.C1,T4.C2] and [T4.H1] represent further conditions on the parameters that must be fulfilled regardless of the reconnection regime: [T4.C1] is a constraint that follows from [T4.E2] and definitions [T4.D2–T4.D3]; conditions [T4.C2a] and [T4.C2] correspond to (10.9) that we have discussed in the text; condition [T4.H1] corresponds to the ansatz (10.5) discussed in the text. Equations [T4.R1a] and [T4.R1b] are two immediate conclusions than can be drawn and allow us to specify hypothesis [T4.H1] in the small- and large-Δ' limits, respectively.

	Warm-reconnection regimes			
	warm-collisionless regime		warm-resistive regime	
Hypothesis 2	[T5.H2]	$\frac{k\delta}{\gamma}\frac{\varphi_1}{\psi_1}\Delta'_{v_y} \sim \frac{2}{\rho_s^2}$	($\psi_1 \sim \frac{k^2\rho_s^2}{\gamma^2}x^2\psi_1''$ in T4.E1, using T4.E2)	
Hypotheses 3	[T5.H3a]	$l_c\delta \sim d_e^2$	[T5.H3b]	$\gamma l_c\delta \sim S^{-1}$
		($\psi_1 \sim d_e^2\psi_1''$ in T4.E1)		($\psi_1 \sim \frac{S^{-1}}{\gamma}\psi_1''$ in T4.E1)
Result 2	[T5.R2]	$\gamma \sim k\rho_s\left(\frac{\delta}{l_c}\right)^{1/2}$		(from T4.C1 and T5.H2)
Result 3	[T5.R3a]	$\gamma \sim k\rho_s\frac{d_e}{l_c}$	[T5.R3b]	$\gamma \sim k^{2/3}\rho_s^{2/3}\frac{S^{-1/3}}{l_c^{2/3}}$
	(from T5.H3a, T5.R2)		(from T5.H3b, T5.R2)	
Result 4	[T5.R4a]	[T5.R4b]	[T5.R4c]	[T5.R4d]
	$\gamma \sim k\Delta'\rho_s d_e$	$\gamma \sim k\Delta'_{v_y}\rho_s d_e$	$\gamma \sim (k\Delta')^{2/3}\rho_s^{2/3}S^{-1/3}$	$\gamma \sim (k\Delta'_{v_y})^{2/3}\rho_s^{2/3}S^{-1/3}$
	($\Delta'\delta \ll 1$)	($\Delta'\delta \gg 1$)	($\Delta'\delta \ll 1$)	($\Delta'\delta \gg 1$)
	(from T4.R1a)	(from T4.R1b)	(from T4.R1a)	(from T4.R1b)
Result 5	[T5.R5a]	[T5.R5b]	[T5.R5c]	[T5.R5d]
	$\delta \sim \Delta' d_e^2$	$\delta \sim \Delta'_{v_y} d_e^2$	$\delta \sim (k\rho_s S)^{-2/3}\Delta'^{1/3}$	$\delta \sim (k\rho_s S)^{-2/3}\Delta'^{1/3}_{v_y}$
	($\Delta'\delta \ll 1$)	($\Delta'\delta \gg 1$)	($\Delta'\delta \ll 1$)	($\Delta'\delta \gg 1$)
	($\delta$is found by reversing T5.R2 for the relevant value of l_c and γ : $\delta \sim (\gamma/(k\rho_s))^2 l_c$)			

TABLE 4. Combining the hypotheses and results reported in table 2 with hypotheses [T5.H2–T5.H3] that are specific of the warm regimes, it is possible to deduce in a self-consistent way the set of equations [T5.R2–T5.R5]. It must be emphasised, however, that the system of condition is not closed in the large-Δ' regime and additional information about Δ'_{v_y} is required to obtain the corresponding scaling laws.

	Cold-reconnection regimes			
	cold-collisionless regime		cold-resistive regime	
Hypothesis 2	[T6.H2]	$\frac{k\delta}{\gamma}\frac{\varphi_1}{\psi_1} \sim O(1)$		($\psi_1 \sim i\frac{k}{\gamma}x\varphi_1$ in T4.E1)
Hypotheses 3	[T6.H3a]	$l_c\delta \sim d_e^2$	[T6.H3b]	$\gamma l_c\delta \sim S^{-1}$
		($\psi_1 \sim d_e^2\psi_1''$ in T4.E1)		($\psi_1 \sim \frac{S^{-1}}{\gamma}\psi_1''$ in T4.E1)
Constraint 3	[T6.C3]	$\frac{l_c+\delta}{l_c\delta} \sim \frac{k\delta}{\gamma}\frac{\varphi_1'}{\psi_1}$	($\psi_1' \sim i\frac{k}{\gamma}(x\varphi_1)'$ and T4.D2, T6.H2)	
Constraint 4	[T6.C4]	$\Delta'_{v_y} \sim \frac{1}{\delta}$	($(\frac{\psi_1}{x})'' \sim i\frac{k}{\gamma}\varphi_1''$ and T4.D2, T4.H2)	
Constraint 5	[T6.C5]	$\gamma^2 \sim 2\frac{k^2\delta^3}{l_c+\delta}$	(from T6.C3, T4.C1 using T6.C4)	
Results 2	[T6.R2a]	$\gamma \sim k\delta^{3/2}\Delta'^{1/2}$ for $\delta\Delta' \ll 1$		(T6.C5 and T4.R1a)
	[T6.R2b]	$\gamma \sim k\delta$ for $\delta\Delta' \gg 1$		(T6.C5, T4.R1b, T6.C5)
Results 3	[T6.R3a]	[T6.R3b]	[T6.R3c]	[T6.R3d]
	$\gamma \sim k\Delta'^2 d_e^3$	$\gamma \sim k\Delta'^2_{v_y} d_e^3$	$\gamma \sim (k\Delta'^2)^{2/5}S^{-3/5}$	$\gamma \sim (k\Delta'^2_{v_y})^{2/5}S^{-3/5}$
		$\sim kd_e$		$\sim k^{2/3}S^{-1/3}$
	($\Delta'\delta \ll 1$)	($\Delta'\delta \gg 1$)	($\Delta'\delta \ll 1$)	($\Delta'\delta \gg 1$)
	(from T4.R1a)	(from T4.R1b)	(from T4.R1a)	(from T4.R1b)
Result 4	[T6.R4a]	[T6.R4b]	[T6.R4c]	[T6.R4d]
	$\delta \sim \Delta' d_e^2$	$\delta \sim \Delta'_{v_y} d_e^2$	$\delta \sim k^{-2/5}\Delta'^{1/5}S^{-2/5}$	$\delta \sim k^{-2/5}\Delta'^{1/5}_{v_y}S^{-2/5}$
		$\sim d_e$		$\sim k^{-1/3}S^{-1/3}$
	($\Delta'\delta \ll 1$)	($\Delta'\delta \gg 1$)	($\Delta'\delta \ll 1$)	($\Delta'\delta \gg 1$)
	(δ is found by reversing T6.C5 using T6.H3a,b for the relevant value of γ)			

TABLE 5. Combining the hypotheses and results reported in table 2 with hypotheses [T6.H2] and [T6.H3] that are specific of the cold regimes, it is possible to deduce in a self-consistent way the set of equations [T6.C3]–[T6.R4]. Note that, in this case, the set of conditions is closed also in the large-Δ' regime thanks to [T6.H2], which leads to the constraint [T6.C4] that sets the scaling of Δ'_{v_y} to be the same of δ^{-1}. All scalings can be this way *a priori* determined without resorting to numerical calculations.

the system of heuristic conditions also in the large-Δ' limit, so as to determine *a priori* the corresponding scaling of Δ'_{v_y}, which here always results to be the same of δ.

In table 4, we specialise the results to the warm-tearing regimes ($\rho_s \neq 0$), both collisionless and resistive: in each regime, we report the further ansatz required to get the sought scalings in both the small- and large-Δ' limits. The 'symmetry' of the scalings written in the small-Δ' limit in terms of Δ' with respect to the scaling written in the large-Δ' limit in terms of Δ'_{v_y} can be in this way appreciated, although the system of equations is not closed in the large-Δ' limit and we must rely on additional information (e.g. numerical calculations performed by following the procedure detailed in previous § 10.3) to explicitly evaluate Δ'_{v_y}.

REFERENCES

Abramowitz, M. & Stegun, I. 1964 *Handbook of Mathematical Functions: with Formulas, Graphs, and Mathematical Tables*. Dover Ed.

Agullo, O., Muraglia, M., Benkadda, S., Poyé, A., Dubuit, N., Garbet, X. & Sen, A. 2017*a* Nonlinear dynamics of turbulence driven magnetic islands. I. Theoretical aspects. *Phys. Plasmas* **24**, 042308.

Agullo, O., Muraglia, M., Benkadda, S., Poyé, A., Dubuit, N., Garbet, X. & Sen, A. 2017*b* Nonlinear dynamics of turbulence driven magnetic islands. II. Numerical simulations. *Phys. Plasmas* **24**, 042309.

Alfvén, H. 1942 Existence of electromagnetic-hydrodynamic waves. *Nature* **150**, 405.

Ali, A., Li, J. & Kishimoto, Y. 2014 On the abrupt growth dynamics of nonlinear resistive tearing mode and the viscosity effect. *Phys. Plasmas* **21**, 052312.

Ara, G., Basu, B., Coppi, B., Laval, G., Rosenbluth, M.N. & Waddell, B.V. 1978 Magnetic reconnection and $m = 1$ oscillations in current carrying plasmas. *Ann. Phys*. **112**, 443–476.

Aschwanden, M.J. 2020 Global energetics of solar flares. IV. Coronal mass ejection energetics. *Astrophys. J*. **903**, 23.

Aschwanden, M.J., Caspi, A., Cohen, C.M.S., Holman, G., Jing, J., Kretzschmar, M., Kontar, E.P., McTiernan, J.M., Mewaldt, R.A., O'Flannagain, A., *et al.* 2019 Global energetics of solar flares and coronal mass ejections. *J. Phys.: Conf. Ser*. **1332**, 012002.

Aschwanden, M.J., Holman, G., O'Flannagain, A., Caspi, A., McTiernan, J.M. & Kontar, E.P. 2016 Global energetics of solar flares. III. Nonthermal energies. *Astrophys. J*. **832**, 27.

Aschwanden, M.J., Xu, Y. & Jing, J. 2014 Global energetics of solar flares. I. Magnetic energies. *Astrophys. J*. **797**, 50.

Attico, N., Califano, F. & Pegoraro, F. 2000 Fast collisionless reconnection in the whistler frequency range. *Phys. Plasmas* **7**, 2381–2387.

Attico, N., Califano, F. & Pegoraro, F. 2001 Charge separation effects in electron-magnetohydrodynamic reconnection. *Phys. Plasmas* **8**, 16.

Axford, W.I. 1984 *Magnetic field reconnection*. Geophysical Monograph Series, vol. 30, p. 1. American Geophysical Union.

Aydemir, A.Y. 1992 Nonlinear studies of $m = 1$ modes in high-temperature plasmas. *Phys. Fluids* B **4**, 3469–3472.

Basu, B. & Coppi, B. 1976 ... *Tech. Rep.* PRR-76/38. M.I.T., Cambridge, MA.

Basu, B. & Coppi, B. 1981 Theory of $m = 1$ modes in collisionless plasmas. *Phys. Fluids* **24**, 465–471.

Batchelor, G.K. 1950 On the spontaneous magnetic field in a conducting luquid in turbulent motion. *Proc. R. Soc. Lond.* A **201**, 405.

Baum, P.J., Bratenahl, A. & White, R.S. 1971 Experimental study of the reconnection process. *Radio Sci*. **8**, 917.

Bender, C.M. & Orszag, S.A. 1978 *Advanced Mathematical Methods for Scientists and Engineers 1: Asymptotic Methods and Perturbation Theory*. Springer.

Bergmans, J. 2001 Vortex interactions in magnetized plasmas. PhD thesis, Technische Universiteit Eindhoven, Eindhoven (The Netherlands).

https://doi.org/10.1017/S0022377822001088 Published online by Cambridge University Press

BERGMANS, J. & SCHEP, T.J. 2001 Merging of plasma currents. *Phys. Rev. Lett*. **87**, 195002.

BERK, H.L., MAHAJAN, S.M. & ZHANG, Y.Z. 1991 $m = 1$ kink mode for layer widths comparable to the ion Larmor radius. *Phys. Fluids* B **3**, 351.

BERTIN, G. 1982 Effects of local current gradients on magnetic reconnection. *Phys. Rev.* A **25**, 1786.

BETAR, H., DEL SARTO, D., OTTAVIANI, M. & GHIZZO, A. 2020 Multiparametric study of tearing modes in thin current sheets. *Phys. Plasmas* **27** (10), 102106.

BETTARINI, L., LANDI, S., RAPPAZZO, F.A., VELLI, M. & OPHER, M. 2006 Tearing and Kelvin–Helmholtz instabilities in the heliospheric plasma. *Astron. Astrophys*. **452**, 321.

BHATTACHARJEE, A., BRUNEL, F. & TAJIMA, T. 1983 Magnetic reconnection driven by the coalescence instability. *Phys. Fluids* **26**, 3332.

BHATTACHARJEE, A., GERMASCHEWSKI, K. & NG, C.S. 2005 Current singularities: drivers of impulsive reconnection. *Phys. Plasmas* **12**, 042305.

BHATTACHARJEE, A., HUANG, Y.M., YANG, H. & ROGERS, B. 2009 Fast reconnection in high-Lundquist-number plasmas due to the plasmoid instability. *Phys. Plasmas* **16**, 112102.

BIAN, N.H. & TSIKLAURI, D. 2009 Compressible magnetohydrodynamics in a strong magnetic field. *Phys. Plasmas* **16**, 064503.

BICKLEY, W.G. 1937 LXXIII. The plane jet. *Lond. Edinb. Dublin Philos. Mag. J. Sci*. **23**, 727.

BIRN, J. & HONES, E.W. JR. 1981 Three-dimensional computer modeling of dynamic reconnection in the geomagnetic tail. *J. Geophys. Res*. **86**, 6802.

BISKAMP, D. 1982 Dynamics of a resistive sheet pinch. *Z. Naturforsch*. **37a**, 840.

BISKAMP, D. 1986 Magnetic reconnection via current sheets. *Phys. Fluids* **29**, 1520.

BISKAMP, D. 1996 Magnetic reconnection in plasmas. *Astrophys. Space Sci*. **242**, 165.

BISKAMP, D. 2000 *Magnetic Reconnection in Plasmas*. Cambridge University Press.

BISKAMP, D. & BREMER, U. 1994 Dynamics and statistics of inverse cascade processes in 2D magnetohydrodynamic turbulence. *Phys. Rev. Lett*. **72**, 3819.

BISKAMP, D. & SATO, T. 1997 Partial reconnection in the nonlinear internal kink mode. *Phys. Plasmas* **4**, 1326.

BISKAMP, D., SCHWARZ, E. & DRAKE, J.F. 1995 Ion-controlled collisionless magnetic reconnection. *Phys. Rev. Lett*. **75**, 3850.

BISKAMP, D., SCHWARZ, E. & DRAKE, J.F. 1997 Two-fluid theory of collisionless magnetic reconnection. *Phys. Plasmas* **4**, 1002.

BISKAMP, D., SCHWARZ, E. & ZEILER, A. 1998 Instability of a magnetized plasma jet. *Phys. Plasmas* **5**, 2485–2488.

BISKAMP, D. & WELTER, H. 1980 Coalescence of magnetic islands. *Phys. Rev. Lett*. **44**, 1069.

BISKAMP, D. & WELTER, H. 1989 Dynamics of decaying two-dimensional magnetohydrodynamic turbulence. *Phys. Fluids* B **1**, 1989.

BOOZER, A.H. 2012 Theory of tokamak disruptions. *Phys. Plasmas* **19**, 058101.

BORGOGNO, D., GRASSO, D., CALIFANO, F., PEGORARO, F. & FARINA, D. 2005 Aspects of three-dimensional magnetic reconnection. *Phys. Plasmas* **12**, 032309.

BOYD, T.J.M. & SANDERSON, J.J. 2003 *The Physics of Plasmas*. Cambridge University Press.

BRAGINSKII, S.I. 1958 Transport phenomena in a completely ionized two-temperature plasma. *J. Expl Theor. Phys*. **6**, 358.

BRATENAHL, A. & YEATES, C.M. 1970 Experimental study of magnetic flux transfer at the hyperbolic neutral point. *Phys. Fluids* **13**, 26962696.

BRENNAN, D.P., STRAIT, E.J., TURNBULL, A.D., CHU, M.S., LA HAYE, R.J., LUCE, T.C., TAYLOR, T.S., KRUGER, S. & PLETZER, A. 2002 Tearing mode stability studies near ideal stability boundaries in DIII-D. *Phys. Plasmas* **9** (7), 2998.

BULANOV, S.V. 2017 Magnetic recoonection: from MHD to QED. *Plasma Phys. Control. Fusion* **59**, 014029.

BULANOV, S.V., PEGORARO, F. & SAKHAROV, A.S. 1992 Magnetic reconnection in electron magnetohydrodynamics. *Phys. Fluids* **8**, 2499–2508.

BULANOV, S.V., SAKAI, J. & SYROVATSKII, S.I. 1979 Tearing-mode instability in approximatively steady MHD configurations. *Sov. J. Plasma Phys*. **5**, 157.

https://doi.org/10.1017/S0022377822001088 Published online by Cambridge University Press

CAFARO, E., GRASSO, D., PEGORARO, F., PORCELLI, F. & SALUZZI, A. 1998 Invariants and geometric structures in nonlinear Hamiltonian magnetic reconnection. *Phys. Rev. Lett*. **80**, 4430.

CARRERAS, B.A., ROSENBLUTH, M.N. & HICKS, H.R. 1981 Nonlinear destabilisation of tearing modes. *Phys. Rev. Lett*. **46**, 1131.

CASSAK, P. & SHAY, M.A. 2012 Magnetic reconnection for coronal conditions: reconnection rates, secondary islands and onset. *Space Sci. Rev*. **172**, 283.

CERRI, S.S., HENRI, P., CALIFANO, F., DEL SARTO, D., FAGANELLO, M. & PEGORARO, F. 2013 Extended fluid models: pressure tensor effects and equilibria. *Phys. Plasmas* **20**, 112112.

CHEN, X.L. & MORRISON, P.J. 1990 Resistive tearing instability with equilibrium shear flow. *Phys. Fluids* B **2**, 495.

CHEN, Q., OTTO, A. & LEE, L.C. 1997 Tearing instability, Kelvin–Helmholtz instability, and magnetic reconnection. *J. Geophys. Res*. **102**, 151.

CHOI, M.J. 2021 Interaction between a magnetic island and turbulence. *Rev. Mod. Plasma Phys*. **9**, 1375.

COMISSO, L. & BHATTACHARJEE, A. 2016 On the value of the reconnection rate. *Phys. Plasmas* **82**, 595820601.

COMISSO, L., GRASSO, D., WAELBROECK, F.L. & BORGOGNO, D. 2013 Gyro-induced acceleration of magnetic reconnection. *Phys. Plasmas* **20**, 092118.

COMISSO, L., HUANG, Y.-M., LINGAM, M., HIRVIJOKI, E. & BHATTACHARJEE, A. 2018 Magnetohydrodynamic turbulence in the plasmoid-mediated regime. *Astrophys. J*. **854**, 103.

CONNOR, J.W., COWLEY, S.C. & HASTIE, R.J. 1990 Micro-tearing stability in tokamaks. *Plasma Phys. Control. Fusion* **32**, 799.

CONNOR, J.W., HASTIE, R.J., MARCHETTO, C. & ROACH, C.M. 2012*a* A one-dimensional tearing mode equation for pedestal stability studies in tokamaks. *J. Plasma Phys*. **84**, 725840301.

CONNOR, J.W., HASTIE, R.J. & ZOCCO, A. 2012*b* Unified theory of the semi-collisional tearing mode and internal kink mode in a hot tokamak: implications for sawtooth modelling. *Plasma Phys. Control. Fusion* **54**, 035003.

COPPI, B. 1964*a* Addendum on inertial interchange modes. *Phys. Lett*. **12**, 213–214.

COPPI, B. 1964*b* Gravitational instabilities in a compressible collisional plasma layer. *Ann. Phys*. **30**, 178.

COPPI, B. 1964*c* Inertial instabilities in plasmas. *Phys. Lett*. **11**, 226–228.

COPPI, B. 1965 Current-driven instabilities in configurations with sheared magnetic fields. *Phys. Fluids* **8**, 2237.

COPPI, B. & DETRAGIACHE, P. 1992 Magnetic topology transitions in collisionless plasmas. *Phys. Lett.* A **168**, 59.

COPPI, B., GALVAO, R., PELLAT, R., ROSENBLUTH, M.N. & RUTHERFORD, P. 1976 Resistive internal kink modes. *Fyz. Plazmy* **2**, 961.

COPPI, B., LAVAL, G. & PELLAT, R. 1966 Dynamics of the geomagnetic tail. *Phys. Rev. Lett*. **16**, 1207–1210.

COPPI, B., MARK, J.W.-K., SUGIYAMA, L. & BERTIN, G. 1979 Reconnecting modes in collisionless plasmas. *Phys. Rev. Lett*. **42**, 1058.

COWLEY, S.C. & HASTIE, R.J. 1988 Electron diamagnetism and toroidal coupling of tearing modes. *Phys. Fluids* **31**, 426.

COWLEY, S.C., KULSRUD, R.M. & HAHM, T.S. 1986 Linear stability of tearing modes. *Phys. Fluids* **29** (10), 3230–3244.

COWLING, T.G. 1933 The magnetic field of sunspots. *Mon. Not. R. Astron. Soc*. **94**, 39.

COWLING, T.G. 1967 Commission de la Magneto-Hydrodynamique et de la Physique des Gaz Ionises. In *Reports on Astronomy/Proceedings of the Thirteenth General Assembly Prague 1967* (ed. L. Perek), p. 965. Springer.

CROSS, M.A. & VAN HOVEN, G. 1971 Magnetic and gravitational energy release by resistive instabilities. *Phys. Rev.* A **4**, 2347.

DAUGHTON, W. 1999 The unstable eigenmodes of a neutral sheet. *Phys. Plasmas* **6**, 1329–1343.

DAUGHTON, W. & KARIMABADI, H. 2005 Kinetic theory of collisionless tearing at the magnetopause. *J. Geophys. Res*. **110**, A03217.

DAUGHTON, W. & SCUDDER, J. 2006 Fully kinetic simulations of undriven magnetic reconnection with open boundary conditions. *Phys. Plasmas* **13**, 072101.

DEL SARTO, D., CALIFANO, F. & PEGORARO, F. 2003 Secondary instabilities and vortex formation in collisionless-fluid magnetic reconnection. *Phys. Rev. Lett*. **91**, 235001.

DEL SARTO, D., CALIFANO, F. & PEGORARO, F. 2005 Current layer cascade in collisionless electron-magnetohydrodynamic reconnection and electron compressibility effects. *Phys. Plasmas* **12**, 012317.

DEL SARTO, D., CALIFANO, F. & PEGORARO, F. 2006 Electron parallel compressibility in the nonlinear development of two-dimensional magnetohydrodynamic reconnection. *Mod. Phys. Lett.* B **8**, 931–961.

DEL SARTO, D., MARCHETTO, C., PEGORARO, F. & CALIFANO, F. 2011 Finite Larmor Radius effects in the nonlinear dynamics of collisionless magnetic reconnection . *Plasma Phys. Control. Fusion* **53**, 035008.

DEL SARTO, D. & OTTAVIANI, M. 2017 Secondary fast reconnecting instability in the sawtooth crash. *Phys. Plasmas* **24**, 012102.

DEL SARTO, D., OTTAVIANI, M., PUCCI, F., TENERANI, A. & VELLI, M. 2018 Spontaneous magnetic reconnection of thin current sheets. In *Comptes-rendues de la* 21^{e} *Rencontre du Non Linéaire, Paris* (ed. É. Falcon, M. Lefranc, F. Pétrélis, & C.-T. Pham), vol. 21, p. 13. Université Paris Diderot, Non-Linéaires Publications.

DEL SARTO, D. & PEGORARO, F. 2017 Shear-induced pressure anisotropization and correlation with fluid vorticity in a low collisionality plasma. *Mon. Not. R. Astron. Soc*. **475**, 181.

DEL SARTO, D., PUCCI, F., TENERANI, A. & VELLI, M. 2016 "Ideal" tearing and the transition to fast reconnection in the weakly collisional MHD and EMHD regimes . *J. Geophys. Res*. **121**, A021975.

DENG, X.H. & MATSUMOTO, H. 2001 Rapid magnetic reconnection in the earth's magnetosphere mediated by whistler waves. *Nature* **401**, 557.

DOERK, H., JENKO, F., PUESCHEL, M.J. & HATCH, D.R. 2011 Gyrokinetic microtearing turbulence. *Phys. Rev. Lett*. **106**, 155003.

DORLAND, W. & HAMMETT, G.W. 1993 Gyrofluid turbulence models with kinetic effects. *Phys. Fluids* B **5**, 812–835.

DRAKE, J.F. & KLEVA, R.G. 1991 Collisionless reconnection and the sawtooth crash. *Phys. Rev. Lett*. **66**, 1458.

DRAKE, J.F. & LEE, Y.C. 1977 Kinetic theory of tearing instabilities. *Phys. Fluids* **20**, 035008.

DRAKE, J.F., SWISDAK, M., SCHOEFFLER, K.M., ROGERS, B.N. & KOBAYASHI, S. 2006 Formation of secondary islands during magnetic reconnection. *Geophys. Res. Lett*. **L13105**, 035008.

DUBROVIN, B.A., NIVIKOV, S.P. & FOMENKO, A.T. 1991 *Modern Geometry. Methods and Applications: Part I. The Geometry of Surfaces, Transformation Groups, and Fields*. Springer.

DUNGEY, J.W. 1950 Some Researches in Cosmic Magnetism. PhD thesis, Cambridge University, Cambridge (UK).

DUNGEY, J.W. 1953 Conditions for the occurrence of electrical discharges in astrophysical systems. *Lond. Edinb. Dubl. Phil. Mag*. **29** (7), 752–738.

EASTWOOD, J.P., HAPGOOD, M.A., BIFFIS, E., BENEDETTI, D., BISI, M.M., GREEN, L., BENTLEY, R.D. & BURNETT, C. 2018 Quantifying the economic value of space weather forecasting for power grids: an exploratory study. *Space Weath*. **16**, 2052.

EINAUDI, G. & RUBINI, F. 1986 Resistive instabilities in a flowing plasma: I. Inviscid case. *Phys. Fluids* **29**, 2563.

ELSASSER, W.M. 1950*a* Induction effects in terrestrial magnetism. Part III. Electric modes. *Phys. Rev*. **72**, 827.

ELSASSER, W.M. 1950*b* The Earth's interior and geomagnetism. *Rev. Mod. Phys*. **22**, 183.

FAGANELLO, M., PEGORARO, F., CALIFANO, F. & MARRADI, L. 2010 Collisionless magnetic reconnection in the presence of a sheared velocity field. *Phys. Plasmas* **17**, 062102.

FEDELE, B., NEGULESCU, C. & OTTAVIANI, M. 2021 Analysis of the kolmogorov model with an symptotic preserving method. *Phys. Lett.* A **127522**, 410.

FINN, J.M. & KAW, P.K. 1977 Coalescence instability of magnetic islands. *Phys. Fluids* **20**, 72.

FIRPO, M.-C. 2015 Microtearing turbulence: magnetic braiding and disruption limit. *Phys. Fluids* **22**, 122511.

FITZPATRICK, R. 2008 Scaling of the peak magnetic reconnection rate in the inviscid Taylor problem. *Nucl. Fusion* **15**, 024503.

FITZPATRICK, R., HASTIE, R.J., MARTIN, T.J. & ROACH, C.M. 1993 Stability of coupled tearing modes in tokamaks. *Nucl. Fusion* **33** (10), 1533.

FRANCI, L., CERRI, S.S., CALIFANO, F., LANDI, S., PAPINI, E., VERDINI, A., MATTEINI, L., JENKO, F. & HELLINGER, P. 2017 Magnetic reconnection as a driver for a sub-ion-scale cascade in plasma turbulence. *Astrophys. J. Lett*. **850**, L16.

FRANCI, L., LANDI, S., MATTEINI, L., VERDINI, A. & HELLINGER, P. 2016 Plasma beta dependence of the ion-scale spectral break of solar windturbulence: high-resolution 2D hybrid simulations. *Astrophys. J*. **883**, 91.

FRANCI, L., PAPINI, E., DEL SARTO, D., HELLINGER, P., BURGESS, D., MATTEINI, L., LANDI, S. & MONTAGUD-CAMPS, V. 2022 Plasma turbulence in the near-Sun and near-Earth solar wind: a comparison via observation-driven 2D hybrid simulations. *Universe* **8**, 453.

FRUCHTMAN, A. 1991 Penetration and expulsion of magnetic fields in plasmas due to the hall field. *Phys. Fluids* B **3**, 1908.

FURTH, H. 1963 Hydromagnetic instabilities due to finite resistivity. In *Propagation and Instabilities in Plasmas – Seventh Lockheed symposium on magnetohydrodynamics (December 1962)* (ed. W.I. Futtermann), pp. 87–102. Stanford University Press.

FURTH, H. 1964 Instabilities due to finite resistivity or finite current-carrier mass. In *Proceedings of the "Enrico Fermi" International School of Physics of the Italian Physical Society, Course XXV. Advanced plasma Theory* (ed. M.N. Rosenbluth), p. 159. Academic Press.

FURTH, H.P., KILLEEN, J. & ROSENBLUTH, M.N. 1963 Finite-resistivity instabilities of a sheet pinch. *Phys. Fluids* **6**, 459–484.

FURTH, H.P., RUTHERFORD, P.H. & SELBERG, H. 1973 Tearing mode in cylindrical tokamak. *Phys. Fluids* **16**, 1054.

GIOVANELLI, R.G. 1946 A theory of chromospheric flares. *Nature* **158**, 81.

GLADD, N.T., DRAKE, J.F., CHANG, C.L. & LIU, C.S. 1980 Electron temperature gradient driven microtearing mode. *Phys. Fluids* **23**, 1182.

GOPALSWAMY, N. 2016 History and development of coronal mass ejections as a key player in solar terrestrial relationship. *Geosci. Lett*. **3** (1), 1.

GOSLING, J.T. & MCCOMAS, D.J. 1987 Field line draping about fast coronal mass ejecta: a source of strong out-of-the-ecliptic interplanetary magnetic fields. *Geophys. Res. Lett*. **14** (4), 355.

GRADSHTEYN, I.S. & RYZHIK, I.M. 2015 *Table of Integrals, Series, and Products (VIII Edition)*. Elsevier.

GRANIER, C., BORGOGNO, D., GRASSO, D. & TASSI, E. 2022 Gyrofluid analysis of electron β_e effects on collisionless reconnection. *J. Plasma Phys.* **88** (1), 905880111.

GRASSO, D., BORGOGNO, D., CALIFANO, F., FARINA, D., PEGORARO, F. & PORCELLI, F. 2004 Numerical solution of a reduced model of collisionless magnetic reconnection in two and three dimensions. *Phys. Plasmas* **164**, 23.

GRASSO, D., BORGOGNO, D. & PEGORARO, F. 2007 Secondary instabilities in two- and three-dimensional magnetic reconnection in fusion relevant plasmas. *Phys. Plasmas* **14**, 055703.

GRASSO, D., BORGOGNO, D., PEGORARO, F. & TASSI, E. 2009 Coupling between reconnection and Kelvin–Helmholtz instabilities in collisionless plasmas. *Nonlinear Process. Geophys*. **16**, 241.

GRASSO, D., BORGOGNO, D., TASSI, E. & PERONA, A. 2020 Asymmetry effects driving secondary instabilities in two-dimensional collisionless magnetic reconnection. *Phys. Plasmas* **2**, 012302.

GRASSO, D., CALIFANO, F., PEGORARO, F. & PORCELLI, F. 2001 Phase mixing and island saturation in Hamiltonian reconnection. *Phys. Rev. Lett*. **86**, 5051.

GRASSO, D., OTTAVIANI, M. & PORCELLI, F. 2001 Linear stability and mode structure of drift tearing modes. *Phys. Plasmas* **8**, 4306.

GRASSO, D., PEGORARO, F., PORCELLI, F. & CALIFANO, F. 1999 Hamiltonian magnetic reconnection. *Plasma Phys. Control. Fusion* **41**, 1497.

GREENE, J.M. 1993 Reconnection of vorticity lines and magnetic lines. *Phys. Fluids* B **5**, 2355.

GU, Y.J., PEGORARO, F., SASAROV, P.V., GOLOVIN, D., YOGO, A., KORN, G. & BULANOV, S.V. 2019 Electromagnetic burst generation during annihilation of magnetic field in relativistic laser-plasma interaction. *Sci. Rep*. **9**, 19462.

HAHM, T.S. 1988 Neoclassical tearing modes in a tokamak. *Phys. Fluids* **31**, 3709–3712.

HAHM, T.S. & KULSRUD, R.M. 1985 Forced magnetic reconnection. *Phys. Fluids* **28**, 2412.

HARRIS, E.G. 1962 On a plasma sheath separating regions of oppositely directed magnetic field. *Il Nuovo Cimento* **23**, 115.

HASEGAWA, A. & UBEROI, C. 1982 *The Alfvén Wave*. Technical Information Centre, U.S. Departement of Energy.

HAUTZ, R. & SCHOLER, M. 1987 Numerical simulations on the structure of plasmoids in the deep tail. *Geophys. Res. Lett*. **14**, 969.

HAZELTINE, R.D. & ROSS, D.W. 1975 Kinetic theory of tearing instability. *Phys. Fluids* **18**, 1778.

HESSE, M., FORBES, T.G. & BIRN, J. 1999 The diffusion region in collisionless magnetic reconnection. *Phys. Plasmas* **6**, 1781.

HESSE, M., FORBES, T.G. & BIRN, J. 2005 On the relation between reconnected magnetic flux and parallel electric fields in the solar corona. *Astrophys. J*. **1227**, 631.

HICKS, H.R., CARRERAS, B.A. & HOLMES, J.A. 1984 The effect of diamagnetic rotation on the nonlinear coupling of tearing modes. *Phys. Fluids* **27**, 909.

HOFMANN, I. 1974 Resistive tearing modes in a sheet pinch with shear flow. *Plasma Phys*. **17**, 143.

HOLOBORODKO, P. 2012 Multiprecision Computing Toolbox for MATLAB.

HONES, E.W. 1979 Transient phenomena in the magnetotail and their relation to substorms. *Space Sci. Rev*. **23** (3), 393.

HOYLE, F. 1949 *Some recent Researches in Solar Physics*. Cambridge University Press.

HUANG, Y.-M. & BHATTACHARJEE, A. 2010 Scaling laws of resistive magnetohydrodynamic reconnection in the high-Lundquist-number, plasmoid-unstable regime. *Phys. Plasmas* **17**, 062104.

JANVIER, M. 2017 Three-dimensional magnetic reconnection and its application to solar flares. *J. Plasma Phys*. **83**, 535830101.

JARDIN, S.C., KREBS, I. & FERRARO, N. 2020 A new explanation of the sawtooth phenomena in tokamaks. *J. Plasma Phys*. **27**, 032509.

KLEVA, R.G., DRAKE, J.F. & WAELBROECK, F.L. 1995 Fast reconnection in high temperature plasmas. *Phys. Plasmas* **2**, 23.

KNIPP, D.J., FRASER, B.J., SHEA, M.A. & SMART, D.F. 2018 On the little-known consequences of the 4 August 1972 ultra-fast coronal mass ejecta: facts, commentary, and call to action. *Space Weath*. **16**, 1635.

KOWAL, G., FALCETA-GONÇALVES, D.A., LAZARIAN, A. & VISHNIAC, E.T. 2020 Kelvin–Helmholtz versus tearing instability: what drives turbulence in stochastic reconnection? *Astrophys. J*. **892**, 50.

KUMAR, P., KARPEN, J.T., ANTIOCHOS, S.K., WYPER, P.F. & DEVORE, C.R. 2019 First detection of plasmoids from breakout reconnection on the Sun. *Astrophys. J. Lett*. **885**, L15.

KUVSHINOV, B.N., PEGORARO, F. & SCHEP, T.J. 1994 Hamiltonian formulation of low-frequency nonlinear plasma dynamics. *Phys. Lett.* A **191**, 296–300.

KUVSHINOV, B.N. & SCHEP, T.J. 1997 Geometrical approach to fluid models. *Phys. Plasmas* **4**, 537.

LÜTJENS, H. & LUCIANI, J.-F. 2002 Linear and nonlinear thresholds of neoclassical tearing modes in tokamaks. *Phys. Plasmas* **9**, 4837.

LAKHINA, G.S. & TSURUTANI, B.T. 2016 Geomagnetic storms: historical perspective to modern view. *Geosci. Lett*. **3**, 1–11.

LANDI, S., DEL ZANNA, L., PAPINI, E., PUCCI, F. & VELLI, M. 2015 Resistive magnetohydrodynamics simulations of the ideal tearing mode. *Astrophys. J*. **806**, 131.

LAVAL, G., PELLAT, R. & VUILLEMIN, M. 1966 *Instabiliteés electromagnetiques des plasmas sans collisions*, vol. 2, p. 259. International Atomic Energy Agency.

LE, A., EGEDAL, J., OHIA, O., DAUGHTON, W., KARIMABADI, H. & LUKIN, V.S. 2013 Regimes of the electron diffusion region in magnetic reconnection. *Phys. Rev. Lett*. **110**, 135004.

LEAMON, R.J., MATTHAEUS, W.H., SMITH, C.W., ZANK, G.P., MULLAN, D.J. & OUGHTON, S. 2000 MHD-driven kinetic dissipation in the solar wind and corona. *Atsrophys. J*. **537** (2), 1054.

LI, J.H. & MA, Z.W. 2012 Roles of super-Alfvenic shear flows on Kelvin–Helmholtz and tearing instability in compressible plasma. *Phys. Scr*. **86**, 045503.

LIN, J., CRANMER, S.R. & FARRUGIA, C.J. 2008 Plasmoids in reconnecting curent sheets: solar and terrestrial contexts compared. *J. Geophys. Res*. **113**, A11107.

LONGCOPE, D.W. & STRAUSS, H.R. 1993 The coalescence instability and the development of current sheets in two- dimensional magnetohydrodynamics. *Phys. Scr.* **5**, 2858.

LOUREIRO, N.F., COWLEY, S.C., DORLAND, W.D., HAINES, M.G. & SCHEKOCHIHIN, A. 2005 X-point collapse and saturation in the nonilnear tearing mode reconnection. *Phys. Rev. Lett.* **95**, 235003.

LOUREIRO, N.F. & HAMMETT, G.W. 2008 An iterative semi-implicit scheme with robust damping. *J. Comput. Phys.* **227**, 4518–4542.

LOUREIRO, N.F., SCHEKOCHIHIN, A. & COWLEY, S.C. 2007 Instability of current sheets and formation of plasmoid chains. *Phys. Plasmas* **14**, 0703.

LOUREIRO, N.F. & UZDENSKY, D.A. 2016 Magnetic reconnection: from the Sweet–Parker model to stochastic plasmoid chains. *Mon. Not. Lett.* **58**, 014021.

LOUREIRO, N.F., UZDENSKY, D.A., SCHEKOCHIHIN, A., COWLEY, S.C. & YOUSEF, T.A. 2009 Turbulent magnetic reconnection in two dimensions. *Mon. Not. Lett.* **399**, L146.

LOVELOCK, D. & RUND, H. 1989 *Tensors, Differential Forms and Variational Principles*. Dover Publ.

LUNDQUIST, S. 1951 On the stability of magneto-hydrostatic fields. *Phys. Rev.* **83**, 307.

LYUTIKOV, M. 2003 Explosive reconnection in magnetars. *Mon. Not. R. Astron. Soc.* **346**, 540.

MACMAHON, A. 1965 Finite gyro-radius corrections to the hydromagnetic equations for a Vlasov plasma. *Phys. Fluids* **8**, 1804.

MAHAJAN, S.M., HAZELTINE, R.D., STRAUSS, H.R. & ROSS, D.W. 1978 Collisionless "current-channel" tearing modes. *Phys. Rev. Lett.* **41**, 1375.

MAHAJAN, S.M., HAZELTINE, R.D., STRAUSS, H.R. & ROSS, D.W. 1979 Unified theory of tearing modes. *Phys. Fluids* **22**, 2147.

MANDT, M.E., DENTON, R.E. & DRAKE, J.F. 1994 Transition to whistler mediated magnetic reconnection. *Geophys. Res. Lett.* **21** (1), 73.

MATTHAEUS, W.H. & LAMKIN, S.L. 1986 Turbulent magnetic reconnection. *Phys. Fluids* **29**, 2513.

MATTHAEUS, W.H. & VELLI, M. 2011 Who needs turbulence? A review of turbulence effects in the Heliosphere and on the fundamental process of reconnection. *Space Sci. Rev.* **160**, 145.

MIGLIUOLO, S., PEGORARO, F. & PORCELLI, F. 1991 Stabilization of collisional drift-tearing modes at the breakdown of the constant-ψ approximation. *Phys. Fluids* B **3**, 1338.

MILITELLO, F., BORGOGNO, D., GRASSO, D., MARCHETTO, C. & OTTAVIANI, M. 2011 Asymmetric tearing mode in the presence of viscosity. *Phys. Plasmas* **18**, 112108.

MILITELLO, F., HUYSMANS, G., OTTAVIANI, M. & PORCELLI, F. 2004 Effects of local features of the equilibrium current density profile on linear tearing modes. *Phys. Plasmas* **11**, 125.

MILOSEVICH, G., MORRISON, P.J. & TASSI, E. 2018 Direction of cascades in a magnetofluid model with electron skin depth and ion sound Larmor radius scales. *Phys. Plasmas* **25**, 072303.

MURAGLIA, M., AGULLO, O., BENKADDA, S., GARBET, X., BEYER, P. & SEN, A. 2009 Nonlinear dynamics of magnetic islands imbedded in small-scale turbulence. *Phys. Rev. Lett.* **103**, 145001.

MURAGLIA, M., AGULLO, O., BENKADDA, S., YAGI, M., GARBET, X. & SEN, A. 2011 Generation and amplification of magnetic islands by drift interchange turbulence. *Phys. Rev. Lett.* **107**, 095003.

NATIONAL RESEARCH COUNCIL 2008 *Severe Space Weather Events: Understanding Societal and Economic Impacts: A Workshop Report*. The National Academies Press.

NELSON, G.A. 2016 Space radiation and human exposures, a primer. *Radiat. Res.* **185**, 349.

NEWCOMB, W.A. 1958 Motions of magnetic lines of force. *Ann. Phys.* **3**, 347.

NISHIKAWA, K.-I. 1982 Stabilizing effect of a normal magnetic field on the collisional tearing mode. *Phys. Fluids* **25**, 1384.

NISHIZUKA, N., KARLICKY, M., JANVIER, M. & BÁRTA, M. 2015 Particle acceleration in plasmoid ejections derived from radio drifting pulsating structures. *Astrophys. J.* **126**, 799.

OFMAN, L., CHEN, X.L., MORRISON, P.J. & STEINOLFSON, R.S. 1991 Resistive tearing mode instability with shear flow and viscosity. *Phys. Fluids* **3**, 1364.

OTTAVIANI, M., ARCIS, N., ESCANDE, D.F., GRASSO, D., MAGET, P., MILITELLO, F., PORCELLI, F. & ZWINGMANN, W. 2004 Progress in the theory of magnetic reconnection phenomena. *Plasma Phys. Control. Fusion* **46**, B201.

OTTAVIANI, M. & PORCELLI, F. 1993 Nonlinear collisionless magnetic reconnection. *Phys. Rev. Lett.* **71**, 3802.

OTTAVIANI, M. & PORCELLI, F. 1995 Fast nonlinear magnetic reconnection. *Phys. Plasmas* **2**, 4104–4117.

PAPINI, E., FRANCI, L., LANDI, S., HELLINGER, P., VERDINI, A. & MATTEINI, L. 2019*a* Statistics of magnetic reconnection and turbulence in Hall-MHD and hybrid-PIC simulations. *Nuovo Cimento C* **42**, 23.

PAPINI, E., LANDI, S. & DEL ZANNA, L. 2019*b* Fast magnetic reconnection: secondary tearing instability and role of the hall term. *Astrophys. J.* **885**, 56.

PARK, W., MONTICELLO, D.A. & WHITE, R.B. 1984 Reconnection rates of magnetic fields including the effects of viscosity. *J. Geophys. Res.* **27**, 137.

PARKER, E.N. 1957 Sweet's mechanism for merging magnetic fields in conducting fluids. *J. Geophys. Res.* **62**, 509.

PARKER, E.N. 1973 The reconnection rate of magnetic fields. *Astrophys. J.* **180**, 247.

PEGORARO, F., BORGOGNO, D., CALIFANO, F., DEL SARTO, D., ECHKINA, E., GRASSO, D., LISEIKINA, T. & PORCELLI, F. 2004 Developments in the theory of collisionless reconnection in magnetic configurations with a strong guide field. *Nonlinear Process. Geophys.* **11**, 567.

PEGORARO, F., KUVSHINOV, B.N., ROMANELLI, M. & SCHEP, T.J. 1995 Scale-invariant plasma motions near X-points. In *Small-Scale Structures in Three-Dimensional Hydrodynamic and Magnetohydrodynamic Turbulence* (ed. M. Meneguzzi, A. Pouquet & P.-L. Sulem), Lecture Notes in Physics, vol. 462, p. 295. Springer.

PEGORARO, F., PORCELLI, F. & SCHEP, T.J. 1989 Internal kink modes in the ion-kinetic regime. *Phys. Fluids* B **1**, 364–374.

PEGORARO, F. & SCHEP, T.J. 1981 Low-frequency modes with high toroidal mode numbers: a general formulation. *Phys. Fluids* **24**, 478.

PEGORARO, F. & SCHEP, T.J. 1986 Theory of resistive modes in the ballooning representation. *Plasma Phys. Control. Fusion* **28**, 647.

PERONA, A., ERIKSSON, L.-G. & GRASSO, D. 2010 Electron response to collisionless magnetic reconnection. *Phys. Plasmas* **17**, 042104.

PETSCHEK, H.E. 1964 Magnetic field annihilation. In *AAS-NASA Symposium on the Physics of Solar Flares: Proceedings of a Symposium Held at the Goddard Space Flight Center, Greenbelt, Maryland, October 28–30, 1963*, vol. 50, p. 425. Scientific and Technical Information Division, National Aeronautics and Space Administration.

PNEUMAN, G.W. 1983 Ejection of magnetic fields from the sun: acceleration of a solar wind containing diamagnetic plasmoids. *Astrophys. J.* **265**, 468.

POGUTSE, I.O., SMOLYAKOV, A.I. & HIROSE, A. 1998 Magnetohydrodynamic equations for plasmas with finite-larmor-radius effects. *J. Plasma Phys.* **60**, 133–149.

PORCELLI, F. 1987 Viscous resistive magnetic reconnection. *Phys. Fluids* **30**, 1734.

PORCELLI, F. 1991 Collisionless $m = 1$ tearing mode. *Phys. Rev. Lett.* **66**, 425.

PORCELLI, F., BORGOGNO, D., CALIFANO, F., GRASSO, D., OTTAVIANI, M. & PEGORARO, F. 2002 Recent advances in collisionless magnetic reconnection. *Plasma Phys. Control. Fusion* **44**, B389.

PORCELLI, F., BOUCHER, D. & ROSENBLUTH, M.N. 1996 Model for the sawtooth period and amplitude. *Plasma Phys. Control. Fusion* **38**, 2163.

PRIEST, E.R. 1976 Current sheet models of solar flares. *Sol. Phys.* **47**, 41.

PRIEST, E.R. & SONNERUP, B.U.Ö. 1975 Theories of magnetic field annihilation. *Geophys. J. Intl* **41**, 405.

PRITCHETT, P.L., LEE, Y.C. & DRAKE, J.F. 1979 Coalescence of magnetic islands. *Phys. Fluids* **22**, 2140.

PRITCHETT, P.L., LEE, Y.C. & DRAKE, J.F. 1980 Linear analysis of double tearing mode. *Phys. Fluids* **23**, 1368.

PUCCI, F. & VELLI, M. 2014 Reconnection of quasi-singular current sheets: the "ideal" tearing mode. *Astrophys. J. Lett.* **780**, L19.

PUCCI, F., VELLI, M., SHI, C., SINGH, K.A.P., TENERANI, A., ALLADIO, F., AMBROSINO, F., BURATTI, P., FOX, W., JARA-ALMONTE, J., *et al.* 2020 Onset of fast magnetic reconnection and particle energization in laboratory and space plasmas. *J. Plasma Phys.* **86**, 535860601.

PUCCI, F., VELLI, M., TENERANI, A. & DEL SARTO, D. 2018 Onset of fast "ideal" tearing in thin current sheets: dependence on the equilibrium current profile. *Phys. Plasmas* **25**, 032113.

https://doi.org/10.1017/S0022377822001088 Published online by Cambridge University Press

ROBERTS, K.V. & TAYLOR, J.B. 1962 Magnetohydrodynamic equations for finite larmor radius. *Phys. Rev. Lett*. **8**, 197.

ROGERS, B.N., KOBAYASHI, S., RICCI, P., DORLAND, W., DRAKE, J. & TATSUNO, T. 2007 Gyrokinetic simulations of collisionless magnetic reconnection. *Phys. Plasmas* **14**, 092110.

SCHEKOCHIHIN, A.A. 2020 MHD turbulence: a biased review. arXiv:2010.00699.

SCHEP, T.J., PEGORARO, F. & KUVSHINOV, B.N. 1994 Generalized two fluid theory of nonlinear magnetic structures. *Phys. Plasmas* **1**, 2843–2852.

SCHNACK, D.D. JR. 1978 Non-linear numerical studies of the tearing mode. PhD thesis, Lawrence Livermore Laboratory, University of California, Livermore, CA.

SCHNACK, D.D. JR. 2009 *Lectures in Magnetohydrodynamics. With An Appendix on Extended MHD*. Springer.

SCHOLER, M. 1987 Earthward plasma flow during near-earth magnetotail reconnection: numerical simulations. *J. Geophys. Res*. **92** (A11), 12425.

SCHOUTEN, J.A. 1989 *Tensors Analysis for Physicists*. Dover Publ.

SERVIDIO, S., DMITRUK, P., GRECO, A., WAN, M., DONATO, S., CASSAK, P.A., SHAY, M.A., CARBONE, V. & MATTHAEUS, W.H. 2011 Magnetic reconnection as an element of turbulence. *Nonlinear Process. Geophys*. **18**, 675.

SERVIDIO, S., MATTHAEUS, W.H., SHAY, M.A., CASSAK, P.A. & DMITRUK, P. 2009 Magnetic reconnection in two-dimensional magnetohydrodynamic turbulence. *Phys. Rev. Lett*. **102**, 115003.

SHAY, M.A, DRAKE, J.F., DENTON, R.E. & BISKAMP, D. 1998 Structure of the dissipation region during collisionless magnetic reconnection. *J. Geophys. Res*. **103**, 9165.

SHIBATA, K. 1998 Evidence of magnetic reconnection in solar flares and a unified model of flares. *Earth Planet. Space* **264**, 129.

SHIBATA, K. & TANUMA, S. 2001 Plasmoid induced-reconnection and fractal reconnection. *Earth Planet. Space* **53**, 473.

SINGH, A., PUCCI, F., TENERANI, A., SHIBATA, K., HILLIER, A. & VELLI, M. 2019 Dynamic evolution of current sheets, ideal tearing, plasmoid formation and generalized fractal reconnection scaling relations. *Phys. Plasmas* **881**, 52.

SMOLYAKOV, A.I., POGUTSE, I.O. & HIROSE, A. 1995 Fluid model of collisionless plasma with finite Larmor radius effects. *Phys. Plasmas* **2**, 4451–4454.

SOMOV, B.V. & VERNETA, A.I. 1988 Magnetic reconnection in a high-temperature plasma of solar flares. III. Stabilizing effect of the transverse magnetic field in a non-neutral current sheet. *Solar Phys*. **117**, 89.

SOMOV, B.V. & VERNETA, A.I. 1989 Magnetic reconnection in a high-temperature plasma of solar flares. IV. Resistive tearing mode in non-neutral current sheets. *Solar Phys*. **120**, 93.

SONNERUP, B.U.Ö. 1973 Magnetic field reconnection and particle acceleration. In *High Energy Phenomena on the Sun Symposium Proceedings NASA-GSFC Doc. X-693-73-193*, p. 357.

STRAUSS, H.R. 1976 Nonlinear three-dimensional magnetohydrodynamics of non-circular tokamaks. *Phys. Rev*. **19**, 134.

STRAUSS, H.R. 1977 Dynamics of high-β tokamaks. *Phys. Rev*. **20**, 1354.

STRAUSS, H.R. 1988 Turbulent reconnection. *Astrophys. J*. **326**, 412.

SWEET, P.A. 1958 The neutral point theory of solar flares. In *Electromagnetic Phenomena in Cosmical Physics. International Astronomical Union Symposium No. 6* (ed. B. Lehnert), p. 123. Cambridge University Press.

SYROVATSKII, S.I. 1966*a* Dynamic dissipation of a magnetic field in particle acceleration. *Sov. Astron*. **10**, 270.

SYROVATSKII, S.I. 1966*b* Dynamic dissipation of magnetic energy in the vicinity of a neutral magnetic field line. *Sov. Phys. JETP* **23**, 754.

SYROVATSKII, S.I. 1981 Pinch sheets and reconnection in astrophysics. *Rev. Astron. Atrophys*. **19**, 163.

TAJIMA, T. & SHIBATA, K. 1997 *Plasma Astrophysics*. Addison-Wesley.

TANUMA, S., YOKOYAMA, T., KUDOH, T. & SHIBATA, K. 2001 Two-dimensional magnetohydrodynamic numerical simulations of magnetic reconnection triggered by a supernova shock in the interstellar medium: generation of X-ray gas in the galaxy. *Astrophys. J*. **551**, 312.

TASSI, E., SULEM, P.-L. & PASSOT, T. 2016 Reduced models accounting for parallel magnetic perturbations: gyrofluid and finite Larmor radius–Landau fluid approaches. *J. Plasma Phys*. **82**, 705820601.

TAVANI, M., BULGARELLI, A., VITTORINI, V., PELLIZZONI, A., STRIANI, E., CARAVEO, P., WEISSKOPF, M.C., TENNANT, A., PUCELLA, G., TROIS, A., *et al.* 2011 Discovery of powerful gamma-ray flares from the Crab Nebula. *Science* **331** (6018), 736–739.

TENERANI, A. & VELLI, M. 2020 Spectral signatures of recursive magnetic field reconnection. *Mon. Not. R. Astron. Soc*. **491**, 4627.

TENERANI, A., VELLI, M., PUCCI, F., LANDI, S. & RAPPAZZO, A.F. 2016 'Ideally' unstable current sheets and the triggering of fast magnetic reconnection. *J. Plasma Phys*. **82**, 535820501.

TENERANI, A., VELLI, M., RAPPAZZO, A.F. & PUCCI, F. 2015 The tearing mode instability of thin current sheets: the transition to fast reconnection in the presence of viscosity. *Astrophys. J*. **801**, 145.

THOMPSON, W.B. 1961 Magnetohydrodynamic equations for finite Larmor radius. *Rep. Prog. Phys*. **24**, 363.

TRUESDELL, C. 1950 The effect of the compressibility of the Earth in its magnetic field. *Phys. Rev*. **78**, 823.

TRUESDELL, C. 1954 *The Kinematics of Vorticity*. Indiana University Press.

TUR, A.V. & YANOVSKY, V.V. 1993 Invariants in dissipationless hydrodynamic media. *J. Fluid Mech*. **248**, 67.

UZDENSKY, D.A. 2011 Magnetic reconnection in extreme astrophysical environments. *Space Sci. Rev*. **160**, 45.

UZDENSKY, D.A., LOUREIRO, N.F. & SCHEKOCHIHIN, A.A. 2010 Fast magnetic reconnection in the plasmoid-dominated regime. *Geophys. Res. Lett*. **105**, 235002.

VAIVADS, A., KHOTYAINTSEV, Y., ANDRÉ, M., RETINO, A., BUCHERT, S.C., ROGERS, B.N., DÉCRÉAU, P., PASCHMANN, G. & PHAN, T.D. 2004 Structure of the magnetic reconnection diffusion region from four-spacecraft observations. *Phys. Rev. Lett*. **93**, 105001.

VAN HOVEN, G. & CROSS, M.A. 1971 Resistive instability of a sheet pinch. *Phys. Fluids* **14**, 1141.

VAN HOVEN, G. & CROSS, M.A. 1973*a* Energy release by magnetic tearing: the nonlinear limit. *Phys. Rev.* A **7**, 1347.

VAN HOVEN, G. & CROSS, M.A. 1973*b* Inertial magnetic field reconnection and magnetospheric substorm. *Phys. Rev. Lett*. **30**, 642.

VASYLIUNAS, V.M. 1975 Theoretical models of magnetic field line merging. *Rev. Geophys*. **13**, 303.

VELLI, M. & HOOD, A.W. 1989 Resistive tearing in line-tied magnetic fields: slab geometry. *Solar Phys*. **119**, 107.

WAELBROECK, F.L., HAZELTINE, R.D. & MORRISON, P.J. 2009 A Hamiltonian electromagnetic gyrofluid model. *Phys. Plasmas* **16**, 032109.

WAELBROECK, F.L. & TASSI, E. 2012 A compressible Hamiltonian electromagnetic gyrofluid model. *Commun. Nonlinear Sci. Numer. Simul*. **17**, 2171–2178.

WAN, M., MATTHAEUS, W.H., SERVIDIO, S. & OUGHTON, S. 2013 Generation of X-points and secondary islands in magnetohydrodynamic turbulence. *Phys. Plasmas* **20**, 042307.

WANG, X. & BHATTACHARJEE, A. 1997 Forced reconnection and mode locking in rotating cylindrical plasmas. *Phys. Plasmas* **4**, 748.

WANG, X. & BHATTCHARJEE, A. 1995 Nonlinear dynamics of the $m = 1$ kink-tearing instability in a modified magnetohydrodynamic model. *Phys. Plasmas* **2**, 171.

WANG, S., LEE, L.C. & WEI, C.Q. 1988 Streaming tearing instability in the current sheet with a super-Alfvénic flow. *Phys. Fluids* **31**, 1544.

WANG, Z.-X., WEI, L., WANG, X., ZHENG, S. & LIU, Y. 2011 Fast linear growth of collisionless double tearing modes in a cylindrical plasma. *Nucl. Fusion* **51**, 033003.

WATSON, P.G. & CRAIG, I.J.D. 1998 Magnetic annihilation and reconnection in two dimensions. *Astrophys. J*. **505**, 363.

WEI, F., HU, Q., FENG, X. & SCHWEN, R. 2000 Simulation of turbulent magnetic reconnection in the small-scale solar wind. *Sci. China* A **43**, 629.

WESSON, J.A. 1986 Sawtooth oscillations. *Plasma Phys. Control. Fusion* **28**, 243.

WESSON, J.A. 1990 Sawtooth reconnection. *Nucl. Fusion* **30**, 2545.
WESSON, J. 2004 *Tokamaks*. Oxford University Press.
WHITE, R.B. 1983 Resistive instabilities and field line reconnection. In *Handbook of Plasma Physics, Vol. I* (ed. A.A. Galeev & R.N. Sudan), p. 611. North Holland Publisher.
WHITE, R.B. 1986 Resistive reconnection. *Rev. Mod. Phys*. **58**, 183.
WILSON, H.R. 2012 Neoclassical tearing modes. *Fusion Sci. Technol*. **61**, 113–121.
WOLTJER, L. 1958 A theorem on force-free magnetic fields. *Proc. Natl Acad. Sci*. **44**, 489.
YAMADA, M., JI, H., HSU, S., CARTER, T., KULSRUD, R., ONO, Y. & PERKINS, F. 1997 Identification of Y-shaped and O-shaped diffusion regions during magnetic reconnection in a laboratory plasma. *Phys. Rev. Lett*. **78**, 3117.
YAMADA, M., KULSRUD, R. & JI, H. 2010 Magnetic reconnection. *Rev. Mod. Phys*. **82**, 603.
YAN, X., XUE, Z., JIANG, C., PRIEST, E.R., KLIEM, B., YANG, L., WANG, J., KONG, D., SONG, Y., FENG, X. *et al.* 2022 Fast plasmoid-mediated reconnection in a solar flare. *Nat. Commun*. **13**, 640.
YU, Q. 2010 Linear and nonlinear stability of drift-tearing mode. *Nucl. Fusion* **50**, 025041.
ZAKHAROV, L. & ROGERS, B. 1992 Two-fluid magnetohydrodynamic description of the internal kink mode in tokamaks. *Phys. Fluids* B **4** (10), 3285–3301.
ZANK, G.P. & MATTHAEUS, W.H. 1992 The equations of reduced magneto- hydrodynamics. *J. Plasma Phys*. **48**, 85.
ZHOU, M., WU, D.H., LOUREIRO, N.F. & UZDENSKY, D.A. 2021 Statistical description of coalescing magnetic islands via magnetic reconnection. *J. Plasma Phys*. **87**, 905870620.
ZOCCO, A., HELANDER, P. & WEITZNER, H. 2020 Magnetic reconnection in 3d fusion devices: non-linear reduced equations and linear current-driven instabilities. *Plasma Phys. Control. Fusion* **63**, 025001.
ZOCCO, A. & SCHEKOCHIHIN, A.A. 2011 Reduced fluid-kinetic equations for low-frequency dynamics, magnetic reconnection, and electron heating in low-beta plasmas. *Phys. Plasmas* **18** (10), 102309.